VOLUME 79 MARCH 13, 1975 NUMBER 6

JPCHAx

THE JOURNAL OF PHYSICAL CHEMISTRY

PUBLISHED BIWEEKLY BY THE AMERICAN CHEMICAL SOCIETY

THE JOURNAL OF

PHYSICAL CHEMISTRY

AMERICAN CHEMICAL SOCIETY, *1155 Sixteenth St., N.W., Washington, D.C. 20036*

Books and Journals Division

JOHN K CRUM *Director*
VIRGINIA E. STEWART *Assistant to the Director*

CHARLES R. BERTSCH *Head, Editorial Processing Department*
D. H. MICHAEL BOWEN *Head, Journals Department*
BACIL GUILEY *Head, Graphics and Production Department*
SELDON W. TERRANT *Head, Research and Development Department*

 Published biweekly by the American Chemical Society at 20th and Northampton Sts., Easton, Pa. 18042. Second-class postage paid at Washington, D.C., and at additional mailing offices.

All manuscripts should be sent to *The Journal of Physical Chemistry*, Department of Chemistry, University of Minnesota, Minneapolis, Minn. 55455.

Additions and Corrections are published once yearly in the final issue. See Volume 78, Number 26 for the proper form.

Extensive or unusual alterations in an article after it has been set in type are made at the author's expense, and it is understood that by requesting such alterations the author agrees to defray the cost thereof.

The American Chemical Society and the Editor of *The Journal of Physical Chemistry* assume no responsibility for the statements and opinions advanced by contributors.

Correspondence regarding accepted copy, proofs, and reprints should be directed to Editorial Processing Department, American Chemical Society, 20th and Northampton Sts., Easton, Pa. 18042. Department Head: CHARLES R. BERTSCH. Associate Department Head: MARIANNE C. BROGAN. Assistant Editor: CELIA B. MCFARLAND. Editorial Assistant: JOSEPH E. YURVATI.

Advertising Office: Centcom, Ltd., 50 W. State St., Westport, Conn. 06880.

Business and Subscription Information

Send all new and renewal subscriptions *with payment* to: Office of the Controller, 1155 16th Street, N.W., Washington, D.C. 20036. Subscriptions should be renewed promptly to avoid a break in your series. All correspondence and telephone calls regarding changes of address, claims for missing issues, subscription service, the status of records, and accounts should be directed to Manager, Membership and Subscription Services, American Chemical Society, P.O. Box 3337, Columbus, Ohio 43210. Telephone (614) 421-7230. For microfiche service, contact ACS Journals Department, 1155 16th St. N.W., Washington, D.C. 20036. Telephone (202) 872-4444.

On changes of address, include both old and new addresses with ZIP code numbers, accompanied by mailing label from a recent issue. Allow four weeks for change to become effective.

Claims for missing numbers will not be allowed (1) if loss was due to failure of notice of change in address to be received before the date specified, (2) if received more than sixty days from date of issue plus time normally required for postal delivery of journal and claim, or (3) if the reason for the claim is "issue missing from files."

Subscription rates (hard copy or microfiche) in 1975: $20.00 for 1 year to ACS members; $80.00 to nonmembers. Extra postage $4.50 in Canada and PUAS, $5.00 other foreign. Supplementary material (on microfiche only) available on subscription basis, 1975 rates: $15.00 in U.S., $19.00 in Canada and PUAS, $20.00 elsewhere. All microfiche airmailed to non-U.S. addresses; air freight rates for hard-copy subscriptions available on request.

Single copies for current year: $4.00. Rates for back issues from Volume 56 to date are available from the Special Issues Sales Department, 1155 Sixteenth St., N.W., Washington, D.C. 20036.

Subscriptions to this and the other ACS periodical publications are available on microfilm. For information on microfilm write Special Issues Sales Department at the address above.

Notice to Authors last printed in the issue of January 16, 1975

THE JOURNAL OF

PHYSICAL CHEMISTRY

Volume 79, Number 6 March 13, 1975

JPCHAx 79(6) 545–670 (1975)

ISSN 0022-3654

COMMUNICATIONS TO THE EDITOR

■ Supplementary material for this paper is available separately, in photocopy or microfiche form. Ordering information is given in the paper.

* In papers with more than one author, the asterisk indicates the name of the author to whom inquiries about the paper should be addressed.

AUTHOR INDEX

THE JOURNAL OF
PHYSICAL CHEMISTRY

VOLUME 79, NUMBER 6 MARCH 13, 1975

Infrared Laser Augmented Decomposition of $H_3B \cdot PF_3$

E. R. Lory, S. H. Bauer,*

Department of Chemistry, Cornell University, Ithaca, New York 14853

and T. Manuccia

Optical Sciences Division, Naval Research Laboratories, Washington, D.C. 20390 *(Received July 8, 1974)*

Consideration of v–v and v–T relaxation rates for polyatomic molecules subsequent to their vibrational excitation by currently available laser fluxes led to a strategy for selecting reactants for which the possibility for successful augmentation of reaction by infrared irradiation is optimized. Several criteria are listed. While these are shown to be useful guides they do not constitute a sufficient set of conditions for predicting augmentation of reactions. The criteria were applied to the selection of reactants for a typical $2AB \rightarrow A_2 + 2B$ reaction, *i.e.*, a self-scavenging system. The thermochemistry, essential vibrational spectroscopy, and kinetic parameters for the $H_3B \cdot PF_3$ decomposition are briefly summarized. The experimental arrangement is described and the results of a series of runs with a CO_2 laser (10.6-μ band) are presented. A number of tests were applied to demonstrate that the induced decomposition was indeed due to vibrational excitation and not to a net rise in temperature. No significant boron isotope effect was found. A mechanism is proposed, based on the observed dependence of per cent decomposition on photon flux, and its specificity for the rotational line used for excitation. Use of a spectrophone greatly facilitated measurement of the optical absorption coefficients. It appears that the rate-determining step is $H_3B + H_3B{\cdot}PF_3^{(v\approx 2)} = B_2H_6 + PF_3$ with the vibrational excitation in specific modes. Similar studies with $H_3B{\cdot}CO$ (9.6-μm band) showed no augmentation.

Introduction

That some reactions can be forced to occur at finite rates, or show augmented rates, as a consequence of photon absorption by the reactants is hardly startling. Photochemical processes induced by visible or ultraviolet radiations have been investigated and effectively utilized for many decades. The current interest in laser augmented reactions stems from the recently developed technology which for the first time makes available high fluxes of photons in the infrared, *i.e.*, photons that carry from 3.3 to ~10 kcal/einstein. The energy load per photon provides a critical criterion for its functional classification. If it is sufficiently large (uv or visible) (i) the absorption cross sections are quite large $\sim 10^{-17}$ to 10^{-18} cm^2; (ii) the absorber is electronically excited and may either dissociate or become highly receptive to attack; (iii) lifetimes for such excited states, or of states into which these relax rapidly, range from microseconds to seconds. In contrast when the energy content is low (ir) (i) the absorption cross sections are generally of the order 10^{-19} cm^2, or smaller; (ii) the absorbers are vibrationally excited but do not pick up sufficient energy to dissociate by such a single event; (iii) collisional lifetimes at ordinary pressures are in the nanosecond range for most molecules of interest.

In view of these unfavorable factors why bother with photochemistry in the infrared? There are several reasons. The most persuasive one is that the currently available high fluxes, 10^{18} to 10^{20} cm^{-2} sec^{-1}, permit the attainment of high populations of vibrationally excited states within the ground electronic state. The objective then is to measure chemical reactivity as a function of specific internal excitation, rather than of the total energy content, which during conventional activation is partitioned according to a Boltzmann distribution among all states. Indirect evidence for the dependence of bimolecular atom exchange reaction rate constants on vibrational energy rather than on total energy was presented about a decade ago.[1] Specifically, studies of ir laser induced reactions may provide an answer to the following question. In binary collisions which lead to reaction, for all entering pairs with total energy content E,

what is the dependence of the cross section, $\sigma(E; \xi)$, on the fraction of the energy ξ that is in vibration? By now about half a dozen experiments have been described[2] which present partial answers to this question. Several extended trajectory analyses[3] have been made to ascertain the relative efficacy of activation energy available as vibration *vs.* translation, and general discussions of the inverse process, the partition of energy among product states, have been published.[4]

A second reason is correlary to the first—the possibility of inducing reactions selectively, that is, of specific molecular species. This hinges on the narrowness of spectral line widths of laser radiations, and on the possibility of matching, accidentally or by tuning, the incident radiation to a characteristic transition of one of several potential reactants present in the mixture. Also, it is theoretically possible[5] that ultrahigh fluxes ($\approx 10^{29}$ cm^{-2} sec^{-1}) may lead to simultaneous multiphoton absorptions, and thus induce dissociations by a novel process. Whatever the motive, considerable effort has been expended in attempts to demonstrate experimentally the occurrence of laser augmented reactions, but few[2] were successful in *unequivocally* proving that the effects they observed were not due to thermalized systems. The inherent limitations are obvious, yet they were not adequately recognized in the design of many experiments. For any specific pumping rate [$\propto$ flux · cross section], the attainable population in *those* vibrationally excited states which favor the desired transformation is determined (to a major extent) by a v–T relaxation time. When the net vibration → translation energy transfer rate is fast compared to the v pumping rate, the excitation of the sample is equivalent to homogeneous heating and conventional thermodynamic and kinetic restrictions apply; if these two rates are comparable one must experimentally discriminate between reaction steps due to heating and those due to excitation of specific states.[2h] Only when $\tau(v\text{–}v) \ll \tau(v\text{–}T)$ are the results unequivocal.[6] However, one must not overlook the intramolecular relaxation time; *i.e.*, the rate for redistribution of vibrational energy within the absorber which controls the drain of excitation from the reaction coordinate. For high levels of vibrational excitation this characteristic time is of the order of picoseconds.[7]

Consideration of these and other factors led us to a strategy for selecting reactants for which the probability of successful augmentation of a reaction by infrared irradiation is optimized. (α) Select reactions with modest E_{act} (20–30 kcal/mol), and use the most energetic photons for which the absorption cross section is high. (β) Select systems for which $\tau_{v,T}$ is much greater than $\tau_{v,v}$ (generally this is the case for molecules that contain few atoms). Alternately, work at low pressures so that the mean free path is comparable to the reactor dimensions. (γ) Adjust conditions for minimal $\Delta T_{T,r}$; operate at sufficiently low pressures such that wall collisions moderate the translational and rotational temperatures of the reactant, or used forced convective cooling. (δ) Introduce scavengers which react rapidly with the vibrationally excited species or with the products of photolysis. Strive for $\tau_{chem} < \tau_{v,v} \ll \tau_{v,T}$. ($\epsilon$) Whether one uses short pulses of very high power or extended irradiation with low power, but with the same integrated absorbed energy, depends on the analytical devices available for following the course of reaction. In view of β, the former is preferred.

Herein we report the successful demonstration of a CO_2 laser induced reaction of the type $2AB \rightarrow A_2 + 2B$, selected on the basis of the above prescription. It is our contention that the decomposition of $H_3B \cdot PF_3$ under the conditions described below is not a consequence of thermal heating of the sample, and that the methodology developed in this experiment can be generally extended so as to ensure that when positive effects are observed they are indeed due to specific vibrational excitation.

Two essential experimental conditions must be fulfilled. First, the reagents should be at a pressure so low that their mean free paths are comparable to the dimensions of the cell and thus maintain the translational and rotational temperatures at the wall temperatures. During the short intervals when these molecules traverse the beam and absorb photons, they become vibrationally hot. Further, it is necessary that the photon flux be very high in order to affect significant conversions. This can be achieved by placing the reactor cell within the laser cavity. The reactants must be present at sufficiently low pressures so that the absorption losses do not quench laser oscillations.

Spectroscopic Preliminaries

The requirement that the mean free path of the reactants be comparable to the cell dimensions restricts the application of this technique to those materials that have very high absorption coefficients at wavelengths for which high laser fluxes are available. Clearly the products of reaction should not absorb the laser frequency. Also, because of the low energy content of the CO_2 laser photons [~3.3 kcal/einstein], the reactants must have a sufficient density of excited states so that successive absorptions can occur.

For $H_3B \cdot PF_3$ we had to supplement the spectroscopic data in the literature with several essential measurements. Over the range of the 10.6-μ CO_2 band, the raman spectrum of liquid $H_3B \cdot PF_3$, as reported by Taylor and Bissot,[8] shows three bands: at 957 cm^{-1} [ν_9(e), P–F str], 944 cm^{-1} [ν_3(a), P–F str], and 920 cm^{-1} [(ν_8–ν_{12}), calculated 920 cm^{-1} for (HBH def)–(PF_3 rock)]. Our raman scan of the vapor (Spex Ramalog) showed only a broad weak scattering at 930 ± 3 cm^{-1}. The other bands check well with the reported frequencies: 2386 ± 1 *vs.* 2385 cm^{-1} for B–H str; 608 ± 1 *vs.* 607 cm^{-1} for P–B str; 441 ± 1 *vs.* 441 cm^{-1} for FPF def. There is no reason to question Taylor and Bissot's assignment of fundamentals, and it is interesting to note that the P–F stretching frequencies *increase* on coordination [ν_1(a) 892 cm^{-1}: ν_2(e) 860 cm^{-1} in PF_3]. A moderate resolution infrared absorption spectrum (Perkin-Elmer No. 521) showed three well-resolved peaks and two shoulders, Figure 1, of which three features, at 957.7, 942.9, and 921.2 cm^{-1}, match the raman spectrum exceptionally well. The two remaining prominent peaks (not reported by Taylor and Bissot) must be assigned to combination bands [$2\nu_{11}$(e) + ν_{12}(e), calcd 937 cm^{-1}, obsd 931 cm^{-1}; higher order combinations possibly account for the 951-cm^{-1} band]. The superposition of absorptions provided the first indication that at a pressure of 1.5 Torr this part of the rotational–vibrational spectrum may consist of a dense array of lines.

The spacing in the pure rotational spectrum, derived from a microwave study,[9] is approximately 10^2 greater than the laser line widths ($\approx 10^2$ MHz). This suggested the possibility that $H_3{}^{10}B \cdot PF_3$ absorptions could be distinguished from $H_3{}^{11}B \cdot PF_3$ in those vibrations which are coupled to the B–P stretch, as the P–F stretch must be. The spectrum obtained by tuning the laser from line to line reproduced the pattern recorded in Figure 1. Absorption coefficients for the natural abundance and the ^{10}B enriched (95%) sam-

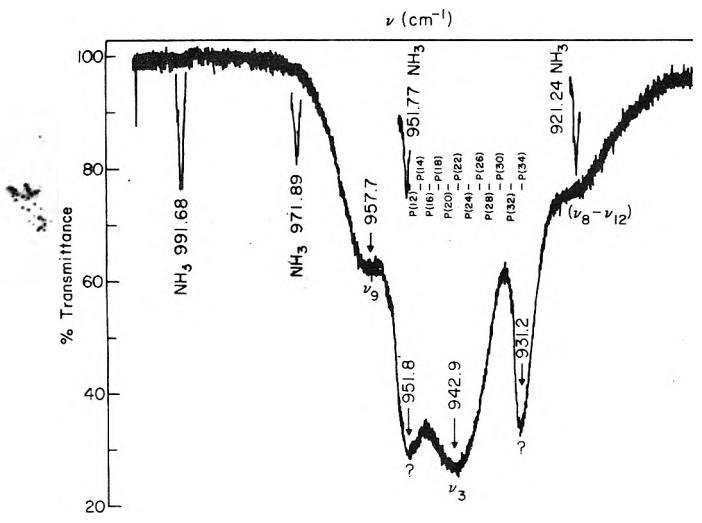

Figure 1. Infrared absorption spectrum of $H_3B \cdot PF_3$ in the 10.6-μ region, as recorded with a Perkin-Elmer No. 521: cell length 7.5 cm; sample pressure 1.5 Torr; spectral resolution 0.2 cm^{-1}.

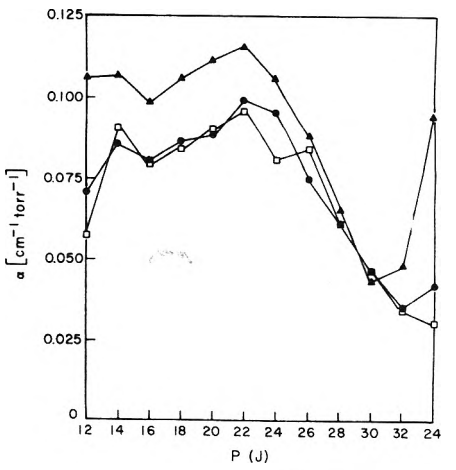

Figure 2. Derived absorption coefficients [$\alpha \equiv (1/pl) \ln (I_0/I)$], $Torr^{-1}$ cm^{-1}, at specified CO_2 laser lines (spectrophone), for $p \geq 250$ mTorr: (□) normal isotopic composition; (●) ^{10}B enriched (95%); (▲) values deduced from trace in Figure 1.

ples of $H_3B \cdot PF_3$ were determined for 12 frequencies, corresponding to laser transitions P(12) to P(34) [00°1 → 10°0 band]. In addition, for the same frequencies absorption coefficients were obtained for SF_6 to provide a check on the reliability of our procedure, which involved the use of a spectrophone cell.[10] The output signal of the laser was reduced in intensity to a level of approximately 0.3 W/cm^2 by interposing a low transmittance germanium flat in the output beam. The spectrophone cell incorporates a Capps condenser microphone which is connected through a suitable preamplifier to a PAR JB-4 lock-in amplifier. The reference signal was generated by a chopper, light source, and a phototransistor detector. Laser power was monitored by a Coherent Radiation power meter, Model 201, and displayed on a strip chart recorder for time averaging. An absolute scale for the coefficients was established by (cell in)/(cell out) recording of the spectrophone signal. Corrections for window absorption were made. The absorption coefficients measured for SF_6 at 450 mTorr were slightly lower than those reported by Shimizu.[11] The difference is probably due to our use of an unstabilized laser, since Shimizu found a large variation in the coefficients as he tuned a stabilized laser across each laser transition. Measurements made with incident power levels 0.04 → 0.30 W/cm^2 gave the same absorption coefficients, indicating the absence of saturation effects.

Three sets of observed absorption coefficients for $H_3B \cdot PF_3$ are shown in Figure 2. Within the uncertainty limits of the data the two isotopic species of boron have the same coefficients for the indicated laser lines, at the level of 0.3 W/cm^2. The magnitudes of the coefficients are lower than those of SF_6 by approximately a factor of 4. It is evident from Figure 2 that the conventionally recorded spectrum gives essentially the same values for the absorption coefficients as those derived for the narrow laser lines. This supports the contention that no saturation effects influenced the spectrophone data, and that at pressures at 250 mTorr, the absorber lines are sufficiently broad such that they constitute a dense array on the scale of laser line widths. For P(28), a line of intermediate absorption intensity, the value of $\alpha(cm^{-1}\ Torr^{-1}) = 0.065 \pm 0.005$, corresponds to a cross section of 2×10^{-18} cm^2; for P(20), $\alpha = 0.085 \pm 0.007$.

We also measured the effect of sample pressure on the absorption coefficient, which is equal to the quantity $\{S/\kappa p\}$, where S is the lock-in amplifier output voltage, κ the overall apparatus constant, and p the pressure of the absorber. (S/p) remained independent of pressure from 1.5 Torr down to 250 mTorr, and then fell off to about 1/10 of its value at 25 mTorr. The addition of He to a low-pressure sample had little effect unless the inert gas was ≳1 Torr; in contrast, added Xe increased the magnitude of α as much, possibly a little more, than the $H_3B \cdot PF_3$. We conclude that significant pressure broadening occurs between 25 and 250 mTorr. Note that the relative magnitude of α for P(28) and P(20) remained essentially unchanged with pressure.

Kinetic Preliminaries

Burg and Fu[12] called attention to the many similarities between the physical and chemical properties of $H_3B \cdot CO$ and $H_3B \cdot PF_3$; the mechanism for decomposition proposed for the former[13] applies to the latter. That is, over the temperature range 0–60°

$$H_3BPF_3 \underset{1}{\overset{-1}{\rightleftharpoons}} H_3B + PF_3 \quad \text{(fast)} \tag{1}$$

$$H_3B + H_3BPF_3 \xrightarrow[2]{} B_2H_6 + PF_3 \quad \text{(rate limiting)} \tag{2}$$

$$-\frac{d[H_3BPF_3]}{dt} = \frac{2k_1k_2[H_3BPF_3]^2}{k_{-1}[PF_3] + k_2[H_3BPF_3]} \tag{3}$$

for the "steady state" condition on H_3B. Arrhenius plots for the carbonyl and trifluorophosphine adducts give, respectively

$$\log\left(\frac{k_1}{k_{-1}}k_2\right) = 13.58 - 26{,}750/4.575T \quad (H_3B{\cdot}CO) \tag{4}$$

$$= 15.84 - 29{,}300/4.575T \quad (H_3B{\cdot}PF_3) \tag{5}$$

These activation energies must be partitioned between the two steps; for $H_3B \cdot PF_3$ a reasonable value for the first is ≈21 kcal, and 8.3 kcal/mol for the second.

Experimental Section

The Apparatus. The experimental arrangement is shown schematically in Figure 3. The laser is a 115-cm section of

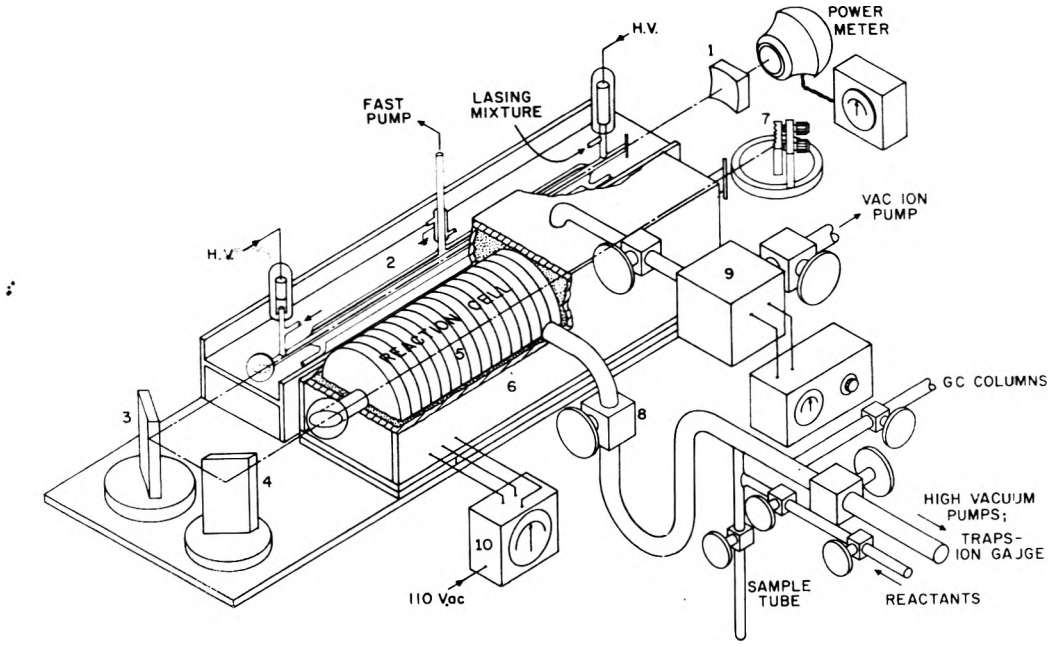

Figure 3. Schematic of experimental arrangement: (1) 95% reflecting, Ge output mirror (focal length 5 m); (2) laser tube, quartz, 115 cm long; (3,4) front surface mirrors; (5) heating coil, on reaction cell; (6) transite box, vermiculite filled; (7) grating 150 lines/mm, blazed for 10 μ; (8) valve to U tube; for sample injection and extraction; (9) MKS-Baratron 77H-1; (10) thermocouple and temperature controller.

13-mm i.d. quartz tube, with Brewster angle windows, and fitted with a water jacket, gas inlet, and pump outlet ports, and electrodes. The discharge, through a rapidly flowing gas mixture of CO_2, N_2, and He (2:3:6), was maintained by a stabilized Voltronics power supply, 0–50 kV; 0–85 mA. The laser was generally operated at 8 kV and 50 mA. The cavity was folded, closed by a 150 lines per millimeter grating for selection of rotational lines, and by a 95% reflecting germanium mirror, to provide a small output signal for monitoring the intracavity power. To check that this signal did measure the intracavity flux the ratio of the signal through the mirror to the intensity reflected from one of the cell windows was measured. This was constant over the range of powers used in these experiments. The total intracavity flux (both directions) was varied over the range 60–160 W, by changing the power supply discharge current. No attempt at intensity stabilization was made. The measured beam diameter at the cell position was 13 ± 1 mm. The reaction cell, a 12-cm diameter stainless steel pipe, 110 cm in length, was fitted with Brewster angle windows and constituted one arm of the folded cavity. It was connected through a high conductance U tube to the vacuum system. A Baratron capacitance manometer, Model 77H1, was attached directly to the cell, which was wrapped with heating tape, enclosed in an oversize transite box and insulated with vermiculite. A thermocouple, attached externally to the reactor wall, approximately near the middle, was connected to a temperature controller and to a recorder. The reactor wall temperature was maintained to ±0.2°.

Experiments were conducted as follows. A sample of $H_3B \cdot PF_3$, prepared by equilibrating B_2H_6 and PF_3 at room temperature for about 30 hr, after several trap-to-trap distillations, was cooled to −160° [2-methylbutane slush bath] and pumped-on to remove residual diborane and trifluorophosphine. The sample was then expanded from a measured pressure in a known small volume, into the sample cell. *No change* in the *laser output* signal was observed when the sample was admitted into the cell. The cell walls had been conditioned with $H_3B \cdot PF_3$ and evacuated to a pressure less than 2×10^{-6} Torr. Most of the experiments were performed with sample pressures between 2 and 3 mTorr. These were chosen so that the mean free paths of the reactant molecules were comparable to the laser beam diameter, and approximately 1/4 of the cell radius. In a few cases additional reagents or an Ar diluent were added to raise the total pressure to 500 mTorr. During irradiation the pressure change and the laser power were continuously recorded. Upon completion of irradiation the cell was opened to the U tube, cooled to −196°. A noncondensible gas was produced during each irradiation; the amount correlated with the degree of reaction observed (15–17% of total). The condensed sample was then transferred either to a small sample tube for mass spectral analysis or directly to the injection volume of a gas chromatograph.

Mass spectra were recorded with a CEC instrument, Model 21-103A. The inlet system was equipped with a capacitance manometer so that the initial sample pressure in the ballast volume could be accurately controlled. A representative (m/e) peak for each component in a sample mixture was measured as a function of time, and extrapolated to zero time, to compensate for the pressure drop in the ballast volume during the analysis. Gas chromatographic analyses were made with a F & M flame ionization unit, Model 609. We used a 20 ft, 0.25-in. diameter column packed with a 30% (wt) mineral oil liquid phase coating on Chrom R (Applied Science Laboratory, Inc.) as the solid support. The column was held at 0° during the analysis. This column effectively separated PF_3 from B_2H_6 or from $H_3B \cdot PF_3$ but did not separate the latter two components. We soon discovered that neither the reactant nor its products generated in the flame sufficient ions for a useful signal. A phototube (1P28; 90 V/dynode) was fitted with a 100-Å hand pass filter centered at 5260 Å and then set up to monitor the flame emission. This detector proved to be highly sensitive to both boron and phosphorus containing samples. The Baratron capacitance manometer was sensitive to pressure changes as small as 0.01 mTorr. Its output

was recorded continuously so that the extent of reaction *vs.* time was monitored throughout the experiment.

Qualitative Observations. Irradiation periods as short as 6 min produced up to 33% decomposition under conditions which produced no measureable thermal decomposition. The extent of reaction was frequency dependent but *not* in proportion to the corresponding ground state absorption coefficients. The extent of reaction increased with the intensity of radiation. When a substantial pressure of Ar was added, the extent of reaction increased, but dilution experiments with borane–carbonyl *at pressures comparable to the reactant* did not enhance the extent of decomposition. Also, the $H_3B \cdot CO$ decomposed only as much as was measured for this material at the wall temperature in the absence of laser radiation.

Significant differences between the relative efficiencies for inducing decomposition were found between P(28) and lower *J* lines. However, within the scatter of our data, no significant difference was found for the P(28) line between the extent of decomposition of $H_3{}^{10}BPF_3$ and $H_3{}^{11}BPF_3$; more about this later. A number of experiments were conducted to eliminate possible contributions to the observed augmentation by factors other than laser radiation. These included (i) operating the laser discharge but blocking laser radiation in a manner that permitted the visible and uv radiation from the discharge to enter the cell. No augmentation was observed. (ii) The sample cell was electrically grounded to prevent high-frequency discharges within the cell. (iii) The laser beam was carefully aligned through the cell and this alignment was frequently checked to make certain that the beam did not impinge on any wall. The cell windows were also inspected for material deposition which might cause local heating.

Quantitative Results

Power Dependence. Figure 4 shows the per cent decomposed as a function of total laser flux in the cavity (forward plus reverse) over the range 53 to 110 W; these data are listed in Table I. The net loss per minute [defined as $[(\text{moles})_i - (\text{moles})_f]/(\text{moles})_i \text{min}$, based on mass spectrometric or gc analyses of the cell contents] are mean values over irradiation times, which ranged from 6 to 240 min. Several features appear. It is clear that irradiation with P(28) is far more effective than irradiation with P(20), even though at pressures (25 → 1000 mTorr) the absorption coefficient for the latter is 20–50% larger than for the former. P(16) was about as effective as P(20); P(24) and P(26) were more, while P(30) and P(32) were less effective. The shape of the decomposition curve is concave upward indicating that the extent of decomposition is at least quadratic, and possibly of higher order in photon flux. The apparent threshold [*e.g.*, 1% for 30 min of irradiation with P(28)] is about 37 W. The early experiments show a large scatter for the normal ($^{10}B/^{11}B$) composition but the three points for the 95% ^{10}B enriched material appear to be mutually consistent and below the "band." This lack of reproducibility was later traced to inadequate conditioning of the cell walls and to the loss of PF_3 on transferring the sample from the cell to the U tube. When a rigid experimental methodology was followed, as in the final set of experiments, the pressure–time curves for a number of runs with ^{n}B and ^{10}B essentially superposed [mean slope 0.54 (0.05) for ^{n}B and 0.64 (0.08) for ^{10}B, with mean deviations indicated]. These observations are consistent with the near equality of their absorption coefficients, and not inconsistent with the mechanism proposed below. The difference in per cent conversions per minute, for the 30- and 120-min irradiations with P(20) is not due merely to depletion of reactant [compare the fourth and sixth columns in Table I]; account should also be taken of the reversibility of reaction 2. In Figure 5, the 6- and 12-min irradiation with P(28) are mutually consistent and show a slope [2.12] which is essentially the same as for the 30-min irradiations with P(20) [2.14]; the longer irradiations for P(20) have a steeper slope [3.61]. For either case, it appears that two to three photons are required for the overall process. A few experiments were conducted with sample pressures of 3.5 mTorr. The slopes for these data were essentially the same as for the lower sample pressures.

Borane–carbonyl does not absorb appreciably in the 10.6-μ band. No signal above the noise level could be obtained with the spectrophone for pressures up to several Torr whereas the $H_3B \cdot PF_3$ showed detectable absorptions at pressures as low as 25 mTorr. This was further checked by irradiating samples of the $H_3B \cdot CO$ under the same conditions as used for the $H_3B \cdot PF_3$. No augmented decomposition was observed. Experiments were then conducted

TABLE I

Sample[a]	Time, min	Measured power × 40	% reaction (per min)	Laser transition P(*J*)	% converted
n	6	72.4	1.4	28	8.4
n	6	70.2	2.2	28	12.9
n	6	64.0	1.9	28	11.3
n	12	89.6	2.8	28	33.0
n	12	89.4	3.3	28	40.0
n	12	85.2	3.0	28	35.9
n	12	80.8	2.7	28	32.1
n	12	76.8	2.8	28	33.6
n	12	70.4	1.6	28	18.7
n	12	70.4	1.5	28	17.7
n	12	68.2	1.7	28	20.0
n	12	64.0	1.8	28	22.0
n	12	63.8	1.0	28	12.5
n	12	55.4	1.3	28	15.3
n	12	53.2	0.8	28	9.4
10	12	85.2	2.0	28	24.0
10	12	68.2	1.1	28	13.1
10	12	55.2	0.7	28	8.6
n	30	110.8	1.2	20	36.9
n	30	98.0	0.90	20	27.1
n	30	89.4	0.81	20	24.3
n	30	81.0	0.56	20	16.8
n	120	106.6	0.58	20	69.0
n	120	106.6	0.55	20	66.4
n	120	89.0	0.27	20	31.8
n	120	89.0	0.21	20	25.2
n	120	80.4	0.14	20	16.3
n	120	70.4	0.12	20	14.5
n	120	70.4	0.09	20	10.3
n	120	21.2	0.00	20	0
n	120	80.6	0.58	28	70.1
n	120	90.8	0.63	26	75.6
n	120	89.0	0.57	26	67.9
n	120	89.0	0.44	24	52.3
n	120	89.0	0.18	16	21.5
n	120	59.4	0.0	10	0

[a] n = natural abundance: 10 = 95% ^{10}B.

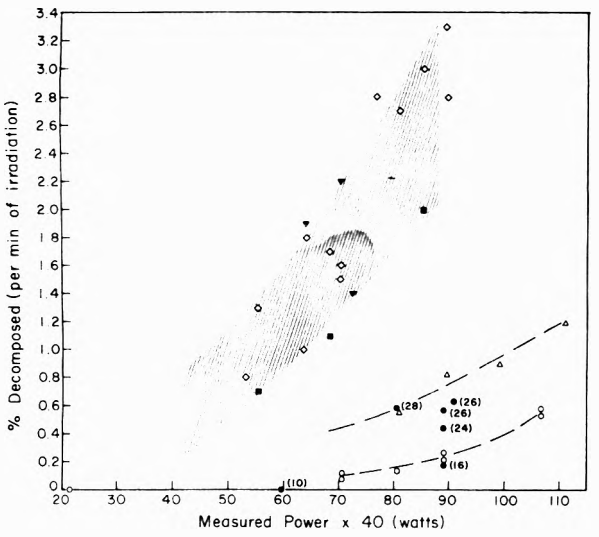

Figure 4. Per cent converted per minute *vs.* intracavity laser power; reduced from data for 6-, 12-, 30-, and 120-min runs. The laser lines used are indicated: (◇) normal isotopic composition, 12 min with P(28); (▼) normal isotopic composition, 6 min with P(28); (■) ^{10}B enriched (95%), 12 min with P(28); (△) normal isotopic composition, 30 min with P(20); (○) normal isotopic composition, 120 min with P(20); (●) normal isotopic composition, 120 min with P(*J*) indicated.

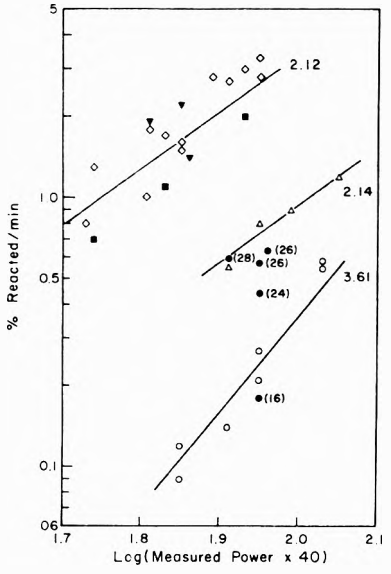

Figure 5. The data in Figure 4 replotted on log–log scales.

with a mixture of 1:1 of $H_3B \cdot PF_3$ and $H_3B \cdot CO$ at a total pressure of 2.5 mTorr. This showed the expected extent of decomposition for the former compound but only the room temperature rate for the latter. The results indicate that the chemical kinetic temperature of the borane–carbonyl was not changed by the radiation nor by collisions with the trifluorophosphine–borane. Additional experiments, with the $H_3B \cdot PF_3$ pressures held constant at 2.5 mTorr while the pressure of the carbonyl was increased, showed a slight increase in the rate as the pressure rose to a total of 10 mTorr; on further addition of $H_3B \cdot CO$ the rate of decomposition of the $H_3B \cdot PF_3$ decreased. This run was monitored by the Baratron capacitance manometer. Finally, the addition of Ar (up to 500 mTorr) or PF_3 (added pressure up to 7 mTorr) resulted in an increased rate of decomposition of the $H_3B \cdot PF_3$.

Discussion of Mechanism

First, let us summarize the evidence that the augmented decomposition of $H_3B \cdot PF_3$ is due to vibrational excitation rather than to an overall temperature rise. (a) The extent of decomposition is dependent on the *J* value of the laser line used but not in proportion to the absorption coefficients; differences in energy between P(20), P(28), and P(30) are trivial, yet their relative chemical efficiencies differ by as much as a factor of 5. (b) Collisional energy transfer to $H_3B \cdot CO$ does not appreciably raise the chemical kinetic temperature of the latter, since there was no augmented decomposition of the carbonyl. Thus, the strategy of using low pressures to maintain translational and rotational temperatures at or near the wall temperature succeeded even though the radius of the cell was about four times the mean free path.

The next step in the analysis of the data is estimation of the fraction of reactant molecules which have absorbed one or more photons. At 2 mTorr the density of $H_3B \cdot PF_3$ is 6.5×10^{13} molecules cm^{-3}, or 0.95×10^{16} molecules in the volume illuminated by the laser beam. Their mean free path is about 1 cm at 300°K; and their mean speed is 3.4×10^4 cm sec^{-1}. The mean time spent by the average molecule in the illuminated portion of the cell depends on the model used to calculate this average; it is of the order of the beam diameter divided by the mean speed ($\approx 4 \times 10^{-3}$ sec). During this time approximately 1.6×10^{19} Φ pass through the cell in both directions, since the net flux at 75 W of 10.6 μ radiation corresponds to 4×10^{21} Φ sec^{-1}. Now, on the basis of the measured low-pressure (at 25 mTorr) absorption cross section the "effective" superposed area obscured by 10^{16} molecules is 2×10^{-3} cm^2, and thus can intercept 2.4×10^{16} Φ. We conclude that under these high flux conditions most molecules which pass through the beam will absorb at least one photon.

The log–log plots of per cent conversion *vs.* laser power (Figure 5) indicate that two to three photons are needed for augmentation of the reaction rate. The surprising feature is the critical dependence of yield on the *J* value of the laser line used; *i.e.*, on the specificity of the mode of excitation rather then on the total energy content. This argues against augmentation of the rate by v–v transfer, wherein encounters between pairs of molecules with $v = 1$ lead to pumping of one of them to $v = 2$, etc. That there is a power dependence at all, even though the flux is high enough to provide a photon for nearly every molecule which passes through the beam, suggests that the cross section for absorption of the second photon is an order of magnitude smaller than for the first. Indeed, we are driven to that assumption by the fact that the extent of conversion is greater for P(28) than for P(20), whereas the measured $v = 0 \rightarrow 1$ absorption coefficient is smaller for the former than for the latter. Since the density of lines in the fundamental region around 10.6 μ is high, as indicated by Figure 2, it is plausible that the first harmonic region is even more dense, and there is no dearth of states for successive photon absorptions. Furthermore, even though the mean free path is about equal to the laser beam width in the cell, a substantial number of collisions do occur in the illuminated region and the absorber gas is thus rotationally thermalized.

The following auxiliary observations also support the assumption that the rate-limiting displacement reaction 2 is accelerated by a specific vibrational excitation. We found that the decomposition of $H_3B \cdot CO$ is not augmented upon illuminating a mixture of the phosphine and the carbonyl

even though one must assume a very high efficiency for collisional energy transfer ($Z_{AB} \leq 5$) between molecules which possess substantial dipole moments and nearly resonant vibrational states. Thus, the mere accumulation of vibrational energy is not sufficient. Indeed, when the pressure of $H_3B \cdot CO$ was increased to a value such that collisions with the carbonyl served to deplete the population of vibrationally excited $H_3B \cdot PF_3$, the rate of decomposition of the phosphine decreased but that of the carbonyl remained low. On the other hand, the addition of Ar or PF_3 increased the rate of decomposition of the $H_3B \cdot PF_3$. These relatively inert molecules served to reduce diffusion of the singly activated $H_3B \cdot PF_3$ from the illuminated region toward the walls. In addition, at the pressures used, these gases may broaden the rotational line widths of the $H_3B \cdot PF_3$ and enhance absorption.

It appears that two criteria must be met. The first concerns energy content; the second concerns the accumulation of energy in a specific vibrational mode. Consider the equilibrium constant for step 1, and of the rate constant for step 2. In an ensemble of AB molecules in thermal equilibrium at T°K, the fraction which has sufficient energy to dissociate or react is given by $\int_{E_c}^{\infty} g(E)e^{-E/kT}\,dE / \int_0^{\infty} g(E)e^{-E/kT}\,dE$, with $E_c = \Delta H°_{diss}$ (step 1) or $E_c = E_{act}$ (step 2). Were each of these reactants to possess an additional 3.3 kcal/mol of vibrational energy [equivalent to 1 einstein of 10.6-μ photons], the corresponding fraction at 300°K could be augmented by $e^{3300/300R} = 2.5 \times 10^2$. Whether this increase is experimentally detectable obviously depends on the background rate; in the absence of radiation this is low for $H_3B \cdot PF_3$ and $H_3B \cdot CO$. However, for

$$H_3B + H_3B{\cdot}PF_3^{(v=n)} \longrightarrow B_2H_6 + PF_3 \qquad (2^*)$$

with $n = 2$ or 3, the augmentation factors are $\approx 6 \times 10^4$ and 10^7, respectively, and the change is much easier to detect. That the net increase in B_2H_6 was not due to a *large* increase in the steady-state concentration of BH_3 follows from the fact that there was no enhancement of the decomposition of the admixed $H_3B \cdot CO$. Indeed, parallel experiments run with the latter compound irradiated with the 9.6-μ band, where it absorbs strongly, gave negative results because of the apparent absence of suitable upper states for sequential absorption [see Appendix]. Apparently, there is a small rise in the steady-state concentration of BH_3, as indicated by our qualitative observations of an increase in the noncondensable gas, presumably hydrogen, due to decomposition of the BH_3 which did reach the walls of the cell after 4–10 collisions. Here, we are making the assumption that $H_3B \cdot PF_3^{(v=1)}$ is deexcited by wall collisions but does not preferentially decompose to PF_3, H_2, and $(BH)_m$.

Conclusion

On reviewing the strategy proposed in the Introduction for reactions which are suitable for augmentation by ir laser radiation, and comparing these with the totality of our experimental effort, we note our statements $\alpha \rightarrow \epsilon$ comprise a list of favorable but not sufficient conditions. Furthermore, there are very few combinations available to us at present which permit reproducing this set of conditions with high fidelity, the most serious limitation is the unavailability of tunable lasers which produce high photon fluxes at the higher frequencies at which many reagents absorb. The high flux of photons generated by the CO_2 laser carry modest energies (per photon) so that sequential absorptions are necessary to significantly augment a reaction rate. In turn this requires accidental coincidences of upper state spacings, which occur with higher probability in the larger and heavier molecules (PF_3 adduct) than in the lighter ones (CO adduct). Were we to limit our studies to radiations which carry <4 kcal/einstein, we would have to embark on a program for measuring absorption coefficients for excited vibrational states. This is an interesting and intriguing aspect of molecular spectroscopy of which very little is known, and merits study for its own sake now that the design of practical experiments appear feasible.

Our final comment pertains to an old problem in a new guise. This is best illustrated by comparing $H_3B \cdot PF_3$ with $H_3B \cdot CO$. The reaction coordinates for both steps 1 and 2 incorporate large extensions of the B–P or B–C bond, respectively. In the former, ν_3 absorption excites extension of the P–F bonds. Indeed, were radiation available at the stretching frequency for B–P [607 cm^{-1}], it would carry a 2/3 penalty in quantum size. In presenting the arguments regarding the anticipated enhancement of the (k_1/k_{-1}) ratio and of k_2, we tacitly postulated that the vibrational energy in $P{\equiv}F_3$ could be effectively utilized for extending the adjacent bond. This is consistent with RRKM theory which accounts well for the behavior of highly excited molecules undergoing unimolecular decompositions.[14] In the latter case, intramolecular vibrational redistribution times are faster than the mean lifetimes of the activated molecules.[7] However, for low states of excitation, a model closer to that proposed by Slater[15] is probably more suitable. We conclude that $H_3B \cdot PF_3$ and $H_3B \cdot CO$ differ because, while extension of the P–F bonds in $H_3B \cdot PF_3$ (950 cm^{-1}) is closely coupled with the H_3B–P stretching vibration, deformation of the HBH angles in $H_3B \cdot CO$ (1100 cm^{-1}) does not significantly couple with the H_3B–CO extension. Another factor which must be considered is the incomplete utilization of the available vibrational energy; thus, in the bimolecular reactions wherein vibrationally activated ozone reacts with NO, $O_2(^1\Delta)$ and SO it appears that only 15–50% of the injected vibrational energy contributes to the acceleration of the rate.[2b]

Acknowledgment. This work was supported by the Army Research Office—Durham, under Contract No. DA-ARO-D-31-124-73-G195.

Appendix. Experiments with $H_3B \cdot CO$

The 9.6-μ CO_2 laser emission is partially absorbed by borane–carbonyl. Two of the HBH deformation vibrations have been designated ν_3(a), at 1073.4 and 1083.1 cm^{-1} for the ^{11}B and ^{10}B adducts, respectively, and ν_3(e) at 1100 cm^{-1}. The carbonyl is another test compound for a $2AB \rightarrow A_2 + 2B$ decomposition reaction, and is a candidate for selectively generating BH_3 to be scavenged by other reagents.

Samples of the borane–carbonyl (natural abundance and ^{10}B enriched) were prepared from corresponding diborane samples according to the standard technique.[16] They were purified by repeated distillations. Relative absorptions at a number of lines in the 9.6-μ band were obtained with a spectrophone. For J values 12–28, absorptions over the R branches were, on the average, four to five times that for the P branch. The largest differences between the ^{10}B enriched and natural abundance boron isotopic samples showed for R(28) and P(18): Figure 6. Because the available laser power is considerably less at R(28), we use the

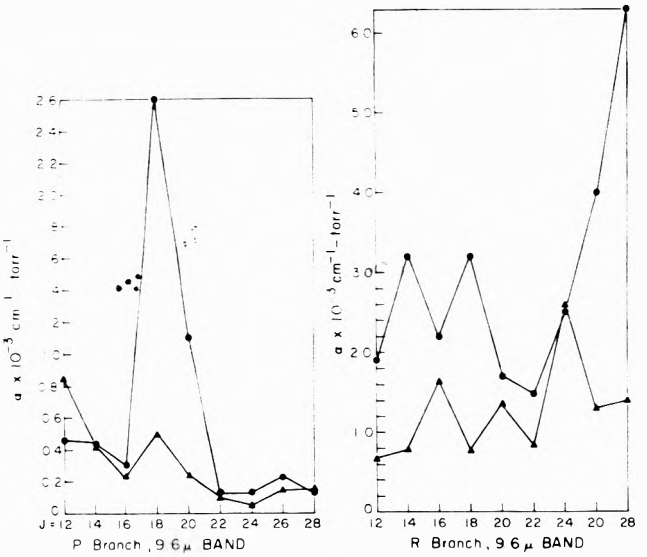

Figure 6. Absorption coefficients of H_3BCO at selected CO_2 laser lines (9.6-μ band): (●) normal isotopic composition; (▲) ^{10}B enriched sample.

P(18) line for which the absorption coefficient for the ^{n}B species was greater by a factor of about 5. Since the natural abundance sample contains about 20% ^{10}B, we deduce that the ^{11}B species has an absorption coefficient approximately 6 times that of the ^{10}B species for this line. For comparison: the borane–trifluorophosphine absorbs, at its optimum in the 10.6-μ band, approximately 30 times as much as the borane–carbonyl does at the P(18) line in the 9.6-μ band.

Numerous tests over a range of conditions show that no thermal reaction was observed with the sample in the cell at ≈2–3 mTorr, at room temperature, whether it was irradiated or not. A finite thermal rate was recorded when the cell temperature was raised to 51°. Irradiation of samples of both isotopic compositions showed a very small enhancement over the thermal rate at 31.1° and no difference was discernible for the two samples. These rates were followed with the Baratron capacitance manometer. Several tests of mixtures of $H_3B \cdot CO$ with N_2O and of $H_3B \cdot CO$ with PF_3, at room temperature, indicated no conversion upon irradiation of these samples in the pressure regime 2–5 mTorr. These negative experiments complement the conclusions we reached relative to the trifluorophosphine adduct, in that two or more photons in the 3.5 kcal/einstein energy range are required to facilitate reaction. Unfortunately due to the lower molecular weight and more open set of states for the carbonyl there is no appropriately positioned level for absorption of the second photon.

References and Notes

(1) S. H. Bauer and E. L. Resler, Jr., *Science*, **146**, 1045 (1964).
(2) (a) $H_2^{+(v)}$ – He: W. A. Chupka and M. E. Russell, *J. Chem. Phys.*, **49**, 5426 (1968); J. A. Rutherford and D. A. Vroom, *ibid.*, **58**, 4076 (1973). $O^+ + N_2^{(v)}$: R. H. Neynaber and G. D. Magnuson, *ibid.*, **58**, 4586 (1973); $K + HCl^{(v)}$: T. J. Odiorne, P. R. Brooks, and J. V. V. Kasper, *ibid.*, **55**, 1980 (1971). (c) O,H + $HCl^{(v)}$: D. Arnoldi and J. Wolfram, *Chem. Phys. Lett.*, **24**, 234 (1974). (d) O + $CN^{(v)}$: H. Schacke, K. J. Schmatjko, and J. Wolfram, *Ber. Bunsenges. Phys. Chem.*, **77**, 248 (1973). (e) $O_3^{(v)}$ + NO: R. J. Gordon and M. C. Lin, *Chem. Phys. Lett.*, **22**, 2621 (1973). $O_3^{(v)}$ + $O_2(^1\Delta)$: M. J. Kurylo, W. Braun, A. Kaldor, S. M. Freund, and R. P. Wayne, submitted to *Int. J. Photochem.* $O_3^{(v)}$ + SO: A. Kaldor, W. Braun, and M. J. Kurylo, submitted for publication. (f) $N_2F_4^{\ddagger}$ diss: J. L. Lyman and R. J. Jensen, *J. Phys. Chem.*, **77**, 883 (1973). (g) $SiF_4^{\ddagger}$ pyr: N. R. Isenor, V. Merchant, R. S. Hallsworth, and M. C. Richardson, *Can. J. Phys.*, **51**, 1281 (1973). (h) $HF^{(v)} + D_2$: R. S. Chang and G. J. Wolga, *Bull. Am. Phys. Soc.*, **18**, 1522 (1973), Abs. EB11. (i) "Laser Induced Photochemical Enrichment of Boron Isotopes," S. M. Freund and J. J. Ritter, (NBS), 4th Conference of Chemical and Molecular Lasers, 1974. (j) "Laser Induced Photochemical Enrichment of Chlorine Isotopes," M. Lamotte, *et al.*, (NBS), 4th Conference on Chemical and Molecular Lasers, 1974.
(3) Examples of 3D trajectory calculations (classical): (a) $H_2^{(v)}$ + I: L. M. Raff, L. B. Sims, D. L. Thompson, and R. N. Porter, *J. Chem. Phys.*, **53**, 1606 (1970). (b) $H_2 + I_2^{(v)}$: J. M. Henry, J. B. Anderson, and R. L. Jaffe, *Chem. Phys. Lett.*, **20**, 138 (1973). (c) H + $HF^{(v)}$: R. L. Wilkins, *J. Chem. Phys.*, **58**, 3038 (1973). (d) AB + CD: M. H. Mook and J. C. Polanyi, *ibid.*, **53**, 4538 (1970). (e) F + $HCl^{(v)}$: L. J. Kirsch and J. C. Polanyi, *ibid.*, **57**, 4498 (1972), etc. (f) F + HD: J. T. Muckerman, *ibid.*, **57**, 3388 (1972). Consideration of transition probabilities for collinear collisions (quantal *vs.* classical): (g) $H_2^{(v)}$ ÷ He: D. G. Truhlar, *ibid.*, **56**, 1481 (1972). (h) H + $H_2^{(v)}$: J. M. Bowman and A. Kupperman, *Chem. Phys. Lett.*, **12**, 1 (1971); D. G. Truhlar and A. Kupperman, *J. Chem. Phys.*, **58**, 2232 (1972).
(4) (a) G. L. Hofacker and R. D. Levine, *Chem. Phys. Lett.*, **9**, 617 (1971); **15**, 165 (1972); (b) J. L. Kinsey, *J. Chem. Phys.*, **54**, 1206 (1971); (c) C. Rebick, R. D. Levine, and R. B. Bernstein, prepublication copy "Energy Requirements and Energy Disposal: Reaction Probability Matrices and a Computational Study of a Model System."
(5) G. J. Pert, *IEEE J. Quant. Elect.*, **QE-9**, 435 (1973).
(6) S. H. Bauer, D. M. Lederman, and E. L. Resler, Jr., *Int. J. Chem. Kinet.*, **5**, 93 (1973); P. Jeffers, D. Hilden, and S. H. Bauer, *Chem. Phys. Lett.*, **20**, 525 (1973).
(7) B. S. Rabinovitch, J. F. Meagher, K. J. Chao, and J. R. Barker, *J. Chem. Phys.*, **60**, 2932 (1974), and previous publications.
(8) R. C. Taylor and T. C. Bissot, *J. Chem. Phys.*, **25**, 780 (1956).
(9) R. L. Kuczkowski and D. R. Lide, Jr., *J. Chem. Phys.*, **46**, 357 (1967).
(10) (a) S. H. Bauer and R. R. Karl, manuscript in preparation. (b) A very sensitive system is described by L. B. Kreuzer, N. D. Kenyon, and C. K. N. Patel, *Science*, **177**, 347 (1972).
(11) F. Shimizu, *Appl. Phys. Lett.*, **14**, 378 (1969).
(12) A. B. Burg and Y. C. Fu, *J. Amer. Chem. Soc.*, **88**, 1147 (1966).
(13) M. E. Garabedian and S. W. Benson, *J. Amer. Chem. Soc.*, **86**, 176 (1964).
(14) P. J. Robinson and K. A. Holbrook, "Unimolecular Reactions," Wiley, New York, N.Y., 1972.
(15) N. B. Slater, "Theory of Unimolecular Reactions," Cornell University Press, Ithaca, N.Y., 1959.
(16) A. B. Burg and H. I. Schlesinger, *J. Amer. Chem. Soc.*, **59**, 780 (1937).

Intercalation Compounds of Metal Hydroxides with Group V Layered Dichalcogenides

G. V. Subba Rao,* M. W. Shafer, and J. C. Tsang

IBM Thomas J. Watson Research Center, Yorktown Heights, New York 10598 *(Received July 1, 1974)*

Publication costs assisted by the IBM Thomas J. Watson Research Center

The layered dichalcogenides of Nb and Ta easily form intercalation compounds with metal hydroxides (alkali, alkaline earth, ammonium hydroxide, and their derivatives) in aqueous solution. The increase per unit layer in the c lattice parameter produced upon intercalation varies from 2 to 6 Å and is dependent on the host dichalcogenide, the metal hydroxide employed, and its solvation number. A formula of the type $TaS_2(MOH)_{0.2-0.3}(H_2O)_{0.5-0.8}$ was obtained from chemical analyses data. The formation of different intercalation stages, structural aspects, and superconductivity of these compounds are described and discussed.

Introduction

Transition metal dichalcogenides offer a wide variety of interesting physical properties ranging from diamagnetic semiconductor to Pauli paramagnetic metal behavior at room temperature, with the group V sulfides and selenides exhibiting superconductivity at low temperatures.[1] The most important property of these materials from the crystallographic point of view is that they possess hexagonal layer structures in which a layer of metal atoms is strongly bonded to, and sandwiched between, two layers of chalcogens. These Ch–M–Ch "slabs" are weakly bonded (presumably by van der Waals forces) and are stacked in the *c* direction giving rise to marked anisotropy in the physical properties. The weak interlayer bonding in these dichalcogenides permits intercalation quite akin to other layer-type materials such as graphite and silicate clay minerals, by which process it is possible to introduce metal ions, inorganic, and organic molecules between the layers. Thus alkali,[2,3] alkaline earth,[4] and 3d transition metals[5] have been successfully intercalated into the layered chalcogenides whereas extensive studies of Gamble, *et al.*,[6] have shown that a large variety of organic and inorganic compounds of the Lewis base type can be easily and successfully intercalated into group IV and V dichalcogenides. Depending on the intercalate, extensive changes in the physical properties of the host dichalcogenide can occur. Thus, metallic behavior and superconductivity can be induced in the diamagnetic and semiconducting group VI dichalcogenides,[3,4] whereas previous studies from this laboratory[7] have shown that Eu intercalation leads to ferromagnetism at low temperatures in all the groups IV, V, and VI dichalcogenides. It has been shown[6] that the superconducting transition temperatures of the group V sulfides are altered by 3–4°K by intercalation with Lewis bases, the change being upward for Ta and downward for Nb compounds.

Thus, intercalation is an excellent process to obtain tailor-made solid state materials, however, the mechanism of the process is little understood and the available literature is scanty on this aspect. Gamble, *et al.*,[6] have noted a few specific points in their studies which are worth mentioning here. (a) Organic and inorganic compounds which are classed as Lewis bases can be intercalated to produce stable isolatable products indicating that the host dichalcogenides are mainly of acidic type or contain Lewis acid-type active sites. (b) The speed of intercalation depends not only on the nature of the intercalate but also on the dichalcogenide (group IV or V) and the particular polymorph. The observed behavior of a variety of materials led Gamble, *et al.*, to interpret their data on the basis of nucleophilic attack of the intercalate on the long Ch–Ch bonds[8] and of opening up the Ch–M–Ch slabs, paving the way for successful insertion of the intercalate into the host. However, as one may surmise, the size of the intercalate also appears to play a significant role in the rate of intercalation as well as the stability of the product. Thus for a given basicity, the smaller the size, the faster would be the rate of intercalation.

Considerable data are available on the intercalation of polar organic compounds into layered clay-minerals,[9a] and recently Hooley[9b] has examined the intercalation of graphite with inorganic materials such as $FeCl_3$, Br_2, etc. He arrived at three important characteristics of the process of intercalation which appear to be quite general in nature and are applicable to the transition metal dichalcogenide systems as well. First, a threshold or minimum concentration of the intercalate should be present in contact with the host material before which intercalation can take place with noticeable speed at any given temperature. This has been amply demonstrated in the case of graphite intercalation with alkali metals[10] and with compounds of the type $FeCl_3$, Br_2, ICl, HNO_3, etc.[9b,10] Secondly, the property of swelling of the crystals on intercalation and expansion of the *c* lattice parameter *via* stages as can be observed by X-rays. Stage I product would correspond to the case where the intercalate is present in between any two layers, stage II corresponding to the case where the intercalate in inserted in between alternate set of layers, etc. (Figure 1). The third and most important criterion appears to be the hysteresis effect or easy deintercalation of an intercalated product where the original layered material is recovered with the original lattice parameters. Studies of Gamble, *et al.*,[6,11] showed that the MCh_2 materials satisfy the last two criteria fairly well.

Gamble, *et al.*,[6] have shown in their preliminary studies that alkali metal hydroxides in aqueous solution intercalate into TaS_2 with ease and rapidity to form stable intercalation products, and that the increase in the *c* lattice parameter of TaS_2 on intercalation is characteristic of the metal hydroxide employed; however, since the alkali metal ions are usually solvated in aqueous solution, the nature of the intercalated species and the stoichiometry of the complex are not known in detail. In the present investigation we re-

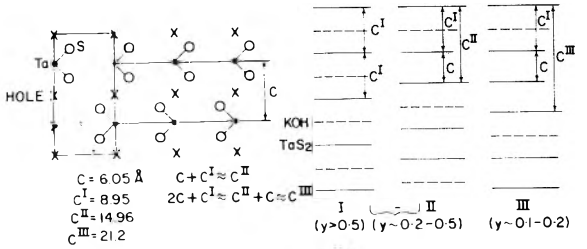

Figure 1. A schematic representation of TaS_2 structure and various intercalation stages obtained with KOH. y represents the concentration of KOH in moles per mole of TaS_2. The relationships between c,c^I, etc. due to the different intercalation stages indicate that KOH produces a constant δ when intercalated and TaS_2 layers stay intact when devoid of the intercalate.

port on the intercalation of group V sulfides and selenides with metal hydroxides, the stability of the products, and the replaceability of the intercalated species in the lattice. In a separate paper[12] we present the results of kinetic studies of hydroxide intercalation into TaS_2 and discuss the possible mechanisms for the intercalation process.

Experimental Section

TaS_2 was prepared by direct combination of constituent high-purity elements in evacuated and sealed quartz tubes at ~1000° using a small amount of iodine as a carrier. The 1s polymorph obtained was ground to powder and annealed at 600° for 4 days and then at 500° for 2 weeks to get pure single phase 2s TaS_2 (single crystals were also obtained by the annealing process). The black, free flowing TaS_2 powder was sieved (through 53- and 149-μ sieves) and used for the intercalation studies. Other group V materials were obtained using similar procedures described in the literature.[13,14] Alkali metal hydroxide aqueous solutions were prepared from high-purity chemicals in CO_2 free water and standardized before use. Saturated alkaline earth metal hydroxide solutions were made from freshly prepared oxides obtained by decomposing the carbonates.

The intercalation was carried out by stirring known amounts of TaS_2 and aqueous hydroxide solutions. The resulting product was filtered with repeated washing followed by drying. Care was taken to see that negligible amounts of CO_2 were absorbed by the hydroxide from atmosphere. The 2s polymorph of TaS_2 is easiest to intercalate. For example, alkali metal hydroxides at fairly high concentrations intercalate within 1 hr at 25° while Nb compounds require longer periods of time (~12 hr). However, prolonged treatment with the concentrated hydroxides chemically decompose the chalcogenides, especially the selenides. Millimolar range of concentrations of the hydroxides were found to be quite suitable for composition variation studies. Usually 1 mmol of TaS_2 of known particle size was treated with varying amounts of (y mmol) hydroxides in a constant volume of 100 ml.

Chemical analysis of the OH^- ion in the intercalated TaS_2 was carried out by treating the complex with known excess of HCl and heating at ~60° (which produced deintercalation) and back titration. Blank runs indicated that dilute HCl solution neither intercalates into, nor decomposes, the TaS_2. For the analysis of the intercalated alkali metal ion, either the sample was deintercalated as above or completely decomposed by treating with hot aqua regia and the metal ion concentrations were estimated by atomic absorption analysis. In a few cases, Ta, S, O, and metal ion concentrations in intercalated crystals were determined by electron beam microprobe analysis. X-Ray powder patterns of the intercalated products were taken using a Norelco diffractometer and a Guinier camera (Cu Kα radiation), and lattice parameters were obtained using the high-angle peaks by least-squares fitting. Thermogravimetric analysis (TGA) was done in air using a Stanton balance in the range 25–800°. Superconductivity tests were made at liquid He temperatures by 11 Hz ac susceptibility method. The onset transition temperature was taken as the highest temperature at which the shielding currents could first be detected.

Results and Discussion

It is known from the work of Gamble, *et al.*,[6] that TaS_2 when treated with excess of pyridine (Py) at 200° results in a stage I intercalation compound (intercalated species between every chalcogenide layer) with a formula $TaS_2(Py)_{0.5}$ for the complex; however, treatment of TaS_2 with 0.25 mol of Py for longer periods of time (at 200°) produces a stage II complex (intercalated species between every other layer). We have observed a similar behavior with metal hydroxide intercalation compounds. As can be seen from Figure 1, depending on the starting mole ratios of TaS_2 and KOH (aq) either a mixture of stages (III and II; II and I) or pure stage I product could be obtained.[15a] The observed empirical relationship between the expanded c lattice parameters of the different intercalated products (Figure 1) indicate that (i) KOH produces a constant increase in the c lattice parameter per unit layer of TaS_2 (δ) irrespective of the stages formed, and (II) TaS_2 layers stay intact with the original c axis spacing wherever intercalate is absent in the van der Waals gap. No evidence of intercalation was noted by X-rays for KOH concentration $y < 0.1$ (moles per mole of TaS_2). This value of $y = 0.1$ may not represent the concentration threshold in the absolute sense but it is the minimum concentration of KOH that should be present in contact with the host TaS_2 to produce noticable intercalation reaction at 25°.

Table I summarizes the X-ray data on the group V dichalcogenide intercalation complexes with metal hydroxides. These intercalations were carried out by stirring with relatively large amounts of the intercalate in aqueous solution at 25°. As can be seen, our data on alkali hydroxide intercalates with TaS_2 are in good agreement with those of Gamble, *et al.*[6] For NbS_2 and $NbSe_2$, a temperature of ~50° was found to be convenient. All the products formed were stage I materials where the intercalate was present between every layer. The a lattice parameter of the hexagonal unit cell is little affected whereas the c axis indicates large expansion in that direction. The δ values observed vary with the metal hydroxide employed and the host dichalcogenide. This shows that the metal ions play a significant role in determining δ.

TaS_2 (NaOH) complex exhibits two distinct intercalated phases, both corresponding to stage I products. The δ values are 2.9 and 5.8 Å and the complex shows interesting behavior with respect to the intercalated H_2O present in the lattice. A freshly prepared product exhibits a δ value of 5.8 Å; keeping the sample in a desiccator (or drying *in vacuo*) overnight converts it to a well-defined crystalline complex with δ of 2.9 Å. Treating this sample with a slightly alkaline aqueous solution regenerates the original complex with δ = 5.8 Å. It is clear that H_2O pick-up by the lattice is involved in this process[15b] and in fact TGA and electron microprobe study of TaS_2–NaOH complex (with δ = 5.8 Å) showed excess O compared to the complex with δ =

TABLE I: Crystal and Superconductivity Data on Hydroxide Intercalation Complexes with Group V Dichalcogenides

MCh_2–OH complex	a, Å	c, Å	δ, Å	n[a]	Cryst radius, Å[b]	Eff radius in soln, Å[a]	T_c, °K[c]
2s TaS_2	3.32	2 × 6.05					0.8
LiOH	3.33_0	$2 \times 8.9_5$	$2,9_0$	4.3	0.74	2.5	(4.5)
NaOH	3.32_3	$2 \times 11.8_7$	5.8_2	2.9	1.02	2.17	3.4
							(4.8)
	3.32_0	$2 \times 8.9_6$	2.9_1	2.9	1.02	2.17	3.4
NaOD		$? \times 11.7_0$[d]	5.6_5				4.2
(in D_2O)		$? \times 9.0_5$	3.0_0				4.2
NaSH		$? \times 11.9_0$	5.8_5	2.9	1.02	2.17	4.2
		$? \times 9.0_9$	3.0_4	2.9	1.02	2.17	4.2
Na[e]		$? \times 7.3_0$	1.2_5		1.02		
K[e]		$? \times 8.0_0$	1.9_5		1.20		
KOH	3.32_8	$2 \times 8.9_5$	2.9_0	1.2	1.38	1.75	4.4
							(5.3)
RbOH	3.32_4	$2 \times 9.1_7$	3.1_2	0.5	1.49	1.53	4.0
							(4.3)
CsOH	3.32_4	$2 \times 9.3_2$	3.2_8	0.0	1.70	1.47	2.7
							(3.8)
TlOH	3.33_0	$2 \times 8.7_5$	2.7_0		1.50	1.23	4.2
Tl	3.33_0	$2 \times 8.0_8$	2.0_5		1.50	1.23	4.2
$Ca(OH)_2$	3.31_9	$2 \times 11.6_8$	5.6_3	7.2	1.00	2.72	4.2[f]
							3.0
$Sr(OH)_2$	3.33_4	$2 \times 11.7_1$	5.6_9	6.7	1.16	2.74	4.0
$Ba(OH)_2$	3.32_6	$2 \times 8.8_0$	2.7_5	5.2	1.36	2.48	3.0
NH_4OH	3.33_0	$2 \times 9.1_0$	3.0_5	1.05	1.48	1.88	(3.3)
$N(CH_3)_4OH$	3.32_5	$2 \times 11.3_7$	5.3_2	2.05			2.9
$N(C_2H_5)_4OH$	3.33_1	$2 \times 11.1_0$	5.0_5	2.83			2.2
3s NbS_2	3.33	3×5.97					5.7
KOH	3.33_4	$3 \times 8.9_7$	3.0_0	1.2	1.38	1.75	
2s $NbSe_2$	3.45	2×6.27					7.1
KOH		$? \times 9.4_0$	3.1_3	1.2	1.38	1.75	
RbOH		$? \times 9.3_5$	3.0_8	0.5	1.49	1.47	

[a] Hydration number (n) of the ions and the effective ionic radii in aqueous solution ($r_{M^{n+}}^{eff}$) are obtained from ref 17 ($n_{OH^-} = 3.5$; $r_{OH^-} = 1.40$ Å; $r_{OH^-}^{eff} = 2.46$ Å). [b] Crystal radii obtained from ref 16. [c] Values in parentheses from ref 6. [d] Accurate lattice parameters not determined; c axis repeat distance obtained from ($00l$) lines of the X-ray diffractograms. [e] Intercalated at −50° by the liquid ammonia method.[4] The observed small δ values indicate the absence of NH_3 in the lattice and in fact the lattice parameters agree well with those reported for $Na_{2/3}TaS_2$ and $K_{2/3}TaS_2$ obtained by ceramic techniques.[2] The samples are fully intercalated but we have not determined the composition. [f] Shows two transitions.

2.9 Å. Identical behavior was exhibited by TaS_2–NaSH and TaS_2–NaOD complexes (Table I).

In Table I we also give the crystal ionic radii,[16] effective ionic radii (of the solvated cations in aqueous solution), and hydration numbers[17] (n) of the intercalate ions in aqueous solution. All the ions except Cs^+ are hydrated (and also OH^- ion) in aqueous solution with varying n, and the effective ionic radii ($r_{M^+}^{eff}$) in solution are significantly different from the crystal radii (r_{M^+}). We also note that r_{M^+} increases through the series Li to Cs whereas $r_{M^+}^{eff}$ decreases. Since the dichalcogenides were intercalated from aqueous solution, undoubtedly some H_2O molecules also were intercalated into the lattice along with the cations and OH^- and indirectly influence the δ value for a given complex.

Certain trends in the observed δ values and the ionic radii are apparent. In the alkali hydroxide series, the δ values are always less than the diameter of the hydrated OH^- ion indicating that the OH^- ions in the intercalated lattice are not hydrated to the same extent as in aqueous solution. For Li, Na, and K, $r_{M^+} < r_{OH^-}$ and hence OH^- must be controlling the observed δ; in fact, LiOH, NaOH, and KOH produce constant δ of 2.9 Å which is only slightly larger than the crystal diameter of the OH^- ion. For Rb and Cs, $r_{M^+} > r_{OH^-}$, and their corresponding TaS_2 hydroxide complexes we note that δ values are only slightly smaller than the respective diameters of the M^+ ions. In the TaS_2–NaOH and its analogs (comparing the higher δ values), NaSH has higher δ compared to NaOH complex as can be expected but NaOD shows the opposite trend. On the other hand, the composition with the lower δ values (*i.e.*, 2.9 Å) are seen to remain almost unchanged for NaOH, NaOD, and NaSH.

In the alkaline earth hydroxide series we see a similar behavior as in the alkali series in that when $r_{M^{2+}} < r_{OH^-}$, OH^- ion controls the δ. The high δ values (Table I) actually encountered might also be due to a large value of n for Ca^{2+} and Sr^{2+}; $r_{Ba^{2+}}$ is only slightly smaller than r_{OH^-} and the low δ value of 2.7 Å indicates negligible solvation of the cation in the lattice. Indeed, electron beam microprobe analysis for Ta, S, Ba, and O on an intercalated crystal has shown the composition to be TaS_2 $[Ba(OH)_2]_{0.2}0.2H_2O$.

TlOH intercalated TaS_2 exhibits an interesting behavior. A complex freshly prepared from dilute TlOH solution

shows a δ of 2.7 Å but after a few hours of standing at 25° δ falls to a constant value of 2.0 Å (the complex with δ of 2.0 Å is also obtained by using aqueous concentrated TlOH ($y \gg 2$) during preparation). A δ value of 2.0 Å is too small for a hydroxide intercalate and in fact the c lattice parameter is identical with Tl_xTaS_2 ($x \sim 0.5$, prepared by heating TaS_2 with Tl metal vapor at 800° for 4 days) indicating some disproportionation of Tl^+ to Tl^{3+} and Tl^0 has occurred in the TaS_2 lattice. $(TlOH)_xTaS_2$ samples prepared from hydroxide could not be completely deintercalated by acid treatment (see Experimental Section); on the other hand, acid treatment regenerates the complex with δ = 2.7 Å. Electron beam microprobe analysis of a crystalline complex (δ = 2.0 Å) obtained from TlOH indicated the composition to be $TaS_2Tl_{0.45}$ and no trace of O in the lattice. A comparison of δ values observed for the same intercalate (KOH) with various dichalcogenides (Table I) indicates that δ is scattered at ~3 Å but definitely depends on the MCh_2 and the particular polymorph. 1s TaS_2 is difficult to intercalate and we have not been able to isolate any intercalated products.

Chemical analysis of TaS_2–hydroxide intercalated materials indicated the presence of both metal and OH^- ions in the TaS_2 lattice. The composition of the complex obtained from the analyses data is scattered in the range 0.2–0.3 MOH unit per TaS_2 in all the hydroxides studied. TGA studies have shown that the hydroxide intercalates are associated with intercalated water, which is lost in 100–300° range.[18a] As evidenced by the X-ray diffraction data, samples heated to this temperature still retain the intercalate species indicating that the increase in the c axis is mainly caused by the metal hydroxide, the water molecules playing a minor role. Based on a large number of chemical analyses combined with TGA on same samples, electron microprobe data on selected crystals and weight gain experiments, a general formula of the type $TaS_2\ (MOH)_{0.2\text{-}0.3}(H_2O)_{0.5\text{-}0.8}$ appears reasonable.

In pure TaS_2, the van der Waals gap is ~2.9 Å and structurally the gap can be visualized as consisting of large octahedral holes (Figure 1). For 2s TaS_2, there is one octahedral hole per Ta atom in the unit cell, and in principle, it should be possible to insert ions of radius <1.4 Å into the octahedral holes without producing an expansion in the c axis. Whenever a salt-like compound (*e.g.*, KOH) consisting of two ions is intercalated, the ion with the largest ionic radius should govern the δ value, as is indeed observed with hydroxides. The negatively charged hydroxide ion is the one which acts as an electron donor to the host TaS_2 and if it occupies one octahedral hole, the K^+ ion will be in its vicinity to form a loosely bound ion pair. Thus, if all the octahedral holes are filled by K^+ and OH^- ions, the limiting composition of the intercalated product will be $TaS_2(KOH)_{1/2}$. However, since H_2O is also present in an intercalated form, the maximum concentration of KOH based on a structure where each ion has a H_2O neighbor occupying the octahedral hole is $TaS_2(KOH)_{1/3}(H_2O)_{1/3}$, (or $TaS_2(KOH)_{1/4}(H_2O)_{1/2}$ for the more dilute case), a formula quite consistent with the chemical analysis data. The intercalated H_2O is more loosely bound to the lattice than K^+ and OH^- and, under proper conditions, the latter should be able to replace the H_2O to achieve the limiting composition of 0.5 KOH.[18b] Unfortunately, TaS_2 decomposes chemically on prolonged treatment with concentrated alkali hydroxide solutions and hence a complete filling of the octahedral holes with K^+ and OH^- ions alone is not feasible. From the above discussion it is clear that a minimum of y = 1/3 of KOH is required to form a stage I intercalated product whereas experimentally we found a value ≥1/2. Complexes exhibiting high δ values (NaOH, $Ca(OH)_2$, etc.) are solvated to a larger extent and a variety of possible configurations are possible for the intercalated species in the lattice.

The TaS_2–MOH intercalated products are stable to air over long periods of time in spite of the reactivity of the free metal hydroxides. This is also true for the tetraethylammonium hydroxide which is known only in solution. Perhaps intercalation may be an excellent way of stabilizing an unstable hydroxide compound. However, the intercalate is not very strongly bonded to the TaS_2 lattice since treatment with a dilute acid quickly produces deintercalation. It appears that the intercalated ion or molecule is replaceable to a certain extent in the lattice. Thus, KOH can replace NaOH in the TaS_2–NaOH intercalated sample by treating it with aqueous KOH solution for 1 hr as has been ascertained by chemical analysis and X-ray data. In general, the replacing Lewis base should be stronger than the one to be replaced, and in the process the lattice should not be dilated to a large extent compared to the original state. Evidence for an *in situ* reaction, $Na + H_2O \rightarrow NaOH + \frac{1}{2}H_2$, within the crystal lattice was obtained when Na metal intercalated TaS_2 crystals (obtained by the liquid ammonia method;[4,7] lattice parameter, c = 7.3 Å and δ = 1.2 Å)[18c] were exposed to air or treated with water at 25°; X-ray diffractometer pattern of the resulting product was identical with that of $(NaOH)_xTaS_2$. Similar behavior was observed with K_xTaS_2 (Table I).

The remarkable ability of the group V chalcogenides (compared to group IV and VI materials) to form intercalation compounds readily with Lewis bases is supposed to be due to their d band structure. The inherent metallic behavior and Pauli paramagnetism indicate a partially filled narrow d band, a model which has been supported by the recent photoemission studies[20] and theoretical calculations.[21] Since the Lewis bases act as electron donors, upon intercalation, some type of electronic charge transfer from the base to the partially filled d band in the chalcogenide can occur leading to a change in the density of states at the Fermi level of the host and/or redistribution of the energies of the s, p, and d band states.[22] These changes are also reflected in the superconductivity behavior at liquid He temperatures. Gamble, *et al.*,[6] reported that the alkali metal hydroxide intercalation compounds of TaS_2 have higher transition temperatures (T_c) compared to pure 2s TaS_2 (0.8°K). We have examined the hydroxide intercalated samples for superconductivity at low temperatures and the data are shown in Table I; all the samples are superconducting below 4.2°K, T_c being dependent on the particular chalcogenide–hydroxide complex. Intercalated water does not seem to affect T_c values in TaS_2–NaOH complexes and their derivatives.

Acknowledgments. We are indebted to R. A. Figat for technical assistance, B. Olson for chemical analyses and TGA runs, and J. D. Kuptsis and F. Cardone for electron microprobe studies. We wish to acknowledge very helpful discussions with Professor F. Jellinek.

References and Notes

(1) For a review on the layered dichalcogenides, see J. A. Wilson and A. D. Yoffe, *Advan. Phys.*, **18**, 193 (1969).

(2) W. P. F. A. M. Omloo and F. Jellinek, *J. Less-Common Metals*, **20**, 121 (1970).
(3) R. B. Somoano and A. Rembaum, *Phys. Rev. Lett.*, **27**, 402 (1971); R. B. Somoano, V. Hadek, and A. Rembaum, *J. Chem. Phys.*, **58**, 697 (1973); A. M. Hermann, R. B. Somoano, V. Hadek, and A. Rembaum, *Solid State Commun.*, **13**, 1068 (1973).
(4) G. V. Subba Rao, M. W. Shafer, S. Kawarazaki, and A. M. Toxen, *J. Solid State Chem.*, **9**, 323 (1974).
(5) J. M. Van der Berg and P. Cossee, *Inorg. Chem. Acta*, **2**, 143 (1968); F. Hulliger and E. Pobitschka, *J. Solid State Chem.*, **1**, 117 (1970).
(6) F. R. Gamble, *et al.*, *Science*, **168**, 568 (1970); **174**, 493 (1971).
(7) G. V. Suoba Rao, M. W. Shafer, and L. J. Tao, AIP Conf. Proc., No. 10 (American Inst. of Phys.), 1973, p. 1173; M. W. Shafer, G. V. Subba Rao, and L. J. Tao, paper presented at the International Conference on Magnetism and Magnetic Materials, Moscow, Aug, 1973.
(8) Looking along the *c* axis of the layered chalcogenide, we can picture the Ch–M–Ch slabs as being joined by long Ch–Ch bonds across the van der Waals gap akin to the case of graphite (Figure 1).
(9) (a) See, for example, W. Eitel, "Silicate Science," Vol. 1, Academic Press, New York, N.Y., 1964; (b) J. G. Hooley, paper presented at the Conference on Layer Compounds, Calif., Aug, 1972 (unpublished).
(10) A. R. Ubbelohde, *Carbon*, **10**, 201 (1972).
(11) F. R. Gamble, *et al.*, *J. Chem. Phys.*, **55**, 3525 (1971).
(12) G. Subba Rao and M. W. Shafer, *J. Phys. Chem.*, following paper.
(13) F. Kadijk, R. Huisman, and F. Jellinek, *Recl. Trav. Chim. Pays-Bas*, **83**, 768 (1964).
(14) J. F. Revelli, Ph.D. Dissertation, Stanford University, 1973.
(15) (a) For starting mole ratios TaS_2:KOH of 1:<0.5, intercalation was allowed to proceed to completion until no free OH^- was present in the solution. (b) Pure H_2O does not intercalate into TaS_2 under ordinary conditions.
(16) (a) R. D. Shannon and C. T. Prewitt, *Acta Crystallogr., Sect. B*, **25**, 925 (1969); (b) B. S. Krumgal'z, *Russ. J. Phys. Chem.*, **45**, 1448 (1971).
(17) C. B. Monk, "Electrolytic Dissociation," Academic Press, New York, N.Y., 1961.
(18) (a) TGA of pure 2s TaS_2 in air has shown that no weight loss or gain occurs up to 600°, when oxidation to Ta_2O_5 occurs. (b) Replacement of H_2O by OH^- involves only a proton transfer compared to the replacement by K^+ ion where diffusion plays a major part (see following paper[12]). (c) Unlike the case with Eu, Yb, and alkaline earth metals[4,7,19] ammonia will not be intercalated along with Na and K into TaS_2.
(19) G. V. Subba Rao, M. W. Shafer, and L. J. Tao, *Mat. Res. Bull.*, **8**, 1231 (1973).
(20) (a) J. C. McMenamin and W. E. Spicer, *Phys. Rev. Lett.*, **29**, 1501 (1972); (b) P. M. Williams and F. R. Shepherd, *J. Phys. C: Solid State Phys.*, **6**, L36 (1973).
(21) L. F. Mattheis, *Phys. Rev. Lett.*, **30**, 784 (1973); *Phys. Rev. B*, **8**, 3719 (1973).
(22) A. R. Beal and W. Y. Liang, *Phil. Mag.*, **27**, 1397 (1973); *J. Phys. C: Solid State Phys.*, **6**, L482 (1973).

Kinetic Studies of Metal Hydroxide Intercalation into Tantalum Disulfide

G. V. Subba Rao* and M. W. Shafer

IBM Thomas J. Watson Research Center, Yorktown Heights, New York 10598 *(Received July 1, 1974)*

Publication costs assisted by the IBM Thomas J. Watson Research Center

The rate of intercalation of KOH and NaOH into 2s TaS_2 in aqueous solution has been studied as a function of hydroxide concentration (y mol per mol of TaS_2) and in the temperature range 2–100° in a constant volume of solution. For $y \leq 0.5$, the rate follows first order until all the hydroxide is consumed but the intercalated product is a mixture of stages; for $y > 0.5$, the end product is of stage I intercalation but the first-order rate law is obeyed only up to t' of the total time ($t' < t$) of reaction and thereafter exhibits a complex behavior with a decreased rate. The data are discussed in terms of the theory of heterogeneous reactions in solution and plausible mechanisms are proposed for the observed falling off of first-order rate and for the process of intercalation.

Introduction

In an earlier paper[1] we have reported on the preparation and characterization of the intercalation compounds formed by the metal hydroxides with group V dichalcogenides. Because of the layer characteristics of these chalcogenides, many molecules (organic and inorganic) and ions can be intercalated where the guest species occupy the van der Waals gap of the host material. However, the speed of intercalation depends on the nature and size of the intercalate and also on the dichalcogenide and particular polymorph.[2] Alkali metal hydroxide species intercalate into TaS_2 fairly rapidly at room temperature to give stable products and have the added advantage of being amenable to easier methods of chemical estimation. In the following we report on the kinetic studies of intercalation of NaOH and KOH into 2s TaS_2 as a function of concentration and temperature. We attempt to explain the observed data in terms of the theory of heterogeneous reactions and suggest possible mechanisms for the hydroxide intercalation process.

Experimental and Results

The 2s polymorph of TaS_2 was prepared by the method described earlier.[1] Powder of known particle size (53–149 μ) was employed in all the kinetic studies; these particles had surface areas ~0.1–0.5 m^2/g, as determined by a scanning electron micrograph. Kinetic studies of NaOH and KOH intercalation of 2s TaS_2 were carried out at various concentrations of the aqueous alkali solutions and in the temperature range 2–100°. NaOH and KOH aqueous solutions were freshly prepared from highly pure chemicals and standardized before use with the usual precautions. Preliminary runs indicated that the millimole range of concentrations was most suitable for the kinetic studies. The subsequent data were obtained using different mole ratios of TaS_2 and KOH (1:y) in a constant volume of solution (100 ml). The intercalated hydroxide was bound to the TaS_2 lattice and chemically inactive and the progress of the intercalation was followed with time by analyzing the amount of hydroxide left over at various time intervals by standard titration methods. In a few cases, the reaction was also followed by

TABLE I: Kinetic Data of Intercalation Reaction of MOH (M = Na, K) with TaS_2

TaS_2–KOH								
y[a]	0.3	0.63	1.0	2.1				
				25°	2°	65°	85°	100°
t',[b] min	40	15	10	15	30	5	5	5
(t)	(40)	(80)	(80)	(30)	(95)	(80)	(60)	(40)
$k_1 \times 10^{-2}$, min^{-1}	7.8	6.3	3.5	1.3	0.9	5.4	5.6	5.4
$k_1' \times 10^{-6}$, $M\ min^{-1}$[c]		5.0	7.1	2.7	1.5	9.3	7.3	6.3
TaS_2–NaOH								
y	0.67	1.1	3.9	3.8[d]				
t' min	20	12	10	10				
(t)	(100)	(50)	(140)	(150)				
$k_1 \times 10^{-2}$, min^{-1}	7.0	5.3	1.8	1.0				
$k_1' \times 10^{-6}$, $M\ min^{-1}$	16.2	4.0	1.5	1.1				

[a] y represents the initial number of millimoles of hydroxide present per millimole of TaS_2 in a constant volume of 100 ml. [b] Time up to which first-order rate law is obeyed to give rate constant k_1. Values in parentheses are the times up to which the reaction was followed. [c] Effective rate constant derived from eq 3 and Figure 2. [d] TaS_2 particles of size <53 μ. In all other cases particles are in the range 53–149-μ size.

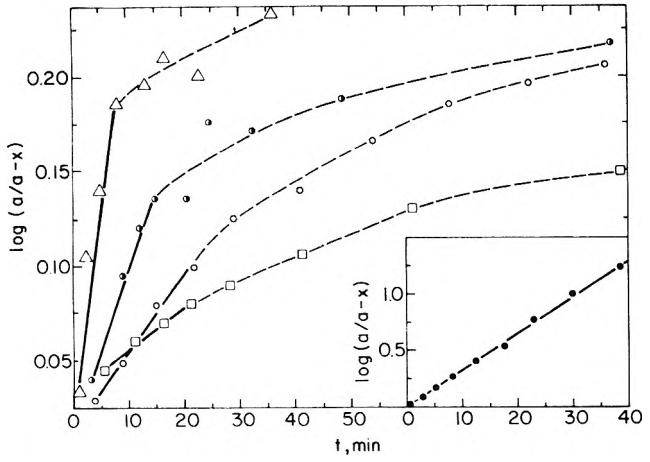

Figure 1. First-order rate law plots for TaS_2–KOH and –NaOH systems [(△) y = 2, 65°; (◑) y = 2, 25°; (○) y = 2, 2°; (●) y = 0.3, 25° all for KOH; (□) y = 3.8, 25° for NaOH]. First-order rate law is obeyed up to certain time and thereafter exhibits complex behavior except for y = 0.3 where the law is obeyed up to the completion of the intercalation reaction. (a is the initial concentration; x is the hydroxide intercalated at time t.)

observing pH changes as a function of time with a pH meter. X-Ray diffraction patterns (taken with Cu Kα radiation and Ni filter) gave good indication of the various phases formed.

It was found that whenever the starting composition (y) of KOH or NaOH was <0.5, the reaction followed strictly first-order kinetics with respect to the alkali concentration up to the completion of the reaction (Figure 1) but the intercalated product was always a mixture of stages I and II as identified by X-rays with no pure TaS_2 phase.[3] The first-order rate constant is fairly high ($\sim 7 \times 10^{-2}$ min^{-1} at 25° for both KOH and NaOH, Table I). Starting hydroxide concentrations greater than y = 1.0 always yielded stage I intercalated products but the first-order rate law was obeyed only up to a certain time (t') less than the total time (t) of the reaction. The value of t' (usually ~15 min) depends on concentration of the alkali (for all $y > 2$) and temperature and is smaller at higher y and greater temperatures. X-Ray data of samples intercalated up to time t' with higher initial concentrations ($y > 2$) showed that stage I intercalation is achieved within this time. After time t', the effective rate of the reaction was retarded by some complex mechanism. Reactions, stopped and examined at times much below t', showed partial intercalation (pure TaS_2 and stage I intercalated phases).

Discussion

The intercalation process, whether it is carried out in solution or in a gas phase, can be mainly considered as a heterogeneous process, and the usual parameters such as particle size of the solid, surface area, number of active sites, concentration of the intercalate, and temperature enter into the mechanism. A mechanism for the complete process of intercalation consists of the following elementary steps: (1) diffusion of the intercalate to the surface (or active centers) of the host material; (2) adsorption of the intercalate on to the surface (or active centers on the surface or at the edges); (3) formation of the activated complex of the intercalate with the host surface atoms and the concomittant opening up of the layers; and (4) diffusion of the intercalate into the lattice forming a stable intercalation compound.

Considering these steps in detail, step 1 is usually the fastest and obviously not rate determining. Step 2 depends on the concentration of active sites on the host and, to some extent, on the basicity or polar nature of the intercalate and its concentration. Since it is fairly well established that only Lewis bases can be intercalated into TaS_2,[2] the active sites involved in the chalcogenide must be acidic in nature and it may be safely assumed that any intercalate of the Lewis base type may easily get adsorbed on the surface; further, the exothermic adsorption energy is fairly small (≤0.05 kcal/mol[4]). Thus, it is highly unlikely that this will be a rate-determining step. Step 3 can be assumed to be akin to the case of chemisorption and involves an energy of activation and most probably is the rate-determining step. This is confirmed by the fact that intercalation involves some type of electronic charge transfer from the guest species to the host chalcogenide (see preceding paper[1]) and the experimental observation that an increase in temperature always leads to an increased rate of intercalation. It is also likely that size effects of the intercalate play a role in the formation of a suitably oriented activated complex. Further, the activation energy involved might be fairly small in the case of hydroxide intercalation (≤10 kcal/mol) since the deintercalation of an intercalated product is easily achieved;[1] in other words, the intercalation process is thermodynamically reversible. It is likely that step 4 is also

rate determining, especially in cases where intercalation has proceeded to a considerable extent, or in other words, step 4 may act as an inhibitor of the intercalation thereby inhibiting the activated complex formation at the active sites by the fresh intercalate molecules due to the inherent slowness of the diffusion of the intercalate into the bulk of the lattice.

According to the absolute theory of reaction rates as applied to surface reactions, the velocity of a heterogeneous reaction is given by[4]

$$v = k_1 c_g c_s \frac{kT}{h} \frac{f^{\ddagger}}{F_g f_s} \exp(-E/RT) \qquad (1)$$

where c_g is the concentration of molecules to be adsorbed (moles/liter or molecules/cc), c_s is the concentration of active sites per unit area of the surface, k_1 is the rate constant, k and h are the Boltzmann and Planck constants, T the absolute temperature, and E the activation energy; $f^{\ddagger}$ and f_s are the total partition functions of the activated complex and that of the adsorption sites, respectively, and F_g is the partition function of the adsorbate species. Now $f^{\ddagger}$ and f_s can be taken as unity, and at a given temperature, E and F_g (which involve mainly translational and rotational partition functions) are constant, and thus for a given surface area, we have

$$v = k_1 c_g \qquad (2)$$

which leads to the first-order rate law. In the usual chemisorption theory, account is taken of the desorption process occurring from the surface sites; however, in the intercalation process, it is the diffusion of the adsorbed species into the bulk of the lattice that is to be taken into account. Therefore, as a first approximation, we may assume that the rate of diffusion is proportional to the concentration of the adsorbed species, *i.e.*, to the concentration of the adsorbate in the bulk of the solution (since diffusion from the bulk to the surface is not rate determining).

As can be seen from Table I and Figure 1, the rate of consumption of the hydroxide obeys a first-order rate law at the low initial concentrations up to the completion of the reaction or up to time t' at high initial concentrations. The deviation from first order and falling off of rate after time t' can be understood by considering examples in the literature[4,5] where a surface reaction is inhibited by the products getting adsorbed on the active sites and thereby acting as poisons; in such cases, an explicit rate law can be derived of the form

$$k_1' = (a/t) \ln (a/a - x) - b(x/t) \qquad (3)$$

where k_1' is the effective first-order rate constant, a the initial concentration, x the number of moles adsorbed (intercalated) at time t, and b a constant. We have applied eq 3 to our data on the TaS_2–KOH and –NaOH systems and as can be seen from Figure 2, a plot of $\{(1/t) \log (a/a - x)\}$ *vs.* (x/t) is found to be a straight line; deviation from linearity occurs only for $t \ll t'$. The effective rate constants (k_1') obtained from eq 3 were orders of magnitude lower ($\sim 10^{-6}$ *vs.* 10^{-2} min^{-1}) than the first-order rate constants (k_1) obtained from plots up to the time t' (Table I).[6] We picture the mechanism of the intercalation as follows. Because of the acidic nature of the active sites present in TaS_2, the alkali hydroxide molecules, or more precisely the ion pairs (with the associated hydration spheres), are adsorbed fairly quickly on the surface, and whenever the relative orientation and thermal energy considerations are satisfied, form a transition state or activated complex. Because of the localized electrical charge on the anions in the activated complex, small localized positive charges (acidic centers) will be developed on the S atoms in TaS_2 which are involved in the formation of the complex. Thus, the transition state is essentially ionic with a large dipole moment. Also, because of the localization of charges on the chalcogen planes in the van der Waals gap, the OH^- ions will be slowly attracted and will diffuse into the bulk of the lattice, leaving the edge or surface (basal plane) states free to act as fresh sites for adsorption. In the initial stages of the intercalation, the rate is rapid and the diffusion of the intercalate into the bulk of the lattice is fast (since the van der Waals gap is empty) and the reaction is completely first order as is observed experimentally. This situation changes drastically after time t' at high initial starting hydroxide concentrations ($y > 2$); essentially, after time t', a stage I intercalation has been achieved in which all the layers of TaS_2 opened up and there is at least one OH^- or KOH unit (with the associated hydration spheres) present between any two Ch–M–Ch slabs (see preceding paper[1]). Because of electrostatic repulsion between OH^- ions, diffusion of fresh OH^- ions from the edges or from basal plane sites is slowed and the activated complex formed at the active sites has a definite probability of breaking up to form the reactants again. In other words, the lifetime of the transition state is increased, the active site is not free to accept fresh intercalate ions, and hence the rate of intercalation is slowed down. Thus, the "product" of the adsorption (intercalation) reaction acts as a poison and inhibits the first-order rate behavior and explains the excellent linearity of $(1/t)$ log $(a/a - x)$ *vs.* (x/t) plots obtained for TaS_2–KOH system at various temperatures (Figure 2). The fact that only partial intercalation is observed for $t < t'$ is consistent with this assumption since under the conditions stage I intercalation is not achieved in all regions of the small TaS_2 crystallites. Also, after t', the intercalation is not complete in the real sense since otherwise the reaction will indicate a zero order. The observation of a mixture of stages (I and II or II and III), whenever low concentrations of KOH (*e.g.*, $y > 0.5$) are allowed to intercalate into TaS_2, can be explained on the assumption that, in these cases, $t' \geq t$ and partial intercalation results until all the OH^- ions in the bulk of the solution are consumed. At this point, the driving force for the intercalation ceases to exist and the ions in

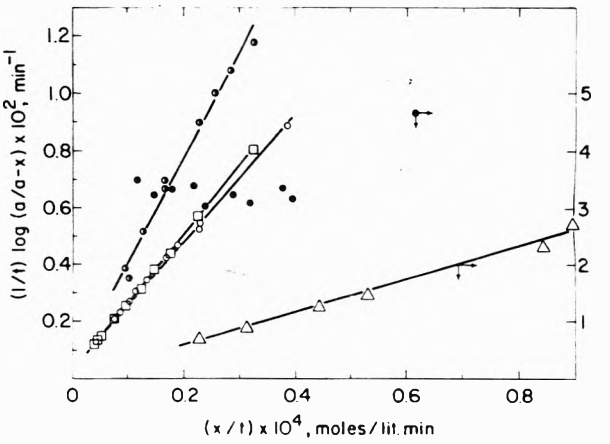

Figure 2. Straight line plots obtained using the data of Figure 1 indicating a mechanism where a first-order rate law is inhibited by the poisoning effect of the products formed in the reaction (intercalation). Symbols refer to the same runs as in Figure 1.

the intercalated regions slowly diffuse into the unintercalated regions. However, this diffusion is not random but occurs in a specific fashion to give rise to a second stage intercalation (where the intercalate is present in every second TaS_2 layer[1]). KOH concentrations of $y < 0.1$ do not produce noticeable intercalation in TaS_2, thereby indicating that the number of OH^- ions available in solution is too low to satisfy the criterion demanded for the formation of an activated complex.

As discussed in an earlier paper,[1] the intercalate ions go to occupy the empty octahedral interstices in the host chalcogenide lattice. 2s TaS_2 has one octahedral hole per Ta atom (two holes in the unit cell). In the initial stages of the intercalation reaction the OH^- ions occupy the first available octahedral sites dragging K^+ ions and the polarized H_2O molecules (hydration sphere) along with them. Since it is experimentally observed that stage I intercalation is reached at time t', this should mean that some of the octahedral sites (assuming each particle of TaS_2 has, *e.g.*, $\sim 10^4$ unit cells) are occupied by H_2O molecules instead of K^+ and OH^- ions to give the compositions we find by analyses, $TaS_2(KOH)_{1/3}(H_2O)_{1/3}$;[1] this is plausible since the polarized H_2O molecules associated with an OH^- ion can effectively act as intercalate species. Continuation of intercalation reaction after t' must then be a replacement of the intercalated H_2O molecules by the OH^- and K^+ ions at the octahedral sites to give the limiting composition $TaS_2(KOH)_{1/2}$. This argument was tested experimentally as follows. One run of TaS_2–KOH reaction was stopped at t' and the product was removed and X-rayed; it showed complete stage I intercalation. Then the sample was kept in high vacuum for 12 hr at 25° after which X-rays showed evidence of partial intercalation indicating that the loosely bound H_2O molecules (possibly, also some KOH) were expelled and the lattice collapsed to the pure TaS_2 phase in certain regions. Unfortunately it is not possible to replace all the H_2O molecules by K^+ and OH^- ions since TaS_2 decomposes chemically after prolonged treatment (~12 hr) with concentrated alkali hydroxides.

The observed first-order rate constants ($t = t'$; $y = 2$; TaS_2–KOH system) at various temperatures (2–100°) were found to roughly obey the Arrhenius equation. The observed value of energy of activation (~3 kcal/mol) was in the range of values encountered for adsorption reactions but far below the values for typical homogeneous reactions in solution (~30 kcal/mol).[4] k_1 is seen to be slightly higher for lower initial concentrations ($y \lesssim 0.5$ KOH) compared to concentrations where $y > 1.0$. It is thus possible, that the reaction is inhibited to a small extent at times less than t' as well, at the high initial concentrations (Table I).

The effect of particle size is not at all considered in the above discussion even though, for the temperature variation studies, TaS_2 particles of same size have been employed. No doubt an increase of particle surface area will enhance the initial reaction velocity which may also depend on the relative ratio of the basal plane *vs.* edge areas if these were to act differently toward the formation of the activated complex.[8] One point is worth mentioning regarding the temperature variation of the first-order rate constants. Although the increase of k_1 with temperature is not very great in the temperature range 2–100°, data on a particular system (of same particle size, starting composition, etc.) are probably significant and real. The low measured activation energy of ~3 kcal/mol is probably inherent to the TaS_2–MOH system, where MOH intercalates with ease and rapidity compared to, for example, pyridine which requires drastic conditions of temperature and pressure.[2]

Summary

For low initial alkali hydroxide concentrations (KOH; $y < 0.5$), the rate of intercalation of TaS_2 follows a first-order rate law but the product is a mixture of different intercalation stages as identified by X-rays. Pure stage I intercalation product is obtained for $y > 0.5$ but the first-order rate law with respect to the alkali concentration (NaOH or KOH) is obeyed only up to t' of the total time ($t' < t$) and thereafter the rate decreases. This falling off of the rate is interpreted as due to the "poisoning" effect of the intercalated product at the surface of TaS_2 and due to the slowness of diffusion of the intercalate species into the host lattice. The significance of t' is that, from a structural point of view, the intercalation reaction is essentially complete at t' where all the available octahedral interstices in TaS_2 are filled by M^+, OH^- ions, and H_2O molecules to give a composition $TaS_2(MOH)_{1/3}(H_2O)_{1/3}$ for the complex. Continuation of the reaction above $t > t'$ is presumed to be the replacement of the intercalated H_2O by fresh M^+ and OH^- ions to give the composition $TaS_2(MOH)_{1/2}$. This limiting composition could not be achieved experimentally. Metal hydroxide intercalation into TaS_2 is an endothermic process with a low energy of activation (~3 kcal/mol).

Acknowledgments. We wish to acknowledge valuable discussions and helpful suggestions on the kinetic aspects with R. A. Ghez. Thanks are also due to R. A. Figat for technical assistance and to C. Aliotta for electron micrographs of TaS_2 powders.

References and Notes

(1) G. V. Subba Rao, M. W. Shafer, and J. C. Tsang, *J. Phys. Chem.*, preceding paper.
(2) F. R. Gamble, *et al.*, *Science*, **174**, 493 (1971).
(3) When the intercalate species are inserted between every two layers of the host TaS_2, the complex is of stage I; when it is inserted between alternate sets of layers, the complex is of stage II, etc. Different stages of intercalation are characterized by varying *c* lattice parameters.[1]
(4) K. J. Laidler, "Chemical Kinetics," McGraw-Hill, New York, N.Y., 1950.
(5) E. S. Amis, "Kinetics of Chemical Change in Solution," Macmillan, New York, N.Y., 1949.
(6) Data exist in the literature[5] where eq 3 is obeyed by the adsorption rate of benzoic acid and iodine by charcoal in solution. We have considered other forms of rate expressions including the Elovic equation.[7] It is possible to fit the observed data at high t values to the Elovic equation, $x = (1/\alpha) \ln (1 + c\alpha t)$ where c and α are constants and x the amount adsorbed (intercalated) at time t. Even though the Elovic equation is best understood in the light of a constant site generation and decay in the course of adsorption, it does not give insight into the mechanism of the intercalation process.
(7) C. Aharoni and F. C. Tompkins in "Advances in Catalysis," Vol. 21, D. D. Eley, H. Pines, and P. B. Weisz, Ed., Academic Press, New York, N.Y., 1970.
(8) We have one set of data at 25° with TaS_2:NaOH of the same initial concentration but of two different particle sizes ($<54\ \mu$ and $53 < p < 149\ \mu$) (Table I). The first-order rate constant is lower with TaS_2 particles of smaller size than with larger size (1.0×10^{-2} *vs.* 1.8×10^{-2} min^{-1}; $t' \sim 10$ min). It might be that the smaller particle size TaS_2 forms a stage I product at shorter times (fast initial intercalation rate) and the inhibition of the reaction might already have started to play a significant role.

Yields of Positive Ions in the Radiolyses of Liquid Hydrocarbons. Propane and Cyclohexane

Toshinori Wada, Shoji Shida,* and Yoshihiko Hatano

Laboratory of Physical Chemistry, Tokyo Institute of Technology, Meguro-ku, Tokyo, Japan *(Received April 29, 1974; Revised Manuscript Received December 13, 1974)*

The yields of positive ions produced in the radiolyses of liquid propane and cyclohexane have been estimated by using a proton acceptor (NH_3) together with an electron scavenger (SF_6) and a radical scavenger (O_2). In liquid propane the G value of fragment ion $C_2H_5^+$ is estimated to be 0.3, which is in good agreement with that obtained by Koob and Kevan making use of perdeuterated propane. The G value of parent-minus-H ion $C_3H_7^+$, which is found to be 0.7, is larger than that for $C_2H_5^+$. In liquid cyclohexane, the formation of parent-minus-H ion c-$C_6H_{11}^+$ is observed with a yield of 0.7. Further, an attempt to estimate the yields of parent ions produced in the radiolyses of liquid propane and cyclohexane has been made on the basis of the presumed ionic processes. These results, especially the relatively large yields of parent-minus-H ions, indicate a characteristic mode of the fragmentation of excited parent ions in liquid hydrocarbons as compared with that in the gas phase.

I. Introduction

The fragmentation of the excited parent ion in the radiolysis of liquid hydrocarbon has been studied by methods using perdeuterated compounds[1] and charge scavengers.[2] From these studies it has generally been recognized that the fragmentation of the excited parent ion occurs to a lesser extent in the liquid phase than in the gas phase. Furthermore, it is now becoming clearer that the mode of the fragmentation in the liquid phase is appreciably different from that in the gas phase.

In a previous paper,[3] yields of fragment ions were estimated in the radiolysis of liquid n-butane with the following results. (1) The yields of fragment ions (carbonium ions) estimated by using charge scavengers are in good agreement with those obtained by use of perdeuterated n-butane.[1c] (2) The formation of parent-minus-H ion $C_4H_9^+$ has been found by using charge scavengers with a relatively large yield compared with the yields of other fragment ions, which seems to be characteristic of the radiolysis of n-alkane in the liquid phase.

In the present work the yields of positive ions in liquid propane and cyclohexane have been measured using charge scavengers in order to generalize the above results. Especially, the formation of parent-minus-H ions has been carefully examined in both cases. Ionic processes in the liquid-phase radiolysis of propane have been studied by Koob and Kevan making use of deuterated propane.[1b] In the method using deuterated compounds the yield of parent-minus-H ion could not be estimated easily. The formation of parent-minus-H ion, c-$C_6H_{11}^+$, in the radiolysis of liquid cyclohexane has been reported by Ward and Hamill with a G value of 0.1 by measuring the yield of adduct c-$C_6H_{11}OC_2H_5$ formed in the presence of ethanol.[4]

II. Experimental Section

Propane supplied by Takachiho Shoji Co., was purified gas chromatographically using a squalane column, followed by trap-to-trap distillations at −78°. Gas-chromatographic analysis using a flame-ionization detector showed its purity to be more than 99.99%. Phillips Research Grade cyclohexane was used after the usual degassing and trap-to-trap distillations. Gas-chromatographic analysis of cyclohexane showed impurities of less than 0.01%, about half of which was 2,4-dimethylpentane. The purities of other materials used were as follows: ammonia (>99%), sulfur hexafluoride (>98%), and oxygen (>99.9%).

About 0.2 ml of propane was filled in vacuo into a Pyrex tube (3 cm long, 0.3 cm i.d.) fitted with a breakable seal. The cyclohexane solution (1 ml) was filled into a sample tube (4 cm long, 0.6 cm i.d.). A known amount of propane or cyclohexane was irradiated at 0° or at room temperature, respectively, by ^{60}Co γ rays at a dose rate of 3.8×10^{19} eV/g hr to a total dose of 1.1×10^{20} eV/g.

The hydrocarbon products (C_1–C_6) formed in the propane solution were analyzed by a gas-chromatograph with a flame ionization detector and a 3-m activated alumina column at 60°. However, a peak of 2,3-dimethylbutane was not completely separated from that of 2-methylpentane. Cyclohexene produced in the cyclohexane solutions was analyzed using a 6-m dimethylsulfolane column at room temperature. Bicyclohexyl, cyclohexanone, and cyclohexanol were also analyzed using a 0.75-m polyethylene glycol 600 column at 100°.

III. Results

Propane. Figure 1 shows the effect of the addition of sulfur hexafluoride on the product yields in the radiolysis of liquid propane. Figure 2 shows the effect of the addition of oxygen on the product yields. "Dimer" products such as n-C_6H_{14}, 2,3-dimethylbutane, and 2-methylpentane which may be produced by radical recombination reactions could not be detected in the presence of oxygen. Figures 3 and 4 show, respectively, the effect of the addition of ammonia on the yields of products from C_3H_8–0.4 M SF_6 mixture and from C_3H_8–0.4 M SF_6–0.02 M O_2 mixture. The yield of C_3H_6 increases greatly upon the addition of NH_3. The increase in the yield of C_2H_4 is accompanied by the decrease in that of C_2H_6. The yield of 2,3-Me_2C_4 + 2-MeC_5 also increases somewhat. As seen in Figure 4, the yield of C_3H_6 from a C_3H_8–SF_6–O_2 mixture attains a maximum value at low NH_3 concentration, and then decreases gradually with increasing NH_3 concentration. The G values of products

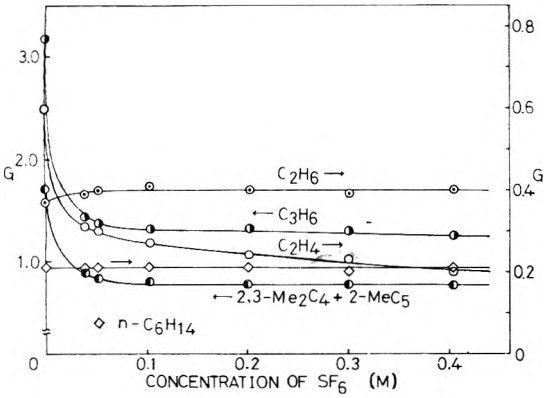

Figure 1. Effect of the addition of sulfur hexafluoride on the product yields from liquid propane.

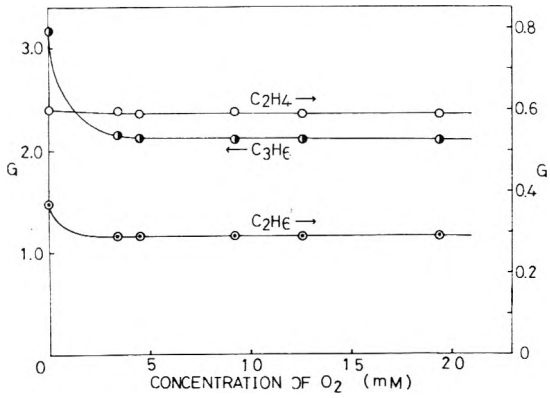

Figure 2. Effect of the addition of oxygen on the product yields from liquid propane.

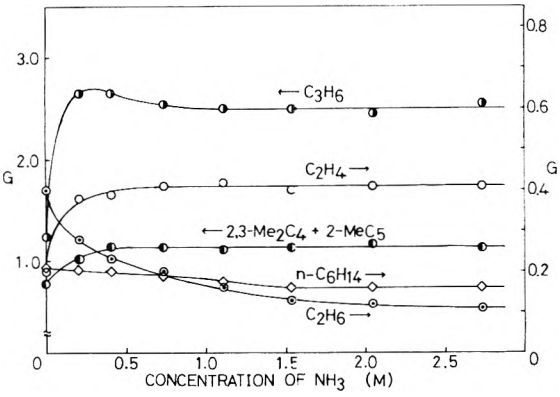

Figure 3. Effect of the addition of ammonia on the product yields from liquid propane containing 0.4 *M* SF_6.

from liquid propane with and without scavengers are summarized in Table I.

Cyclohexane. The G values of c-C_6H_{10} and $(c\text{-}C_6H_{11})_2$ from pure cyclohexane are 3.1 ± 0.1 and 1.9 ± 0.1, respectively. So far, the G value of c-C_6H_{10} was reported[5] to be in the region of 3.0~3.3, and that of $(c\text{-}C_6H_{11})_2$ in the region of 1.7~2.0. Figure 5 shows the effect of the addition of sulfur hexafluoride on these products. The decrements of these yields are in good agreement with those reported previously.[6] Table II shows the effect of the addition of oxygen on the yield of c-C_6H_{10}. The yield of c-C_6H_{10} sharply decreases at low oxygen concentration (~0.004 *M*) and attains a constant value. As shown in Table III, the yield of

TABLE I: G Values of Products Formed in the Radiolysis of Liquid Propane with and without Various Scavengers[a-c]

	Additive[d]					
Product	None	SF_6	SF_6 + NH_3	O_2	O_2 + SF_6	O_2 + SF_6 + NH_3
CH_4	0.67	0.46	0.28	0.37	0.30	0.20
C_2H_6	0.37	0.40	0.11	0.29	0.38	0.14
C_2H_4	0.60	0.20	0.41	0.59	0.24	0.42
C_3H_6	3.17	1.24	2.49	2.10	0.25	0.98
$(2,3\text{-}Me_2C_4 + 2\text{-}MeC_5)$	1.72	0.77	1.14			
n-C_6H_{14}	0.21	0.21	0.16			

[a] Dose 1.13×10^{20} eV/g. [b] Irradiation temperature 0°. [c] Probable errors in G values ±5%. [d] Concentration SF_6 0.4 *M*, NH_3 2.7 *M*, and O_2 0.02 *M* in all runs in this table.

TABLE II: Effect of the Addition of Oxygen on the Yield of c-C_6H_{10}

$10^{-2}[O_2]$, *M*	0	0.14	0.23	0.35	0.55	1.00	1.23
$G(c\text{-}C_6H_{10})$	3.14	1.77	1.69	1.68	1.70	1.65	1.60

TABLE III: G Values of Products Formed in the Radiolysis of Liquid Cyclohexane with and without Various Scavengers[a-c]

	Additive[d]					
Product	None	SF_6	SF_6 + NH_3	O_2	O_2 + SF_6	O_2 + SF_6 + NH_3
c-C_6H_{10}	3.14	1.28	2.53	1.64	0.39	1.14
$(c\text{-}C_6H_{11})_2$	1.85	1.04	1.84	0.28	0.17	0.25
c-$C_6H_{10}O$				2.92	3.23	0.33
c-$C_6H_{11}OH$				2.97	3.96	5.53

[a] Dose 1.07×10^{20} eV/g. [b] Irradiation at room temperature. [c] Probable errors in G values ±5%. [d] Concentration SF_6 0.4 *M*, NH_3 0.7 *M*, and O_2 0.01 *M* in all runs in this table.

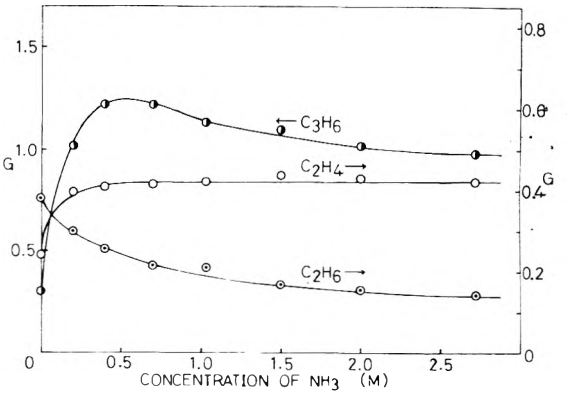

Figure 4. Effect of the addition of ammonia on the product yields from liquid propane containing 0.4 *M* SF_6 and 0.02 *M* O_2.

$(c\text{-}C_6H_{11})_2$ also decreases upon the addition of O_2 (~0.01 *M*). New oxygen-containing products, cyclohexanone and cyclohexanol, are formed in place of c-C_6H_{10} and $(c\text{-}C_6H_{11})_2$. This fact is due to the scavenging of cyclohexyl

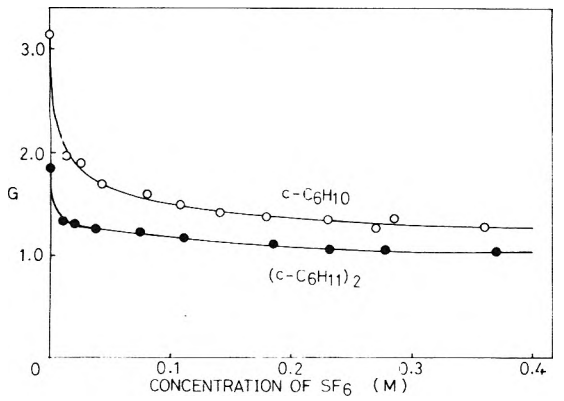

Figure 5. Effect of the addition of sulfur hexafluoride on the products c-C_6H_{10} and $(c$-$C_6H_{11})_2$ from liquid cyclohexane.

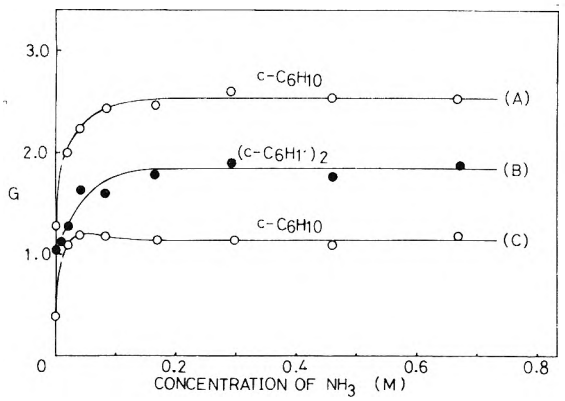

Figure 6. Effect of the addition of ammonia on the product c-C_6H_{10} from a c-C_6H_{12}–0.4 M SF_6 mixture (curve A), on the product $(c$-$C_6H_{11})_2$ from a c-C_6H_{12}–0.4 M SF_6 mixture (curve B), and on the product c-C_6H_{10} from a c-C_6H_{12}–0.4 M SF_6–0.01 M O_2 mixture (curve C).

radicals by the oxygen added. Figure 6 shows the effects of the addition of ammonia on the yields of c-C_6H_{10} (curve A) and $(c$-$C_3H_{11})_2$ (curve B) from c-C_6H_{12}–0.4 M SF_6 mixture, and on the yield of c-C_6H_{10} (curve C) from c-C_6H_{12}–0.4 M SF_6–0.01 M O_2 mixture, respectively. The G values of products from liquid cyclohexane with and without scavengers are summarized in Table III. The G values of products are determined in this experiment with the probable errors of ±5%.

IV. Discussion

Yield of Fragment Ion $C_2H_5^+$ in Liquid Propane. The fragment ion $C_2H_5^+$ formed by the C–C bond cleavage of the excited parent ion $C_3H_8^{+*}$ undergoes hydride-ion transfer reaction 1 competing with neutralization reaction 2 in the liquid phase. When sulfur hexafluoride is added,

$$C_2H_5^+ + C_3H_8 \longrightarrow C_2H_6 + C_3H_7^+ \quad (1)$$

$$C_2H_5^+ + e^- \longrightarrow C_2H_4 + H \quad (2)$$

the electron is converted into the sulfur hexafluoride negative ion which is less diffusive than the electron itself, and the $C_2H_5^+$ undergoes the hydride-ion transfer more efficiently than in the absence of SF_6. As seen in Figure 1, $G(C_2H_6)$ slightly increases upon the addition of SF_6, and also increases by about 30% upon the addition of SF_6 to a C_3H_8–O_2 mixture (Table I). When ammonia is added together with SF_6 (Figure 3), the yield of C_2H_6 decreases with increasing NH_3 concentration, while the yield of C_2H_4 increases complementarily. These facts are undoubtedly due to proton transfer 3 from $C_2H_5^+$ to NH_3 prior to hydride-

$$C_2H_5^+ + NH_3 \longrightarrow C_2H_4 + NH_4^+ \quad (3)$$

ion transfer 1. The G value of the fragment ion $C_2H_5^+$ may be estimated from the decrement of C_2H_6 yield upon the addition of NH_3 to C_3H_8–SF_6 mixture to be 0.3. According to reaction 3, the yield of C_2H_4 should be increased by 0.3, whereas the increment is only 0.2 (Table I). As a plausible explanation for this difference, the condensation reaction 4

$$C_2H_5^+ + NH_3 \longrightarrow C_2H_5NH_3^+ \quad (4)$$

which does not lead to the formation of C_2H_4 is assumed to occur between $C_2H_5^+$ and NH_3. As shown in Table I, the decrement of $G(C_2H_6)$ upon the addition of NH_3 to a C_3H_8–SF_6–O_2 mixture is slightly smaller than in a C_3H_8–SF_6 mixture. This may suggest that in the presence of SF_6 alone, $C_2H_5^+$ in part undergoes neutralization (5) with

$$C_2H_5^+ + SF_6^- \longrightarrow C_2H_5 + SF_6 \quad (5)$$

SF_6^- besides hydride-ion transfer 1. The C_2H_5 radical formed abstracts a hydrogen atom from propane to give C_2H_6. On the other hand, in a C_3H_8–SF_6–O_2 mixture the C_2H_5 radical resulting from reaction 5 should be scavenged by O_2.

The G value of fragment ion $C_2H_5^+$ estimated above by using a proton acceptor NH_3 can be compared with that obtained by Koob and Kevan[1b] making use of perdeuterated propane. They accounted for the yield of bimolecular ethane (C_2D_5H) in a C_3H_8–C_3D_8–O_2 mixture by hydride-ion transfer reaction 6, and estimated the G value of ethyl

$$C_2D_5^+ + C_3H_8 \longrightarrow C_2D_5H + C_3H_7^+ \quad (6)$$

ion to be 0.27. This value is in good agreement with that obtained by use of NH_3 in this work. In the radiolysis of liquid n-butane,[3] it was also confirmed that the yields of fragment ions in both estimations were in good agreement with each other. Thus, it may be concluded that generally in the liquid-phase radiolysis of n-alkane both methods give the same yields of fragment ions (carbonium ions).

Yields of Parent-minus-H Ions $C_3H_7^+$ in Liquid Propane and c-$C_6H_{11}^+$ in Liquid Cyclohexane. (*A*) *Yield of $C_3H_7^+$.* The carbonium ion which is formed by the C–H bond cleavage of the excited parent ion is called parent-minus-H ion.[7] The formation of parent-minus-H ion $C_3H_7^+$ in liquid propane is indicated by the increase of the propylene yield upon the addition of NH_3. As seen in Figure 4, the G value of C_3H_6 from a C_3H_8–SF_6–O_2 mixture attains a maximum value at low NH_3 concentration, and then decreases gradually with increasing NH_3 concentration. At low NH_3 concentration, $C_3H_7^+$ ions produced both by the primary decomposition of the parent ion $C_3H_8^+$ and by hydride-ion transfer reaction 1 (and its analog of fragment ions other than $C_2H_5^+$) undergo proton transfer reaction 7

$$C_3H_7^+ + NH_3 \longrightarrow C_3H_6 + NH_4^+ \quad (7)$$

to give C_3H_6. At high NH_3 concentration, however, the $C_2H_5^+$ ion has already been intercepted by NH_3, and does not give the $C_3H_7^+$ ion by hydride-ion transfer reaction 1.

As seen in Figures 3 and 4, the increase in the G value of C_3H_6 from a C_3H_8–SF_6 mixture upon the addition of NH_3 is considerably larger than that from a C_3H_8–SF_6–O_2 mixture. In the former case, ammonia scavenges not only $C_3H_7^+$ but also parent ion $C_3H_8^+$, both of which contribute to the formation of C_3H_6. The C_3H_7 radical formed by proton transfer reaction 8 partly gives C_3H_6 via disproportion-

$$C_3H_8^+ + NH_3 \longrightarrow C_3H_7 + NH_4^+ \quad (8)$$

ation of C_3H_7 radicals. On the other hand, in a C_3H_8–SF_6–O_2 mixture the C_3H_7 radical is scavenged by O_2. The increment of $G(C_3H_6)$ upon the addition of NH_3 is only attributed to proton transfer reaction 7.

Thus, the G value of parent-minus-H ion $C_3H_7^+$ can be estimated to be 0.7 from the increment of $G(C_3H_6)$ in a C_3H_8–SF_6–O_2 mixture at high NH_3 concentration (Table I). Previously, Tanno et al.[2c] reported a value of 1.1 as the G value of $C_3H_7^+$ in the radiolysis of liquid propane. However this value was obtained from the increment of $G(C_3H_6)$ in a C_3H_8–SF_6 mixture upon the addition of NH_3. Namely, it corresponds to the value of 1.3 in this work (Table I), in which the additional contribution of parent ion is included.

The yield of $C_3H_7^+$, 0.7, obtained here is larger than that of $C_2H_5^+$, 0.3. A similar result has already been reported in the case of liquid n-butane.[3] This fact indicates that the excited parent ions of n-alkane in the liquid phase dissociate preferably at C–H bonds rather than at C–C bonds. This seems to be characteristic of the radiolysis of n-alkane in the liquid phase.

(B) Yield of c-$C_6H_{11}^+$. In the radiolysis of liquid cyclohexane, it has so far been implicitly assumed that the positive species except for the parent ion are not produced with appreciable yields. In the analogy from the results of liquid n-alkane, we can expect the G value of parent-minus-H ion c-$C_6H_{11}^+$ to be more than 0.5 in the radiolysis of liquid cyclohexane. In fact, Figure 6 shows the formation of parent-minus-H ion c-$C_6H_{11}^+$ in liquid cyclohexane. The yield of c-C_6H_{10} increases upon the addition of NH_3 to a c-C_6H_{12}–SF_6–O_2 mixture and to a c-C_6H_{12}–SF_6 mixture. In a way similar to that for $C_3H_7^+$ described before, the G value of c-$C_6H_{11}^+$ can be estimated from the increment of c-C_6H_{10} yield upon the addition of NH_3 to a c-C_6H_{12}–SF_6–O_2 mixture. The increase in the yield of c-C_6H_{10} in this mixture is only due to proton transfer reaction 9. Allowing for the pos-

$$c\text{-}C_6H_{11}^+ + NH_3 \longrightarrow c\text{-}C_6H_{10} + NH_4^+ \quad (9)$$

$$c\text{-}C_6H_{11}^+ + NH_3 \longrightarrow c\text{-}C_6H_{11}NH_3^+ \quad (10)$$

sibility that the c-$C_6H_{11}^+$ ion in part may undergo condensation reaction 10 with added NH_3, we can estimate the G value of parent-minus-H ion c-$C_6H_{11}^+$ to be at least 0.7.

Ward and Hamill[4] made an attempt to measure yields of carbonium ions in hydrocarbon–alcohol liquid mixtures. The G value of c-$C_6H_{11}^+$ was estimated to be only about 0.1 by measuring the yield of adduct c-$C_6H_{11}OC_2H_5$ formed in a cyclohexane–ethanol mixture. As was pointed out by them, however, proton transfer from c-$C_6H_{11}^+$ to C_2H_5OH should be considered to compete with adduct formation.

Thus, it is confirmed that in the radiolysis of liquid cycloalkane as well as liquid n-alkane the parent-minus-H ion is produced with a fairly large yield.

Yields of Parent Ions c-$C_6H_{12}^+$ and $C_3H_8^+$. The yields of positive ions in liquid cyclohexane which undergo proton transfer to C_2H_5OD or ND_3 added as a proton acceptor have been estimated by Buchanan and Williams.[9] If a G value of about 4 is accepted as the yield of total ionization in liquid cyclohexane,[10] the G value of the parent ion is expected to be about 3.3 from the present results. We make here an attempt to estimate the yield of the parent ion.

As shown in Figure 6, the yield of $(c\text{-}C_6H_{11})_2$ from a c-C_6H_{12}–SF_6 mixture increases upon the addition of NH_3. The yield of c-C_6H_{10} from a c-C_6H_{12}–SF_6 mixture increases more than that from a c-C_6H_{12}–SF_6–O_2 mixture. These increases in the yields of $(c\text{-}C_6H_{11})_2$ and c-C_6H_{10} may be ascribed to radical reaction 12 of c-C_6H_{11} which is formed by proton transfer 11 from the parent ion c-$C_6H_{12}^+$. In the

$$c\text{-}C_6H_{12}^+ + NH_3 \longrightarrow c\text{-}C_6H_{11} + NH_4^+ \quad (11)$$

$$2c\text{-}C_6H_{11} \longrightarrow \begin{cases} c\text{-}C_6H_{10} + c\text{-}C_6H_{12} \\ (c\text{-}C_6H_{11})_2 \end{cases} \quad (12)$$

absence of NH_3, the parent ion undergoes neutralization 13 with SF_6^- instead of an electron, which may not produce

$$c\text{-}C_6H_{12}^+ + SF_6^- \longrightarrow \text{not } c\text{-}C_6H_{11} \quad (13)$$

the c-C_6H_{11} radical,[6,8] while the c-$C_6H_{11}^+$ ion undergoes neutralization 14 with SF_6^- to give the c-C_6H_{11} radical fol-

$$c\text{-}C_6H_{11}^+ + SF_6^- \longrightarrow c\text{-}C_6H_{11} + SF_6 \quad (14)$$

lowed by radical reaction 12 to give c-C_6H_{10} and $(c\text{-}C_6H_{11})_2$. The increment of c-C_6H_{10} yield upon the addition of NH_3 to a c-C_6H_{12}–SF_6 mixture (curve A) is 1.3, where the formation of c-C_6H_{10} produced by proton transfer reaction 9 of c-$C_6H_{11}^+$ (0.7 G value) is included. The increment of $(c\text{-}C_6H_{11})_2$ yield upon the addition of NH_3 to a c-C_6H_{12}–SF_6 mixture (curve B) is 0.8. From these results, the yield of the parent ion c-$C_6H_{12}^+$ may be estimated to be $2(1.3 + 0.8) - 0.7 = 3.5$, which is in good agreement with the value 3.3 expected above. The sum of the estimated yields of the parent ion and the c-$C_6H_{11}^+$ ion is 4.2.

Since, however, G(c-$C_6H_{12}^+$) estimated here is based on the increment in the product yields at the highest concentration of NH_3 in the presence of SF_6, the fact that the above estimation may suffer from certain ambiguities caused by the subsequent reactions of NH_4^+ and SF_6^- should be pointed out. It has qualitatively been suggested that the final neutralization between NH_4^+ and SF_6^- occurs to form an insoluble product NH_4F, possibly together with SF_5.[8] Little information on the reactivity of SF_5 is available.[11] If SF_5 could abstract a H atom from the cyclohexane molecule to form an additional c-C_6H_{11} radical, the yield of the parent ion estimated here would be overestimated. If SF_5 could react in part with the c-C_6H_{11} radical, the parent ion yield would be underestimated.

In a way similar to that for cyclohexane, an attempt to estimate the G value of the parent ion $C_3H_8^+$ produced in liquid propane has been made. As seen in Figure 3 and Table I, the yields of C_3H_6 and dimer products (C_6) increase by 1.3 and 0.3, respectively, upon the addition of NH_3 to a C_3H_8–SF_6 mixture. These increases might be ascribed to the radical reaction of C_3H_7 which is formed by proton transfer 8 from the parent ion $C_3H_8^+$, but the formation of C_3H_6 due to proton transfer reaction 7 of $C_3H_7^+$ (0.7 G value) is included in this increment of C_3H_6. Thus, the G value of the propane parent ion $C_3H_8^+$ is estimated to be 2.5.

A Comparison of the Fragmentation of the Excited Propane Parent Ion in the Liquid Phase with that in the Gas Phase. A lot of quantitative information is available concerning the fragmentation of the parent ion and the subsequent reactions from radiolytic and mass spectrometric studies carried out in the gas phase. However, the fragmentation processes in the liquid phase have not been fully elucidated. Although the present work has not resolved this problem clearly, the features characterizing the fragmentation of the excited parent ion in the liquid phase have been at least partly revealed.

The G values of fragment ions, parent-minus-H ion $C_3H_7^+$, and parent ion $C_3H_8^+$ produced by the radiolysis of

TABLE IV:

		Liquid phase		Gas phase
		a	*b*	*c*
$C_3H_8^{**} \rightarrow$	$C_2H_3^{\cdot} + CH_3 + H_2$		0.13	0.27
	$C_2H_4^{\cdot} + CH_4$		0.15	0.62
	$C_2H_5^{\cdot} + CH_3$	0.3	0.27	1.30
	$C_3H_5^{\cdot} + H_2 + H$		0.13	0.25
	$C_3H_7^{\cdot} + H$	0.7		0.37
	$C_3H_8^{\cdot}$	2.5		0.94
Total positive ions		3.9		3.8

[a] This work; liquid phase, 0°. [b] Koob and Kevan; liquid phase, 35°. [c] Bone, Sieck, and Futrell; gas phase, 35°, 1 atm, *G* values calculated from M/N yields in ref 12.

propane in the liquid phase and in the gas phase are summarized in Table IV, together with the results by Koob and Kevan[1b] for the liquid phase and by Bone, Sieck, and Futrell[12] for the gas phase.

In the gas phase at 1 atm, the yield of fragment ion $C_2H_5^+$ is the largest of all positive ions. The yield of the parent ion is considerably smaller than that of $C_2H_5^+$, and the yield of parent-minus-H ion $C_3H_7^+$ is still smaller than that of fragment ion $C_2H_4^+$. In the liquid phase, however, most of the positive ions consists of the parent ion and the formation of fragment ions is much smaller than in the gas phase. The phase change from gas at 1 atm to liquid causes fragmentation of the excited parent ion to be greatly reduced. It is also clearly shown that the relative importance in the primary modes of the fragmentation of the excited parent ion is greatly affected by the phase change. The yields of fragment ions $C_2H_5^+$ and $C_2H_4^+$ which occupy the most part of the positive ions in the gas phase reduce greatly in the liquid phase. On the other hand, parent-minus-H ion $C_3H_7^+$ is produced with a fairly large yield compared with the yields of other fragment ions in the liquid phase. It seems to be characteristic of the radiolysis of liquid *n*-alkane that C–H bond cleavage of the excited parent ion takes place more easily than C–C bond cleavage. The cage effect in the liquid phase may be at least in part responsible for this phenomenon.

In spite of the great difference in the primary modes of the fragmentation of the excited propane ion between the gas phase and the liquid phase, the *G* values of the total positive ions in both phases seem to be in good agreement with each other. This seems to show apparently a little difference between the *G* value of ionization in the liquid phase and that obtained from the *W* value in the gas phase. The *G* value of ionization in the liquid phase described here is defined as the scavengeable yield.

References and Notes

(1) (a) A. A. Scala and P. Ausloos, *J. Chem. Phys.*, **47**, 5129 (1967); (b) R. D. Koob and L. Kevan, *Trans. Faraday Soc.*, **64**, 706 (1968); (c) N. Fujisaki, S. Shida, Y. Hatano, and K. Tanno, *J. Phys. Chem.*, **75**, 2852 (1971).

(2) (a) K. Tanno, T. Miyazaki, K. Shinsaka, and S. Shida, *J. Phys. Chem.*, **71**, 4290 (1967); (b) K. Tanno, S. Shida, and T. Miyazaki, *ibid.*, **72**, 3496 (1968); (c) K. Tanno and S. Shida, *Bull. Chem. Soc. Jap.*, **42**, 2128 (1969).

(3) N. Fujisaki, T. Wada, S. Shida, and Y. Hatano, *J. Phys. Chem.*, **77**, 755 (1973).

(4) J. A. Ward and W. H. Hamill, *J. Amer. Chem. Soc.*, **89**, 5116 (1967).

(5) (a) P. J. Dyne and J. A. Stone, *Can. J. Chem.*, **39**, 2381 (1961); (b) J. W. Falconer and M. Burton, *J. Phys. Chem.*, **67**, 1743 (1963); (c) W. G. Burns and J. R. Parry, *Nature (London)*, **210**, 814 (1964); (d) S. K. Ho and G. R. Freeman, *J. Phys. Chem.*, **68**, 2189 (1964); (e) J. Y. Yang and I. Marcus, *J. Chem. Phys.*, **42**, 3315 (1965).

(6) N. H. Sagert and A. S. Blair, *Can. J. Chem.*, 45, 1351 (1967).

(7) Although this positive ion has been suggested to occur in the liquid-phase radiolysis of propane[2c] and *n*-hexane,[8] this term for that carbonium ion was first used in the previous paper.[3]

(8) K. Shinsaka and S. Shida, *Bull. Chem. Soc. Jap.*, **43**, 3728 (1970).

(9) (a) F. Williams, *J. Amer. Chem. Soc.*, **86**, 3954 (1964); (b) J. W. Buchanan and F. Williams, *J. Chem. Phys.*, **44**, 4377 (1966).

(10) (a) G. P. Freeman and E. D. Stover, *Can. J. Chem.*, **46**, 3235 (1968); (b) J. M. Warman, K.-D. Asmus, and H. Schuler, *J. Phys. Chem.*, **73**, 931 (1969).

(11) (a) J. W. F. van Ingen and W. A. Cramer, *J. Phys. Chem.*, **74**, 1134 (1970); (b) P. T. Holland and J. A. Stone, *Can. J. Chem.*, **48**, 3277 (1970); (c) J. Niedzielski and J. Gawlowski, *J. Phys., Chem.*, **77**, 2853 (1973).

(12) L. I. Bone, L. W. Sieck, and J. H. Futrell, "The Chemistry of Ionization and Excitation," G. R.A. Johnson and G. Scholes, Ed., Taylor and Francis, London, 1967, pp. 223–235.

Selective Hydrogen Atom Abstraction by Hydrogen Atoms in Photolysis and Radiolysis of Neopentane–Alkane Mixtures at 77 K

Tetsuo Miyazaki* and Takeshi Hirayama

Department of Synthetic Chemistry, Faculty of Engineering, Nagoya University, Chikusa-ku, Nagoya, Japan *(Received July 24, 1974)*

Selective hydrogen atom abstraction in the photolysis and radiolysis of neopentane containing a small amount of alkane has been studied by esr spectroscopy and product analysis with mass spectrometer. When neo-C_5H_{12}–i-C_4H_9D–HI is illuminated with ultraviolet light at 77 K, t-C_4H_9 radical, H_2, and HD are formed. A remarkable isotope effect is observed in the abstraction reaction. H atoms migrate a long distance through the matrix without reacting with neopentane molecules. The selective hydrogen atom abstraction reaction occurs efficiently in the solid at 77 K, while it does not occur at all in the solid at 198 K and in the liquid at 262 K. When pure neopentane is γ irradiated at 77 K, neo-C_5H_{11}, t-C_4H_9, and unidentified radicals are produced. A remarkable preirradiation effect is observed on the formation of t-C_4H_9 and the unidentified radical. t-C_4H_9 and the unidentified radicals are not formed directly by the decomposition of neopentane, but by the reaction of H atoms, which are produced by the radiolysis of neopentane, with impurities or products. When neopentane containing a small amount of alkanes is γ irradiated at 77 K, the solute alkyl radicals are formed predominantly. H_2 and HD are formed in the radiolysis of neo-C_5H_{12}–i-C_4H_9D at 77 K, while D_2 is not formed at all. The solute radicals are formed by the selective hydrogen atom abstraction from the solute alkane by H atoms produced by the fragmentation of neopentane.

Introduction

We can easily investigate solid-state reactions at 77 K by irradiation with ultraviolet light or γ rays. The studies on the solid alkane at 77 K have indicated that the reactions exhibit remarkable selectivity and seem to he strongly affected by the condition of the matrix or the crystalline field. Miyazaki, *et al.*, found that when isobutane is exposed to γ irradiation[1] or hydrogen atom attack[2] at 77 K, the isobutyl radical is formed in the polycrystalline state, while the tertiary butyl radical is formed in the glassy state. In the radiolysis of 2,3-dimethylbutane at 77 K, the $\cdot CH_2CH(CH_3)CH(CH_3)_2$ radical is formed in crystal I, while the $CH_3\dot{C}(CH_3)CH(CH_3)_2$ radical is formed in crystal II.[3] When neopentane containing a small amount of other alkane is subjected to γ irradiation at 77 K, alkyl radicals from solute alkanes rather than neopentyl radicals are selectively formed.[4] Willard and Henderson found that when glassy 3-methylalkanes are exposed to γ irradiation, hot atom attack, hot radical attack, or photosensitization by aromatic solutes, radicals are formed predominantly by the rupture of secondary C–H bonds rather than weaker tertiary or more abundant primary bonds.[5]

Recently we have reported preliminary results that H atoms produced by the photolysis of hydrogen iodide in neopentane containing a small amount of alkane react selectively with the solute alkane at 77 K.[6] The previous communication reserved the following questions for further studies. (1) Since only the solute alkyl radical was observed by esr spectroscopy, the possibility that the solute radical is formed by the hydrogen atom abstraction from the solute alkane by neopentyl radicals was not completely excluded in the previous study. (2) If the reaction is caused by H atoms, what is the character of the reaction?

The research described herein was undertaken to resolve the above questions.

* On leave to Laboratório de Radioquimica, Instituto de Energia Atômica, C.P. 11049 (Pinheiros), 01000 São Paulo, Sp, Brazil, until July 1975.

The radiolysis of pure solid neopentane has been studied by esr spectroscopy by several investigators.[7-9] Quite different esr spectra, however, have been reported by them. When neopentane–alkane mixtures are γ irradiated at 77 K, the solute alkyl radical is predominantly formed.[4a] It was suggested previously[4b] that its formation is due to excitation transfer from neopentane to the alkane or to the selective hydrogen atom abstraction reaction by H atoms. The formation of radicals in the radiolysis of pure neopentane and neopentane–alkane mixture is discussed here in comparison with the results obtained in the photolysis.

Experimental Section

A sample of neopentane, >99.9 mol %, supplied by the Tokyo Kagaku Seiki Co. was used in the photolysis and radiolysis of alkane mixtures and another, >99.997%, supplied by the American Petroleum Institute was used in the radiolysis of pure neopentane. Isobutane, supplied by the Takachiho Shoji Co., was more than 99.7%. Isobutane-2-d_1, synthesized by the Grignard reaction of *tert*-butylmagnesium bromide with D_2O, was purified by passing it through a column of freshly activated alumina and then through a column of fresh soda lime. Mass spectrometric analysis indicated that at least 95% of the isobutane-2-d_1 was correctly labeled with the deuterium atom at the tertiary position. Spectrograde cyclohexane was passed through a 1-m column packed with silica gel and then distilled on a vacuum line before use. The D content of dodecadeuteriocyclohexane was more than 99%. Hydrogen iodide was the same as used before.[2]

Uv illumination was provided by a Toshiba medium-pressure mercury lamp and γ irradiation by Co-60 at a dose rate of 4.2×10^{19} eV/g hr.

H_2 and HD were analyzed by a gas buret connected to a Toepler pump and mass spectrometer (RMS-4 Hitachi mass spectrometer). The esr measurement were done on a JES-3BX esr spectrometer.

TABLE I: Formation of Hydrogen in the Photolysis of neo-C_5H_{12}–i-C_4H_9D–HI and the Radiolysis of neo-C_5H_{12}–i-C_4H_9D[a]

	Irradiation[b]	Temp, K	Phase	Composition of hydrogen, mol % H_2	HD	Yield of hydrogen[c]
neo-C_5H_{12}–i-C_4H_9D–HI	Uv	77	Solid	83	17	10
neo-C_5H_{12}–i-C_4H_9D–HI	Uv	198	Solid	100	0	13
neo-C_5H_{12}–i-C_4H_9D–HI	Uv	262	Liquid	100	0	64
neo-C_5H_{12}–i-C_4H_9D	γ	77	Solid	60	40	10
neo-C_5H_{12}–i-C_4H_9D	γ	198	Solid	98	2	6
neo-C_5H_{12}–i-C_4H_9D	γ	266	Liquid	100	0	6

[a] Concentrations of isobutane and hydrogen iodide are 2.0 and 0.5 mol %, respectively. Yields are averages of two runs. [b] Illumination time with uv light was 10 min. Total dose of γ rays was 5.9×10^{20} eV/g. [c] Yield of hydrogen at 77 K is taken as 10.

TABLE II: Formation of Radicals in the Photolysis of neo-C_5H_{12}–Alkane–HI and the Radiolysis of neo-C_5H_{12}–Alkane[a]

	Irradiation	Temp, K	Yield of solute alkyl radical[b]	Yield of neo-C_5H_{11} radical[b]
neo-C_5H_{12}–i-C_4H_{10}–HI	Uv	77	10	
neo-C_5H_{12}–i-C_4H_9D–HI	Uv	77	6	
neo-C_5H_{12}–i-C_4H_{10}–HI	Uv	117	10	
neo-C_5H_{12}–i-C_4H_9D–HI	Uv	117	1.5	
neo-C_5H_{12}–c-C_6H_{12}–HI	Uv	77	4.5	
neo-C_5H_{12}–c-C_6D_{12}–HI	Uv	77	0.5	1.5
neo-C_5H_{12}–i-C_4H_{10}	γ	77	10	5
neo-C_5H_{12}–i-C_4H_9D	γ	77	8.7	4
neo-C_5H_{12}–c-C_6H_{12}	γ	77	12.3	2
neo-C_5H_{12}–c-C_6D_{12}	γ	77	2	5
neo-C_5H_{12}, 99.997%	γ	77	3	4
neo-C_5H_{12}, 99.9%	γ	77	4	4

[a] Concentrations of solute alkane and hydrogen iodide are 2.0 and 0.5 mol %, respectively. Yields are averages of two runs. Yields of t-C_4H_9 radicals in the photolysis of neo-C_5H_{12}–i-C_4H_{10}–HI or in the radiolysis of neo-C_5H_{12}–i-C_4H_{10} at 77 K are taken as 10. Since illumination times with uv light at 77 and 117 K were 2 and 1 min, respectively, yields are amounts of radicals per minute. Total dose of γ rays was 6.9×10^{18} eV/g. [b] The yields of the radicals were measured by double integration of the first-derivative esr signal of the radicals. Since only solute alkyl radical is formed selectivity in the photolysis of neo-C_5H_{12}–alkane–HI systems except for neo-C_5H_{12}–c-C_6D_{12}HI system, serious overlapping of the spectra of the solute radical and the neopentyl radical does not occur. The errors of radical yields are about 10%. In the radiolysis of neo-C_5H_{12}–alkane systems or in the photolysis of the neo-C_5H_{12}–c-C_6D_{12}–HI system, neopentyl and solute alkyl radicals are formed comparably, but the unidentified radical, which is produced in the radiolysis of pure neopentane, is not formed. A standard esr spectrum of neopentyl radical was obtained by the γ irradiation of neopentane containing N_2O (*cf.* ref 15). The yields of neopentyl radical were obtained from the height of central peak in the esr spectrum and the standard spectrum of neopentyl radical. The yields of solute radical were obtained by subtracting the yields of neopentyl radical from the total radical yields. The errors of radical yields are about 20% in this case. In the radiolysis of pure neopentane the yield of the solute alkyl radical represents the sum of the yields of t-C_4H_9 and unidentified radicals.

Results

Table I shows the yields of hydrogen and its isotopic composition in the photolysis of neo-C_5H_{12}–i-C_4H_9D–HI and the radiolysis of neo-C_5H_{12}–i-C_4H_9D in the solid and liquid. The dose of γ rays in the product analysis in this table is much higher than that in the esr measurement of radicals in Table II. Since the esr spectrum in the radiolysis of neo-C_5H_{12}–i-C_4H_9D at a dose of 5.9×10^{20} eV/g is approximately the same as that at a dose of 6.9×10^{18} eV/g, the dose effect may be negligible in this system.

Table II shows the yields of radicals in the photolysis of neo-C_5H_{12}–alkane–HI and the radiolysis of neo-C_5H_{12}–alkane. The yields of the radicals were measured by double integration of the first derivative esr signals of the radicals. The microwave power level used did not result in saturation of any of the signals. The radicals do not decay at all at 77 K, even if the sample is stored for 5 hr. When the sample is stored at 117 K, however, the radicals begin to decay in several minutes. Therefore the sample was illuminated for 1 min with uv light at 117 K and then measured at 77 K. In this case, the decay of the radical is negligible.

Figure 1 shows esr spectra of γ-irradiated pure neopentane at 77 K. Figure 1a is the spectrum obtained by the irradiation of 6.9×10^{18} eV/g. After the sample is preirradiated at 77 K with a dose of 3.4×10^{19} eV/g and melted, it is irradiated at 77 K with a dose of 6.9×10^{18} eV/g and its spectrum is shown in Figure 1b. The spectrum of three broad lines, indicated by ↕, is ascribed to the neo-C_5H_{11} radical. The spectrum of eight narrow lines, indicated by ↓, is ascribed to the t-C_4H_9 radical. The spectrum, indicated by ↓, is not identified as yet.

Figure 2 shows the preirradiation effect on the yields of t-C_4H_9 and unidentified radicals in the radiolysis of pure neopentane at 77 K. The peak heights of the unidentified radical and the t-C_4H_9 radical are normalized to 10 at the preirradiation dose of zero and 3.4×10^{19} eV/g, respectively.

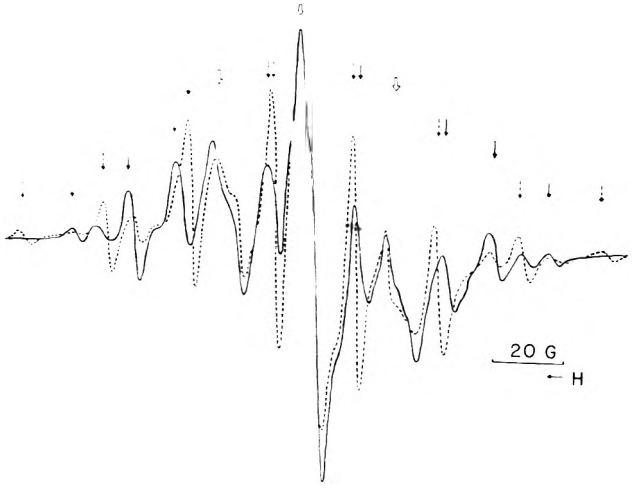

Figure 1. Esr spectra of γ-irradiated pure neopentane (>99.997%) at 77 K (a, solid line) and after the sample was preirradiated at 77 K with a dose of 3.4 × 10^{19} eV/g and melted (b, broken line).

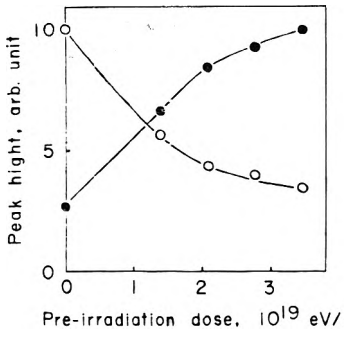

Figure 2. Preirradiation effect on the yields of t-C_4H_9 and unidentified radicals in the radiolysis of pure neopentane (>99.997%) at 77 K: ●, t-C_4H_9 radical; O, unidentified radical. The yields of t-C_4H_9 and unidentified radicals were determined by the measurement of peak heights of some lines, where the overlapping of the spectra of the two radicals are not serious. The peak heights of unidentified and t-C_4H_9 radicals are taken as 10 at the preirradiation doses of zero and 3.4 × 10^{19} eV/g, respectively.

Discussion

Selective Hydrogen Atom Abstraction by H Atoms. It was reported previously that solute alkyl radicals are formed selectively at 77 K by the photolysis of neopentane containing a small amount of alkane and hydrogen iodide.[6] One possible explanation for the selective formation of solute radicals is that hydrogen iodide and the alkane form a complex and dissolve in juxtaposition in the neopentane matrix. The possibility, however, may be quite small for the following three reasons. First, there is no evidence to support the idea that hydrogen iodide forms a complex with the alkane except neopentane. Since the yields of solute radicals in the photolysis of neo-C_5H_{12}–i-C_4H_{10}(1%)–HI(0.1%) are about 6 times as high as those in the photolysis of neo-C_5H_{12}–C_3H_8(1%)–HI(0.1%), it is expected from the complex hypothesis that isobutane is more favorable for the formation of the complex than propane. The propyl radical, however, is selectively formed in the photolysis of i-C_4H_{10}–C_3H_8(1%)–HI(0.1%) at 77 K.[6] Therefore, the results cannot be explained by the hypothesis of complex formation. Secondly, it has been observed that a large fraction of 3-methylpentyl radicals produced by the photolysis of HI in 3-methylpentane glass at 77 K decays within a few minutes, apparently by combination with iodine atoms formed near the same locations in the matrix when HI is dissociated.[10] The t-C_4H_9 radicals produced by the photolysis of HI in a neopentane–isobutane(1%) mixture, however, do not decay at all at 77 K, even if the sample is stored for 5 hr after the photolysis. Thirdly, it is shown in a later section that solute radicals are selectively formed at 77 K in the radiolysis of neopentane containing a small amount of alkane by the reaction of H atoms produced by the radiolysis of neopentane. The results show conclusively that the selective hydrogen atom abstraction does occur in the absence of hydrogen iodide.

If t-C_4H_9 radicals are formed by hydrogen atom abstraction by neopentyl radical in the photolysis of neo-C_5H_{12}–i-C_4H_9D–HI at 77 K, it is expected that only H_2 is formed.

$$HI \xrightarrow{h\nu} H + I \quad (1)$$

$$H + \text{neo-}C_5H_{12} \longrightarrow H_2 + C_5H_{11} \quad (2)$$

$$C_5H_{11} + i\text{-}C_4H_9D \longrightarrow C_5H_{11}D + t\text{-}C_4H_9 \quad (3)$$

Formation of HD in Table I, however, demonstrates clearly that hydrogen atoms produced in reaction 1 migrate through the neopentane matrix to react with i-C_4H_9D at 77 K

$$H + i\text{-}C_4H_9D \longrightarrow HD + t\text{-}C_4H_9 \quad (4)$$

H_2 is also formed in the photolysis of neo-C_5H_{12}–i-C_4H_9D–HI at 77 K. Since the neo-C_5H_{11} radical is not formed in the photolysis, H_2 may be formed by the concerted reaction between neo-C_5H_{12} and HI, which was proposed in the photolysis of HI in 3-methylpentane,[11] or by the reaction between H atom and HI.

Reaction 4 has the following specific characteristics.

(1) The results in Table I show that the formation of HD in the photolysis is completely suppressed at 198 and 262 K. Table II shows that the yield of the t-C_4H_9 radical in the photolysis of neo-C_5H_{12}–i-C_4H_9D–HI at 117 K is lower than that at 77 K. The yields of HD and t-C_4H_9 radicals represent the occurrence of reaction 4 and their temperature effects are shown in Figure 3. The reaction occurs favorably with decreasing temperature. Table I shows that similar temperature effects on the formation of HD are also observed in the radiolysis of neo-C_5H_{12}–i-C_4H_9D, where HI does not exist.

(2) The results in Table II show that remarkable isotope effects are observed in the photolysis of neo-C_5H_{12}–isobutane–HI at 117 K and neo-C_5H_{12}–cyclohexane–HI at 77 K.

(3) The yield of t-C_4H_9 radicals in the photolysis of neo-C_5H_{12}–i-C_4H_{10}–HI(0.05%) at 77 K was studied as a function of concentration of isobutane. The yields reach a plateau over 0.2 mol % of isobutane. H atoms collide with a number of neopentane molecules (about 500 molecules) before they react with isobutane. As discussed in a later section, H atoms produced by the radiolysis of neopentane react more selectively with the solute, where the concentration of the solute is less than 0.003%.

When H atoms are hot, we must assume that they migrate a long distance through the neopentane crystal without losing their kinetic energies at 77 K. This assumption, however, seems very improbable.

When H atoms are thermal, they react also with hydrogen iodide, because the activation energy for reaction 6 is nearly zero.[12]

$$HI \xrightarrow{h\nu} H + I \quad (1)$$

$$H + i\text{-}C_4H_{10} \longrightarrow t\text{-}C_4H_9 + H_2 \quad (5)$$

$$H + HI \longrightarrow I + H_2 \quad (6)$$

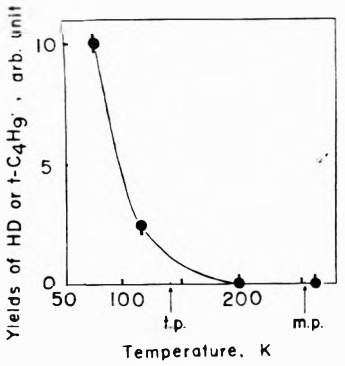

Figure 3. Temperature effect on the yields of HD and the t-C_4H_9 radical in the photolysis of neo-C_5H_{12}–i-C_4H_9D(2%)–HI(0.5%): ●, HD; ●, t-C_4H_9 radical. The yields are quoted from Tables I and II, and the values at 77 K are taken as 10.

Since reaction 5 competes with reaction 6, we must assume that the activation energy for (5) is also nearly zero at 77 K. It should be emphasized that reaction 5 in the gas phase needs 7.4 kcal/mol[13] as an activation energy. The low activation energy in the solid phase at 77 K may be explained by two effects. Sprague, *et al.*,[14] found that a thermal methyl radical abstracts a hydrogen atom from a matrix molecule at 77 K and ascribed the reaction to quantum mechanical tunneling (tunneling effect). As was described in the Introduction, C–H bond rupture reaction in solid alkane is affected remarkably by the condition of matrix. The potential energy surface of reaction in the crystalline field may be quite different from that in the gas phase. The activation energy may be lowered in special conditions, such as near defects, of the crystal (matrix effect). If the solute alkanes behave as defects, H atoms react selectively with the solute alkane rather than neopentane.

The temperature effect may be explained as follows. Since reaction 6 occurs without activation energy its rate at 77 K is approximately equal to that at 117 K. Figure 3 shows that the rate of reaction 4, which competes with reaction 6, increases with decreasing temperature. Though radicals do not decay at all at 77 K, they decay fast at 117 K. This fact indicates that the matrix at 117 K is much softer than that at 77 K. It seems that a drastic modification of the potential energy surface of reaction 4 is caused more efficiently in the rigid matrix at 77 K than in the soft matrix at 117 K. Therefore reaction 4 occurs more easily at 77 K than at 117 K.

The isotope effects can be explained by the difference in the mass between H and D,[14b] or the difference in the zero-point energy arising from the frequencies of C–H and C–D stretching.[11]

The discovery of the selective hydrogen atom abstraction reaction has proposed interesting problems in the reaction kinetics in the solid phase at 77 K.

Radical Formation in the Radiolysis of Pure Neopentane and Neopentane–Alkane Mixtures at 77 K. Smaller and Matheson[7] reported the esr spectrum of γ-irradiated neopentane at 77 K. Since both t-C_4H_9 and neo-C_5H_{11} radicals are formed, they considered that C–C bond rupture as well as C–H bond rupture occurs in the radiolysis of solid neopentane. Lin and Williams[15] also found t-C_4H_9 radicals in the radiolysis of neopentane and attributed the C–C bond rupture to neutralization reaction. Roncin[8] and Thyrion, *et al.*,[9] however, obtained quite different esr spectrum of γ-irradiated neopentane at 77 K. They found that t-pentyl(t-C_5H_{11}) and neo-C_5H_{11} radicals in the radiolysis of solid neopentane. It is difficult, however, to explain the formation of the t-pentyl radical by the fragmentation of the neopentane molecule.

Miyazaki, *et al.*,[4a] reported previously that t-C_4H_9 and neo-C_5H_{11} radicals are formed in the radiolysis of neopentane at 77 K. Recently we have found that the esr spectra depend appreciably upon the purity of the neopentane. Though neopentane used in the previous study was 99.9%, here we have used neopentane of 99.997%. Figure 1 shows the esr spectra of γ-irradiated neopentane (99.997%) at 77 K. The spectrum, which is similar to that reported by Roncin[8] and Thyrion, *et al.*,[9] indicates the formation of neo-C_5H_{11} radical and the unidentified radical. When the sample is preirradiated with a small dose, the yield of the unidentified radical decreases, while that of the t-C_4H_9 radical increases complementary (Figures 1b and 2). The results show that the formation of the t-C_4H_9 radical competes with that of the unidentified radical. Both radicals are not formed by the direct decomposition of the irradiated neopentane, but by the secondary process in the radiolysis. When a small amount of alkane is added to neopentane, the formation of the both radicals is suppressed and the solute alkyl radical is formed predominantly. As discussed later, the formation of solute radical in the radiolysis of neopentane–alkane mixtures is due to the reaction of H atoms produced by the fragmentation of neopentane. Therefore it seems that the unidentified radical is formed by the reaction of H atoms with the impurities (<0.003%) in the neopentane and the t-C_4H_9 radical by the reaction of H atoms with the products, such as isobutene or isobutane, which are formed in the yield of 0.4-G unit at 77 K.[16]

Miyazaki, *et al.*, studied the formation of the solute alkyl radical in the radiolysis of neopentane–alkane mixtures at 77 K.[4a] Since the formation of the alkyl radical is not affected by the addition of electron scavengers, such as N_2O, CO_2, and C_2H_5Cl, or a hole scavenger, such as tetramethylethylene, it was concluded that the alkyl radical is formed by the nonionic process.[4b] The following observations obtained here show that the solute alkyl radical is not formed by the excitation transfer from the irradiated neopentane to the solute, but by the selective hydrogen atom abstraction from the solute. (1) If excitation transfer is responsible for the formation of the solute alkyl radical, D_2 should be formed in the radiolysis of neo-C_5H_{12}–i-C_4H_9D at 77 K.

$$\text{neo-}C_5H_{12} \rightsquigarrow C_5H_{12}^* \quad (7)$$

$$C_5H_{12}^* + i\text{-}C_4H_9D \longrightarrow C_5H_{12} + C_4H_8D^* \quad (8)$$

$$C_4H_8D^* \longrightarrow i\text{-}C_4H_9 + D \quad (9)$$

$$D + C_4H_9D \longrightarrow i\text{-}C_4H_9 + D_2 \quad (10)$$

$$2D \longrightarrow D_2 \quad (11)$$

where $C_5H_{12}^*$ represents the excited neopentane molecule. Though HD is formed remarkably in the radiolysis of this system at 77 K, D_2 is not formed at all (Table I). (2) The fragmentation of the excited neopentane molecule produces only the neo-C_5H_{11} radical in the radiolysis at 77 K. According to the mechanism of the excitation transfer, the yield of neo-C_5H_{11} radical should decrease upon the addition of solute alkane. The yield, however, does not decrease upon the addition of i-C_4H_{10} or i-C_4H_9D (Table II). (3) When neo-C_5H_{12}–c-C_6H_{12}(2%) mixture is irradiated at 77 K by γ rays, the cyclohexyl radical and a small amount of the neopentyl radical are formed. When isobutene is added to

the mixture, the formation of the cyclohexyl radical is suppressed, while t-C_4H_9 radical is produced complementary by the addition of H atoms to isobutene.[17] The formation of the neopentyl radical is not affected by the addition of isobutene. (4) Temperature and isotope effects are also observed in neopentane–alkane mixtures (Tables I and II). These effects are quite similar to those in the hydrogen abstraction reaction of H atoms.

Therefore the mechanism of the formation of solute alkyl radical in the radiolysis of neo-C_5H_{12}–i-C_4H_9D at 77 K may be represented as follows:

$$\text{neo-}C_5H_{12} \rightsquigarrow C_5H_{12}^* \quad (7)$$

$$C_5H_{12}^* \longrightarrow \text{neo-}C_5H_{11} + H \quad (12)$$

$$H + i\text{-}C_4H_9D \longrightarrow t\text{-}C_4H_9 + HD \quad (4)$$

H atoms produced by the fragmentation of excited neopentane molecules react selectively with i-C_4H_9D to form t-C_4H_9 radicals and HD. It was reported that the radiolysis of solid 3-methylpentane-d_{14} produces no trapped D atoms,[18] while trapped H atoms are observed in the radiolysis of solid CH_4.[7,19] The formation of H atoms in the radiolysis of solid neopentane does not coincide with the result in the radiolysis of 3-methylpentane glass. It is not clear at present that the reactive H atoms in reaction 12 are the same ones as the trapped H atoms. This problem requires further studies in future. According to the reaction scheme, the yield of the t-C_4H_9 radical should be equal to that of the neo-C_5H_{11} radical. Table II shows, however, that the yield of the solute radical is much higher than that of the neo-C_5H_{11} radical. Therefore we must consider another origin of hydrogen atoms, for example

$$C_5H_{12}^* + C_5H_{12} \longrightarrow C_{10}H_{22} + 2H \quad (13)$$

Acknowledgment. The authors wish to express their appreciation to Professor Zen-ichiro Kuri of Nagoya University for his encouragement, and to Dr. Kozo Matsumoto of Nagoya University for mass spectrometric analysis.

References and Notes

(1) (a) T. Miyazaki, T. Wakayama, K. Fueki, and Z. Kuri, *Bull. Chem. Soc. Jap.*, **42**, 2086 (1969); (b) T. Wakayama, T. Miyazaki, K. Fueki, and Z. Kuri, *J. Phys. Chem.*, **74**, 3584 (1970); (c) Y. Saitake, T. Wakayama, T. Kimura, T. Miyazaki, K. Fueki, and Z. Kuri, *Bull. Chem. Soc. Jap.*, **44**, 301 (1971).
(2) T. Wakayama, T. Miyazaki, K. Fueki, and Z. Kuri, *Bull. Chem. Soc. Jap.*, **44**, 2619 (1971).
(3) M. Fukaya, T. Wakayama, T. Miyazaki, Y. Saitake, and Z. Kuri, *Bull. Chem. Soc. Jap.*, **46**, 1036 (1973).
(4) (a) T. Miyazaki, T. Wakayama, M. Fukaya, Y. Saitake, and Z. Kuri, *Bull. Chem. Soc. Jap.*, **46**, 1030 (1973); (b) M. Kato, Y. Saitake, T. Miyazaki, and Z. Kuri, *ibid.*, **46**, 2004 (1973).
(5) D. J. Henderson and J. E. Willard, *J. Amer. Chem. Soc.*, 91, 3014 (1969).
(6) T. Wakayama, T. Miyazaki, K. Fueki, and Z. Kuri, *J. Phys. Chem.*, **77**, 2365 (1973).
(7) B. Smaller and M. S. Matheson, *J. Chem. Phys.*, **28**, 1169 (1958).
(8) J. Roncin, *Mol. Cryst.*, **3**, 117 (1967).
(9) F. Thyrion, J. Dodelet, C. Fauquenoit, and P. Claes, *J. Chim. Phys.*, **65**, 227 (1968).
(10) W. G. French and J. E. Willard, *J. Phys. Chem.*, **72**, 4604 (1968).
(11) L. Perkey and J. E. Willard, *J. Chem. Phys.*, **60**, 2732 (1974).
(12) J. H. Sullivan, *J. Chem. Phys.*, **30**, 1292 (1959); **36**, 1925 (1962).
(13) B. A. Thrush, *Progr. React. Kinet.*, **3**, 89 (1965).
(14) (a) E. D. Sprague and F. Williams, *J. Amer. Chem. Soc.*, **93**, 787 (1971); (b) R. J. LeRoy, E. D. Sprague, and F. Williams, *J. Phys. Chem.*, **76**, 546 (1972); (c) A. Campion and F. Williams, *J. Amer. Chem. Soc.*, **94**, 7633 (1972); (d) E. D. Sprague, *J. Phys. Chem.*, **77**, 2066 (1973).
(15) J. Lin and F. Williams, *J. Phys. Chem.*, **72**, 3707 (1968).
(16) W. H. Taylor, S. Mori, and M. Burton, *J. Amer. Chem. Soc.*, **82**, 5817 (1960).
(17) M. Kato, T. Miyazaki, and Z. Kuri, unpublished results.
(18) D. Timm and J. E. Willard, *J. Phys. Chem.*, **73**, 2403 (1969).
(19) (a) D. W. Brown, R. E. Florin, and L. A. Wahl, *J. Phys. Chem.*, **66**, 2602 (1962); (b) W. Gordy and R. Morehouse, *Phys. Rev.*, **151**, 207 (1966).

A Photoelectron–Photoion Coincidence Study of the Ionization and Fragment Appearance Potentials of Bromo- and Iodomethanes

Bilin P. Tsai, Tomas Baer,* Arthur S. Werner, and Stephen F. Lin

William R. Kenan, Jr. Laboratory of Chemistry, University of North Carolina, Chapel Hill, North Carolina 27514
(Received September 23, 1974)

The ionization and fragment appearance potentials of CH_3Br, CH_2Br_2, $CHBr_3$, CH_3I, CH_2I_2, and CHI_3 have been derived from an analysis of zero kinetic energy photoelectron–photoion coincidence spectra in the energy range 9–14 eV. Such coincidence spectra yield more precise appearance potentials than integral photoionization scans because of the inherently sharper onsets and the discrimination against competing processes such as ion-pair formation and collisionally induced dissociation.

Introduction

The ionization and fragmentation of the halogenated alkanes exhibit a number of unusual properties. The highest filled molecular orbitals have the predominant character of the halogen lone pairs and the resulting first photoelectron bands exhibit the features which are characteristic of the removal of nonbonding electrons.[1,2] Nevertheless the molecular ions, which under these circumstances might be expected to be very stable, in fact readily fragment. Both the C–X and the C–H bond energies decrease with increasing halogen substitution resulting, in the case of carbon tetrachloride[3] and carbon tetrafluoride,[4] in unstable parent ions. The driving force for this trend is the stability of the

planar halogenated methyl ions which have a closed shell electronic structure.

A characteristic feature in the fragmentation of the chloromethane ions produced by photoionization below 13.5 eV is the absence of hydrogen loss even though this reaction in CH_3Cl is energetically favored over chlorine loss. In all the other chloro-, bromo-, and iodomethanes, halogen atom loss is energetically favored, and in two molecules (CH_3Br and CH_3I) which we studied with sufficient mass resolution to resolve the H loss fragment, we again found no evidence for H loss. We can rule out an activation barrier because electron impact experiments such as those of Lossing[5] produce strong onsets for hydrogen loss in CH_3Cl^+ at precisely the thermodynamic appearance potential. This point is discussed further elsewhere.[6]

Little work has been done on the ionization and especially the fragment appearance potentials of the bromo- and iodomethanes. There are two investigations in which the photoelectron spectra (PES) of all the molecules in this study were obtained.[1,2] In addition other workers have reported PES of the monohalomethanes.[7-9] Several electron impact investigations have been reported,[10-18] however, none have dealt with CH_2I_2 or CHI_3 and only one[16] with $CHBr_3$. With the exception of one study,[19] the available photoionization spectra (PI) have been measured without mass analysis and at low photon resolution.[20-22] As a result much of the published work concerns only the parent ionization potentials.

We have undertaken this study of the bromo- and iodomethanes in order to establish reliable values for fragment ion appearance potentials and heats of formation.

Experimental Section

The apparatus, presented in detail in a previous paper,[3] will only briefly be described here. A hydrogen "many-line" light source dispersed by a 1-m vacuum uv monochromator to give 2-Å resolution ionized the molecules in a photoionization chamber; the sample gas pressure was approximately 10^{-4} Torr. Ions were mass analyzed with a quadrupole mass filter and/or by time of flight. A nominally zero kinetic energy (ZKE) electron analyzer[23] was used to provide both the "start" of the ion time of flight as well as to obtain ZKE photoelectron spectra. The ion flight time distribution was displayed on a multichannel pulse height analyzer and the appropriate region was read out. During a scan, ZKE electrons, total ions, ZKE electron–ion coincidences, as well as photon intensity and sample gas pressure were counted for preset time intervals. The data were reduced by normalizing to the photon intensity and sample gas pressure. All spectra were taken at room temperature. The quadrupole mass filter was used only on CH_3Br and CH_3I because the masses of the other molecules exceeded the limit of our quadrupole.

Results

In our previous study[3] of the chloromethanes and carbon tetrabromide, we developed a general procedure for fitting calculated photoionization spectra to the experimental curves. The purpose of this was to take into account the contribution of hot bands and variations in the ionization transition probability in calculating ionization and fragment appearance potentials. This procedure is particularly necessary for accurately determining the latter. The calculated photoionization yield, PY, at a photon energy, E, is given by eq 1 in which $g(\epsilon)$ is the density of states of the

$$\mathrm{PY}(E) = \int_0^\infty d\epsilon \int_0^{E+\epsilon-E_0} dx\ g(\epsilon)e^{-\epsilon/kT}p(x) \quad (1)$$

ground state molecule, and $p(x)$ is the ionization transition probability at an energy, x, above the ionization potential. E_0 is the adiabatic ionization or fragment appearance potential. The density of states can be determined by direct count, and $p(x)$ is known from PES. By using the PES for $p(x)$ we neglect the contribution of autoionization, an assumption which can be justified only for certain systems. For example, the PI spectrum of CH_3I[24] shows numerous autoionization peaks between threshold and 0.7 eV above the first ionization potential. However, for the molecules studied here, the fragmentation onsets were in regions which exhibited relatively little autoionization.

In the present study we found that the hot bands contribute significantly more to the total ionization than they did in the chloromethanes. In addition, autoionization increases with increasing mass of the halogen. As a result the analysis of the bromo- and iodomethanes was considerably more difficult. In order to sharpen up the onsets as well as to discriminate against autoionization and possible competing processes such as ion-pair formation and collisionally induced fragmentation we analyzed the ZKE electron–ion coincidence curves. For such curves, eq 1 reduces to eq 2 in which integration over the distribution of ejected electron energies is eliminated.

$$\mathrm{CY}(E) = \int_0^\infty d\epsilon\ g(\epsilon)e^{-\epsilon/kT}p(E+\epsilon-E_0) \quad (2)$$

Figures 1–4 show the ZKE electron–ion coincidence spectra in which the counts are normalized to the total light intensity. A summary of the derived ionization and fragment appearance potentials of the molecules investigated is shown in Tables I and II along with the results of other workers. The values for the heats of formation were derived without regard to a possible correction due to kinetic energy release. These values are thus upper limits. The kinetic energy release for Cl loss from $CH_2Cl_2^+$ has been measured by Cooks et al.[25] and found to be less than 0.015 eV.

As in $CH_2Cl_2^+$, both $CH_2Br_2^+$ and $CH_2I_2^+$ show collisional dissociation to give CH_2X^+ as evidenced by the long slowly rising tails on the daughter PI curves below the true appearance potentials. The intensity of this bimolecular contribution decreases with decreasing sample gas pressure, but due to the high cross section for collisional dissociation[26] the tails are evident even in the lowest pressure runs. Although the tail cannot be totally suppressed in the ion curve, the coincidence curves do effectively suppress the contribution of the bimolecular reaction because of the displaced flight time of the collisionally induced CH_2X^+ fragments.

Discussion

CH_3Br. The photoionization curve of methyl bromide is well known[19-21] and will not be presented in this paper. The first ionization potential is due to the ejection of an electron from a nonbonding $4p\pi_e$ orbital localized on the bromine atom. The onset is very sharp and gives an ionization potential, 10.54 eV, in good agreement with those obtained from photoelectron, photoionization, and absorption spectroscopy (Table I). The coincidence spectrum for the CH_3^+ fragment is similar to the photoionization spectrum of Krauss[19] except that our onset is sharper. Our threshold

TABLE I: First Ionization Potentials

	CH_3Br^+	$CH_2Br_2^+$	$CHBr_3^+$	CH_3I^+	$CH_2I_2^+$	CHI_3^+
$\Delta H^\circ_f(298)$, kcal mol^{-1} [a]	234.6 ± 0.3	241.5 ± 1.5	245.6 ± 0.4	222.9 ± 0.3	245.1 ± 0.6	263.2 ± 0.4
Technique	Ionization potentials, eV					
Photoionization	10.54 ± 0.01[b] 10.528 ± 0.005[c] 10.53 ± 0.01[d,e]	10.52 ± 0.05[b] 10.49 ± 0.02[d]	10.48 ± 0.02[b] 10.51 ± 0.02[d]	9.533 ± 0.01[b,f] 9.54 ± 0.01[d] 9.550 ± 0.006[c] 9.55 ± 0.1[e]	9.46 ± 0.02[b]	9.25 ± 0.02[b]
Photoelectron spectroscopy	10.53 ± 0.01[h] 10.53 ± 0.02[i] 10.53 ± 0.03[j] 10.54[k,l]	10.61[k] 10.63[l]	10.47[k] 10.44[l]	9.50 ± 0.03[j] 9.52 ± 0.02[i] 9.54[k] 9.55[l]	9.46[k] 9.52[l]	9.26 ± 0.02[l]
Electron impact	10.5[m,n] 10.53 ± 0.02[o] 10.56[p] 10.8 ± 0.01[q]	10.8 ± 0.01[q]		9.50[m,n] 9.51 ± 0.02[o] 9.59[p]		
Penning ionization	10.54 ± 0.04[r]			9.55 ± 0.04[r]		
Absorption spectroscopy	10.488 ± 0.003[s] 10.541 ± 0.003[t]			9.49 ± 0.003[s] 9.538[t] 9.54[u]		

[a] Based on our ionization potentials and the following heats of formation:[10,30] CH_3Br (−8.4); CH_2Br_2 (−1); $CHBr_3$ (4); Br (26.74); CH_3I (3.1); CH_2I_2 (27); CHI_3 (50); I (25.5); H (52.1). The values are in kcal mol^{-1}. [b] This work. [c] Reference 21. [d] Reference 20. [e] Reference 19. [f] Reference 24. [g] Reference 22. [h] Reference 7. [i] Reference 8. [j] Reference 9. [k] Reference 1. [l] Reference 2. [m] Reference 14. [n] Reference 15. [o] Reference 11. [p] Reference 12. [q] Reference 13. [r] Reference 29. [s] Reference 28. [t] Reference 27. [u] Reference 31.

TABLE II: X Loss Appearance Potentials

	CH_3^+/CH_2Br	CH_2Br^+/CH_2Br_2	$CHBr_2^+/CHBr_3$	CH_3^+/CH_3I	CH_2I^+/CH_2I_2	CHI_2^+/CHI_3
$\Delta H^\circ_f(298)$, kcal mol^{-1} [a]	260.0 ± 0.6	234.0 ± 0.4	223.9 ± 0.4	260.0 ± 0.6	244.6 ± 0.4	249.7 ± 0.4
Technique	Appearance potentials, eV					
Photoionization	12.80 ± 0.03[b]	11.35 ± 0.02[b]	10.70 ± 0.02[b]	12.25 ± 0.03[b]	10.55 ± 0.02[b]	9.77 ± 0.02[b]
Electron impact	12.77[c]	10.93 ± 0.04[d] 11.5 ± 0.01[e]	10.80 ± 0.01[d]	12.2 ± 0.05[f] 12.22 ± 0.03[g] 12.36 ± 0.02[b] 12.4 ± 0.2[i]		

[a] Based on our appearance potentials and the neutral heats of formation listed under Table I. [b] This work. [c] Reference 19. [d] Reference 16. [e] Reference 13. [f] Reference 15. [g] Reference 18. [h] Reference 17. [i] Reference 14.

analysis yields an appearance potential of 12.80 eV, which is precisely the thermodynamic onset for Br loss.

As mentioned previously, only bromine loss is detected, however, the appearance potential (AP) of CH_2Br^+ from CH_3Br^+ can be determined from a knowledge of the heat of formation of CH_2Br^+ (see Table II). According to eq 3, the

$$AP(CH_2Br^+) = \Delta H^\circ_f(H) + \Delta H^\circ_f(CH_2Br^+) - \Delta H^\circ_f(CH_3Br) + KE = 12.77 \text{ eV} + KE \text{ released} \quad (3)$$

thermodynamic AP of CH_2Br^+ neglecting kinetic energy release is 12.77 eV, which makes it nearly isoenergetic with Br loss.

CH_2Br_2. Figure 1 shows the coincidence curves for $CH_2Br_2^+$ and CH_2Br^+. The fourfold degenerate halogen lone pair electron states are split into three peaks which are poorly resolved in Figure 1. However three peaks are clearly visible in the PES[1,2] which indicates that one is a composite of two states. It was impossible to fit the $CH_2Br_2^+$ coincidence curve with our fitting procedure and as a result no reliable IP was derived. The slow onset between 10.4 and 10.5 eV could possibly be attributed to autoionization from hot bands, although Price's PES[1] also exhibits an anomalously slow onset. Our best guess is that the IP of CH_2Br_2 is 10.52 ± 0.05 eV. The low value is chosen partly to allow the ionization potentials of successively higher substituted methyl bromides to monotonically decrease in a manner similar to that in the series of methyl iodides.

The CH_2Br^+ onset was very sharp and strong. The thermodynamic appearance potential for H loss is 12.02 eV. However lack of sufficient mass resolution did not allow us to determine whether H loss does occur.

$CHBr_3$. In the bromoform ion the $4p\pi_e$ degenerate state splits into four states, two of which remain degenerate. The coincidence curve, shown in Figure 2, was obtained by time-of-flight mass analysis of the ion product in which the photoelectron and photoion provided the start and stop signals, respectively. The coincidence scan shows only the

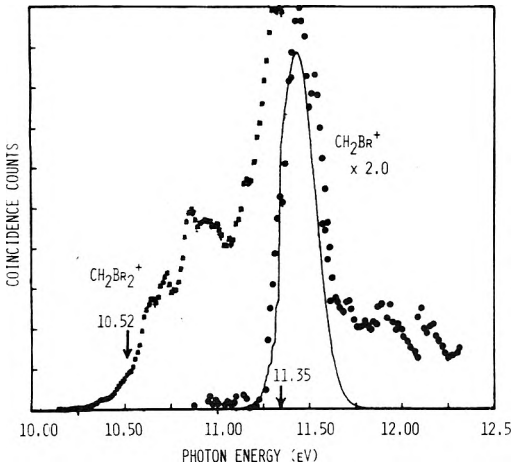

Figure 1. The ZKE electron–ion coincidence spectrum of CH_2Br_2 and its fragment. The parent ion data beyond 11.3 eV is not plotted because it nearly overlaps the daughter ion signal. The points are experimental values and the solid lines are calculated fits. The parent ion curve could not be fit. (See Text.)

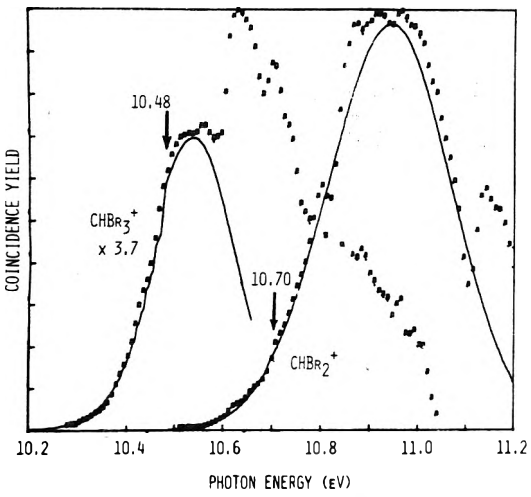

Figure 2. The ZKE electron–ion coincidence spectrum of $CHBr_3$ and its fragment. The points are experimental values and the solid lines are calculated fits.

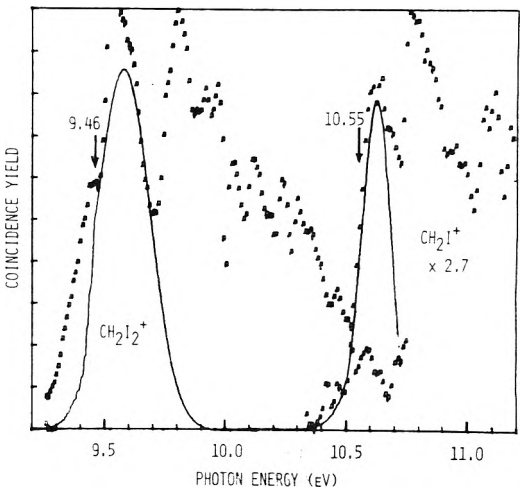

Figure 3. The ZKE electron–ion coincidence spectrum of CH_2I_2 and its fragment. The points are experimental values and the solid lines are calculated fits.

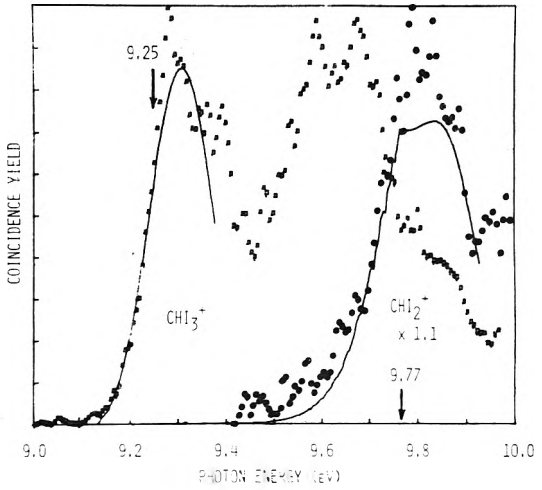

Figure 4. The ZKE electron–ion coincidence spectrum of CHI_3 and its fragment. The points are experimental values and the solid lines are calculated fits.

first state and the calculated fit gives an IP of 10.48 eV, 40 meV above Turner's PES peak.[2] Our value is further supported by a reported PES value[1] of 10.47 eV. This leads us to suspect the low value which Turner assigned to the first PES peak. The slow rise in the threshold region indicates a substantial hot band contribution. The peak at 10.65 eV is assigned to AI since there is no electronic state observed[1,2] in that region. The fragment ion threshold, like that of the parent, rises very gradually and the derived appearance potential is 10.70 eV. The thermodynamic appearance potential for H loss from $CHBr_3^+$ was calculated to be 12.23 eV using a value[3] for $\Delta H°_f$ (CBr_3^+) of 233.7 kcal mol^{-1} however lack of high-resolution mass analysis prevented us from distinguishing the parent ion from the H loss fragment ion.

CH_3I. The photoionization curve of CH_3I has been published by several workers,[19-22] and most recently by us[24] and will not be shown here. Like CH_3Cl and CH_3Br, the first electron ejected is from the valence $np\pi_e$ orbital localized on the iodine atom. Our ionization potential, 9.533 eV, agrees well with the spectroscopic value,[27] 9.538 eV. The second state of the doublet occurs at 10.158 eV giving a spin–orbit separation of 0.622 eV, in precise agreement with Price's value, 0.622 eV. There is a great deal of autoionization from Rydberg states of the series converging to the upper state, $^2E_{1/2}$.

Although the I loss produced a strong CH_3^+ onset at 12.25 eV, no H loss was observed, the thermodynamic onset for the latter process being 12.74 eV.

CH_2I_2. The coincidence curves of $CH_2I_2^+$ and CH_2I^+ were obtained by TOF mass analysis of the ions and are shown in Figure 3. Besides two PES[1,2] studies there have been no other data reported for the ionization and fragment appearance potentials of CH_2I_2. Like CH_2Br_2, four states result from the splitting of the degenerate $4p\pi_e$ state: b_2 at 9.5 eV; a_2 at 9.8 eV; a_1 at 10.3 eV; and b_1 at 10.6 eV.[1,2]

The first two electronic states are shown in the parent coincidence curve. The best fit to this curve in the threshold region yields an IP of 9.46 eV. There is a great deal of autoionization: the shoulder on the low-energy side of the threshold, as well as the structure from 9.9–10.3 eV, are assigned to autoionization from initially excited vibrational states of the neutral. The second electronic state occurs at 9.80 eV which agrees well with the PES value.

As in the other dihalomethanes, $CH_2I_2^+$ undergoes collisional dissociation to yield CH_2I^+. However the coincidence technique effectively reduces interference due to fragmentation by ion–molecule collisions. The derived daughter appearance potential is 10.55 eV.

The calculated appearance potential of CHI_2^+ is 11.92 eV but lack of high-resolution mass analysis did not allow us to distinguish the parent ion from the H loss fragment ion.

CHI_3. Since CHI_3 has an m/e >200, the ionization products were TOF mass analyzed and the coincidence scans (Figure 4) were studied. There are no literature values except for PES data[2] for the ionization potential of CHI_3 with which to compare our results. Since the PES data shows a broad first peak, a precise onset cannot be determined from it. The four electronic states of CHI_3^+ have not been identified with certainty although two are known to be degenerate. The states corresponding to the first two PES peaks are evident in our coincidence scan. From our data, the IP of CHI_3 is 9.25 eV.

In the threshold fit for the fragmentation process, the transition probability, $p(x)$, was approximated by a sum of two gaussians corresponding to the second and third PES peaks. The resulting calculated onset is 9.77 eV.

Acknowledgment. We are grateful for financial support from the following agencies: the U.S. Army Research Office, Durham; the Research Corporation; and the Petroleum Research Fund, administered by the American Chemical Society.

References and Notes

(1) A. W. Potts, H. J. Lempka, D. G. Streets, and W. C. Price, *Phil. Trans. Roy. Soc., Ser. A*, **268**, 59 (1970).
(2) D. W. Turner, C. Baker, and C. R. Brundle, "Molecular Photoelectron Spectroscopy," Wiley, London, 1970.
(3) A. S. Werner, B. P. Tsai, and T. Baer, *J. Chem. Phys.*, **60**, 3650 (1974).
(4) C. J. Noutary, *J. Res. Natl. Bur. Stand.*, **72**, 479 (1968).
(5) F. P. Lossing, *Bull. Soc. Chim. Belg.*, **81**, 125 (1972).
(6) T. Baer, A. S. Werner, B. P. Tsai, and S. F. Lin, *J. Chem. Phys.*, **61**, 5468 (1974).
(7) T. A. Hashmall and E. Heilbronner, *Angew. Chem., Int. Ed. Engl.*, **9**, 305 (1970).
(8) F. Brolgi and E. Heilbronner, *Helv. Chim. Acta*, **54**, 1423 (1971).
(9) T. L. Ragle, I. A. Stenhouse, D. C. Frost, and C. A. McDowell, *J. Chem. Phys.*, **53**, 178 (1970).
(10) J. L. Franklin, J. G. Dillard, H. M. Rosenstock, J. T. Herron, K. Draxl, and F. H. Field, *Nat. Stand. Ref. Data Ser., Nat. Bur. Stand.*, **No. 26** (1969).
(11) D. C. Frost and C. A. McDowell, *Proc. Roy. Soc., Ser. A*, **241**, 194 (1957).
(12) J. M. Williams and W. H. Hamill, *J. Chem. Phys.*, **49**, 4467 (1968).
(13) H. Gutbier, *Z. Naturforsch A*, **9**, 348 (1954).
(14) V. H. Dibeler and R. M. Reese, *J. Res. Nat. Bur. Stand.*, **54**, 127 (1955).
(15) S. Tsuda, C. E. Melton, and W. H. Hamill, *J. Chem. Phys.*, **41**, 689 (1964).
(16) R. I. Reed and W. Snedden, *Trans. Faraday Soc.*, **55**, 876 (1956).
(17) C. A. McDowell and B. C. Cox, *J. Chem. Phys.*, **20**, 1496 (1952).
(18) F. P. Lossing and G. P. Semeluk, *Can. J. Chem.*, **48**, 955 (1970).
(19) M. Krauss, J. A. Walker, and V. H. Dibeler, *J. Res. Nat. Bur. Stand., Sect. A*, **72**, 281 (1968).
(20) K. Watanabe, T. Nakayama, and J. Mottl, *J. Quant. Spectrosc. Radiat. Transfer*, **2**, 369 (1962).
(21) A. J. C. Nicholson, *J. Chem. Phys.*, **43**, 1171 (1965).
(22) J. D. Morrison, H. Hurzeler, M. G. Inghram, and H. E. Stanton, *J. Chem. Phys.*, **33**, 821 (1960).
(23) T. Baer, W. B. Peatman, and E. W. Schlag, *Chem. Phys. Lett.*, **4**, 243 (1969).
(24) (a) T. Baer and B. P. Tsai, *J. Electron Spectrosc.*, **2**, 25 (1973); (b) B. P. Tsai and T. Baer, *J. Chem. Phys.*, **61**, 2047 (1974).
(25) E. G. Jones, J. H. Beynon, and R. G. Cooks, *J. Chem. Phys.*, **57**, 2652 (1972).
(26) T. Baer, L. Squires, and A. S. Werner, *Chem. Phys.*, **6**, 325 (1974).
(27) W. C. Price, *J. Chem. Phys.*, **4**, 539 (1936).
(28) H. Sponer and E. Teller, *Rev. Modern Phys.*, **13**, 75 (1941).
(29) V. Cermak, *Collect. Czech. Chem. Commun.*, **33**, 2739 (1968).
(30) D. D. Wagman, W. H. Evans, V. B. Parker, I. Halow, S. M. Bailey, and R. H. Schumn, *Nat. Bur. Stand. Tech. Note*, **No. 270-3** (1968).
(31) R. A. Boschi and D. R. Salahub, *Mol. Phys.*, **24**, 289 (1972).

Heats of Hydrogenation of Large Molecules. I. Esters of Unsaturated Fatty Acids

Donald W. Rogers* and Nafees A. Siddiqui

Chemistry Department, The Brooklyn Center, Long Island University, Brooklyn, New York 11201 *(Received August 16, 1974)*

Publication costs assisted by the National Institutes of Health

We have developed a hydrogen microcalorimeter for the purpose of determining heats of hydrogenation and heats of formation of large molecules, particularly those of biochemical significance. This paper reports and interprets results obtained for the seven unsaturated and polyunsaturated methyl esters of palmitoleic, palmitelaidic, oleic, elaidic, linoleic, linoelaidic, and linolenic acids. The heats of formation follow from the heats of formation of the saturated reaction products, methyl palmitate and methyl stearate, by Hess' law addition. We believe that these molecules are the largest ever studied by hydrogen calorimetry and that the sample size on which reliable data can be obtained, about 15 μg, is among the smallest. Standard deviations of six replicate samples of each ester were about 0.3 kcal/mol per double bond.

Introduction

Recently we described a hydrogen microcalorimeter[1] with which we were able to determine the heats of hydrogenation of micromolar quantities of unsaturated hydrocarbons dissolved in an inert solvent. We developed this variant on liquid-phase hydrogen calorimetry as it is usually practiced[2-4] for two principal reasons. The method requires very little material, making it applicable to biologically interesting substances which are commercially available in great variety but usually in small quantities and at considerable expense. Second, the rapidity of the method offers

one the chance of gathering a statistically meaningful collection of data in a reasonable amount of time.

The first class of compounds we wished to study was the class of methyl esters of long-chain unsaturated fatty acids. The fatty acid portion of the molecule is of obvious interest biochemically. We chose the methyl esters because the analytical chemistry of reactants and saturated products is simpler, or at least better documented, than the analytical chemistry of the free fatty acids or the glycerides which we mean to make the subject of subsequent papers.

Theory

By far the most widely used method of determining enthalpies of formation has been and will no doubt continue to be combustion calorimetry. Large molecules, however, present special problems. They are usually far more difficult to purify than small molecules and, more fundamental, the heats of combustion of large molecules are numerically much greater than the energy differences we seek. Thus, one might rely on combustion data to determine the relatively small heat of isomerization between *cis*- and *trans*-2-butene but the same calculation[5,6] for *cis*- and *trans*-octadec-9-enoic acids (oleic and elaidic acids) would be highly suspect because of the magnitudes of their heats of combustion and the probable absolute error involved. The obvious and serious limitation on hydrogen thermochemistry is that it is applicable only to molecules which are unsaturated and can be quantitatively hydrogenated to give a single, well-defined product. Nevertheless, hydrogen calorimetry, when these conditions are met, retains the advantage of giving small numbers, making it applicable to problems in cis–trans isomerism[7,8] resonance enthalpies,[9,10] conjugation and hyperconjugation enthalpies,[10,11] ring strain,[12] molecular crowding and neighboring group interactions,[13,14] and molecular conformations.[3,15]

Experimental Section

Reagents. All samples of fatty acid methyl esters were obtained from Analabs Inc.[16] and certified by the manufacturer to be 99+% pure as demonstrated by glc, tlc, or both. Samples were provided by the manufacturer in ampoules sealed under an inert atmosphere. Upon receipt, samples were refrigerated until use. All data reported below were obtained within 2 or 3 hr of the time the ampoule was opened.

Sources of all other reagents and materials have been given.[1]

Procedure. The apparatus and experimental method followed have been described in detail elsewhere.[1] Briefly, it consists of hydrogenating a standard solution of 1-hexene in *n*-hexane by direct injection into the calorimeter followed by hydrogenation of a similar solution of the unknown ester. Assuming that the heat of hydrogenation of 1-hexene is known, one computes ΔH_h of the ester from the ratio of its heat output per millimole to that of the standard.

Specific Procedure for Fatty Acid Methyl Esters. We quickly found it best to have the standard solution and unknown solution at such concentrations that they gave off about the same amount of heat upon hydrogenation. This was not difficult to do because, even in the case of reactions which differed greatly in exothermicity, we could control the concentrations of standard and sample so as to make them *thermochemically* equivalent. In these experiments, we guessed at the heat of hydrogenation of the ester in question on the basis of number of double bonds and the cis–trans isomerism and made up the standard accordingly. Sample size was 80 μl of an approximately 20% solution of ester in *n*-hexane. If the deflections of standard and unknown differed by more than 5%, their ratio was used to make up a new standard which would produce a deflection as close as possible to that of the unknown. Thus, by selection of the proper concentration for the standard, we had already determined the heat of hydrogenation to within better than 5%, about 1–2 kcal/mol for a monounsaturated ester, and the remainder of the experiment was devoted to reducing this uncertainty as much as possible.

Diagnostic Tests. We used both gas chromatography and mass spectroscopy to test for completeness of hydrogenation. In a typical example, the calorimeter was opened immediately after the last hydrogenation and the reaction slurry was filtered to remove the catalyst. The filtrate (1 μl) was injected into a gas chromatograph[17] the column of which was packed with 3% silicone on Chromosorb W.[18] Helium was the carrier gas having a flow rate of 20 ml/min and the effluent was monitored by means of a hydrogen flame ionization detector. The attenuation was set at 50× and, in all cases reported here, only peak was observed. Next, an aliquot portion of the reaction mixture was "doped" with a small amount of the appropriate unsaturated fatty acid ester and the chromatogram taken again. Two peaks appeared in the second chromatogram, a small one, due to the unsaturate at shorter retention time[19] and the main peak, identical with the one previously observed. By measuring the area under the two peaks at attenuation of 200× or 500× for the main peak and 20× or 50× for the small peak, we estimated the per cent contamination of the reaction product by the unsaturated reactant. In a typical example, at a column temperature of 200°, an estimated 0.42% of methyl linoleate produced a clearly discernable peak 0.2-in. high and 0.4-in. broad at the base, well separated from the main peak due to methyl stearate. The unadulterated reaction mixture showed a perfectly level base line at this retention time leading us to believe that any methyl linoleate present must have been at a concentration well under 0.1%. Retention times at 200° were about 7.5 and 9 min for methyl linoleate and stearate. Separation was less favorable for methyl elaidate and stearate necessitating a reduction to 182° for good separation with a corresponding increase in retention times to 14 and 16 min for the minor and major peaks, respectively. Methyl palmitate showed good separation from its unsaturates at 150°.

Mass spectroscopic verification of completeness of reaction was carried out by evaporating off the hexane from a sample of used calorimeter fluid leaving a waxy residue of methyl stearate or palmitate which was introduced into a mass spectrometer[20] by means of a solids probe. The parent peak of methyl stearate or palmitate was located at mass 296.46 or 268.41, respectively, along with the satelite $n + 1$ peaks[21] at 297.46 and 269.41. At full scale amplification, there was no evidence of an $n - 2$ peak such as would have been expected if a trace of unsaturate had been present. Intentionally contaminated samples led us to believe that this would have been an extremely sensitive method of detecting incomplete reactions. Since, however, the mass spectrometer was "down" throughout most of the time occupied by these studies, mass spectroscopic verifications of completeness of reaction are far more fragmentary than we would have hoped. Suffice it to say that no mass spectra we

obtained indicated any contamination of the reaction product by unsaturate. We feel that either the glc criterion or the mass spectroscopic criterion is sufficient to establish completeness of hydrogenation. All methyl esters reported here have passed the first test and several have passed the second.

Results and Discussion

Heats of formation of most unsaturated fatty acids, esters, and glycerides are either unknown or too inaccurately known to be useful. Domalski, in his critical review,[22] lists only four heats of formation for unsaturated acids having more than 12 carbon atoms: oleic, elaidic, erucic, and brassidic acids (the cis and trans isomers, respectively, of ocadecenonic and docosenoic acids). Of these four references, the latter two[23,24] are more than 80 years old and the most recent reference, to the former two,[5] is 44 years old.

Among the methyl esters of the unsaturated fatty acids, only methyl oleate and methyl elaidate have been investigated, these by Keffler[6] in 1937.

We do not wish to imply that all old data are bad data but that, in thermochemistry, which depends most strongly on the known purity of the sample, data on fatty acids and esters which predate the purification techniques of glc, liquid chromatography, and tlc are so highly suspect as to be useless no matter how carefully or well the thermochemistry was done. Possible exceptions are some the late data of Keffler[6] in which he obtained consistent values of −1.6 kcal/mol for the cis to trans conversion of methyl, *n*-propyl, and *n*-butyl esters of oleic and elaidic acids. These plausible results are, however, given along with the implausible value of +0.7 kcal/mol for isomerization of ethyl oleate to ethyl elaidate which throws doubt on the remaining three results, particularly as there is nothing to distinguish his experiments on the ethyl esters from the others.

Our preliminary results indicated that the heat of hydrogenation of the cis double bond in oleic acid is exothermic to the extent of about 35 kcal/mol. This seemed unreasonably high to the senior author and to one of his correspondents.[25] We have also noted that enthalpimetric determinations of unsaturated acids and esters show an unaccountably high experimental scatter and are generally less reliable than enthalpimetric data on simple olefins.[26]

While there is no precedent for it in the literature and it is not predicted theoretically, we felt that the possibility of destabilizing effect of very long chains on an internal double bond should be investigated. If such a destabilizing effect did exist, one would expect it to be progressive in nature and for the beginning of the trend to be observable in C_8 and C_{10} hydrocarbons with cis double bonds. Interpolating between 3-hexene with ΔH = −28.57 kcal/mol and approximately −35.0 kcal/mol, one anticipates that if a progressive effect exists, ΔH will become more negative by 0.53 kcal/mol per carbon atom. This leads to values of −29.10, −29.63, and −30.69 kcal/mol for the cis isomers of 3-heptene, 4-octene, and 5-decene, respectively. Our results in Table I show that this trend is not observed and that the difference between anticipated and experimental values is well outside of experimental error, particularly in the case of 5-decene.

Injection of solutions of stearic acid, which is, of course, already hydrogenated, gave off heat to the extent of about one sixth that of an equivalent amount of oleic acid. Adsorption of fatty acids on charcoal is known[27] and we speculate that this was the cause. The exothermic effect rapidly diminished, however, and reached zero after about six injections, possibly due to saturation of the available adsorption sites by acid. No diminution of catalytic activity was observed.

TABLE I: Heats of Hydrogenation of Some Larger Alkenes

Compound (all cis)	Purity,[a] %	ΔH_h, kcal/mol	ΔH_f (lit.),[b] kcal/mol
2-Butene			−28.57 ± 0.02[c]
3-Hexene	98	−23.57 ± 0.29	−28.09 ± 0.16[d]
3-Heptene	98	−23.01 ± 0.68	
4-Octene	98	−23.62 ± 0.52	−27.39 ± 0.14[e]
5-Decene	97	−23.56 ± 0.35	

[a] According to manufacturer's statement. [b] 1 kcal = 4.184 kJ. [c] From ref 10. [d] From H. F. Bartolo and F. D. Rossini, *J. Phys. Chem.*, 64, 1685 (1960). [e] From ref 14.

TABLE II: Heats of Hydrogenation and Formation of the Methyl Esters of Seven Common Unsaturated Fatty Acids

Fatty acid methyl ester	ΔH_h, kcal/mol	ΔH_h per double bond, kcal/mol	ΔH_f, kcal/mol
Palmitoleate	−29.30 ± 0.24	−29.30 ± 0.24	−161.16
Palmitelaidate	−32.43 ± 0.60	−32.43 ± 0.60	−158.03[a]
Oleate	−29.14 ± 0.26	−29.14 ± 0.26	−173.91
Oleate	−29.38 ± 0.30	−29.38 ± 0.30	
Elaidate	−28.29 ± 0.15	−28.29 ± 0.15	−174.88
Linoleate	−58.60 ± 0.39	−29.30 ± 0.20	−144.57
Linoelaidate	−55.70 ± 0.13	−27.85 ± 0.06	−147.47
Linolenate	−85.40 ± 0.58	−28.70 ± 0.19	−117.77

[a] Doubtful value; see text.

Injection of unsaturated fatty acid esters was also decreasingly exothermic, reaching a constant value after about six samples had been run. Consequently, the values given in Table II were, with one exception, calculated from the last 6 of a series of 20 or more injections (40 or more including the standard). We feel that whatever competing thermochemical effect was responsible for the abnormally exothermic behavior at the beginning of the series, it had ceased to be operative and the values given represent only the heat of hydrogenation.

The exception was methyl palmitelaidate, only 100 mg of which was available to us and which was diluted to only 1 ml total volume with hexane. The value given in Table II is the average of the last six of eight injections and reflects, we think, interference from the extraneous thermochemical effect just described. Both the value of ΔH and the large standard deviation indicate that constant exothermicity had not yet been reached and that the value given is not reliable. This is unfortunate because we wished to compare the cis–trans isomerization enthalpy between methyl palmitoleate and methyl palmitelaidate with methyl oleate–methyl elaidate.

There is no published value for the heat of formation of methyl stearate or methyl palmitate but the methyl esters of saturated acids of chain length C_5 to C_{15} have been studied by Adriaanse, Dekker, and Coops.[28] These remarkably self-consistent data follow the equation

$$\Delta H = -88.288 - 5.7032n - 0.018055n^2$$

where n is the number of carbon atoms in the molecule (one more than the chain length). The standard deviation from the equation above as determined by a least-squares procedure is only 0.22 kcal/mol for the 11 points. Extrapolation of this equation to $n = 17$ for methyl palmitate and $n = 19$ for methyl stearate leads to −190.46 and −203.17, respectively, for their expected heats of formation. Using these values, we calculated the heats of formation of the seven unsaturated fatty acid esters shown in Table II.

The experimental enthalpies of isomerization of methyl oleate to methyl elaidate are −0.85 and −1.09 kcal/mol obtained from the third, fourth, and fifth entries in Table II. Both of these values are in excellent agreement with Kistiakowsky's value[29] for vapor-phase hydrogenation of *cis*- to *trans*-2-butene (−0.95 kcal/mol), that of Turner[14] for 1,1,8,8-tetramethyl-4-octene in acetic acid solution (−0.86 kcal/mol), and −1.28 kcal/mol predicted for any straight-chain cis to trans isomerization by the method of Franklin.[30] All of these values are somewhat lower than the average of −1.5, −1.5, and −1.7 kcal/mol for the corresponding methyl, n-propyl, and *n*-butyl esters obtained by Keffler.[6]

Acknowledgment. We wish to acknowledge support of this work by the National Institutes of Health.

References and Notes

(1) D. W. Rogers, P. M. Papadimetriou, and N. A. Siddiqui, *Mikrochem. Acta*, in press.
(2) R. B. Williams, *J. Amer. Chem. Soc.*, **64**, 1395 (1942).
(3) R. B. Turner, W. R. Meador, and R. E. Winkler, *J. Amer. Chem. Soc.*, **79**, 4116 (1957).
(4) T. Flirtcroft, H. A. Skinner, and M. C. Whiting, *Trans. Faraday Soc.*, **53**, 784 (1957).
(5) L. J. P. Keffler, *J. Phys. Chem.*, **34**, 1319 (1930).
(6) L. J. P. Keffler, *J. Phys. Chem.*, **41**, 715 (1937).
(7) J. B. Conant and G. B. Kistiakowsky *Chem. Rev.*, **20**, 181 (1937).
(8) K. MacKenzie in "The Chemistry of Alkenes," S. Patai, Ed., Interscience, New York, N.Y., 1964, Chapter 7.
(9) G. W. Wheland, "Resonance in Organic Chemistry," Wiley, New York, N.Y., 1955, p 78 *ff.*
(10) K. S. Pitzer, "Quantum Chemistry," Prentice Hall, Englewood Cliffs, N.J., 1953, p 184 *ff.*
(11) See, however, M. J. S. Dewar and S. Schmeising, "Conference on Hyperconjugation," Pergamon Press, New York, N.Y., 1959, p 83 *ff.*
(12) R. B. Turner, *et al.*, *J. Amer. Chem. Soc.*, **90**, 4315 (1968).
(13) R. B. Turner, D. E. Nettleton, Jr., and M. Perelman, *J. Amer. Chem. Soc.*, **80**, 1430 (1958).
(14) R. B. Turner, A. D. Jarrett, P. Goebel, and B. J. Mallon, *J. Amer. Chem. Soc.*, **95**, 790 (1973).
(15) D. W. Rogers and F. J. Mc Lafferty *Tetrahedron*, **27**, 3765 (1971).
(16) Analabs Inc., North Haven, Conn. 06473.
(17) Perkin Elmer Co., Norwalk, Conn., Model 800.
(18) Varian Aerograph, Springfield, N.J. 07081. Packed analytical column 6 ft × ⅛ in.
(19) J-P. Thenot, *et al.*, *Anal. Lett.*, **5**, 217 (1972).
(20) Varian Associates, Palo Alto, Calif. 94303.
(21) F. W. Mc Lafferty, "Interpretation of Mass Spectra: An Introduction," W. A. Benjamin, New York, N.Y., 1967, p 23 *ff.*
(22) E. S. Domalski, *J. Phys. Chem. Ref. Data*, **1**, 221 (1972).
(23) F. Stohmann, unpublished data quoted in C. Liebermann, *Berichte*, **25**, 90 (1892).
(24) F. Stohmann, *Z. Phys. Chem.*, **10**, 410 (1892).
(25) E. S. Domalski, private communication.
(26) D. W. Rogers and R. J. Sasiela, *Mikrochem. Acta*, 33 (1973).
(27) A. W. Adamson, "Physical Chemistry of Surfaces," 2nd ed, Interscience, New York, N.Y., 1967, p 402 *ff.*
(28) N. Adriaanse, H. Dekker, and J. Coops, *Recl. Trav. Chim. Pays-Bas*, **84**, 393 (1965).
(29) G. B. Kistiakowsky, J. R. Ruhoff, H. A. Smith, and W. E. Vaughan, *J. Amer. Chem. Soc.*, **57**, 876 (1935).
(30) J. L. Franklin, *Ind. Eng. Chem.*, **41**, 1070 (1949).

Alkali Metal Chromates. Enthalpy of Formation, ΔH_f° $(CrO_4^{2-})(g)$. Charge Distribution of Gaseous Chromate Ion and Total Lattice Potential Energies of Sodium, Potassium, Rubidium, and Cesium Chromates

H. D. B. Jenkins,* Anne Winsor,

Department of Molecular Sciences, University of Warwick, Coventry CV4 7AL, England

and T. C. Waddington

Department of Chemistry, University of Durham, Durham City, England *(Received April 15, 1974; Revised Manuscript Received September 24, 1974)*

This theoretical study reports the assignment of a charge of $q_0 = -0.61$ proton units to each of the oxygen atoms in the CrO_4^{2-} ion. The following values for the heat of formation of the chromate ion and the total lattice potential energies of the chromates are assigned: $\Delta H_f^\circ(CrO_4^{2-}) = -705$ kJ mol^{-1}; $U_{POT}(Na_2CrO_4) = 1836$ kJ mol^{-1}; $U_{POT}(K_2CrO_4) = 1714$ kJ mol^{-1}; $U_{POT}(Rb_2CrO_4) = 1653$ kJ mol^{-1}; $U_{POT}(Cs_2CrO_4) = 1596$ kJ mol^{-1}. A value for the absolute oxide ion affinity of the oxyacid CrO_3, corresponding to the process $CrO_3(g) + O^{2-}(g) \rightarrow CrO_4^{2-}(g)$, is estimated to be approximately -1224 kJ mol^{-1}.

Introduction

Considerable work has been done on the calculation of lattice energies of salts containing singly charged complex anions and cations. The complex ions, NH_4^+,[1] CO_3^{2-},[2,3] HF_2^-,[4] N_3^-,[5] and NO_3^-,[6] have recently been examined. Neckel and Vinek[7] have also considered lattice energies of the bifluorides as have Van Gool, Bruinink, and Bottelberghs.[8] The CN^- ion has been discussed by Ladd[9] although there is some dispute regarding the reference energy levels employed[10,11] in this latter work.

In many cases values of the lattice energies are susceptible to direct experimental checks and, in general, agreement between values computed based on an ionic model and experiment is good. Little work has been done on the calculation of lattice energies of salts containing doubly charged negative ions and the work which does exist[12-14] generally involves ions of the transition metals; the aim of this work is to extend calculations to salts containing the CrO_4^{2-} ion. Though checks with experiment are much more difficult, where they can be made, agreement is satisfactory. It seems sensible to extend these calculations to doubly charged oxyanions and to relate the calculations to the estimation of the absolute oxide O^{2-} ion affinity of strong anhydrooxyacid systems such as SO_3 and CrO_3. This paper represents an attempt to calculate such data for the alkali metal chromates.

Lattice Energy Calculations

We now examine the CrO_4^{2-} ion, where a distributed charge q_{Cr} is assigned to the chromium atom and q_0 to each of the four oxygen atoms. These charges are related by the equation

$$q_{Cr} = -2[1 + 2q_0] \quad (1)$$

Total lattice potential energies, $U_{POT}(M_2CrO_4)$, are computed as single-parameter functions of q_0 for the four alkali metal salts corresponding to M = Na, K, Rb, and Cs. Using the thermochemical cycle

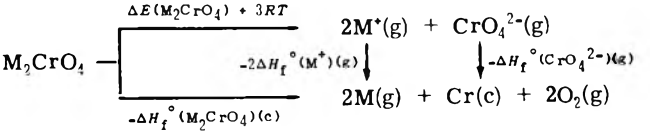

We find that $U_{POT}(M_2CrO_4)$ for each salt is related to $\Delta H_f^\circ(CrO_4^{2-})(g)$ by the equation

$$\Delta H_f^\circ(CrO_4^{2-})(g) = \Delta H_f^\circ(M_2CrO_4)(c) + \Delta E(M_2CrO_4) - 2\Delta H_f^\circ(M^+)(g) + 3RT \quad (2)$$

where, at 298 K

$$\Delta E(M_2CrO_4) = U_{POT}(M_2CrO_4) \quad (3)$$

where $\Delta E(M_2CrO_4)$ is the total internal energy of the crystalline chromate salt, and $\Delta H_f^\circ(M_2CrO_4)(c)$ and $\Delta H_f^\circ(M^+)(g)$ are the standard enthalpies of formation of the crystalline chromate and of the corresponding alkali metal ion, respectively. The combined equation

$$\Delta H_f^\circ(CrO_4^{2-})(g) = \Delta H_f^\circ(M_2CrO_4)(c) + U_{POT}(M_2CrO_4) - 2\Delta H_f^\circ(M^+)(g) + 3RT \quad (4)$$

can be expressed in the parametric form[2,3]

$$\Delta H_f^\circ(CrO_4^{2-})(g) = \sum_{i=0}^{2} A_i q_0^i \quad (5)$$

Solution of equations of the above general form enables a value for $\Delta H_f^\circ(CrO_4^{2-})(g)$, which is alkali metal ion independent, and for q_0 to be assigned for the chromate ion.

The total lattice potential energy is given by

$$U_{POT}(M_2CrO_4) = U_{ELEC} + U_D - U_R \quad (6)$$

where U_{ELEC} is the electrostatic lattice energy, corresponding to the process

$$M_2CrO_4(c) \longrightarrow 2M^+(g) + CrO_4^{2-}(g)$$

U_D and U_R are the dispersion and repulsion energies of the lattice, respectively. The Bertaut[15] method is employed to calculate the Madelung constant and energy associated with the hypothetical process

$$M_2CrO_4(c) \longrightarrow 2M^+(g) + Cr^{q_{Cr}}(g) + 4O^{q_0}(g)$$

TABLE I: Parameterization of Equations for the Chromates[a]

	Na_2CrO_4	K_2CrO_4	Rb_2CrO_4	Cs_2CrO_4
α_0	2.287772	2.239607	2.119129	2.096907
α_1	7.903739	8.047681	7.970842	8.057652
α_2	12.307207	12.231810	12.148100	12.273957
L	1.5837	1.5895	1.5780	1.6099
B_0	2,006.9	1,957.5	1,865.7	1,809.5
B_1	6,933.5	7,034.0	7,017.7	6,953.4
B_2	10,796.5	10,691.0	10,695.5	10,591.8
C_1	−7,009.8	−6,943.8	−6,946.2	−6,879.2
C_2	−10,800.0	−10,698.5	−10,701.4	−10,598.9
D_1	−76.2	90.1	71.5	74.2
D_2	−3.5	−7.5	−5.9	−7.0
U_D	13.2	26.8	33.6	49.0 α for I^{-d}
U_D	8.0	17.9	23.0	32.4 α for SO_4^{2-e}
U_D av	10.6	22.4	28.3	40.7 average value taken
U_R	226.2	208.3	194.8	205.9
$\Delta H_f°(M_2CrO_4)(c)$	−1,328.8[b]	−1,382.8[b]	−1,380.7	−1,389.5
		−1,388.7[c]		
$\Delta H_f°(M^+)(g)$	609.8	514.2	494.9[b]	460.6[b]
A_0	−749.4 (II)	−632.2[b]	−664.0	−658.9
	(I)	−638.1[c]		
A_1	−76.2	90.1	71.5	74.2
A_2	−3.5	−7.5	−5.9	−7.0

[a] L is shortest Cr-O distance to which Madelung parameters are referred. Energies quoted are in kJ mol^{-1}. [b] Reference 35. [c] Reference 34. [d] Reference 23. [e] Reference 24.

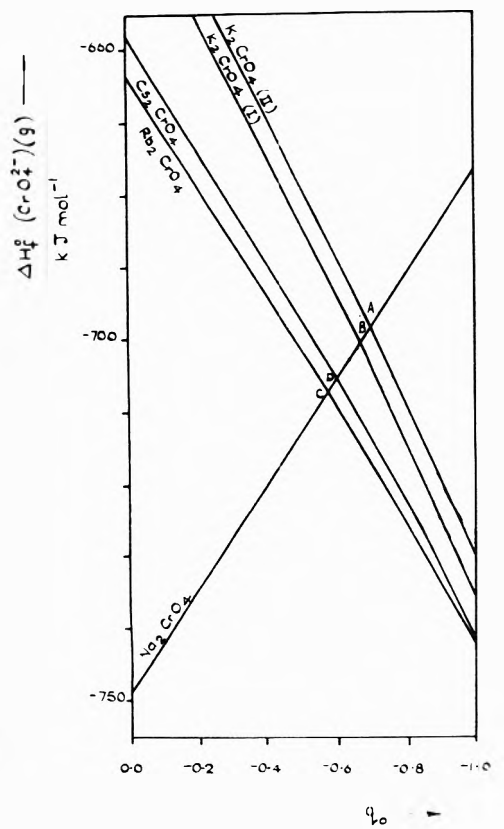

Figure 1.

and employing the truncation procedure and convergence check suggested by Jenkins[16] the values given in Table I are obtained.

The CrO_4^{2-} ion "self energy," U_{SE}, is added to U_M to generate an equation for U_{ELEC}. The equations involved take the usual forms[2]

TABLE II: Intersection Points of Figure 1

Intersection	Point	$\Delta H_f°(CrO_4^{2-})$ (g), kJ mol^{-1}	q_0, proton units
Na–K(II)	A	−689.5	−0.69
Na–K(I)	B	−701.0	−0.66
Na–Rb	C	−707.1	−0.57
Na–Cs	D	−705.6	−0.59
Average	(all points)	−703.0	−0.63
Average	(A,C,D)	−703.7	−0.62
Average	(B,C,D)	−704.6	−0.61

$$M = \sum_{j=0}^{2} \alpha_j q_0^j \tag{7}$$

$$U_M = \sum_{j=0}^{2} B_j q_0^j \tag{8}$$

$$U_{SE} = \sum_{k=1}^{2} C_k q_0^k \tag{9}$$

$$U_{ELEC} = B_0 + \sum_{l=1}^{2} (B_l + C_l) q_0^l = B_0 + \sum_{m=1}^{2} D_m q_0^m \tag{10}$$

The dispersion energy, U_D, is calculated employing the formulae

$$U_D = \frac{1}{2}[C_{++} S_6^{++} + C_{--} S_6^{--}] + C_{+-} S_6^{+-} \tag{11}$$

where

$$C_{++} = 0.75 \epsilon_+ \alpha_+^2 \tag{12}$$

$$C_{--} = 0.75 \epsilon_- \alpha_-^2 \tag{13}$$

$$C_{+-} = (1.5 \epsilon_+ \epsilon_- \alpha_+ \alpha_-)/(\epsilon_+ + \epsilon_-) \tag{14}$$

TABLE III: Calculation of Absolute Oxide Ion Affinity of CrO_3 and Estimate for SO_3

Average	$A_{CrO_3}{}^{O^{2-}}$	$A_{CrO_3}{}^{O^{2-}}$, kJ mol^{-1} $\Delta H_f°(O^{2-})(g)$	$A_{CrO_3}{}^{O^{2-}}$, kJ mol^{-1} $\Delta H_f°(CrO_3)(g)$	$\Delta H_f(CrO_4{}^{2-})(g)$ (this work)
−1224 ± 46	−1244 ± 63	925 ± 63[a]	−385.8[d]	−705
	−1202 ± 29	883 ± 29[b]	−385.8[d]	−705
	−1227	908[c]	−385.8[d]	−705
Average	$A_{SO_3}{}^{O^{2-}}$	$A_{SO_3}{}^{O^{2-}}$, kJ mol^{-1} $\Delta H_f°(O^{2-})(g)$	$\Delta H_f°(SO_3)(g)$	$\Delta H_f(SO_4{}^{2-})(g)$
−1242 ± 46	−1270 ± 63	925 ± 63[a]	−395.72[d]	−741[e]
	−1236 ± 63	925 ± 63[a]	−395.72[d]	−707[f]
	−1279 ± 63	925 ± 63[a]	−395.72[d]	−750[g]
	−1228 ± 29	883 ± 29[b]	−395.72[d]	−741[e]
	−1194 ± 29	883 ± 29[b]	−395.72[d]	−707[f]
	−1237 ± 29	883 ± 29[b]	−395.72[d]	−750[g]
	−1253	908[c]	−395.72[d]	−741[e]
	−1219	908[c]	−395.72[d]	−707[f]
	−1262	908[c]	−395.72[d]	−750[g]

[a] Reference 41. [b] Reference 42. [c] Reference 43. [d] Reference 40. [e] Reference 46. [f] Reference 50. [g] Reference 51.

TABLE IV: Literature Values for Charge Distribution on $CrO_4{}^{2-}$ Ion

Source	q_0
Reference 36	−0.66
Reference 22	−0.69
Reference 37[a]	−0.69
References 38, 39	−0.67
Av lit. value	−0.67
This work	−0.61

[a] Assigning an oxidation state of $CrO_4{}^{2-}$ ion as +0.78 and linearly interpolating.

$$S_6^{++} = 2\sum_i^{\infty}(1/R_{M^+M^+_i})^6 \quad (15)$$

$$S_6^{--} = \sum_j^{\infty}(1/R_{CrCr_j})^6 \quad (16)$$

$$S_6^{+-} = 2\sum_k^{\infty}(1/R_{M^+Cr_k})^6 \quad (17)$$

where $R_{M^+M^+_i}$, R_{CrCr_j}, and $R_{M^+Cr_k}$ are the distances of the ith M^+ ion and jth Cr atom a *reference* M^+ ion or chromium atom (which is excluded from the summation). ϵ_+, the characteristic energy of the alkali metal ion M^+, is taken as 0.75 of the second ionization potential of the ion ($M^+ \rightarrow M^{2+}$), values being taken from Moore.[17] ϵ_- is the characteristic energy of the $CrO_4{}^{2-}$ ion, the value of which is taken from Von Halben and Litmanowitsch,[18] Viste and Gray,[19] Waggoner and Chambers,[20] Campbell,[21] and Oleari, De Michelis, and Di Sipio[22] all of whom have examined the most intense absorption band in the ultraviolet spectrum of the ion and found it to lie at λ 270 mμ. α_+ and α_- are the polarizabilities of the cation and anion, respectively, the former polarizabilities are taken from Mayer[23] but the latter, have not, to our knowledge, been measured. Values of α_- for the chromate ion were used which (a) assumed α_- to be the same as that for an I^- ion and (b) values of α_- for $SO_4{}^{2-}$ in the corresponding sulfates as calculated by Tessman, Kahn, and Shockley.[24]

U_R is calculated using the equation

$$U_R = U_R^{++} + U_R^{--} + U_R^{+-} \quad (18)$$

where, following Huggins[25]

$$U_R^{++} = \tfrac{1}{2}bc_{++}\exp(2r_+/\rho)\sum_i \exp(-R_{M^+M^+_i}/\rho) \quad (19)$$

$$U_R^{+-} = bc_{+-}'\exp([r_+ + r_-]/\rho)\sum_j \exp(-R_{M^+O_j}/\rho) \quad (20)$$

$$U_R^{--} = \tfrac{1}{2}bc_{--}'\exp(2r_-/\rho)[\sum_k \exp(-R_{OO_k}/\rho) - \exp(-R_{OO'}/\rho) - \exp(-R_{OO''}/\rho) - \exp(-R_{OO'''}/\rho)] \quad (21)$$

where the model taken for the $CrO_4{}^{2-}$ ion consists solely of the four oxygen atoms, the chromium ion at the center of the tetrahedra not specifically being considered. The Huggins radii for the alkali metal ions are well established; for the oxygen atoms, comprising the $CrO_4{}^{2-}$ ion, a value of the "basic radii," $r_- = 1.23$ Å, is taken from previous work on the NO_3^- ion described elsewhere by Jenkins and Waddington.[6] ρ was taken to be 0.345 $Å^{-1}$. $R_{OO'}$, $R_{OO''}$, and $R_{OO'''}$ are the distances between the reference O^{q_0} ion and the other three oxygen atoms in the same $CrO_4{}^{2-}$ ion unit. b is is a constant and following Pauling[26]

$$c_{++}' = [1 + (2q_+/n_+)] \quad (22)$$

$$c_{--}' = [1 + (2q_-/n_-)] \quad (23)$$

$$c_{+-}' = [1 + (q_+/n_+) + (q_-/n_-)] \quad (24)$$

where q_+ is the cationic charge (+1) and n_+ the number of electrons in the valence shell of the M^+ ion (=8). q_- is the anionic charge of −2 and n_- was assigned the value 8. Combining eq 6 and 10

$$U_{POT}(M_2CrO_4) = B_0 + \sum_{m=1}^{2} D_m q_0{}^m + U_D - U_R = \sum_{n=0}^{2} E_n q_0{}^n \quad (25)$$

where

$$E_0 = (B_0 + U_D - U_R) \quad (26)$$

and

$$E_n = D_n \text{ for } n \neq 0 \quad (27)$$

consequently in eq 5

$$A_0 = E_0 + \Delta H_f^\circ(M_2CrO_4)(c) - 2\Delta H_f^\circ(M^+)(g) + 3RT \quad (28)$$

$$A_i = E_i \text{ for } i \neq 0 \quad (29)$$

Figure 1 shows $\Delta H_f^\circ(CrO_4^{2-})(g)$ as a function of q_0.

Results

The alkali metal chromates show various structure types.[27]

Sodium chromate is orthorhombic having a space group, V_h^{17} ($Cmcm$) and unit cell lengths (a_0 = 7.138 Å, b_0 = 5.861 Å, c_0 = 9.259 Å).[28] Potassium, rubidium, and cesium chromates have the K_2SO_4 arrangement with the following cell lengths: K_2CrO_4 (a_0 = 7.61 Å, b_0 = 5.92 Å, c_0 = 10.40 Å);[29-31] Rb_2CrO_4 (a_0 = 7.983 Å, b_0 = 6.288 Å, c_0 = 10.704 Å);[32] and Cs_2CrO_4 (a_0 = 8.429 Å, b_0 = 6.302 Å, c_0 = 11.19 Å).[33] Table I cites details of the coefficients and energy parameters calculated in this work. There are several points to note. (i) The value of U_D, the dispersion energy used in these calculations, corresponded to the average value of $U_D^{(a)}$, calculated assuming the CrO_4^{2-} ion to have the same polarizability as an I^- ion (Mayer[23]) and a value $U_D^{(b)}$ calculated taking the polarizability for the ion to be that of the SO_4^{2-} ion in the corresponding alkali metal sulfate (Tessman, *et al.*[24]). (ii) For K_2CrO_4, the value of $\Delta H_f^\circ(K_2CrO_4)(c)$ as cited by Muldrow and Hepler[34] generates curve I while the older NBS data generate curve II. The fact that the interaction point B is closer to points C and D generated by the other chromates suggests that the values of Muldrow and Hepler are more reliable. This illustrates a feature of this type of calculation, which we have noted before,[1,4] namely, that when there are two differing values of the lattice parameters or two differing values for enthalpy data (as in this case) then from the curves of $\Delta H_f^\circ(X^{n-})(g)$ *vs.* distributed charge it is often possible to make a value judgment between them. (iii) The equations for the total lattice potential energies of the chromates take the form

$$U_{POT}(Na_2CrO_4) = 1792.3 - 76.2q_0 - 3.5q_0^2 \quad (30)$$

$$U_{POT}(K_2CrO_4) = 1771.6 + 90.1q_0 - 7.5q_0^2 \quad (31)$$

$$U_{POT}(Rb_2CrO_4) = 1699.2 + 71.5q_0 - 5.9q_0^2 \quad (32)$$

$$U_{POT}(Cs_2CrO_4) = 1644.3 + 74.2q_0 - 7.0q_0^2 \quad (33)$$

(iv) Table II gives the ordinates and abcissae of the intersection points of the graph of $\Delta H_f^\circ(CrO_4^{2-})(g)$ as a function of q_0.

The average value of $\Delta H_f^\circ(CrO_4^{2-})(g)$ obtained by using the points (B, C, and D) which are generated by using the more modern data (avoiding the older NBS values) is probably the most reliable.

Accordingly we assign a value for

$$\Delta H_f^\circ(CrO_4^{2-})(g) = -705 \text{ kJ mol}^{-1} \quad (34)$$

which is probably accurate to ±20 kJ mol^{-1}, and a value of q_0 for the chromate ion

$$q_0 = -0.61 \text{ proton units} \quad (35)$$

(v) Since data are available for $\Delta H_f^\circ(CrO_3)(g)$ and $\Delta H_f^\circ(SO_3)(g)$[40] and for $\Delta H_f^\circ(O^{2-})(g)$[41-43] it is possible to estimate a value for the absolute oxide ion affinity of the anhydro oxyacid CrO_3, $A_{CrO_3}^{O^{2-}}$

$$CrO_3(g) + O^{2-}(g) \xrightarrow[A_{CrO_3}^{O^{2-}}]{} CrO_4^{2-}(g)$$

and for the absolute oxide ion affinity of the oxyacid SO_3, $A_{SO_3}^{O^{2-}}$

$$SO_3(g) + O^{2-}(g) \xrightarrow[A_{SO_3}^{O^{2-}}]{} SO_4^{2-}(g)$$

whereupon

$$A_{CrO_3}^{O^{2-}} = \Delta H_f^\circ(CrO_4^{2-})(g) - \Delta H_f^\circ(CrO_3)(g) - \Delta H_f^\circ(O^{2-})(g) \quad (36)$$

with an analogous equation for $A_{SO_3}^{O^{2-}}$, and as shown in Table III a value of −1224 kJ mol^{-1} emerges for $A_{CrO_3}^{O^{2-}}$ with a probable error of about ±50 kJ mol^{-1} and a value of −1242 kJ mol^{-1} can be estimated for $A_{SO_3}^{O^{2-}}$ with a rather larger uncertainty owing to the uncertainty about a value for $\Delta H_f^\circ(SO_4^{2-})(g)$.

Discussion

$\Delta H_f^\circ(CrO_4^{2-})(g)$ is a thermodynamic quantity, the value of which has never previously been assigned to our knowledge. The value obtained for q_0 seems satisfactory although the present work places considerable reliance on the curve for Na_2CrO_4 since this curve is the discriminant, used when examining the mutual intersections of the curves. The crystal structure of Li_2CrO_4, had it been determined, would have enabled us to ascertain with even more confidence a value for $\Delta H_f^\circ(CrO_4^{2-})(g)$. The values of $U_{POT}(M_2CrO_4)$, the total lattice potential energies, are found to be

$$U_{POT}(Na_2CrO_4) = 1836.5 \text{ kJ mol}^{-1} \quad (37)$$

$$U_{POT}(K_2CrO_4) = 1713.8 \text{ kJ mol}^{-1} \quad (38)$$

$$U_{POT}(Rb_2CrO_4) = 1653.4 \text{ kJ mol}^{-1} \quad (39)$$

$$U_{POT}(CsCrO_4) = 1596.4 \text{ kJ mol}^{-1} \quad (40)$$

and correspond to a value for q_0 of −0.61 proton units. The only values of lattice energies of chromates which appear in the literature are those quoted by Samsanov[44] which originate from Yatsimirskii's work[45] and are, for Na_2CrO_4, 1979 kJ mol^{-1} and, for K_2CrO_4, 1816 kJ mol^{-1} and differ from the current values by 6–8%, which is the order of accuracy claimed for the Yatsimirskii empirical equation. Agreement seems satisfactory.

Values of −705 kJ mol^{-1} for $\Delta H_f^\circ(CrO_4^{2-})(g)$ and of −1224 kJ mol^{-1} for $A_{CrO_3}^{O^{2-}}$ can be compared with an estimated value from −707 to −750 for $\Delta H_f^\circ(SO_4^{2-})(g)$ and of −1242 kJ mol^{-1} for $A_{SO_3}^{O^{2-}}$. These figures show clearly that CrO_3 is a Lewis oxyacid of *quantitatively* very similar strength to SO_3 perhaps the *strongest* uncharged Lewis acid known. Unfortunately, at the present time, there are insufficient data to make a comparison with MoO_3 and SeO_3 possible.

A number of calculations for q_0 exist in the literature. These range from semiempirical estimates[22,36,37] to a full *ab initio* calculation[38,39] and our current value is in fair agreement with these (Table IV).

Acknowledgments. We wish to thank Professor Yosio Sakamoto of the University of Hiroshima for his interest

and kindness in reading the manuscript prior to publication and for his helpful suggestions.

References and Notes

(1) A. L. Goodliffe, H. D. B. Jenkins, S. V. Martin, and T. C. Waddington, *Mol. Phys.*, **21**, 76 (1971).
(2) H. D. B. Jenkins and T. C. Waddington, *J. Chem. Phys.*, **56**, 5323 (1972).
(3) H. D. B. Jenkins and T. C. Waddington, *Nature (London), Phys. Sci.*, **232**, 5 (1971).
(4) H. P. Dixon, H. D. B. Jenkins, and T. C. Waddington, *J. Chem. Phys.*, **57**, 4388 (1972).
(5) H. P. Dixon, H. D. B. Jenkins, and T. C. Waddington, *Chem. Phys. Lett.*, **10**, 600 (1971).
(6) H. D. B. Jenkins and T. C. Waddington, *J. Inorg. Nucl. Chem.*, **34**, 2465 (1972).
(7) A. Neckel and G. Vinek, *Z. Naturforsch. A*, **26**, 569 (1971).
(8) W. Van Gool, J. Bruinink, and P. H. Bottelberghs, *J. Inorg. Nucl. Chem.*, **34**, 3631 (1972).
(9) M. F. C. Ladd, *Trans. Faraday Soc.*, **65**, 2712 (1969).
(10) H. D. B. Jenkins and T. C. Waddington, *Nature (London), Phys. Sci.*, **238**, 126 (1972).
(11) M. F. C. Ladd, *Nature (London), Phys. Sci.*, **238**, 125 (1972).
(12) M. Mori, R. Tsuchiya, E. Kyuno, and T. Nichide, *Bull. Chem. Soc. Jap.*, **33**, 1510 (1960).
(13) A. B. Blake and F. A. Cotton, *Inorg. Chem.*, **2**, 906 (1963).
(14) J. Beck, R. H. Wood, and N. N. Greenwood, *Inorg. Chem.*, **9**, 86 (1970).
(15) E. F. Bertaut, *J. Phys. Radium*, **13**, 499 (1952).
(16) H. D. B. Jenkins, *Chem. Phys. Lett.*, **9**, 473 (1971).
(17) C. E. Moore, *Nat. Bur. Stand., Circ.* No. **467** (1958).
(18) H. Ver. Halben and M. Ehmanowitsch, *Helv. Chim. Acta*, **24**, 44 (1941).
(19) A. Viste and H. B. Gray, *Inorg. Chem.*, **3**, 1113 (1964).
(20) W. H. Waggoner and M. E. Chambers, *Talanta*, **5**, 121 (1960).
(21) J. A. Campbell, *Spectrochim. Acta*, **21**, 1333 (1965).
(22) L. Oleari, G. De Michelis, and L. Di Sipio, *Mol. Phys.*, **10**, 111 (1966).
(23) J. E. Mayer, *J. Chem. Phys.*, **1**, 270 (1938).
(24) J. R. Tessman, A. H. Kahn, and W. Shockley, *Phys. Rev.*, **92**, 890 (1953).
(25) M. L. Huggins, *J. Chem. Phys.*, **5**, 143 (1937).
(26) L. Pauling, *Z. Kristallogr.*, **6**, 377 (1928).
(27) R. W. G. Wyckoff, "Crystal Structures," Vol. 3, 2nd ed, Interscience, New York, N.Y., 1965.
(28) A. Niggli, *Acta Crystallogr.*, **7**, 776 (1954).
(29) K. Hermann, M. Hosenfeld, and N. Schonfeld, *Wiss. Veroff. Siemenskonz*, **5**, 119 (1926).
(30) M. Y. Colby, *Z. Kristallogr.*, **78**, 168 (1931).
(31) W. H. Zachariasen and G. E. Zeigler, *Z. Kristallogr.*, **80**, 164 (1931).
(32) H. W. Smith, Jr., and M. Y. Colby, *Z. Kristallogr.*, **101**, 90 (1940).
(33) J. J. Miller, *Z. Kristallogr.*, **99A**, 32 (1938).
(34) C. N. Muldrow, Jr., and L. G. Hepler, *J. Amer. Chem. Soc.*, **79**, 4045 (1957).
(35) F. D. Rossini, *et al.*, *Nat. Bur. Stand., Circ.*, **No. 500** (1952).
(36) S. S. Batsanov, *Zhur. Neorg. Khim.*, **9**, 1322 (1964).
(37) G. De Michelis, L. Oleari, and L. Di Sipio, *Coord. Chem. Rev.*, **1**, 18 (1966).
(38) I. H. Hillier and V. R. Saunders, *J. Chem. Soc. D*, 1275 (1969).
(39) I. H. Hillier and V. R. Saunders, *Proc. Roy. Soc., Ser. A*, **320**, 161 (1970).
(40) D. D. Wagman, W. H. Evans, V. B. Parker, I. Halow, S. M. Bailey, and R. H. Schumm, *Nat. Bur. Stand., Tech. Note*, **No. 270-4** (1969).
(41) M. L. Huggins and Y. Sakamoto, *J. Phys. Soc. Jap.*, **12**, 241 (1957).
(42) D. F. C. Morris, *Proc. Roy Soc., Ser. A*, **242**, 116 (1957).
(43) T. C. Waddington, *Advan. Inorg. Chem. Radiochem.*, **1**, 157 (1959).
(44) G. V. Samsonov, *Vysokotemp*, **119** (1965).
(45) K. B. Yatsimirskii, *KOX, **26**, 9 (1956).
(46) M. F. C. Ladd and W. H. Lee, *J. Inorg. Nucl. Chem.*, **21**, 216 (1961).
(47) K. B. Yatsimirskii, *J. Gen. Chem. USSR*, **26**, 2655 (1956).
(48) K. B. Yatsimirskii, *Zhur. Obshch. Khim.*, **26**, 2376 (1956).
(49) N. M. Selivanova and M. Ch. Karapet'yants, *Izv. Vyssh. Uchneb. Zaved., Khim. Khim. Tekhnol.*, **6**, 891 (1963).
(50) M. F. C. Ladd and W. H. Lee, *J. Inorg. Nucl. Chem.*, **30**, 330 (1968).
(51) H. D. B. Jenkins, *J. Chem. Phys.*, **56**, 5065 (1972).

Partial Molal Heat Capacities of Caffeine and Theophylline in Pure Water

J. H. Stern* and L. R. Beeninga

Department of Chemistry, California State University, Long Beach, California 90840 *(Received July 31, 1974; Revised Manuscript Received December 9, 1974)*

Calorimetric enthalpies of solution of the biochemically important methylated xanthines, caffeine and theophylline, to very low concentrations in water have been measured from 288 to 308°K. The temperature derivatives of the enthalpies yield the appropriate partial molal heat capacity differences between the aqueous solutes and the pure crystalline solids, with values of 100 and 90 cal/deg mol at 298°K for caffeine and theophylline, respectively. These results, combined with the estimated heat capacities of the crystalline solids, give the anomalously high partial molal heat capacities of 160 and 140 cal/deg mol at 298°K for caffeine and theophylline, respectively, and are evidence of the complex structuring induced by the two solutes. The CH_2 group contribution to the partial molal heat capacities deduced from these two xanthines is approximately the same as that for various aqueous aliphatic nonelectrolytes, showing that limited group contribution predictions for partial molal heat capacities of aqueous nonelectrolytes may be possible when more data becomes available.

Introduction

Aqueous methylated xanthines are important biochemical solutes[1] with very interesting but poorly understood physicochemical properties.[2] A previous paper[3] included a study of the enthalpies of solution of crystalline caffeine in pure water at 298°K, as a function of concentration. This contribution reports on the partial molal heat capacities of caffeine and theophylline at very low concentrations in pure water via measurement of the enthalpies of solution from 288 to 308°K. The interaction of these solutes with water and their effect on aqueous solution structure should be of particular interest since both xanthines have similar pharmacodynamical properties, particularly as diuretics.[4]

It has been observed that the anomalous partial molal heat capacity difference $\Delta C^\circ_{p_2}$ between a pure and a dissolved solute at low concentrations in water, or the absolute partial molal heat capacity of the aqueous solute $\bar{C}^\circ_{p_2}$,

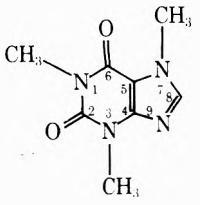

caffeine
1,3,7-trimethylxanthine

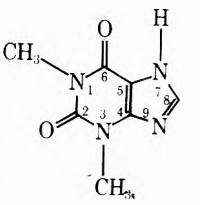

theophylline
1,3-dimethylxanthine

are very sensitive indicators of aqueous solution structure changes. The few $\Delta C^\circ_{p_2}$ values for aliphatic nonelectrolytes which have been reported to date[5-10] are positive, and generally increase with the size of the nonpolar groups or number of alkyl groups in the nonelectrolyte. The positive value of $\Delta C^\circ_{p_2}$ can be interpreted as evidence of increased structure induced in the water by the presence of the dissolved nonelectrolyte. The systems of aqueous nonelectrolytes upon which these conclusions are based include a few alkanes, hydrogen bonding hydrophilic low molecular weight aliphatic alcohols, alkyl amines,[8,9] ethyl acetate,[5] nitromethane,[6] and acetic acid.[7] This study appears to be the first involving the effect of two related heterocyclic ring compounds on water

Experimental Section

The calorimeter and calorimetric procedure have been described elsewhere.[11] The pure crystalline anhydrous caffeine was identical with that used in the previous study[3] and the anhydrous theophylline was obtained from the Nutritional Biochemical Corp. Elemental analysis of theophylline gave the following percentage results: calcd, C, 46.85; H, 4.48; N, 31.10; O, 17.73: found, C, 46.85; H, 4.58; N, 30.94; O, 17.51. In each run 480 g of distilled and deionized water were weighed into the dewar to ±0.05 g.

Results and Discussion

The means of the observed enthalpies of solution of caffeine and theophylline in pure water, ΔH°_2 (obsd), with their standard deviations are shown in Table I. The very low overall final molality in this study ranges from ca. 0.002 to 0.006 *m*. No variation in enthalpies over this concentration range was observed within the limits of the reported uncertainties. The enthalpies may thus be considered as infinite dilution values, with no evidence of possible self-association that may take place at higher concentrations.[2,3,12-14] The calculated enthalpies, ΔH°_2 (calcd), in kcal/mol are from eq 1 and 2 for caffeine and theophylline,

$$\Delta H^\circ_2(\text{caffeine}) = 314.6 - 2.185T + 3.83 \times 10^{-3}T^2 \quad (1)$$

$$\Delta H^\circ_2(\text{theophylline}) = 238.9 - 1.667T + 2.95 \times 10^{-3}T^2 \quad (2)$$

respectively, with values of the constants determined via least squares. The $\Delta C^\circ_{p_2}$ analytical equations in cal/deg mol are obtained directly from the temperature derivatives of eq 1 and 2:

$$\Delta C^\circ_{p_2}(\text{caffeine}) = -2185 + 7.66T \quad (3)$$

$$\Delta C^\circ_{p_2}(\text{theophylline}) = -1667 + 5.90T \quad (4)$$

The difference in values of $\Delta C^\circ_{p_2}$ for the two xanthines may be considered as the contribution to $\Delta C^\circ_{p_2}$ by a CH_2 group. In the midrange of measurement (298–303°K), eq 3 and 4 show that this contribution is 10–15 cal/deg mol. Examination of heat capacity data for low molecular weight aliphatic alcohols and amines,[8,9] alkyl ammonium, and fatty acid salts[10] shows that $\Delta C^\circ_{p_2}$ increases by approximately 15 cal/deg mol per CH_2 group added. It appears then that the CH_2 group contribution is approximately constant, whether in an aliphatic or heterogeneous aromatic ring compound. In this connection it may be noted that measurements with the biochemically similar isomer of theophylline, theobromine (3,7-dimethylxanthine), were unsuccessful because of the very slow rate of dissolution in water. However, in view of the observed regularity, it can be assumed that the heat capacity behavior and consequently the effect on aqueous solution structure of the two isomers may be the same or very similar.

TABLE I: Enthalpies of Solution of Caffeine and Theophylline in Pure Water

T, °K	No. of runs	ΔH°_2 (obsd), kcal/mol	ΔH°_2 (calcd), kcal/mol
		Caffeine	
288	11	3.00 ± 0.06	3.00
298[a]	22	3.60 ± 0.06	3.61
303	6	4.20 ± 0.12	4.19
308	11	4.97 ± 0.14	4.97
		Theophylline	
288	10	3.91 ± 0.07	3.91
293	2	4.12 ± 0.18	4.15
298	5	4.67 ± 0.01	4.54
303	3	4.94 ± 0.03	5.07
308	7	5.80 ± 0.19	5.76

[a] Reference 3.

It would be desirable to obtain absolute values of the partial molar heat capacities $\bar{C}^\circ_{p_2}$ of the aqueous solutes by combining $\Delta C^\circ_{p_2}$ with the heat capacity of the crystalline solids $C^\circ_{p_2}(s)$: $\bar{C}^\circ_{p_2} = \Delta C^\circ_{p_2} + C_{p_2}(s)$. However, direct experimental values of $C_{p_2}(s)$ are not available for caffeine and theophylline. Estimated values of $C_{p_2}(s)$ at 298°K were calculated as follows: $C_{p_2}(s)$ (caffeine) = $C_{p_2}(s)$ (xanthine) + $3C_{p_2}(s)$ (CH_2) and $C_{p_2}(s)$ (theophylline) = $C_{p_2}(s)$ (xanthine) + $2C_{p_2}(s)$ (CH_2), where $C_{p_2}(s)$ (CH_2) is the CH_2 contribution to the heat capacity of the solid. The experimental value of $C_{p_2}(s)$ (xanthine) is 36.5 cal/deg mol.[15] The calculated value of $C_{p_2}(s)$ (CH_2) was obtained from the difference between the experimental values of the heat capacities of crystalline 2-methylnaphthalene and naphthalene:[16] $C_{p_2}(s)$ (CH_2) = $C_{p_2}(s)$ (2-methylnaphthalene) − $C_{p_2}(s)$ (naphthalene) = 47.2 − 39.7 = 7.5 cal/deg mol. In this way the estimated values of $C_{p_2}(s)$ were calculated to be 59 and 52 cal/deg mol for caffeine and theophylline, respectively. It may be noted that Kopp's 100 year old rules on additivity of atomic heat capacities[17-19] yield values within 2 cal of the above more reliable estimates. Thus at 298°K, rounded off $\bar{C}^\circ_{p_2}$ is 160 and 140 cal/deg mol for caffeine and theophylline, respectively. These remarkably high positive values show the large degree of structuring induced by these two molecules. Equations 3 and 4 also show that $\Delta C^\circ_{p_2}$ for both systems increases sharply with temperature, contrary to the behavior generally observed for low molecular weight aliphatic nonelectrolytes which show negative temperature coefficients of $\Delta C^\circ_{p_2}$ (methanol excepted[8]). The lack of data for other systems and possible inflection points over wider temperature spans preclude any satisfactory models at this time.

Acknowledgment. The authors wish to express their gratitude to Hendrik Tuinstra for help with the least-squares calculations, and to the Long Beach California State University Foundation for financial assistance.

References and Notes

(1) W. S. Hoffman, "Biochemistry of Clinical Medicine," 4th ed, Year Book Medical Publishers, Chicago, Ill., 1970.
(2) D. Guttman and T. Higuchi, *J. Amer. Pharmacol. Ass., Sci. Ed.*, **46**, 4 (1957).
(3) J. H. Stern, J. A. Devore, S. L. Hansen, and O. Yavuz, *J. Phys. Chem.*, **78**, 1922 (1974).
(4) G. deStevens, "Diuretics, Chemistry and Pharmacology," Academic Press, New York, N.Y., 1963.
(5) J. H. Stern and A. Hermann, *J. Phys. Chem.*, **72**, 364 (1968).
(6) J. H. Stern and T. Swearingen, *J. Phys. Chem.*, **74**, 167 (1970).
(7) J. H. Stern, O. Yavuz, and T. Swearingen, *J. Chem. Eng. Data*, 17, 182 (1970).
(8) F. Franks in "Hydrogen-Bonded Solvent Systems," A. K. Covington and P. Jones, Ed., Taylor and Francis, London, 1968.
(9) F. Franks in "Water, A Comprehensive Treatise," Vol. 2, F. Franks, Ed., Plenum Press, New York, N.Y., 1973.
(10) J. S. Sarma and J. C. Ahluwalia, *Chem. Soc. Rev. (London)*, **2**, 203 (1973).
(11) J. H. Stern and C. W. Anderson, *J. Phys. Chem.*, **68**, 2528 (1964).
(12) D. Guttman and T. Higuchi, *J. Pharm. Sci.*, **60**, 1267 (1971).
(13) A. L. Thakkar, L. G. Tensmeyer, and W. L. Williams, *J. Pharm. Sci.*, **60**, 1267 (1971).
(14) J. Kirschbaum, *J. Pharm. Sci.*, **62**, 109 (1973).
(15) R. D. Stiehler and H. M. Huffman, *J. Amer. Chem. Soc.*, **57**, 1741 (1935).
(16) J. P. McCullough, H. L. Finke, J. F. Messerly, S. S. Todd, J. C. Kinchenloe, and G. Waddington, *J. Phys. Chem.*, **61**, 1105 (1957).
(17) H. Kopp, *Ann. Chem. Pharm. Suppl.*, **3**, 1, 289 (1864).
(18) L. Pauling, "General Chemistry," 2nd ed, W. H. Freeman, San Francisco, Calif., 1959, p 638.
(19) G. N. Lewis and M. Randall, "Thermodynamics," revised by K. S. Pitzer and L. Brewer, McGraw-Hill, New York, N.Y., 1961, p 58.

Partial Specific Volumes in Highly Concentrated Protein Solutions. I. Water–Bovine Serum Albumin and Water–Bovine Hemoglobin

J. Bernhardt* and H. Pauly

Institut für Physikalische und Medizinische Strahlenkunde der Universität Erlangen-Nürnberg, 8520 Erlangen, West Germany

(Received July 23, 1974; Revised Manuscript Received November 25, 1974)

Measurements of the specific volume of highly concentrated and salt-free solutions of bovine serum albumin (BSA) and bovine hemoglobin (Hb) at 25° were carried out by using a digital densimeter. The protein mass fractions in the binary mixture were determined by measuring the dry weight with an accuracy of better than 0.01%. We found that the specific volumes of both solutions are not linear functions of the protein mass fraction. There exist very small deviations from linearity, more in BSA solutions than in Hb solutions. The data were approximated by a power series. The partial specific volumes for water and hydrated proteins were determined with the aid of this power series. The partial specific volume of water increases with increasing protein mass fraction. The maximum increase for BSA solutions is about 0.4% (at 0.34 BSA mass fraction) and for Hb solutions about 0.3% (at 0.44 Hb mass fraction). According to this increase there is a decrease of the partial specific volume of the hydrated proteins. We found for the partial specific volume of BSA in infinitely diluted solution a value of $v_{BSA}^{\infty} = 0.73604$ cm^3 g^{-1} and for Hb $v_{Hb}^{\infty} = 0.75460$ cm^3 g^{-1}.

I. Introduction

Measurements of the specific volume of highly concentrated protein solutions were not of particular interest in the past. As only the limiting values v_p^{∞} of the partial specific volume of protein in infinitely diluted solutions were needed, measurements were made only with rather diluted protein solutions. Because of the increasing interest in the state of water in the living cell and in protein solutions of physiological concentrations measurements of the specific volume may now have a new bearing. However, until now there has been no report of a concentration dependence of the partial specific volumes in protein solutions.[1-3]

In order to understand better the behavior of water in the living cell, many experiments have been reported in scientific literature. As was resumed by Pauly,[4] measurements of some properties of protein solutions, e.g., the dielectric constant and the electrical conductivity (Pauly and Schwan[5]), the heat of melting (Hasl and Pauly[6,7]), and the partial specific heat (Milber[8]), have led to the result that approximately 0.2–0.4 g of water per gram of dry protein are bound in mixtures of protein and water, and the rest behaves like normal water.

After Kratky et al.[9] had developed the digital densimeter, it has become possible to measure easily and with sufficient accuracy the specific volume of small amounts of highly viscous solutions. However in order to detect changes of the partial specific volumes, the protein concentration of the solutions has to be determined with an accuracy of 0.01% or better. We determined the partial specific volume v_w of water in bovine erythrocytes and stated a small, but significant increase of v_w in erythrocytes.[10] As we were not able to separate the influence of the proteins from that of the salts on the partial specific volume of water, we used salt-free protein solutions as simple models and measured their specific volume. The results given in this paper show that the removal of water from protein so-

lutions is followed by an increase of the partial specific volume of water and by a corresponding decrease of the partial specific volume of the hydrated proteins.

II. Experimental Section

Proteins. Bovine serum albumin (BSA) was supplied by the Behring Werke (Marburg). Aqueous solutions with a BSA mass fraction of 0.1 were prepared, deionized (conductivity below 5×10^{-6} Ω^{-1} cm^{-1}), and then lyophilized.[7,11] The freeze dried BSA was used for preparing solutions with a mass fraction of about 0.25; we degassed the solutions and after having removed the foam we concentrated these solutions at 18–20° in a rotatory vaporizer, Rotavapor-R of Büchi. In its final state the BSA mass fraction was about 0.33. The final solutions were viscous like honey and without air bubbles and foam. All other samples were prepared by diluting the solutions with water. After careful mixing, each sample was degassed once more before the measurement of the specific volume.

Bovine hemoglobin (Hb) was prepared by first using the techniques of Drabkin[12] and Hinson.[13] The hemoglobin solution, free of particles, which was obtained by this method, was then deionized and concentrated by applying a technique developed by Pfister and Tretter.[14] For the deionization the ion-exchange mixed-bed resin AG 501-X8 (D) of Bio-Rad Corp. was used. The conductivity of the hemoglobin solutions (10 wt % Hb) was smaller than 5×10^{-6} Ω^{-1} cm^{-1}. In order to concentrate the solutions, a Sartorius ultrafiltration system was used. Solutions with a Hb mass fraction up to 0.44 were obtained.[15] Small samples of the final solution were packed into plastic bags, frozen, and stored at −30° for further experiments. After having thawed a sample we diluted it step by step with water for the measurements of the specific volume. In measuring the optical density there was no indication of methemoglobin. Furthermore a gel filtration (using Sephadex G 150) proved that there was no denaturation of the hemoglobin by broken or aggregated Hb molecules.[16]

Measurements of the Specific Volume. The specific volume (reciprocal density) of the protein solutions was measured at 25° by using the digital densimeter DMA-02 of Heraeus/Paar developed by Kratky et al.[9] In this densimeter an exactly defined volume of the sample takes part in the undamped oscillation of a mechanical oscillator, thereby changing its natural frequency. Two thermostats provided an accuracy of the temperature of 0.01°. The densimeter was calibrated with air and water. In order to check the linearity of the scale we measured the specific volume of mercury. The specific volume of mercury is tabulated[17] as $v_{Hg} = 0.073890$ cm^3 g^{-1} at 25°. We measured a value of $v_{Hg} = 0.073886 \pm 1 \times 10^{-6}$ cm^3 g^{-1}. Furthermore, we measured the specific volume of a concentrated NaCl solution (NaCl Suprapur of Merck) with a mass fraction of 0.200015. We measured a value of $v = 0.873105 \pm 1 \times 10^{-5}$ cm^3 g^{-1} at 25°. The extrapolated value taken from the International Critical Tables is $v = 0.873126$ cm^3 g^{-1}. By comparing these two measurements we feel sure that the deviation of 2×10^{-5} for the NaCl solution is not due to a nonlinearity of the scale. We therefore conclude from the experiments that we can measure the specific volume near the calibration point "water" in the range between 1.002964 cm^3 g^{-1} (the specific volume of pure water at 25°[18]) and 0.8 cm^3 g^{-1} to better than 10^{-5} without systematic deviation. The main error source was small invisible air bubbles in the samples. Therefore those measurements were discarded for which no constant value for the specific volume could be attained, or for which a too large value of the specific volume was obtained compared with the correlation specific volume–protein mass fraction, which was calculated later (for details of this procedure see section III).

Dry Weight Determinations. The protein mass fraction of the solutions was determined by measuring the dry weight. Because of the high accuracy of the density measurements the determination of the dry weight was made very carefully and was more accurate than described in literature so far. All weight determinations were carried out with a Cahn gram electrobalance. In order to improve precision and accuracy, a portion of the sample weight was tared and fine electrical ranges were used. The sample containers of a volume of 1 ml were made of aluminum foil and possessed empty weights of about 45 mg (weight accuracy 5 μg). After each density measurement a container was filled with sample solution, until a total weight of ca. 1 g was reached. The water evaporation during filling and weighing was taken into consideration (weight accuracy 0.05 mg). Then the samples were placed into weighing bottles. The drying of the samples was carried out in a similar way as described by Hunter.[19] Freeze drying over P_2O_5 was followed by drying at 110° in a vacuum oven for 48 hr. After the drying process air was allowed to enter the oven through a drying tube filled with P_2O_5. Then the bottles were capped as quickly as possible while still in the oven at 110°. The bottles were transferred into a special glove box made from lucite which contained vessels with P_2O_5 and the weighing assembly of the Cahn gram electrobalance. The weighing bottles were opened 24 hr later and the samples were weighed (weight accuracy 0.01 mg). The weights did not change during the weighing process.

It was stated[19] that the drying process in the vacuum oven without P_2O_5 must be repeated three or four times until the dry weight reached a nearly constant value within our accuracy. This could be avoided by using P_2O_5 in the vacuum oven. The P_2O_5 was in an open vessel and covered with a thick layer of glass wool. For the second drying process we used this method with P_2O_5.

For the weighing process we calculated an error smaller than 0.002% for the value of the protein mass fraction. When comparing the measured values with the relation between specific volume and mass fraction one can determine a mean deviation of the points from the mean value of about 0.005 to 0.01%. Because the accuracy of the density measurements is better by a factor 10 this must be due to the incomplete removal of water during the drying process and perhaps to the adsorption of water when determining the dry weights (see Discussion).

III. Results

Bovine Serum Albumin Solutions. Table I shows the values of the specific volume v (reciprocal density) and of the mass fraction w (g of protein/g of solution) of the bovine serum albumin (BSA) gained by 113 measurements (we used the symbol $w_p = w$ for the protein mass fraction and $w_w = 1 - w$ for the water mass fraction).

As is shown later, the values empirically obtained were fitted in a least-squares curve. By comparing this curve with the data, those values were graphically discarded whose deviation from the calculated curve was larger than 0.02%. For this procedure Figures 1 and 2 were used. Almost all discarded points (about 10% of all points were dis-

TABLE I: Specific Volumes and Protein Mass Fractions of Salt-Free Solutions of Bovine Serum Albumin at 25° [a]

Protein mass fraction w	Specific volume v, cm^3 g^{-1}	Protein mass fraction w	Specific volume v, cm^3 g^{-1}
0.00031	1.00289	0.12786	0.968822
0.00039	1.00286	0.1308	0.96793
0.00078	1.00276	0.137	0.96637
0.00144	1.00259	0.13715	0.966337
0.002125	1.002386	0.14231	0.964846
0.00212	1.002384	0.1432	0.964715
0.00234	1.002386	0.1489	0.96312
0.003876	1.001922	0.1524	0.96217
0.006348	1.001281	0.1545	0.96156
0.00665	1.001201	0.15452	0.961516
0.009223	1.000523	0.1573	0.96077
0.00974	1.000385	0.1597	0.96011
0.0104	1.0002	0.1628	0.95936
0.01219	0.999726	0.16452	0.958834
0.012687	0.999604	0.1654	0.95862
0.015749	0.998774	0.1682	0.957841
0.015799	0.998752	0.1688	0.95768
0.0159	0.99874	0.1716	0.9570
0.01977	0.997726	0.1733	0.95648
0.019955	0.997641	0.17657	0.955611
0.02123	0.99733	0.17753	0.955299
0.02405	0.996561	0.18515	0.953307
0.025032	0.996298	0.19558	0.950456
0.0272	0.99574	0.19779	0.949856
0.02800	0.995507	0.20609	0.947658
0.029988	0.994955	0.21353	0.945633
0.03152	0.994532	0.21860	0.944272
0.03312	0.994199	0.22242	0.943265
0.0338	0.994	0.23271	0.940472
0.035633	0.993466	0.24191	0.937956
0.035794	0.993431	0.24914	0.936010
0.040545	0.992132	0.25766	0.933643
0.04209	0.991707	0.26237	0.932383
0.04328	0.991453	0.26676	0.931210
0.0475	0.99033	0.27297	0.929419
0.051126	0.989301	0.27984	0.927626
0.0540	0.98857	0.28192	0.927041
0.05784	0.987473	0.28866	0.925117
0.061489	0.986547	0.29296	0.923969
0.0633	0.98606	0.29535	0.923328
0.064548	0.985754	0.30244	0.921237
0.0730	0.98345	0.30372	0.920952
0.07365	0.983263	0.31044	0.919068
0.073784	0.983251	0.31279	0.918474
0.0819	0.98104	0.31415	0.917975
0.08631	0.979921	0.31592	0.917556
0.086431	0.979881	0.31732	0.917189
0.08913	0.979093	0.32024	0.916155
0.0911	0.97865	0.32199	0.915856
0.0983	0.97674	0.32341	0.915327
0.10173	0.975786	0.32667	0.914561
0.10436	0.975014	0.32749	0.914225
0.10552	0.974824	0.32827	0.913978
0.11640	0.971893	0.32922	0.913836
0.11882	0.9711	0.33125	0.913240
0.1234	0.96994	0.33728	0.911260
0.12695	0.969081		

[a] Less accurate values are included, they are the result from our first measurements.

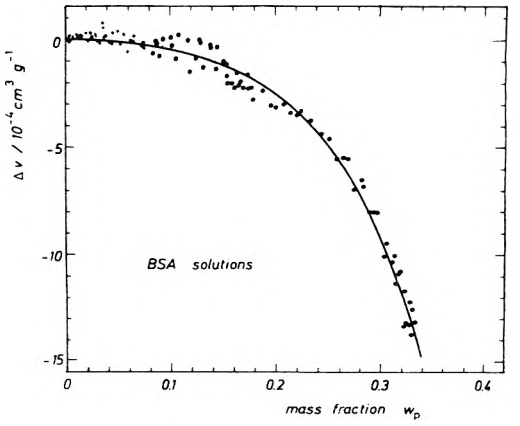

Figure 1. Experimental deviations Δv_i of the individual values v_i of the specific volume from the linear part of the function in eq 1, $\Delta v_i = v_i - v_w^0 - b_1 w$, for BSA solutions. The smooth curve is a representation of the specific volume by eq 3.

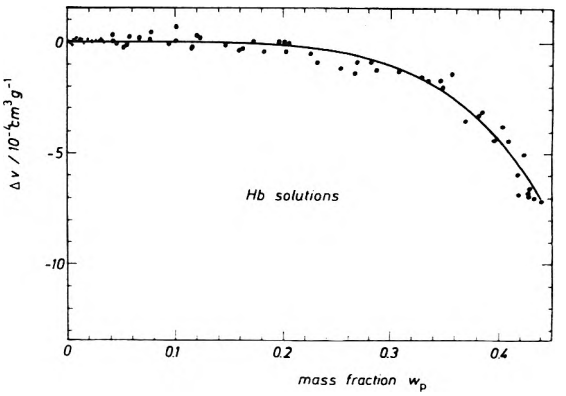

Figure 2. Experimental deviations Δv_i of the individual values v_i of the specific volume from the linear part of the function in eq 1, $\Delta v_i = v_i - v_w^0 - b_1 w$, for Hb solutions. The smooth curve is a representation of the specific volume by eq 4.

carded) were above the calculated curve, indicating thus those samples whose density was measured too low or whose dry substances contained traces of water. The remaining 113 points are given in Table I. These values were then used for all further calculations.

Bovine Hemoglobin Solutions. The values of the specific volume and the protein mass fraction of bovine hemoglobin solutions (Hb) gained by 72 measurements are shown in Table II.

Mathematical Description. It was stated that the specific volumes v were not linear functions of the protein mass fractions w, but that the specific volume slightly deviated negatively from a straight line. We therefore tried a least-squares fit of the experimental data using power series of the form

$$v(w) = v_w^0 + \sum_{j=1}^{n} b_j w^j \qquad (1)$$

$v_w^0 = 1.002964$ cm^3 g^{-1} is the specific volume of pure water at 25° (we used the improved value tabulated by Bigg[18]). We found that the small experimental deviations Δv_i of the individual values v_i of the specific volume from the linear part of the function in eq 1

$$\Delta v_i = v_i - v_w^0 - b_1 w \qquad (2)$$

cannot be approximated with a desired accuracy by a single term $b_j w^j$, $j \leq 2$, in case of BSA solutions. Two coefficients

TABLE II: Specific Volumes and Protein Mass Fractions of Salt-Free Solutions of Bovine Hemoglobin at 25°

Protein mass fraction w	Specific volume v, cm^3 g^{-1}	Protein mass fraction w	Specific volume v, cm^3 g^{-1}
0.0022725	1.002406	0.14554	0.966813
0.002676	1.002308	0.15863	0.963535
0.0035377	1.002071	0.16275	0.962515
0.004449	1.001866	0.17018	0.960699
0.0047911	1.001785	0.18092	0.957994
0.0067576	1.001301	0.19580	0.954347
0.007995	1.000998	0.20282	0.952552
0.0098825	1.000527	0.20502	0.952050
0.010222	1.000445	0.22577	0.946846
0.011011	1.000254	0.23148	0.945386
0.014250	0.999448	0.25217	0.940222
0.014603	0.999360	0.26749	0.936391
0.015434	0.999134	0.26782	0.936363
0.017930	0.998524	0.28157	0.932948
0.021558	0.997614	0.28645	0.931699
0.021822	0.997540	0.30708	0.926576
0.025210	0.996709	0.32756	0.921461
0.028558	0.995882	0.33260	0.920193
0.030533	0.995397	0.34401	0.917363
0.032075	0.995010	0.34563	0.916926
0.032522	0.994888	0.35719	0.914119
0.040503	0.992941	0.36785	0.911255
0.041267	0.992724	0.37945	0.908395
0.046541	0.991404	0.38462	0.907130
0.051237	0.990216	0.39016	0.905680
0.055541	0.989156	0.39560	0.904282
0.056503	0.988951	0.40252	0.902625
0.67361	0.986258	0.40836	0.901113
0.076504	0.984010	0.41696	0.898817
0.076536	0.983965	0.41794	0.898484
0.092195	0.980069	0.42362	0.897355
0.099194	0.978399	0.42761	0.896084
0.09938	0.978292	0.42780	0.896025
0.11580	0.974181	0.42878	0.895826
0.11880	0.973490	0.43260	0.894834
0.12211	0.972661	0.43888	0.893257

b_j, however, are sufficient. Values of the coefficients b_j, $2 \leq j \leq 5$, are shown in Table III for BSA solutions and in Table IV for Hb solutions. Furthermore, the sixth column lists the sums of the squares of the deviations between the observed and the calculated values. As can be seen, the linear part of eq 1 only leads to a poor fit of the data, but the use of one more coefficient b_j, $j \geq 2$, gives a better fit. The fit can even be improved by using a coefficient of a higher order. Only a small further improvement of the fit can be obtained by adding two more coefficients to the linear part of eq 1.

We have chosen a power curve with the coefficients b_2 and b_5 by two reasons. First, the sum of the squares of the residues is smaller (for BSA solutions) or (for Hb solutions) comparable to that of other combinations of coefficients. Second we demand the same sign for all coefficients by physical perception, because it can be shown that only with this assumption the partial specific volumes are smooth functions without turning point of the protein mass fractions.

The best fit found for BSA solutions is

$$v = 1.002964 - 0.266929w - 0.004559w^2 - 0.213153w^5 \qquad 0 \leq w \leq 0.34 \quad (3)$$

and for Hb solutions

$$v = 1.002964 - 0.248364w - 0.00001514w^2 - 0.04285w^5 \qquad 0 \leq w \leq 0.44 \quad (4)$$

In order to estimate our fitting we plotted the deviations Δv_i in Figure 1 for BSA solutions and in Figure 2 for Hb solutions, as defined in eq 2, vs. the protein mass fraction w.

The smooth curves correspond to the functions

$$\Delta v = b_2 w^2 + b_5 w^5 \quad (5)$$

Both figures show the quality of our fit and furthermore the accuracy of our measurements. The maximum values for Δv are $\Delta v = -1.5 \times 10^{-3}$ cm^3 g^{-1} (≈0.17%) for BSA solutions with a BSA mass fraction of 0.34, and $\Delta v = -0.7 \times 10^{-3}$ cm^3 g^{-1} (≈0.078%) for Hb solutions with a Hb mass fraction of 0.44.

Evaluation of the Partial Specific Volumes. By using the relation for the partial specific volume v_w of the water[20]

$$v_w = v - w\left(\frac{\partial v}{\partial w}\right)_{T,P} \quad (6)$$

and of the protein, v_p, in a binary mixture

$$v_p = v + (1 - w)\left(\frac{\partial v}{\partial w}\right)_{T,P} \quad (7)$$

one obtains from eq 6, 7, and 3 for BSA solutions

TABLE III: Coefficients for the Representation of the Specific Volume by Eq 1 and the Sums of the Squares of the Deviations between the Observed and the Calculated Values for BSA Solutions

b_1	b_2	b_3	b_4	b_5	$\sum[v_i - v(w_i)]^2$
−0.269532	0	0	0	0	56.613×10^{-7}
−0.265213	−0.016458	0	0	0	6.274×10^{-7}
−0.266800	0	−0.036847	0	0	4.027×10^{-7}
−0.267354	0	0	−0.099684	0	3.355×10^{-7}
−0.267646	0	0	0	−0.285720	3.407×10^{-7}
−0.267527	0.00714	−0.052304	0	0	3.807×10^{-7}
−0.267156	−0.001437	0	−0.091505	0	3.330×10^{-7}
−0.266926	−0.004559	0	0	−0.213153	2.977×10^{-7}
−0.267372	0	0.001107	−0.102643	0	3.355×10^{-7}
−0.267332	0	−0.012945	0	−0.187821	3.162×10^{-7}
−0.267478	0	0	−0.056242	−0.125030	3.278×10^{-7}

TABLE IV: Coefficients for the Representation of the Specific Volume by Eq 1 and the Sums of the Squares of the Deviations between the Observed and the Calculated Values for Hb Solutions

b_1	b_2	b_3	b_4	b_5	$\sum[v_i - v(w_i)]^2$
−0.249271	0	0	0	0	11.705×10^{-7}
−0.247282	−0.005549	0	0	0	2.757×10^{-7}
−0.247967	0	−0.009608	0	0	1.942×10^{-7}
−0.248224	0	0	−0.019784	0	1.553×10^{-7}
−0.248367	0	0	0	−0.042951	1.381×10^{-7}
−0.248742	0.005664	−0.01886	0	0	1.674×10^{-7}
−0.248505	0.001490	0	−0.024567	0	1.502×10^{-7}
−0.248364	−0.00001514	0	0	−0.042850	1.381×10^{-7}
−0.248468	0	0.008274	−0.036370	0	1.449×10^{-7}
−0.248420	0	0.001143	0	−0.047807	1.375×10^{-7}
−0.248436	0	0	0.008731	−0.061661	1.362×10^{-7}

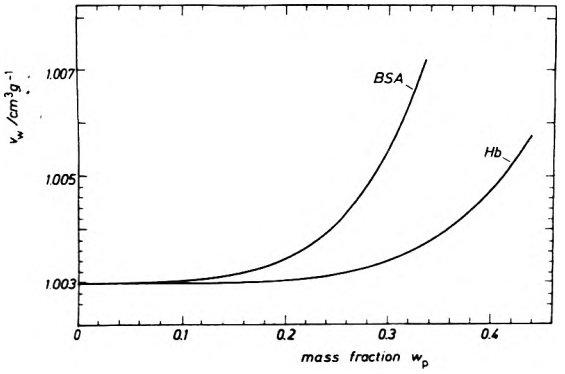

Figure 3. Calculated values of the partial specific volume v_w of water by eq 8 for BSA solutions and by eq 10 for Hb solutions.

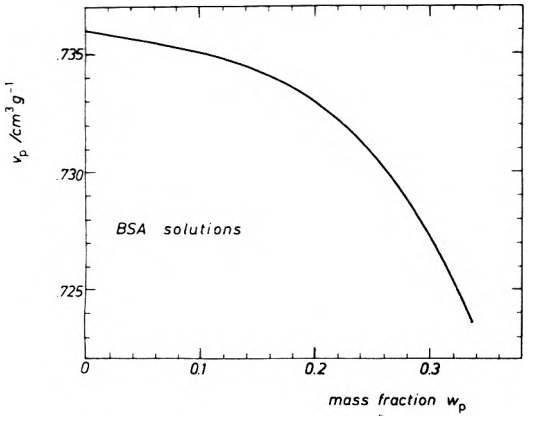

Figure 4. Calculated values of the partial specific volume v_p of the protein by eq 9 for BSA solutions.

$$v_w = 1.002964 + 0.004559w^2 + 0.852612w^5 \quad (8)$$

$$v_p = 0.736035 - 0.009118w + 0.004559w^2 - 1.065765w^4 + 0.852612w^5 \quad (9)$$

For Hb solutions one obtains from eq 6, 7, and 4

$$v_w = 1.002964 + 0.00001514w^2 + 0.1714w^5 \quad (10)$$

$$v_p = 0.756400 - 0.00003028w + 0.00001514w^2 - 0.21425w^4 + 0.1714w^5 \quad (11)$$

The partial specific volumes and their dependence on the protein mass fraction, resulting from eq 8–11 and plotted by an electronic plotter, are shown in Figures 3–5.

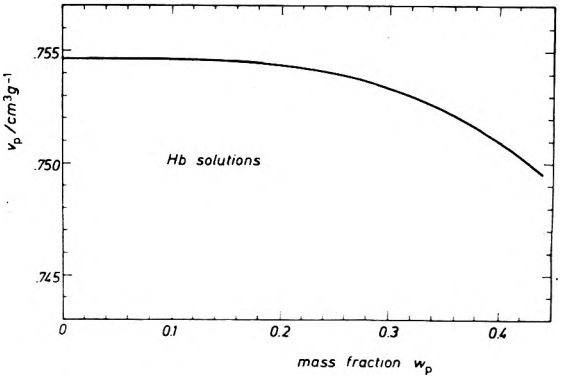

Figure 5. Calculated values of the partial specific volume v_p of the protein by eq 11 for Hb solution.

Errors in the Evaluation of the Partial Specific Volumes. For the errors in the partial specific volume we obtain from eq 6 and 7

$$\delta v_p = \delta v_w = \sqrt{(\delta v)^2 + \left(\frac{\partial v}{\partial w}\,\delta w\right)^2} \quad (12)$$

By assuming an error of $\delta v = 10^{-5}$ cm^3 g^{-1} in the specific volume and an error of $\delta v = 10^{-4}$ in the protein mass fraction, we obtained for BSA solutions values of $\delta v_p = \delta v_w$ between 2.8 and 3.0×10^{-5} cm^3 g^{-1}, depending on the mass fraction, and for Hb solutions values of $\delta v_p = \delta v_w$ between 2.7 and 2.8×10^{-5} cm^3 g^{-1}.

The errors calculated for Δv are of the same order. We can compare these errors with the root mean square deviations between the observed and the calculated values of the specific volumes. They can be calculated by means of the sixth column of the Tables III and IV. We found $\delta v = 5.2 \times 10^{-5}$ cm^3 g^{-1} for BSA solutions and $\delta v = 4.4 \times 10^{-5}$ cm^3 g^{-1} for Hb solutions.

IV. Discussion

The least-squares fit of the measured results was purely mathematically without considering any model of interaction between water and protein. Two criteria let us choose the coefficients: first a minimum value of the sum of the square deviations between the observed and the calculated values, second the physical perception of that the partial specific volumes should be smooth functions without turning point of the protein mass fractions. We believe our fitting is good enough so that nothing or little of the concentration dependence of the partial specific volumes calculat-

ed in this paper will be changed whatever physical model of interactions between water and protein, or among water molecules or hydrated protein molecules themselves may be found later. Furthermore, we believe that eq 3 and 4 can be used in order to determine the protein concentration of salt-free solutions of BSA or Hb, respectively, more accurately than previously.

As far as we know, there has been no description in the literature which dealt with the concentration dependence of the partial specific volumes in highly concentrated salt-free protein solutions found by us.[1-3] Although Pilz and Czerwenka[3] used solutions with protein concentrations up to 220 mg/cm^3, they could not observe a dependence of the specific volume on the concentration. However, we are sure that our accuracy in determining the protein concentration is absolutely necessary to detect small values of Δv (our accuracy is more precise by two orders of magnitude). Furthermore, we used solutions up to much higher protein mass fractions. If there is salt in the solutions this will cause electrostriction of the water which will result in an opposite effect of the volume to that observed by us with pure salt-free protein solutions. The two effects are overlapping. Nevertheless, we can detect the volume deviation from linearity and separate these two effects within our accuracy.[23]

The "true" water content of the dried protein samples is an unsolved problem. We are sure that the values of the dry weight are reproducible within 0.01%. But according to Huber[21,22] one has to reckon with up to 20 molecules of water which are tightly bound within a protein molecule of a molecular weight of approximately 20,000. It is possible that this number is different for various kinds of proteins. However, one may consider the fact that only the hydration water (reproducible within 0.01%) may be removed during the drying process, but the water molecules within the protein structure may not be removable. Therefore one may define a "true" value w_p' of the protein mass fraction $w_p' = [(1 - \bar{w})/(1 - \bar{w}w)]w$, where $\bar{w} = m_w'/(m_w' + m_p')$ (m_p' is the "true" mass of the dry protein; m_w' is the mass of water within the protein molecule). Each coefficient b_n is growing by a factor $[(1 - \bar{w}w)/(1 - \bar{w})]^n = A^n$. By using $\bar{w} = 0.001$ and $w = 0$, one obtains $A = 1.01$, and by using $\bar{w} = 0.01$ and $w = 0.4$, $A = 1.006$. We found out that the removal of water from protein solutions is a process accompanied by an increase of the partial specific volume v_w of water (see Figure 3). The reason may be a changed interaction among the molecules at higher protein concentrations, i.e., interactions between water and water, between water and hydrated protein, and among the hydrated protein. The increase of v_w hints at a growing order with the water molecules by protein concentration, which may be due to the so-called Frank–Evans[24] water structures around nonpolar groups.

One can understand the negative volume deviations observed by us by considering the following model. We assume that water exists at least in two states with different properties ("hydrated" and "free" water). Caused by Brownian molecular movement, there exists for every concentration a certain probability that the hydrated protein molecules build dimers and aggregates of higher order for a short time. During this process a part of water in the overlapping hydration shells may go into the free water and may change its properties. Assuming a larger value for the specific volume of the hydrated water than that of free water, the specific volume of the protein solution will show a negative deviation from linearity on the increase of protein concentration. Measurements of the specific volume at different temperatures could be a test for this model. As results from calorimetric measurements[8,25] the amount of hydration water increases with decreasing temperature. This could also show in the deviation of the specific volume of protein solutions from linearity.[23]

Similarly negative changes of an excess function for the specific volume were observed by Bøje and Hvidt[26] with polymer solutions. The excess function for the specific volume defined by Bøje and Hvidt is based on 1 g of the polymer, in our case Δv is based on 1 g of solution. We used this function in order to show the deviation of the specific volume from a straight line.

The increase of v_w is larger in BSA solutions than in Hb solutions. This may partly be a consequence of the elongated form of the BSA molecules, which form also is probably responsible for the high viscosity of salt-free BSA solutions. Another possibility which cannot be excluded,[27] is that the increase of v_w is caused by the small change of pH of the salt free protein solutions during the dilution with water.[23,30] The maximum increase of v_w for BSA solutions is about 0.4% (at 0.34 BSA mass fraction), and for Hb solutions about 0.3% (at 0.44 Hb mass fraction). According to the increase of v_w there is a decrease of the partial specific volumes v_p of the hydrated proteins (see Figures 4 and 5). Our value of $v_{BSA}^{\infty} = 0.73604$ cm^3 g^{-1} for the hydrated BSA in infinitely diluted solutions is within the range given in literature. Among the publications of the last 10 years there is one by Hunter[19] who found a value of $v_{BSA}^{\infty} = 0.7348$ cm^3 g^{-1}, and one by Bull and Breese[1] who found a value of $v_{BSA}^{\infty} = 0.7376$ cm^3 g^{-1}. We found a value of $v_{Hb}^{\infty} = 0.75460$ cm^3 g^{-1} for hydrated bovine *oxy*hemoglobin in infinitely dilute solutions. We have been unable to find a value for v_p of bovine *oxy*hemoglobin in the literature. Bull and Breese[1] found $v_{Mb} = 0.7583$ cm^3 g^{-1} for bovine methemoglobin. Recently Behlke and Wandt[28] also published a value for bovine *met*hemoglobin of about 0.7503 cm^3 g^{-1} at 25°. There is a value of 0.758 cm^3/g for the specific volume of dry BSA which was determined by Berlin and Pallansch[29] by helium at 25°. This signifies that the function $v(w)$ must have a turning point which may appear between $w = 0.5$ and $w = 0.7$. For the partial specific volumes this signifies that between $w = 0.5$ and $w = 1$, v_p shows an increase and v_w a decrease with protein concentration. We feel, at the present time, that we should not speculate about this as long as we know so little about what happens with the volume of a "dry" protein molecule when it is dissolved in water.

References and Notes

(1) H. B. Bull and K. Breese, *J. Phys. Chem.*, **72**, 1817 (1968).
(2) M. J. Hunter, *J. Phys. Chem.*, **71**, 3717 (1967).
(3) I. Pilz and G. Czerwenka, *Makromol. Chem.*, **170**, 185 (1973).
(4) H. Pauly, *Biophysik*, **10**, 7 (1973).
(5) H. Pauly and H. P. Schwan, *Biophys. J.*, **6**, 621 (1966).
(6) G. Hasl and H. Pauly, *Biophysik*, **8**, 141 (1972).
(7) G. Hasl and H. Pauly, *Biophysik*, **10**, 125 (1973).
(8) P. Milbers, Dissertation, Universität Erlangen-Nurnberg, 1973.
(9) O. Kratky, H. Leopold, and H. Stabinger, *Z. Angew. Phys.*, **27**, 273 (1969).
(10) J. Bernhardt and H. Pauly, Report presented at Jahrestagung der Deutschen Gesellschaft für Biophysik, Jülich, 1973.
(11) H. Pfister, Dissertation, Universität Erlangen-Nürnberg, 1971.
(12) D. L. Drabkin, *J. Biol. Chem.*, **164**, 703 (1946).
(13) J. A. Hinson and T. L. McMeekin, *Biochem. Biophys. Res. Commun.*, **35**, 94 (1969).
(14) H. Pfister and N. Tretter, manuscript in preparation.
(15) N. Tretter and W. Schmid, to whom we are grateful for the preparation of the Hb solutions.

(16) H. Schüssler, to whom we are grateful for carrying out the gel chromatography.
(17) "Handbook of Chemistry and Physics," 46th ed, The Chemical Rubber Publishing Co., Cleveland, Ohio, 1965.
(18) P. H. Bigg, *Brit. J. Appl. Phys.*, **18**, 521 (1967).
(19) M. J. Hunter, *J. Phys. Chem.*, **70**, 3285 (1966).
(20) E. A. Guggenheim, "Thermodynamics," 5th ed, Amsterdam, North-Holland Publishing Co., Amsterdam, 1967.
(21) R. Huber, personal communication.
(22) R. Huber, D. Kutla, W. Steigemann, J. Deisenhofer, and T. A. Jones in "2nd International Research Conference on Proteinase Inhibitors (Bayer Symposium V)," H. Fritz, H. Tschesche, L. J. Greene, and E. Truscheit, Ed., Springer Verlag, New York, N. Y., in press.
(23) We presently measured the specific volume of hemoglobin solutions at different temperatures, as well as the dependence of Δv on the salt content and the pH of the solutions.
(24) H. S. Frank and M. J. Evans, *J. Chem. Phys.*, **13**, 507 (1945).
(25) G. Hasl, Habilitationsschrift, Universität Erlangen-Nürnberg, 1973.
(26) L. Bøje and A. Hvidt, *Biopolymers*, **11**, 2357 (1972).
(27) A. Hvidt, personal communication.
(28) J. Behlke and I. Wandt, *Acta Biol. Med. Ger.*, **31**, 383 (1973).
(29) E. Berlin and M. J. Pallansch, *J. Phys. Chem.*, **72**, 1887 (1968).
(30) We do not believe that this is the reason for the volume deviation observed. First, the deviation is also observed for Hb solutions of high concentration and there may by only a small change of pH because of its isoelectric point near 7.0. Second, we have also observed small negative deviations of Δv for suspensions of erythrocytes of different salt content; in this case one can assume that the pH remains constant.

Temperature Dependence of Excess Thermodynamic Properties of *n*-Heptane–Toluene, Methylcyclohexane–Toluene, and *n*-Heptane–Methylcyclohexane Systems[1]

J. K. Holzhauer and W. T. Ziegler* [2,3]

School of Chemical Engineering, Georgia Institute of Technology, Atlanta, Georgia 30332 *(Received September 11, 1974)*

Heat capacities of the following pure components and mixtures were determined by adiabatic calorimetry: *n*-heptane (182–312 K), methylcyclohexane (144–312 K), toluene (162–312 K), five mixtures of *n*-heptane and toluene (182–312 K), five mixtures of methylcyclohexane and toluene (162–312 K), and one mixture of *n*-heptane and methylcyclohexane (182–312 K). These data were used to compute the molar excess thermodynamic functions C_p^E, G^E, H^E, and S^E of the mixtures over the temperature range of the heat capacity measurements. Densities of the pure components and their mixtures were measured at 293.15 K; excess volumes were derived from these data. The derived excess thermodynamic properties of the *n*-heptane–toluene and methylcyclohexane–toluene systems were interpreted using the conformal solution theory, a theory of Rowlinson and Sutton assuming directional intermolecular forces, and a theory by Flory for mixtures of nonspherical molecules. Only the theory of Rowlinson and Sutton was able to explain the observed temperature dependence of the excess thermodynamic functions, which suggests that directional forces are important in these systems. However, the theory of Flory succeeded best in predicting the observed excess volumes.

Introduction

The dependence of excess thermodynamic properties of binary liquid mixtures on composition has been investigated by many workers.[4–6] Many of the results are summarized in monographs by Rowlinson[7] and Prigogine.[8] Most of these studies are limited to one temperature or a narrow temperature range. Clearly, more information could be obtained by studying the dependence of these properties on both composition and temperature for selected systems. Such studies have been made by Hwa and Ziegler[9] and Brown[10] for several alcohol–hydrocarbon systems.

The *n*-heptane–toluene and methylcyclohexane–toluene systems were selected as suitable representatives of two important classes of mixtures: aliphatic–aromatic and alicyclic–aromatic hydrocarbons. Limited measurements were also made on the *n*-heptane–methylcyclohexane system. Such mixtures are of technical interest because they occur frequently in petroleum processing. The low freezing points of all components permit the determination of excess thermodynamic properties over a wide temperature range. A point of special interest is that at room temperature, the *n*-heptane–toluene and methylcyclohexane–toluene systems show relatively high values of H^E, G^E, and S^E[11–14] whereas the *n*-heptane–methylcyclohexane system is almost ideal.[11,15]

Since the excess thermodynamic functions G^E, H^E, S^E, and C_p^E are related by thermodynamic equations it is sufficient to determine the temperature dependence of one of these properties to establish the temperature dependence of the other properties. It was chosen to measure the heat capacities of the pure components and their mixtures and to derive excess heat capacities from these data. The other excess properties were then obtained from C_p^E by integration.

Experimental Section

Heat Capacity Measurements. The heat capacity measurements were carried out in a precision adiabatic shield calorimeter similar in design to the one described by Scott, *et al.*[16] The calorimeter has been described elsewhere[17] and has been used previously for liquid heat capacity measurements.[9,10,17,18] The cryostat assembly was surrounded by a constant temperature bath. Depending on the temperature of measurement, four different baths were used: liquid ni-

trogen up to about 201 K, ethanol–solid CO_2 from about 195 to 279 K, ice from about 273 to 298 K, and water from about 292 to 312 K. The overlap between adjacent temperature ranges was necessary to verify that the change in bath temperature did not significantly affect the measurements. The sample temperature was measured with a platinum resistance thermometer which had been calibrated by the National Bureau of Standards on the International Practical Temperature Scale of 1948 (IPTS-48). The temperatures were converted to the International Practical Temperature Scale of 1968 (IPTS-68) using the difference between the two scales tabulated by Barber.[19] For the conversion from degrees Celsius to kelvins, the relation $T(K) = t(°C) + 273.15$ was used. All temperatures are reported on IPTS-68 unless otherwise noted. The molecular weights are based on the C 12 scale: *n*-heptane, 100.206; methylcyclohexane, 98.190; and toluene, 92.142.

For the heat capacity measurements the calorimeter can, which had a liquid volume of about 160 cm^3, was filled with about 150 cm^3 of liquid. Calculations showed that the heat capacity of the gas phase (essentially nitrogen) and the effect of sample evaporation were negligible. Since the effect of pressure on the heat capacity is negligible below about 1 atm, the results are reported as heat capacity at constant pressure, C_p. These measurements are discussed in greater detail below.

Density Measurements. Densities were measured with a single-stem, Bingham-type pycnometer following essentially the procedure recommended by the American Society for Testing and Materials.[20] The pycnometer was immersed in a water bath which was held at 20 ± 0.005°. The bath temperature was monitored with a platinum resistance thermometer calibrated by the National Bureau of Standards. The pycnometer was calibrated using freshly boiled, distilled water which had been redistilled from $KMnO_4$. All weighings were carried out using an analytical balance, with a reproducibility of ±0.2 mg. They were corrected for buoyancy. All densities given are averages of at least two determinations, with individual values differing by 0.00001 g/cm^3 or less from the average.

Materials and Purification. All hydrocarbons were obtained from the Phillips Petroleum Co. The methylcyclohexane was Research Grade, and was used without further purification. The *n*-heptane and toluene were Pure Grade, and were further purified by fractional distillation. The melting point of the pure substances and the mole fraction of impurity were determined calorimetrically by measuring the fraction melted as a function of temperature. The usual assumptions were made that the impurity was insoluble in the solid phase and formed an ideal solution in the liquid phase. The details of this method have been outlined by Rossini.[21]

Table I lists the mole fraction of impurity, the melting point of the pure substance, and the density at 293.15 K. For comparison, the densities and melting points given by the API[22] are also listed. The melting points given in this work agree with the API values within the uncertainty of the measurement (±0.03°). The density of the methylcyclohexane sample agrees with the API value within the uncertainty of the measurement (±0.00003 g/cm^3). The densities of the *n*-heptane and toluene samples are 0.00011 g/cm^3 higher and 0.00048 g/cm^3 lower, respectively, than the corresponding API values. As these differences exceed the uncertainty of the measurement they are attributed to impurities.

TABLE I: Melting Points, Purities, and Densities of Materials

	n-Heptane	Methylcyclohexane	Toluene
Mp, K	182.586 ± 0.030	146.550 ± 0.030	178.166 ± 0.030
Mole fraction impurity	0.0027 ± 0.0010	0.0012 ± 0.0005	0.0024 ± 0.0010
Mp, K (API[22])[a]	182.569	146.554	178.184
Density,[b] g/cm^3	0.68387	0.76941	0.86648
Density,[b] g/cm^3 (API[22])	0.68376	0.76939	0.86696

[a] Corrected to IPTS-68. [b] At 20°.

TABLE II: Sample Composition and Temperature Range of Heat Capacity and Density Measurements

System	Composition mole fraction, x_1	Temperature range of C_p measurements, K	Temperature of density measurements, K
n-Heptane		182–312	293.15
Methylcyclohexane		141–312	293.15
Toluene		162–312	293.15
n-Heptane (1)–toluene	0.18810	182–312	293.15
n-Heptane (1)–toluene	0.34751	182–312	293.15
n-Heptane (1)–toluene	0.50341	182–312	293.15
n-Heptane (1)–toluene	0.66119	182–312	293.15
n-Heptane (1)–toluene	0.82359	182–312	293.15
Methylcyclohexane (1)–toluene	0.16728	162–312	293.15
Methylcyclohexane (1)–toluene	0.31372	162–312	293.15
Methylcyclohexane (1)–toluene	0.53541	162–312	293.15
Methylcyclohexane (1)–toluene	0.66700	162–312	293.15
Methylcyclohexane (1)–toluene	0.82676	162–312	293.15
n-Heptane (1)–methylcyclohexane	0.48910	182–312	293.15

Discussion of the Heat Capacity Data. The sample compositions and the temperature range of the measurements are given in Table II. The experimental molar heat capacities, C_p, of the pure components and their mixtures are listed in Table III.[23] The heat capacities of the pure components were fitted by polynomials of the form:

$$C_p = a_0 + a_1T^1 + a_2T^2 + a_3T^3 + a_4T^4 \quad (1)$$

using the method of least squares. The coefficients of the polynomials are given in Table IV. Apart from a few exceptional points the polynomials represent the experimental data within 0.1%.

TABLE IV: List of Polynomials Representing the Heat Capacity Data of the Pure Substances (J/(mol K))

	n-Heptane	Methylcyclohexane	Toluene
a_0	8.6618820 (+2)[a]	1.2988277 (+2)	1.8743814 (+2)
a_1	−9.9628490 (+0)	−5.4107773 (−2)	−7.3026493 (−1)
a_2	5.4561085 (−2)	7.9975642 (−4)	2.9613602 (−3)
a_3	−1.3079634 (−4)	0	−2.8661704 (−6)
a_4	1.1957392 (−7)	0	0
z[b]	0.0745	0.1045	0.0748

[a] Numbers in parentheses indicate the power of ten by which the coefficients have to be multiplied. [b] Standard deviation.

A comparison of the heat capacity of *n*-heptane with good literature values shows that the results of this work are about 0.15–0.35% lower than the data reported by McCullough and Messerly[24] and about 0.05% lower than the data of Douglas, *et al.*[25] Both Douglas, *et al.*, and McCullough and Messerly claim an accuracy of 0.1%. The discrepancy could at least partly be attributed to the impurity of the *n*-heptane sample used in this work (0.27%). The agreement with Brown,[10] who used the same calorimeter and a sample from the same lot, and who claims an accuracy of 0.2%, is very good, except for the room temperature region, where Brown's values are up to 0.2% higher than the results of this work. This difference may be due to the fact that in the present work a water bath at 293 K was used at higher temperatures to reduce radiation from the calorimeter shield, whereas Brown used an ice bath for the same temperature range.

The heat capacity of methylcyclohexane has been measured by Douslin and Huffman[26] and by Hwa.[9] Both claim an accuracy of 0.2%. The results of this work agree with the data of Douslin and Huffman with an average deviation of 0.1% and a maximum deviation of 0.2%, but are consistently about 0.15% lower than the data of Hwa. This may be due to a failure by Hwa to include the buoyancy correction for the sample weight, which would lower his heat capacity values by about 0.14%, in excellent agreement with the results of this work.

The heat capacity of toluene has been measured by Scott, *et al.*,[27] and by Hwa.[9] The agreement with Scott, *et al.*, is good between about 200 and 280 K, but at the highest and lowest temperatures of measurement, the values of Scott, *et al.*, are up to 0.25% higher than the data reported here. The data of Hwa are, on the average, about 0.1% higher than the results of this work. An inclusion of the buoyancy correction would lower his values by 0.12%, making the agreement even better.

This comparison shows that the data reported here for the pure components generally agree well with those of other workers using precision calorimetry. It is concluded that the accuracy of the heat capacities is 0.2%.

Derived Excess Thermodynamic Functions

Method of Derivation. The molar excess thermodynamic functions G^E, H^E, S^E, $C_p{}^E$, and V^E, of a binary mixture are defined by the following relations:

$$G^E = [G - (x_1G_1 + x_2G_2) - RT(x_1 \ln x_1 + x_2 \ln x_2)]_{P,T} \quad (2)$$

$$H^E = [H - (x_1H_1 + x_2H_2)]_{P,T} \quad (3)$$

$$S^E = [S - (x_1S_1 + x_2S_2) + R(x_1 \ln x_1 + x_2 \ln x_2)]_{P,T} \quad (4)$$

$$C_p{}^E = [C_p - (x_1C_{p1} + x_2C_{p2})]_{P,T} \quad (5)$$

$$V^E = [V - (x_1V_1 + x_2V_2)]_{P,T} \quad (6)$$

The functions G^E, H^E, S^E, and $C_p{}^E$ are related by the equations:

$$\left[\partial \frac{(G^E/T)}{\partial T} = -H^E/T^2\right]_{P,x} \quad (7)$$

$$[\partial H^E/\partial T = C_p{}^E]_{P,x} \quad (8)$$

$$[TS^E = H^E - G^E]_{P,T,x} \quad (9)$$

If G^E and H^E are known as functions of composition at one temperature, the temperature dependence of these functions can be computed for the compositions used in the heat capacity measurements by integrating eq 7 and 8. S^E is then computed using eq 9.

The experimental heat capacities of the pure components and their mixtures were not determined at exactly the same temperatures. In order to apply eq 5, the heat capacities of the pure components were computed from the polynomials given in Table IV. The derived experimental excess heat capacities are listed in Table III.[23]

In order to avoid a restriction to certain compositions, all $C_p{}^E$ values for each system were fitted by a single function of temperature and compositon using the method of least squares. The form used was

$$C_p{}^E = x_1x_2[A_0(T) + A_1(T)(x_1 - x_2) + A_2(T)(x_1 - x_2)^2] \quad (10)$$

which corresponds to the Redlich–Kister equation,[28] but with (in general) temperature-dependent coefficients. These equations represent the experimental excess heat capacities of the systems *n*-heptane–toluene and methylcyclohexane–toluene with a standard deviation of about 0.1 J/(mol K), corresponding to about 2–18% of the excess heat capacity or about 0.05–0.07% of the total heat capacity. The excess heat capacity of the single mixture of *n*-heptane and methylcyclohexane studied was also represented by a polynomial. All these $C_p{}^E$ functions are given in Table V.

Literature Data for G^E and H^E. Where more than one set of G^E or H^E data were available, for a particular system, the set with the best internal consistency was selected to provide the integration constants for eq 7 and 8.

For the *n*-heptane–toluene system the excess enthalpy measured by Lundberg[11] and the excess Gibbs free energy measured by Surovy and Heinrich[14] both at 298.15 K, were chosen. Lundberg claimed an accuracy of 1%. Surovy and Heinrich did not state the accuracy of their values; from the scatter of their data it is estimated to be about 12 J/mol, or about 4% of the maximum G^E value. No corrections were made for the imperfection of the vapor since the pressures are very low.

For the methylcyclohexane–toluene system the H^E data of Sosnkowska-Kehiahian[13] at 293.15 K and the G^E data of Schneider[12] at 333.15 K were selected. The excess enthalpy is claimed to be accurate to ±20 J/mol, or about 4% of the maximum value. The excess Gibbs free energy is claimed to be accurate within 1%; the reported values include corrections for the imperfection of the vapor. Since the C_p measurements only cover the range up to 312 K, these had to be extrapolated about 21° to derive the temperature dependence of G^E. However, G^E is quite insensitive to any er-

TABLE V: Functions Representing the Derived Excess Thermodynamic Properties

n-Heptane (1)–Toluene (2) System
Temperature Range 182–312 K
Units J, mol, cm^3, K

$G^E = x_1x_2[(16451.814 - 843.97284T - 0.8360739T^2 + 9.7291136 \times 10^{-4}T^3 - 5.8287258 \times 10^{-7}T^4 + 170.41964T \ln T) + (-1040.0338 + 16.3744678T - 2.318104T \ln T)(x_1 - x_2) + (527.75221 - 9.6607141T + 1.384904T \ln T)(x_1 - x_2)^2]$

$H^E = x_1x_2[(16451.814 - 170.41964T + 0.8360739T^2 - 1.94582273 \times 10^{-3}T^3 + 1.74861875 \times 10^{-6}T^4) + (-1040.0338 + 2.318104T)(x_1 - x_2) + (527.75221 - 1.384904T)(x_1 - x_2)^2]$

$S^E = x_1x_2[(673.5532 + 1.6721478T - 2.9187341 \times 10^{-3}T^2 + 2.3314903 \times 10^{-6}T^3 - 170.41964 \ln T) + (-14.056574 + 2.318104 \ln T)(x_1 - x_2) + (8.2758101 - 1.384904 \ln T)(x_1 - x_2)^2]$

$C_p^E = x_1x_2[(-170.41964 + 1.6721478T - 5.8374682 \times 10^{-3}T^2 + 6.9944750 \times 10^{-6}T^3) + 2.318104(x_1 - x_2) - 1.384904(x_1 - x_2)^2]$

$V^E = x_1x_2[0.58544 + 2.532 \times 10^{-2}(x_1 - x_2)]$

(293.15 K)

Methylcyclohexane (1)–Toluene (2) System
Temperature Range 162–312 K
Units J, mol, cm^3, K

$G^E = x_1x_2[(-639.4904 + 342.53415T + 0.53712445T^2 - 7.1421085 \times 10^{-4}T^3 + 4.5461617 \times 10^{-7}T^4 - 78.249165T \ln T) + (65.078891 - 3.6981461T + 0.577025T \ln T)(x_1 - x_2) + (954.67449 - 22.449973T + 3.371621T \ln T)(x_1 - x_2)^2]$

$H^E = x_1x_2[(-639.4904 + 78.249165T - 0.53712445T^2 + 1.4284217 \times 10^{-3}T^3 - 1.3638485 \times 10^{-6}T^4) + (65.078891 - 0.577025T)(x_1 - x_2) + (954.67449 - 3.371621T)(x_1 - x_2)^2]$

$S^E = x_1x_2[(-264.28498 - 1.0742489T + 2.14263255 \times 10^{-3}T^2 - 1.8184647 \times 10^{-6}T^3 + 78.249165 \ln T) + (3.1211211 - 0.577025 \ln T)(x_1 - x_2) + (19.078352 - 3.371621 \ln T)(x_1 - x_2)^2]$

$C_p^E = x_1x_2[(78.249165 - 1.0742489T + 4.285265 \times 10^{-3}T^2 - 5.455393 \times 10^{-6}T^3 - 0.577025(x_1 - x_2) - 3.371621(x_1 - x_2)^2]$

$V^E = x_1x_2[1.55397 + 0.18259(x_1 - x_2)]$

(293.15 K)

n-Heptane (1)–Methylcyclohexane (2) System
Temperature Range 182–312 K
Mixture composition 0.48910 mole fraction *n*-heptane
Units J, mol, cm^3, K

$G^E = 5370.5959 - 330.60088T - 0.33652798T^2 + 3.8757364 \times 10^{-4}T^3 - 2.2840533 \times 10^{-7}T^4 + 67.489297T \ln T$

$H^E = 5370.5959 - 67.489297T + 0.33652798T^2 - 7.7514727 \times 10^{-4}T^3 + 6.8521600 \times 10^{-7}T^4$

$S^E = 263.11158 + 0.67305596T - 1.16272091 \times 10^{-3}T^2 + 9.1362133 \times 10^{-7}T^3 - 67.489297 \ln T$

$C_p^E = -67.489297 + 0.67305597T - 2.3254418 \times 10^{-3}T^2 + 2.7408640 \times 10^{-6}T^3$

$V^E = -0.011$

(293.15 K)

rors in C_p^E due to the double integration involved in the derivation, and the uncertainty introduced by the extrapolation is believed to be very small.

For the *n*-heptane–methylcyclohexane system the H^E data of Lundberg[11] at 298.15 K were used. Vapor–liquid equilibrium data for this system have been measured by Brandt and Roeck[15] at 304.65 K. Neglecting the small effect of vapor imperfection, they found G^E to be 0 ± 4 J/mol over the entire concentration range.

These selected literature data for G^E and H^E at the specified temperatures were used to provide integration constants when integrating the C_p^E equations. These selected data for G^E and H^E were fitted by Redlich–Kister equations of the form

$$E^E = x_1x_2[C_0 + C_1(x_1 - x_2) + C_2(x_1 - x_2)^2] \quad (11)$$

using the method of least squares. The values of the parameters are given in Table VI. Combinations of these equations with general expressions developed for C_p^E (see Table V) permitted the development of general expressions for H^E, G^E, and S^E. These general expressions are given in Table V.

Excess Volumes. The excess volumes derived from the density measurements were fitted by Redlich–Kister equations of the form

$$V^E = x_1x_2[D_0 + D_1(x_1 - x_2)] \quad (12)$$

The experimental data and the equations representing the smoothed data are given in Tables VII[23] and V, respectively.

Figure 1 shows the excess volumes reported in this work together with data taken from the literature. Excess volumes of the *n*-heptane–toluene system were measured at 298.15 K by Tsao and Smith[29] and Mathieson and Thynne.[30] Although the results of the present work were obtained at 293.15 K, the influence of this temperature difference is believed to be small. The agreement with the data of Tsao and Smith is good, although the latter scatter considerably. Mathieson and Thynne report only two data points, which are about 60% higher than the data reported here.

For the methylcyclohexane–toluene system no excess volumes were found in the literature.

Excess volumes of the *n*-heptane–methylcyclohexane system at 293.15 K have been measured by Brandt and Roeck.[15] Although they report a positive excess volume as opposed to the negative value found in this work, the agreement is considered satisfactory since the absolute values are very small.

Discussion of the Derived Excess Functions. The derived excess thermodynamic properties given in Table VI are shown in Figures 2–6 and values of these properties and the derived activity coefficients are listed in Table VIII[23] at 10° and 0.1 mole fraction intervals. The excess heat capacities are considered to be accurate within 0.25 J/(mol K). The error of the derived excess enthalpies should be no larger than 50 J/mol at the lowest temperature and decrease to about 20 J/mol at room temperature. The derived excess Gibbs free energies are believed to be accurate within 25 J/mol at the lowest temperature and 15 J/mol at room temperature. An analysis of the excess entropy data showed that the accuracy is about 0.24 J/(mol K) at the lowest temperature and 0.12 J/(mol K) at room temperature. The accuracy of the excess volume measurements is estimated to be 0.01 cm^3/mol, corresponding to 6.8% of the maximum value for the *n*-heptane–toluene system and 2.6% for the methylcyclohexane–toluene system.

The dependence of the excess thermodynamic properties on composition is very nearly parabolic for both toluene

TABLE VI: Constants Used in Fitting Selected Literature Data by Redlich–Kister Equations

Quantity fitted	T, K	C_0, J/mol	C_1, J/mol	C_2, J/mol	$\bar{z}$,[a] J/mol	Ref
		n-Heptane–Toluene System				
G^E	298.15[b]	1177.99	−95.78	0.00	11.51	14
H^E	298.15[b]	2209.07	−348.89	114.84	0.92	11
H^E	323.15	2094.90	−315.65	124.25	0.75	11
		Methylcyclohexane–Toluene System				
G^E	333.15[b]	859.68	−50.34	0.00	2.05	12
G^E	353.15	800.95	−52.45	0.00	1.36	12
G^E	363.15	772.13	−34.59	0.00	1.90	12
G^E	373.15	733.27	−42.53	0.00	2.04	12
H^E	283.15[b]	2113.72	−98.31	0.00	3.75	13
H^E	298.15[b]	2070.48	−90.23	0.00	10.52	13
		n-Heptane–Methylcyclohexane System				
G^E	304.65[b]	0.00	0.00	0.00		15
G^E	320.64	0.00	0.00	0.00		15
G^E	353.10	0.00	0.00	0.00		15
H^E	298.15[b]	136.33	−27.68	0.00	0.58	11
H^E	323.15	75.63	−17.78	0.00	0.08	11

[a] Standard deviation. [b] Integration constants used in this work.

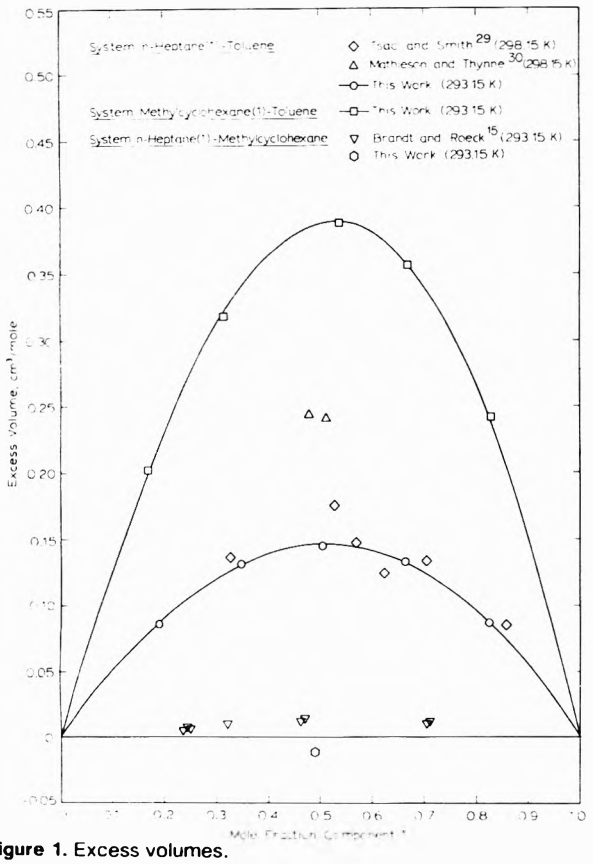

Figure 1. Excess volumes.

systems, in accordance with the general behavior of mixtures formed by nonpolar molecules of similar size. The only exception is the asymmetry shown by the excess heat capacity of the system *n*-heptane–toluene near room temperature. However, the absolute values are very small in this region, and the relative error is large. The shape of the curve will therefore depend on the type of fit chosen.

The following discussion will be limited to the excess thermodynamic functions for equimolar mixtures.

The *n*-heptane–toluene and methylcyclohexane–toluene systems show a very similar temperature dependence of the excess Gibbs free energy, enthalpy, and entropy. All these functions increase with decreasing temperature. The excess Gibbs free energy of an equimolar mixture of *n*-heptane and toluene reaches 450 J/mol at 180 K; the corresponding value for methylcyclohexane–toluene is 440 J/mol at 160 K. These values are unusually high for hydrocarbon mixtures and show that the mixtures are close to the point of phase separation. Cloud point experiments with approximately equimolar mixtures, however, showed no phase separation down to the freezing point for the two systems.

The excess heat capacity curves of both systems are very similar above 240 K. Below this temperature, the excess heat capacity of the *n*-heptane–toluene system becomes rapidly more negative, whereas the excess heat capacity of the methylcyclohexane–toluene system levels off and even shows a slight increase below 200 K. This difference in the C_p^E curves, however, has only a small effect on the derived excess enthalpies and entropies. Below 240 K, the excess enthalpy and entropy of the *n*-heptane–toluene system increase faster with decreasing temperature than the corresponding functions for methylcyclohexane–toluene. The excess volumes of the two systems at 293.15 K are quite different, with a maximum value of 0.15 cm³/mol for *n*-heptane–toluene and 0.39 cm³/mol for methylcyclohexane–toluene.

The derived excess thermodynamic properties for the mixture of *n*-heptane and methylcyclohexane, which is practically equimolar, are shown in Figure 6 and listed in Table VIII.[23] Although the mixture is almost ideal at room temperature, the excess enthalpy and entropy show a strong increase at lower temperatures, especially below about 240 K. The excess heat capacity curve is similar to that of the *n*-heptane–toluene system. However, G^E remains relatively small over the whole temperature range. The excess volume is near zero at 293.15 K.

Theoretical Correlations of the Derived Excess Thermodynamic Properties

Correlations Based on the Conformal Solution Theory. The theory of conformal solutions was developed by Longuet-Higgins.[4] Derivations of the pertinent mathematical expressions can be found in the original paper and in books by Prigogine[8] and Hill[31] and will not be presented here. The main assumption of the theory is that the potential, u_{ij}, of a pair of molecules conforms to a universal function.

$$u_{ij} = \epsilon_{ij} u(r_{ij}/\sigma_{ij}) \tag{13}$$

where r_{ij} denotes the distance between the centers of the molecules. All molecular pairs involved must have very nearly the same energy parameters ϵ_{ij} and length parameters σ_{ij}. Whereas the second assumption seems reasonable for the mixtures considered here, the first is clearly not fulfilled because the molecules under consideration are nonspherical.

Rowlinson and Sutton[5] have modified the conformal solution theory to make it applicable to nonspherical molecules. They assume that the intermolecular potential may be represented as

$$u_{ij} = 4\epsilon_{ij}[(\sigma_{ij}/r_{ij})^{12} - (\sigma_{ij}/r_{ij})^6(1 + a_{ij}g_{ij}(\omega_{ij}))] \tag{14}$$

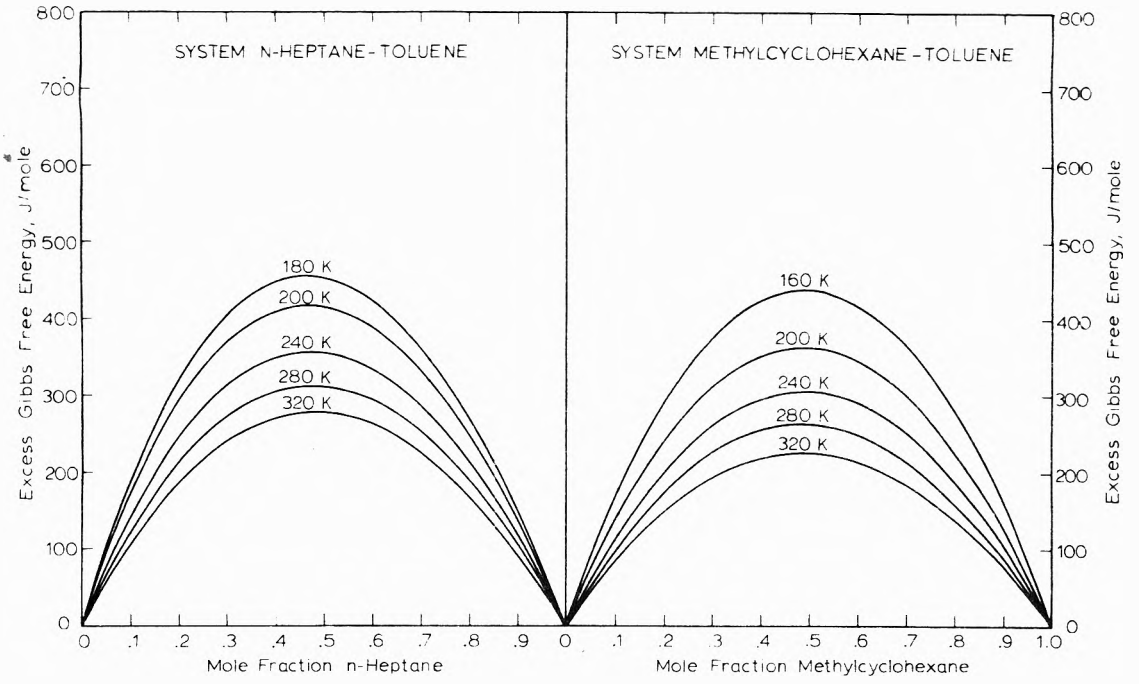

Figure 2. Excess Gibbs free energy of the *n*-heptane–toluene and methylcyclohexane–toluene systems.

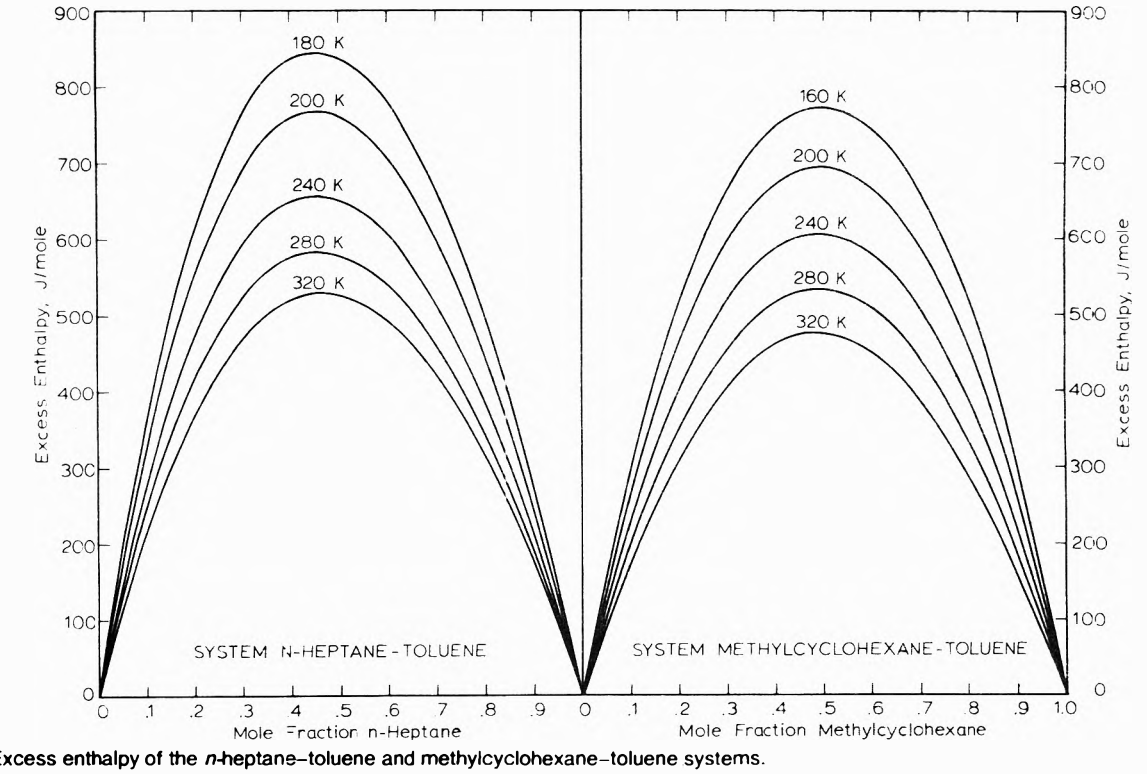

Figure 3. Excess enthalpy of the *n*-heptane–toluene and methylcyclohexane–toluene systems.

which corresponds to a Lennard-Jones potential with an orientation-dependent part. The quantity ω_{ij} denotes all coordinates describing the mutual orientations of a molecular pair, a_{ij} is a constant, and g_{ij} is defined such that

$$\int g_{ij}\, d\omega_{ij} = 0 \qquad (15)$$

with the integration taken over all possible mutual orientations.

An obvious deficiency of the treatment of Rowlinson and Sutton is the assumption that the repulsive part of the potential is spherical. There is some reason, however, to believe that the nonideal behavior of aliphatic–aromatic hydrocarbon mixtures is mainly due to the influence of directional attractive forces. Mixtures of saturated hydrocarbons are usually fairly ideal, although the shapes of the molecules (and thus the repulsive potential) are far from spherical. Typical examples are the systems *n*-hexane–cyclohexane, *n*-heptane–methylcyclohexane, and *n*-octane–tetraethylmethane.[7] On the other hand, quantum mechanical calculations of the lattice energy of crystalline ben-

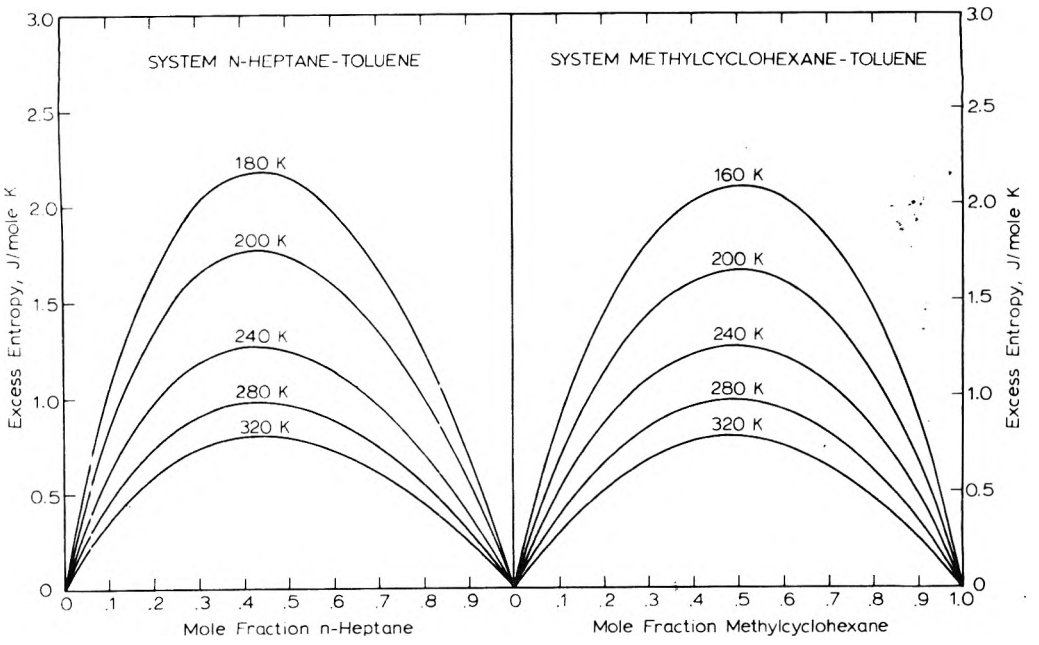

Figure 4. Excess entropy of the *n*-heptane–toluene and methylcyclohexane–toluene systems.

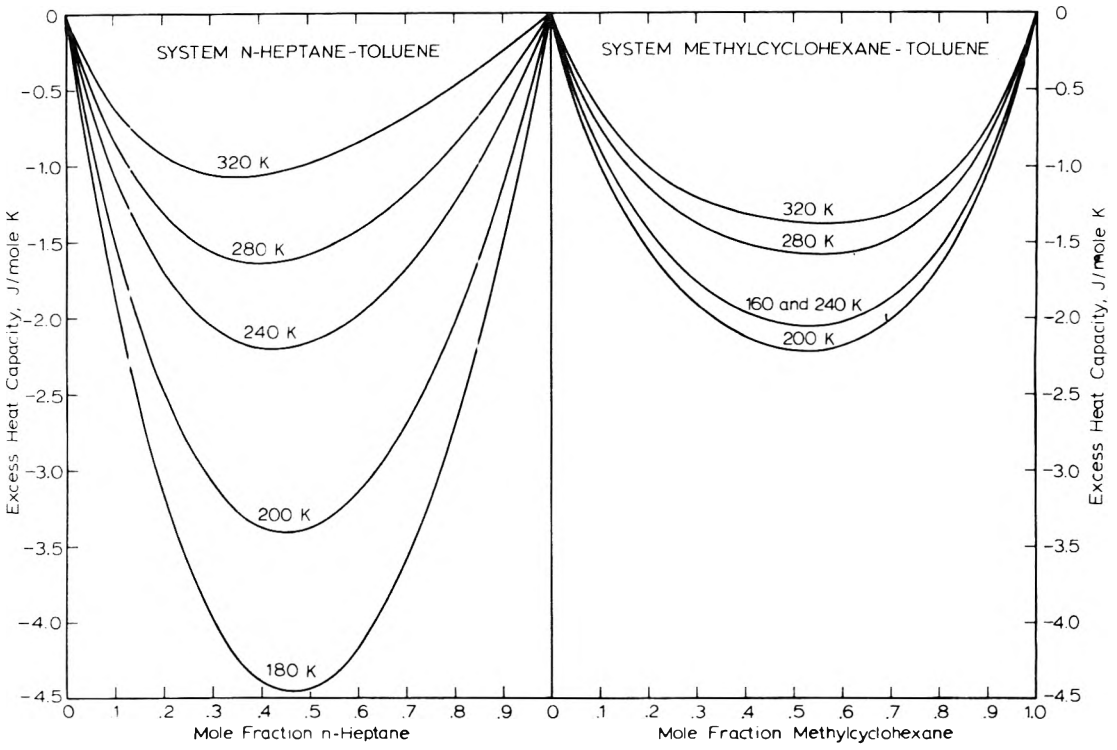

Figure 5. Excess heat capacity of the *n*-heptane–toluene and methylcyclohexane–toluene systems.

zene[32,33] show that the attractive forces vary strongly with molecular orientation, due to the highly anisotropic polarizability of the π-electron systems. Also, the attractive forces between benzene molecules are unusually strong. The π electrons contribute 40% of the lattice energy, although they represent only 20% of all valence electrons.

Although the structure of liquid benzene is certainly much less ordered than that of the solid, the molecules still can be expected to favor orientations for which the attractive energy is large. This effect will decrease with increasing temperature since the thermal motion of the molecules counteracts any order in the liquid.

When benzene is mixed with another liquid which shows no orientation effects, some of the strong π–π electron interactions between neighboring benzene molecules are broken, resulting in a positive excess enthalpy. This effect will be larger at lower temperatures, where the benzene molecules are statistically more likely to assume orientations with large attractive energies. Since the orientational forces in the mixture are weaker than in pure benzene, increased

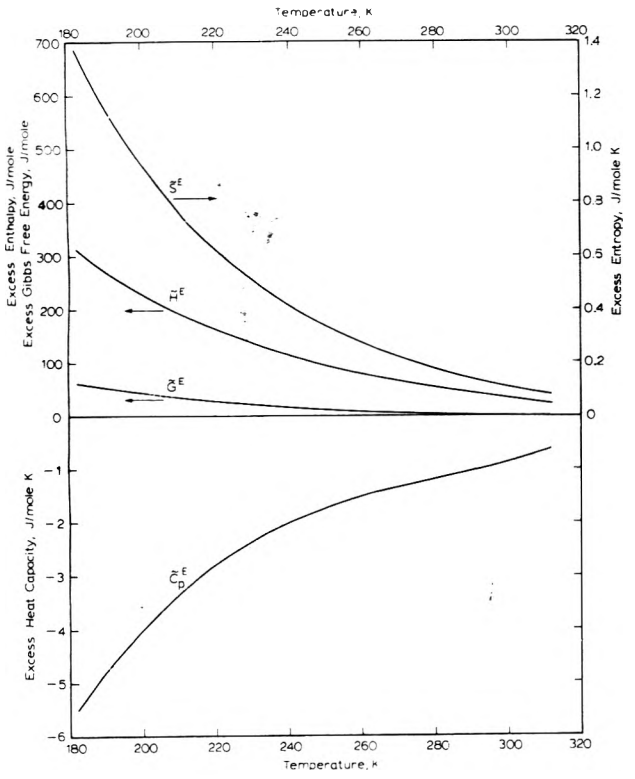

Figure 6. Excess thermodynamic functions of mixture of *n*-heptane (1)–methylcyclohexane mixture (x_1 = 0.4891).

randomness of orientation results, causing a positive excess entropy.

These effects have been found in mixtures of benzene with saturated hydrocarbons.[7,8] Mixtures containing toluene instead of benzene show the same effects, although the excess thermodynamic properties are smaller than for corresponding benzene mixtures. This can readily be explained by the more aliphatic character of toluene (16.7% of the valence electrons are π electrons *vs.* 20% in benzene) and by the larger intermolecular distances (due to the larger molar volume), which weaken the π–π electron interactions.

If the following parameters[34] are introduced

$$e_{12} = (2\epsilon_{12} - \epsilon_{11} - \epsilon_{22})/\epsilon_{00} \quad (16)$$

$$s_{12} = (2\sigma_{12} - \sigma_{11} - \sigma_{22})/\sigma_{00} \quad (17)$$

$$\delta_{ij} = (a_{ij}^2\epsilon_{ij}/kT)(\int g_{ij}^2\, d\omega_{ij}/\int d\omega_{ij}) \quad (18)$$

$$d_{12} = (2\delta_{12} - \delta_{11} - \delta_{22})T \quad (19)$$

where the indices 1 and 2 refer to components of the mixture and 0 to a reference species, the excess thermodynamic properties are given[5] by

$$G^E = x_1x_2[e_{12}U_0 - 3s_{12}RT + d_{12}(2U_0/T + R)] \quad (20)$$

$$H^E = x_1x_2[e_{12}(U_0 - T(\partial U_0/\partial T)_p) + d_{12}(4U_0/T - 2(\partial U_0/\partial T)_p + R)] \quad (21)$$

$$S^E = x_1x_2[-e_{12}(\partial U_0/\partial T)_p + s_{12}(3R) + d_{12}(2U_0/T^2 - 2(\partial U_0/\partial T)_p/T)] \quad (22)$$

$$V^E = x_1x_2[-e_{12}T(\partial V_0/\partial T)_p + s_{12}(3V_0) + d_{12}(-V_0/T - 2(\partial V_0/\partial T)_p)] \quad (23)$$

where U_0 and V_0 denote the configurational energy and the volume, respectively, of a reference liquid.

If the parameter d_{12} is set equal to zero, the equations reduce to those given by the conformal solution theory. Because the reference species must satisfy the same criteria as a component of the mixture, it is convenient to choose one of the components for this purpose. Toluene is used here because it is the common component of the two systems mainly considered here.

The configurational energy of liquid toluene was computed using the relation

$$U_0(T) = -H_v(T_0) - \int_{T_0}^{T}(C_p, \text{gas} - C_p, \text{liquid})\, dT + RT \quad (24)$$

The quantity C_p,gas was calculated from the vibrational frequencies given by Scott, *et al.*,[27] assuming free rotation of the methyl group; T_0 was taken to be 298.15 K; the heat of vaporization H_v at T_0 used was 37991 J/mol (API[22]). The configurational energy of liquid toluene between 160 and 370 K was found to be (J, mol, K):

$$U_0 = -63693.102 + 154.86636T - 0.32404623T^2 + 5.053086 \times 10^{-4}T^3 - 3.2640018 \times 10^{-7}T^4 \quad (25)$$

The density of liquid toluene is listed in the API Tables at 10° intervals from 183.15 to 383.15 K. From these values, the molar volumes were computed and fitted by a polynomial (cm^3, mol, K):

$$V_0 = 80.430085 + 7.4025442 \times 10^{-2}T + 1.1405825 \times 10^{-5}T^2 + 1.2595624 \times 10^{-7}T^3 \quad (26)$$

The theory predicts a quadratic dependence on composition for all excess thermodynamic properties, which is very nearly the case for the systems considered here. It is therefore sufficient to examine the excess thermodynamic functions of the equimolar mixtures.

Equations 20–23 contain three adjustable parameters, e_{12}, d_{12}, and s_{12}. In principle, these parameters could be determined to give a best fit of any of the excess properties over the whole range of temperature. In practice, however, it is preferable to fit G^E since H^E and S^E can both be derived from it. A good fit of either S^E or H^E alone would not guarantee a good fit of G^E because the latter is obtained from either of the former by integration and thus also depends on an integration constant.

The parameters e_{12} and d_{12} were determined by fitting the theoretical excess free energy, G^E_{th}, as given by eq 20, to the experimental excess free energy, G^E_{expt}, as given in Table V, for the equimolar mixture over the temperature range of the experimental data. A least-squares method was used which consisted in minimizing the integral over the squares of the residuals

$$I = \int_{T_1}^{T_2}(G^E_{expt} - G^E_{th})^2\, dT \quad (27)$$

Here T_1 and T_2 are the lowest and highest temperatures of the C_p measurements, respectively. The minimum could be found analytically, but if a computer is available it is less cumbersome to evaluate the integral numerically for several trial values of e_{12} and d_{12} and to determine the minimum by iteration. The other thermodynamic functions can then be computed using eq 21, 22, and 23.

The influence of the parameter s_{12} on G^E, H^E, and S^E is very small. However, s_{12} has a large effect on V^E since it is,

by definition, closely related to the intermolecular distances.

Several types of fits were attempted. Each method used has been assigned a number. The parameters obtained in these fits are shown in Table IX. The excess thermodynamic properties derived from this model are given as a function of temperature in Table X,[23] and compared with experiments in Figures 7–9.

Method 1. $e_{12} \neq 0$; $d_{12} = s_{12} = 0$. This model corresponds to the original conformal solution theory without inclusion of the volume parameter s_{12}. The best fit is found by adjusting the parameter e_{12} such that I (as given by eq 27) becomes a minimum.

Method 2. $e_{12} \neq 0$; $d_{12} = 0$; $s_{12} \neq 0$. Since the parameter s_{12} is mainly related to the excess volume, it was determined by inserting the experimental excess volume into eq 23, giving one relation between e_{12} and s_{12} which is used to eliminate s_{12} from eq 20. e_{12} is then found again by minimizing I.

The inclusion of s_{12} has very little effect on the predicted values of G^E, H^E, and S^E. It is impossible, however, to predict V^E from a knowledge of G^E using the parameter e_{12}. The predicted excess volume for *n*-heptane–toluene is larger than for methylcyclohexane–toluene, in disagreement with the experimental findings. For both systems, the predicted temperature dependence of G^E is too small. The discrepancy between theory and experiment becomes much more pronounced for H^E and S^E, which are obtained from G^E by differentiation and therefore very sensitive to any deviations. Not only is the quantitative agreement poor, but the predicted temperature dependence is much too small.

Method 3. $e_{12} = s_{12} = 0$; $d_{12} \neq 0$. This model illustrates the effect of the noncentral forces.

Method 4. $e_{12} = 0$; $d_{12} \neq 0$; $s_{12} \neq 0$. The parameters d_{12} and s_{12} are determined by fitting the excess volume at 293.15 K exactly and by least-squares fitting the excess free energy as a function of temperature.

The variation of G^E with temperature predicted by methods 3 and 4 is too large. The predicted H^E and S^E values are too large and show a much greater temperature dependence than the experimental values. These effects are exactly the opposite to the results of the conformal solution theory (methods 1 and 2).

Method 5. $e_{12} \neq 0$; $d_{12} \neq 0$; $s_{12} = 0$. This model applies when the influence of both central and noncentral forces is important and a fit of the excess volume is not desired.

Method 6. $e_{12} \neq 0$; $d_{12} \neq 0$; $s_{12} \neq 0$. The parameters are determined by fitting the excess volume at 293.15 K exactly and by least-squares fitting the excess Gibbs free energy as a function of temperature.

Method 5 and 6 allow a fit of G^E over the temperature range covered in this work well within the experimental accuracy. The H^E and S^E values predicted by the theory fit the experimental values very well in the case of *n*-heptane–toluene and reasonably well in the case of methylcyclohexane–toluene.

Table XI shows the contributions of the various parameters to the excess functions as computed from method 6. Again, the results are similar for both systems. The contribution of the directional forces (represented by d_{12}) to both H^E and S^E is greater than the contribution of the central forces (represented by e_{12}), especially at low temperatures. However, both terms contribute about equally to G^E. The contribution of the volume parameter s_{12} to G^E and S^E is only a few per cent, and it does not enter the expression for H^E (eq 21) at all. The contributions of the three parameters to V^E are of the same magnitude. The theory predicts V^E to be almost independent of temperature. Measurements on the related system cyclohexane–benzene show that the excess volume is independent of temperature over the range from 293.15 to 343.15 K,[7] which gives some support to the theoretical predictions.

The success of the theory of Rowlinson and Sutton in correlating the excess thermodynamic properties of *n*-heptane–toluene and methylcyclohexane–toluene suggests that the temperature dependence of these properties may be predictable from a knowledge of their values at room temperature alone. Two methods of prediction were attempted.

Method 7. The experimental values of G^E and H^E at 293.15 K are inserted into eq 20 and 21, respectively. The parameters e_{12} and d_{12} are determined from these two equations. The parameter s_{12} is assumed to be zero.

Method 8. The experimental values of G^E, H^E, and V^E at 293.15 K are inserted into eq 20, 21, and 23, respectively. The parameters e_{12}, d_{12}, and s_{12} are determined from these equations. The excess thermodynamic functions computed from these fits are shown in Figures 7–9 and in Table X.[23]

As in the previous fits, the predicted values of G^E, H^E, and S^E are not significantly affected by the parameter s_{12}. For the *n*-heptane–toluene system the predicted excess free energy, enthalpy, and entropy agree with the experimental data well within the accuracy of measurement down to the lowest temperatures. For the methylcyclohexane–toluene system the agreement is not quite as good, but still very satisfactory considering that the prediction covers a range of more than 130°, from 293.15 to 162 K.

Correlations Using the Theory of Flory. Flory[6] has proposed a theory for mixtures of nonspherical molecules which is more empirical than the theories presented in the preceding section. Only a brief discussion will be given here; the original paper should be consulted for details. Flory's notation will be followed here although it is not always consistent with the notation used in the rest of this paper.

Flory assumed that the forces between polyatomic molecules effectively arises from the surfaces of adjoining molecules. Each molecule is divided into r segments, each of which has s contact sites. The number of segments is proportional to the volume of the molecule. The total number of contact sites per molecule, rs, is proportional to the surface area of the molecule. The mean intermolecular energy of the liquid, E_0, is assumed to be inversely proportional to the volume per segment

$$E_0 = N r s \eta / 2v \qquad (28)$$

where N is the number of molecules, v is the volume of a segment, and η is a constant characterizing the energy of interaction for a pair of neighboring sites. Starting from these assumptions, Flory derived a reduced equation of state:

$$\tilde{p}\tilde{v}/\tilde{T} = \tilde{v}^{1/3}/(\tilde{v}^{1/3} - 1) - 1/\tilde{v}\tilde{T} \qquad (29)$$

The reduced quantities $\tilde{v}$, $\tilde{T}$, and $\tilde{p}$ are defined as

$$\tilde{v} = v/v^* \qquad (30)$$

$$\tilde{P} = p/p^* \qquad (31)$$

$$\tilde{T} = T/T^* \qquad (32)$$

v denotes the molar volume, and v^*, p^*, and T^* are characteristic quantities for each liquid.

TABLE IX: Comparison of Various Fits of the Derived Excess Thermodynamic Properties for Equimolar Mixtures

Method no.	Quantities fitted	e_{12}	d_{12}, K	s_{12}	V^E (293.15 K), cm^3/mol
		n-Heptane–Toluene System			0.1464 (expt)
		Conformal Solution Theory[a]			
1	G^E (182–312 K)	−0.03636	0	0	0.3016
2	G^E (182–312 K) V^E (293.15 K)	−0.03606	0	−0.001916	(0.1464)
		Theory of Rowlinson and Sutton[b]			
3	G^E (182–312 K)	0	−4.343	0	0.6394
4	G^E (182–312 K) V^E (293.15 K)	0	−4.239	−0.006108	(0.1464)
5	G^E (182–312 K)	−0.02136	−1.820	0	0.4451
6	G^E (182–312 K) V^E (293.15 K)	−0.01994	−1.918	−0.003834	(0.1464)
7	G^E (293.15 K) H^E (293.15 K)	−0.02194	−1.737	0	0.4451
8	G^E (293.15 K) H^E (293.15 K) V^E (293.15 K)	−0.02007	−1.904	−0.003770	(0.1464)
		Theory of Flory[c]			
9	H^E (182–312 K)				0.2639
10	H^E (298.15 K)				0.2641
		Methylcyclohexane–Toluene System			0.3885 (expt)
		Conformal Solution Theory[a]			
1	G^E (162–312 K)	−0.03216	0	0	0.2667
2	G^E (162–312 K) V^E (293.15 K)	−0.03236	0	−0.001506	(0.3885)
		Theory of Rowlinson and Sutton[b]			
3	G^E (162–312 K)	0	−3.600		0.5300
4	G^E (162–312 K) V^E (293.15 K)	0	−3.576	−0.001828	(0.3885)
5	G^E (162–312 K)	−0.01478	−1.978	0	0.4139
6	G^E (162–312 K) V^E (293.15 K)	−0.01466	−1.986	−0.000373	(0.3885)
7	G^E (293.15 K) H^E (293.15 K)	−0.01283	−2.248	0	0.4375
8	G^E (293.15 K) H^E (293.15 K) V^E (293.15 K)	−0.01251	−2.276	−0.000633	(0.3885)
		Theory of Flory[c]			
9	H^E (162–312 K)				0.3557
10	H^E (298.15 K)				0.3491

[a] Reference 4. [b] Reference 5. [c] Reference 6.

The theory is extended to a binary mixture by introducing a parameter X_{12} which characterizes the difference in the energy of interaction between neighboring molecules of different species from the average of the interactions in the pure component liquids:

$$X_{12} = s_1(\eta_{11} + \eta_{22} - \eta_{12})/2\nu^{*2} \tag{33}$$

The quantity ν^* is defined as

$$\nu^* = \nu/v \tag{34}$$

and is the same for all species. Flory has shown that the reduced temperature of a binary mixture is given by the expression:

$$\tilde{T} = (\Phi_1 p_1^* \tilde{T}_1 + \Phi_2 p_2^* \tilde{T}_2)/(\Phi_1 p_1^* + \Phi_2 p_2^* - \Phi_1 \theta_2 X_{12}) \tag{35}$$

where the segment fractions, Φ_1 and Φ_2, are defined as

$$\Phi_2 = 1 - \Phi_1 = x_2/(x_2 + x_1 r_1/r_2) \tag{36}$$

and the site fraction θ_2 by

$$\theta_2 = \Phi_2/(\Phi_2 + \Phi_1 s_1/s_2) \tag{37}$$

The molar excess free energy, enthalpy, entropy, and volume are:

$$G^E = x_1 p_1^* v_1^* \left[\tilde{v}_1^{-1} - \tilde{v}^{-1} + 3\tilde{T}_1 \ln\left(\frac{\tilde{v}_1^{1/3} - 1}{\tilde{v}^{1/3} - 1}\right)\right] + x_2 p_2^* v_2^* \left[\tilde{v}_2^{-1} - \tilde{v}^{-1} + 3\tilde{T}_2 \ln\left(\frac{\tilde{v}_2^{1/3} - 1}{\tilde{v}^{1/3} - 1}\right)\right] + x_1 v_1^* \theta_2 X_{12} \tilde{v}^{-1} \tag{38}$$

$$H^E = x_1 p_1^* v_1^* (\tilde{v}_1^{-1} - \tilde{v}^{-1}) + x_2 p_2^* v_2^* (\tilde{v}_2^{-1} - \tilde{v}^{-1}) + x_1 v_1^* \theta_2 X_{12} \tilde{v}^{-1} \tag{39}$$

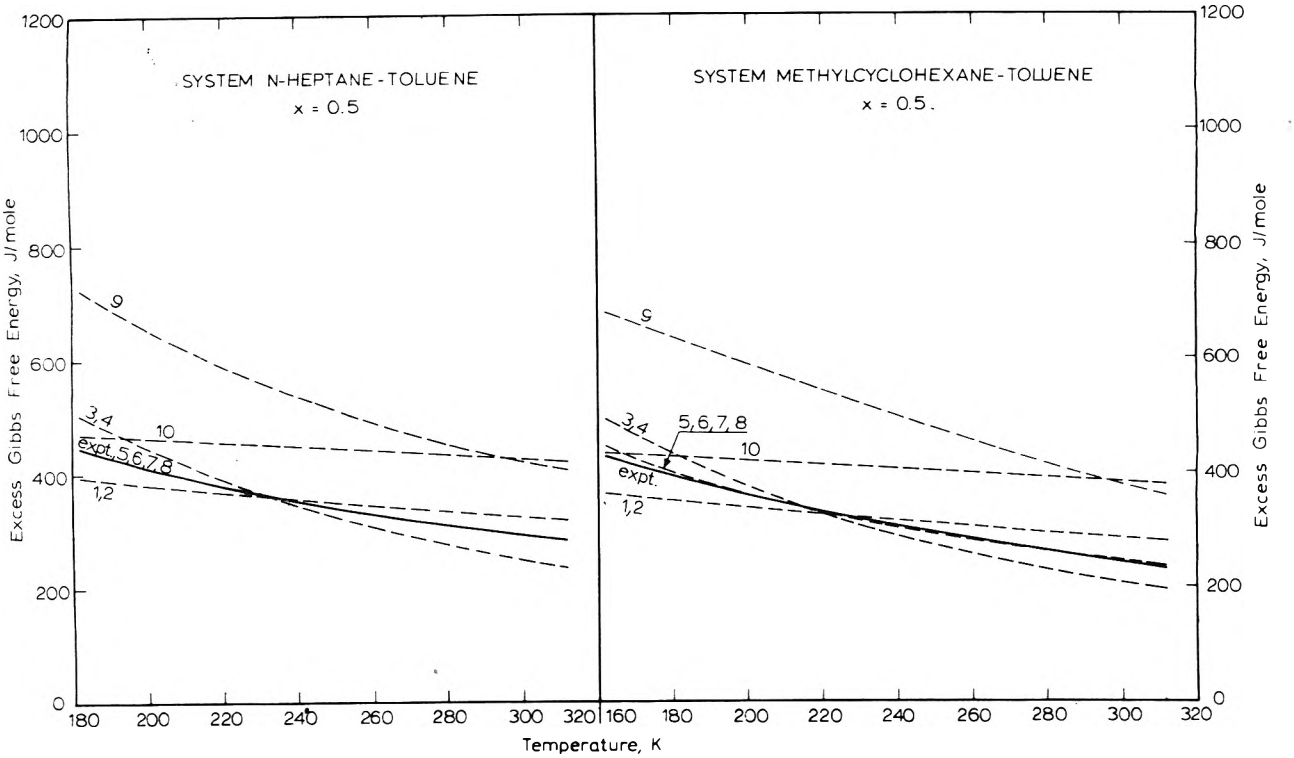

Figure 7. Predicted excess Gibbs free energy of the *n*-heptane–toluene and methylcyclohexane–toluene systems.

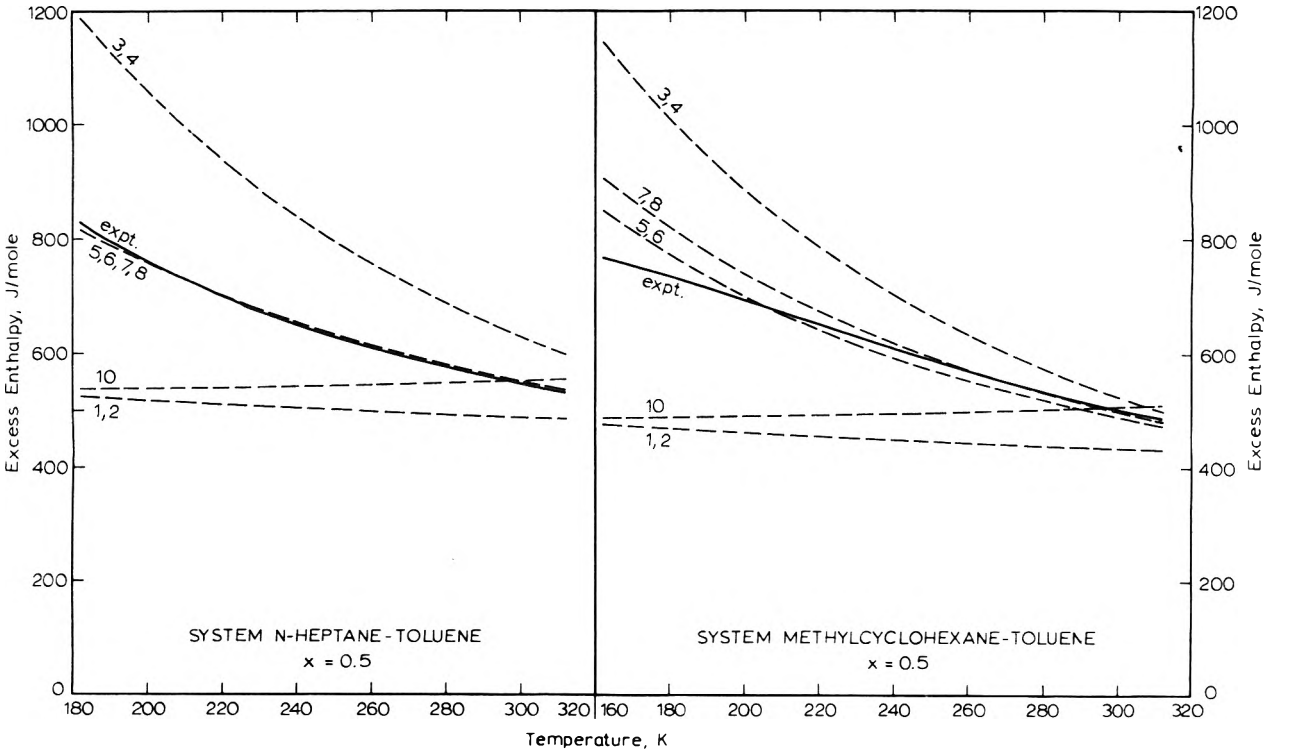

Figure 8. Predicted excess enthalpy of the *n*-heptane–toluene and methylcyclohexane–toluene systems.

$$S^E = -3\left[\frac{x_1 p_1^* v_1^*}{T_1^*}\ln\left(\frac{\tilde{v}_1^{1/3}-1}{\tilde{v}^{1/3}-1}\right) + \frac{x_2 p_2^* v_2^*}{T_2^*}\ln\left(\frac{\tilde{v}_2^{1/3}-1}{\tilde{v}^{1/3}-1}\right)\right] \quad (40)$$

$$V^E = (x_1 v_1^* + x_2 v_2^*)(\tilde{v} - \Phi_1\tilde{v}_1 - \Phi_2\tilde{v}_2) \quad (41)$$

At zero pressure, the reduced equation of state becomes

$$\tilde{T} = (\tilde{v}^{1/3} - 1)/\tilde{v}^{4/3} \quad (42)$$

Equation 42 can be differentiated with respect to temperature and rearranged to give

$$\tilde{v} = (1 + 4\alpha T/3)/(1 + \alpha T)^3 \quad (43)$$

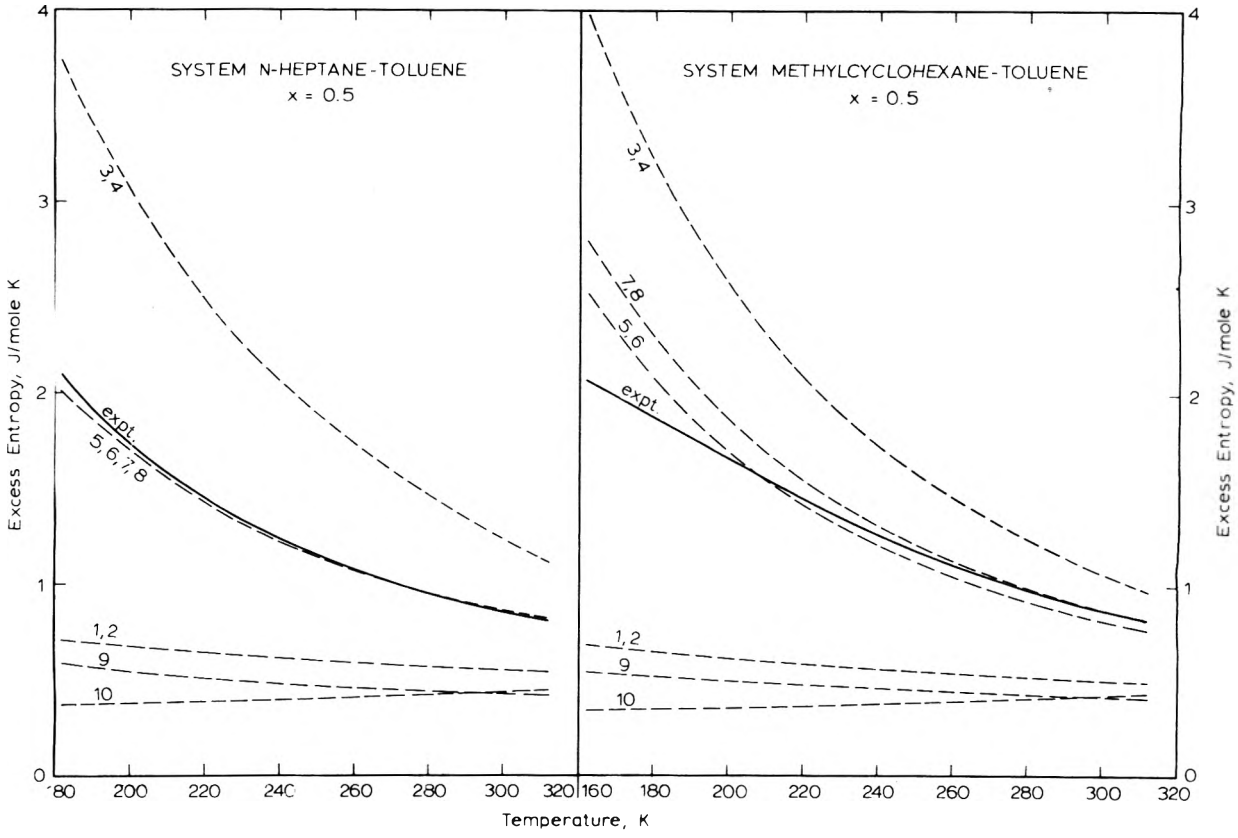

Figure 9. Predicted excess entropy of the *n*-heptane–toluene and methylcyclohexane systems.

Equation 43 permits the determination of $\tilde{v}$ if the coefficient of thermal expansion, α, is known at a certain temperature. If the molar volume, v, is known at the same temperature, the characteristic volume, v^*, can be computed from eq 30. Equation 42 serves to determine the corresponding value of $\tilde{T}$, which is inserted into eq 32 to determine T^*.

Differentiation of eq 29 with respect to pressure yields for the limit of zero pressure:

$$p^* = \tilde{T}\tilde{v}^2\alpha/\beta \tag{44}$$

This equation serves to determine the characteristic pressure, p^*, from the isothermal compressibility, β.

Table XII lists the parameters used for the pure components. All compressibilities were determined from isothermal measurements. The compressibility of *n*-heptane was measured by Eduljee, *et al.*,[35] and the compressibilities of methylcyclohexane and toluene were measured by Shinoda and Hildebrand.[36] Molar volumes and thermal expansion coefficients were computed from densities reported in the API tables.[22]

Abe and Flory[37] applied this theory to a wide variety of binary mixtures of nonpolar molecules. They determined the interaction parameter X_{12} by fitting the experimental excess enthalpy and then computed the other excess functions from X_{12}. This procedure was adopted here.

Since the number of segments, r, was chosen proportional to the volume of the molecule it follows that

$$r_1/r_2 = v_1^*/v_2^* \tag{45}$$

The number of contact sites, rs, was assumed to be proportional to the surface of the molecules. For spherical molecules, this leads to the relation

$$s_1/s_2 = (v_2^*/v_1^*)^{1/3} \tag{46}$$

Thus the quantities ϕ_2 and θ_2 can be determined from eq 36 and 37.

For nonspherical molecules, the ratio s_1/s_2 depends not only on the ratio v_2^*/v_1^*, but also on the shape of the molecules. For simplicity, however, eq 46 is adopted here. A change in the ratio s_1/s_2 would only affect the numerical value of X_{12} (which is treated here as an adjustable parameter), but not the derived excess thermodynamic properties.

Equations 35, 39, and 42 contain three unknown quantities, X_{12}, $\tilde{v}$, and $\tilde{T}$. Equations 35 and 42 can be combined to give

$$X_{12} = \frac{\phi_1 p_1^* \tilde{T}_1 + \phi_2 p_2^* \tilde{T}_2}{\phi_1\theta_2(\tilde{v}^{1/3} - 1)/\tilde{v}^{4/3}} + \frac{\phi_1 p_1^* + \phi_2 p_2^*}{\phi_1\theta_2} \tag{47}$$

Equation 39 is rearranged to yield

$$X_{12} = [H^E - x_1 p_1^* v_1^*(\tilde{v}_1^{-1} - \tilde{v}^{-1}) - x_2 p_2^* v_2^*(\tilde{v}_2^{-1} - \tilde{v}^{-1})]/x_1 v_1^* \theta_2 \tilde{v}^{-1} \tag{48}$$

The reduced volume, $\tilde{v}$, is adjusted by trial and error to make the quantity X_{12} equal for both equations. As a first guess, $\tilde{v}$ was taken to be

$$\tilde{v} = \phi_1\tilde{v}_1 + \phi_2\tilde{v}_2 \tag{49}$$

which corresponds to a zero excess volume. The value of $\tilde{v}$ was then improved by iteration until it changed by less than 10^{-6} from one step to the next one. The quantities G^E, S^E, and V^E were then determined from $\tilde{v}$ using eq 38, 40, and 41, respectively.

If the assumptions of Flory's theory were exact, X_{12}

TABLE XI: Contributions of Various Interaction Parameters to the Predicted Excess Thermodynamic Properties Using the Theory of Rowlinson and Sutton[a] (Based on Method 6, See Table IX)

Parameter	Temp, K 182	208	234	260	286	312
			n-Heptane–Toluene System			
			Excess Gibbs Free Energy, J/mol			
e_{12}	217.1	207.2	197.9	189.2	180.8	172.8
d_{12}	225.5	187.7	158.7	136.0	117.6	102.6
s_{12}	4.4	5.0	5.6	6.2	6.8	7.5
Total	447.0	399.9	362.3	331.4	305.3	282.9
			Excess Enthalpy, J/mol			
e_{12}	289.1	283.9	279.0	274.6	270.6	267.0
d_{12}	531.0	450.2	388.1	339.1	299.6	267.2
Total	820.1	734.0	667.1	613.7	570.3	534.3
			Excess Entropy, J/(mol K)			
e_{12}	0.395	0.368	0.346	0.329	0.314	0.302
d_{12}	1.679	1.262	0.980	0.781	0.636	0.528
s_{12}	−0.024	−0.024	−0.024	−0.024	−0.024	−0.024
Total	2.050	1.607	1.303	1.086	0.926	0.806
			Excess Volume, cm^3/mol			
e_{12}	0.082	0.099	0.117	0.137	0.159	0.183
d_{12}	0.337	0.316	0.301	0.291	0.284	0.280
s_{12}	−0.273	−0.280	−0.287	−0.295	−0.303	−0.312
Total	0.146	0.134	0.130	0.132	0.139	0.151
			Methylcyclohexane–Toluene System			
			Excess Gibbs Free Energy, J/mol			
e_{12}	165.6	156.8	148.6	141.0	133.9	127.1
d_{12}	272.8	217.1	177.2	147.5	124.5	106.2
s_{12}	0.4	0.4	0.5	0.6	0.7	0.7
Total	438.8	374.3	326.4	289.1	259.0	234.0
			Excess Enthalpy, J/mol			
e_{12}	215.6	211.0	206.7	202.8	199.4	196.3
d_{12}	633.3	514.8	429.5	365.5	316.0	276.6
Total	848.8	725.8	636.2	568.3	515.4	473.0
			Excess Entropy, J/(mol K)			
e_{12}	0.308	0.283	0.262	0.245	0.232	0.222
d_{12}	2.225	1.551	1.136	0.865	0.679	0.546
s_{12}	−0.002	−0.002	−0.002	−0.002	−0.002	−0.002
Total	2.531	1.831	1.396	1.108	0.909	0.766
			Excess Volume, cm^3/mol			
e_{12}	0.052	0.065	0.080	0.096	0.114	0.135
d_{12}	0.373	0.340	0.318	0.304	0.295	0.290
s_{12}	−0.026	−0.027	−0.028	−0.029	−0.029	−0.030
Total	0.399	0.378	0.370	0.371	0.379	0.394

[a] Reference 6.

would have to be a constant over the whole range of composition and temperature. The calculations show that X_{12} is indeed very nearly independent of composition for both systems, but is strongly temperature dependent. Table XIII[23] lists X_{12} as a function of composition for 298.15 K and as a function of temperature for the equimolar mixture.

The variation of G^E, H^E, and S^E with temperature calculated by this model (method 9) for an equimolar mixture is shown in Figures 7–9 and in Table X.[23] It will be noted that the predicted excess entropy is much too low over the whole temperature range, which means that the predicted excess Gibbs free energy is too high (see Figure 7). Similar results were obtained by Abe and Flory[37] for the system cyclohexane–benzene, *n*-hexane–benzene, and *n*-heptane–benzene, for which the predicted excess entropies are one-third to one-half of the experimental values. Although the theory of Flory is not restricted to spherical molecules, it does not take any orientational effects into account, which is the most likely reason for its failure to explain the observed excess entropy. The theory, however, correctly predicts the excess volume of the system *n*-heptane–toluene to be smaller than that of the system methylcyclohexane–toluene, although the numerical agreement is poor for the former system (the predicted excess volume is 80% higher than the experimental value for the system *n*-heptane–toluene and 9% lower for the system methylcyclohexane–toluene).

TABLE XII: Parameters Used in the Theory of Flory (T = 298.15 K)

	n-Heptane	Methylcyclohexane	Toluene
α, K^{-1}	1.251×10^{-3}	1.137×10^{-3}	1.070×10^{-3}
β, cm^3/J	1.470×10^{-3}	1.203×10^{-3}	9.480×10^{-4}
v, cm^3/mol	147.47	128.34	106.86
p^*, J/cm^3	426.78	458.30	536.13
v^*, cm^3/mol	113.70	100.65	84.67
T^*, K	4657.3	4884.8	5041.9

Another way of testing Flory's theory is to predict the temperature dependence of the excess thermodynamic properties from a knowledge of the interaction parameter, X_{12}, at room temperature.

The parameter X_{12} was determined from the excess enthalpy at 298.15 K as described above. By combining eq 35 and 42, the parameter $\tilde{T}$ can be eliminated and $\tilde{v}$ can be determined. Assuming that X_{12} is independent of temperature, G^E, H^E, S^E, and V^E can be computed as functions of temperature from eq 38–41. The results for equimolar mixtures of *n*-heptane–toluene and methylcyclohexane–toluene are shown in Table X[23] and Figures 7–9 (method 10). For both systems, the predicted excess Gibbs free energy and enthalpy are practically independent of temperature, in disagreement with experiment. The predicted excess entropy is much too small and decreases with decreasing temperature. The predicted excess volume also decreases with decreasing temperature. Apparently this method of predicting the temperature dependence of the excess thermodynamic properties delivers no better results than the simple assumption that these properties are independent of temperature.

Comparison of the Theories. The results of the preceding sections clearly show that the theory of Rowlinson and Sutton is superior in correlating the excess enthalpy, free energy, and entropy of the *n*-heptane–toluene and methylcyclohexane–toluene systems. The conformal solution theory and the theory of Flory (both of which assume no orientation-dependent intermolecular forces) fail to represent the temperature dependence of the excess thermodynamic functions even qualitatively. This suggests that directional interactions play an important role in these systems.

For the two systems investigated here, the theory of Rowlinson and Sutton allows a fairly good prediction of H^E, G^E, and S^E at low temperatures if these data are known at room temperature. More data on aliphatic–aromatic and alicyclic–aromatic mixtures are needed to decide whether this holds for all systems of these types.

The theory of Rowlinson and Sutton has two comparatively minor deficiencies. (1) Excess volumes cannot be predicted reliably from the other excess properties. In this respect, the theory of Flory gives better results. This is probably due to the fact that the latter theory uses experimental parameters for both pure components and therefore gives a more realistic equation of state for the mixture. (2) The excess enthalpy and entropy of the *n*-heptane–toluene system below about 220 K show a larger temperature dependence than the corresponding functions for the methylcyclohexane–toluene system. This different behavior is not predicted by the theory of Rowlinson and Sutton. It is interesting to note that the *n*-heptane–methylcyclohexane system, which is almost ideal at room temperature, shows a strong increase in H^E and S^E in the same temperature region. This suggests that both effects may have the same cause. A possible explanation is presented here in a qualitative manner.

Whereas methylcyclohexane and toluene are relatively rigid molecules, *n*-heptane is a chain molecule which is quite flexible at sufficiently high temperatures. The molecules alternately coil up, stretch, assume S shapes, etc. No significant orientation effects would be expected in such a liquid. At lower temperatures, however, the molecules become more rigid and assume a more defined shape. They are now more likely to line up with their neighbors in some preferred orientation, similar to the orientation in aromatic liquids assumed in the treatment above. By analogous reasoning, this would explain why *n*-heptane mixes almost ideally with methylcyclohexane at room temperature, whereas the mixture has a considerable excess enthalpy and entropy at low temperatures. The combination of the attractive orientational forces in toluene and the repulsive orientational forces in *n*-heptane would also explain why mixtures of these two components have higher H^E and S^E values at low temperatures than mixtures of methylcyclohexane and toluene.

Supplementary Material Available. Tables III, VII, VIII, X, and XIII will appear following these pages in the microfilm edition of this volume of the journal. Photocopies of the supplementary material from this paper only or microfiche (105 × 148 mm, 24× reduction, negatives) containing all the supplementary material for papers in this issue may be obtained from the Journals Department, American Chemical Society, 1155 Sixteenth St. N.W., Washington, D.C. 20036. Remit check or money order for $6.00 for photocopy or $2.00 for microfiche, referring to code number JPC-75-590.

References and Notes

(1) Based on a thesis submitted by J.K.H. in partial fulfillment of the requirements for Ph.D. Degree, Georgia Institute of Technology, 1970. See *Diss. Abstr. Int. B*, **31**, 6587 (1971).
(2) School of Chemical Engineering, Georgia Institute of Technology, Atlanta, Ga. 30332.
(3) To whom correspondence concerning this paper should be addressed.
(4) H. C. Longuet-Higgins, *Proc. Roy. Soc., Ser. A*, **205**, 247 (1951).
(5) J. S. Rowlinson and J. R. Sutton, *Proc. Roy. Soc., Ser. A*, **229**, 271 (1955).
(6) P. J. Flory, *J. Amer. Chem. Soc.*, **87**, 1833 (1965).
(7) J. S. Rowlinson, "Liquids and Liquid Mixtures," Butterworths, London: 1st ed, 1959; 2nd ed, 1969.
(8) I. Prigogine, "The Molecular Theory of Solutions," North-Holland Publishing Co., Amsterdam, 1957.
(9) S. C. P. Hwa, Ph.D. Thesis, Georgia Institute of Technology, Atlanta, (1963); S. C. P. Hwa and W. T. Ziegler, *J. Phys. Chem.*, **70**, 2572 (1966).
(10) G. N. Brown, Jr., Ph.D. Thesis, Georgia Institute of Technology, Atlanta, (1970).
(11) G. W. Lundberg, *J. Chem. Eng. Data*, **9**, 193 (1964).
(12) G. Schneider, *Z. Phys. Chem. (Frankfurt am Main)* **27**, 171 (1961).
(13) K. Sosnkowska-Kehiahian, unpublished results (communicated by H. Kehiahian).
(14) J. Surovy and J. Heinrich, *Sb. Pr. Chem. Fak. SVST (Slov. Vys. Sk. Tech.)*, 201 (1966).
(15) H. Brandt and H. Roeck, *Chem. Ing. Tech.*, **29**, 397 (1957).
(16) R. B. Scott, C. H. Meyers, R. D. Rands, Jr., F. G. Brickwedde, and N. Bekkedahl, *J. Res. Nat. Bur. Stand.*, **35**, 39 (1945).
(17) H. A. McGee, Jr., Ph.D. Thesis, Georgia Institute of Technology, Atlanta, 1955.
(18) K. F. Liu and W. T. Ziegler, *J. Chem. Eng. Data*, **11**, 187 (1966).
(19) C. R. Barber, *Metrologia*, **4**, 35 (1969).
(20) ASTM Standard D 1217-54, American Society for Testing and Materials, Pittsburgh, Pa., 1965.
(21) F. D. Rossini, "Chemical Thermodynamics," Wiley, New York, N.Y., 1950, p 454.
(22) American Petroleum Institute Research Project 44, Selected Values of Properties of Hydrocarbons and Related Compounds, College Station, Tex.
(23) See paragraph at end of text regarding supplementary material.

(24) J. P. McCullough and J. F. Messerly, *U.S. Bur. Mines, Bull*, **No. 596** (1961).
(25) T. B. Douglas, G. T. Furukawa, R. E. McCoskey, and A. F. Ball, *J. Res. Nat. Bur. Stand*, **53**, 139 (1954).
(26) D. R. Douslin and H. M. Huffman, *J. Amer. Chem. Soc.*, **68**, 173 (1946).
(27) D. W. Scott, G. B. Guthrie, J. F. Messerly, and S. S. Todd, *J. Phys. Chem.*, **66**, 911 (1962).
(28) O. Redlich and A. T. Kister, *Ind. Eng. Chem.*, **40**, 345 (1948).
(29) C. C. Tsao and J. M. Smith, *Chem. Eng. Progr. Symp. Ser.*, **7**, 107 (1953).
(30) A. R. Mathieson and J. C. J. Thynne, *J. Chem. Soc.*, 3708 (1956).
(31) T. L. Hill, "An Introduction to Statistical Thermodynamics," Addison-Wesley, Reading, Mass., 1960, Chapter 20.
(32) K. Banerjee and L. Salem, *Mol. Phys.*, **11**, 405 (1966).
(33) A. I. M. Rae and R. Mason, *Proc. Roy. Soc., Ser. A*, **304**, 487 (1968).
(34) Rowlinson and Sutton[5] use a parameter $\Delta_{12} = d_{12}/T$. Δ_{12} is inversely proportional to T, and d_{12} is a true constant having the dimension of temperature.
(35) H. E. Eduljee, D. M. Newitt, and K. E. Weale, *J. Chem. Soc.*, 3086 (1951).
(36) K. Shinoda and J. H. Hildebrand, *J. Phys. Chem.*, **65**, 183 (1961).
(37) A. Abe and P. J. Flory, *J. Amer. Chem. Soc.*, **87**, 1838 (1965).

Application of the Polanyi Adsorption Potential Theory to Adsorption from Solution on Activated Carbon. VI. Adsorption of Some Binary Organic Liquid Mixtures[1]

Timothy W. Schenz and Milton Manes*

Chemistry Department, Kent State University, Kent, Ohio 44242 *(Received September 5, 1974)*

Publication costs assisted by Calgon Corporation

Adsorption isotherms on a previously studied activated carbon have been determined for the following dilute binary solutions of miscible (a) and of partially miscible (b) components: (a) benzene and/or toluene in methanol, *n*-hexane (C_6), *n*-heptane (C_7), *n*-octane (C_8), *n*-decane (C_{10}), and 2,2,4-trimethylpentane (TMP); and C_{10} in C_8 and TMP; and (b) C_7, C_8, C_9, C_{10}, and TMP in methanol. Except for C_9, vapor-phase isotherms on the same carbon were determined for all components. Except for some upward deviation (higher capacity) for methanol at low capacities (presumably due to chemisorption), the vapor-phase isotherms of methanol, benzene, and toluene were in good agreement with expectations from the Polanyi theory. The paraffins all showed significant downward deviations in the low capacity range that increased with increasing molecular size. The adsorption of benzene and of toluene in the paraffins, over the experimental mole fraction range of the order of 10^{-2} to 10^{-5}, was well accounted for by incorporating the experimental vapor-phase data into the Hansen–Fackler modification of the Polanyi theory. The adsorption of benzene and of toluene in methanol could be accounted for by application of an empirical scale factor to the adsorption potential of methanol in the theoretically derived adsorption isotherm (without the presumed chemisorptive effects). The adsorption of the paraffins in methanol could be accounted for in terms of an earlier Polanyi-based treatment of partially miscible systems, and the adsorption of C_{10} in C_8 and in TMP could be accounted for by the Hansen–Fackler treatment; however, it was here necessary to use the theoretically derived isotherms for the paraffin solutes, *i.e.*, without regard for the observed vapor-phase deviations that accounted for their behavior as solvents.

Introduction

Earlier work in this series[2,3] has dealt with the application of the Polanyi adsorption potential theory[4] to account for the adsorption onto activated carbon of partially and completely miscible organic liquids from water solution. The present study progresses to the adsorption of partially and completely miscible binary organic liquid mixtures. Although there is considerable earlier work on such mixtures, most of which has been reviewed by Kipling,[5] this work is largely concerned with adsorption isotherms (or "composite isotherms") over the entire composition range, and does not deal with highly dilute solutions. By contrast, the present study has emphasized the dilute to trace concentration range, which is of particular interest to the final purification of compounds by adsorption, as distinguished from bulk separation. Moreover, we expected the low concentration range to be particularly amenable to theoretical treatment by the earlier-used modifications of the Polanyi theory.

The miscible systems comprised benzene and/or toluene in methanol, *n*-hexane (C_6), *n*-heptane (C_7), *n*-octane (C_8), *n*-decane (C_{10}), and 2,2,4-trimethylpentane (TMP). The partially miscible systems comprised C_7, C_8, C_9, C_{10}, and TMP in methanol. (C_9 was not used as a solvent for budgetary reasons.) Except for C_9, vapor-phase adsorption isotherms were determined for all of the solution components.

Following the procedures of the earlier work on water solutions, we constructed theoretical liquid-phase adsorption isotherms from the corresponding vapor-phase isotherms of the individual components. However, whereas estimated vapor-phase isotherms had previously sufficed in the calculations, some of the present liquid-phase isotherms showed strong deviations from expectations; these deviations appeared to be ascribable to deviations from theory of the sol-

vent vapor-phase isotherms, which led to the extensive vapor-phase determinations.

Methanol was chosen as a relatively weakly competing solvent for both the paraffins and the aromatic solutes, on the basis of its relatively low refractive index. Benzene and toluene were similarly expected to be adsorbed from the paraffins, which could therefore be observed both as solvents and as solutes.

The characterization of a particular isotherm as normal or anomalous was considerably facilitated by the use of a carbon sample on which there was a considerable background of adsorption data.

Theoretical

The underlying theory, which is here briefly summarized, is more fully explained in the cited references.[2-4,6,7]

The Polanyi theory[4] assumes a heterogeneous "adsorption space" within which a molecule from the bulk phase loses an amount of potential energy (the "adsorption potential," ϵ), that for a given molecule is independent of temperature (because it arises from temperature-independent London forces), and increases with closer proximity to the solid surface; ϵ is highest in fissures or within fine pores. In vapor-phase adsorption the vapors are concentrated in the adsorption space, relative to the bulk phase, to an extent that depends on the local value of ϵ. Wherever ϵ suffices to concentrate the vapor to saturation concentration, the vapor liquefies; this liquefaction accounts for practically all of the physical adsorption on the solid.

In the adsorption from solution of a solid or of a partially miscible liquid, one similarly gets condensation of either the solid or liquid solute in the adsorption space; here, however, the driving force for adsorption, ϵ_{sl}, is equal to the (vapor-phase) adsorption potential of the solute, reduced by that of an equal volume of the displaced solvent.

In the adsorption of miscible mixtures, according to the Hansen–Fackler[6] modification of the Polanyi theory, the driving force for adsorption is the same. Here, however, there is no phase separation in the adsorption space; instead, the adsorbate concentration varies continuously throughout the adsorption space and the resulting change in the solution concentration is calculated by integration over the entire adsorption space.

In vapor-phase adsorption the adsorbate volume comprises that volume in which the adsorption potential either equals or exceeds the value required for condensation, which Polanyi gives as

$$\epsilon \geq RT \ln p_s/p \tag{1}$$

where p_s is the saturation pressure of the liquid and p the equilibrium pressure. A plot of the adsorbate volume against the equilibrium value of ϵ, as calculated from eq 1, is called a "characteristic curve." It depends for a given adsorbate on the nature and structure of the adsorbent, but is temperature independent. It is readily calculated from an adsorption isotherm at any convenient temperature; the reverse calculation of an adsorption isotherm from the characteristic curve makes it possible to calculate adsorption isotherms over a wide temperature range from one experimental isotherm.

Since the ratio of the adsorption potentials of any two adsorbates in any equivalent location should be constant over the entire adsorption space, the Polanyi theory predicts that all characteristic curves for a given adsorbent should be the same, except for a constant scale factor for each adsorbate in the adsorption potential abscissa. Dubinin[8] suggested that this scale factor should be proportional to the adsorbate molar volume, at least approximately, so that a plot of the adsorbate volume against $\epsilon/\bar{V}$ (now called a "correlation curve") should be the same for all adsorbates. It turns out that whereas a single correlation curve describes the adsorption of a series of similar compounds (*e.g.*, the lower homologous paraffins),[9] significant differences do exist, and they turn out to be crucial for liquid-phase adsorption.

For the adsorption of a solid from solution (and, by extension, for the adsorption also of a partially miscible liquid), Polanyi gives the equations

$$\epsilon_{sl} \equiv RT \ln c_s/c = \epsilon_s - \epsilon_l(V_s/V_l) \tag{2}$$

or

$$\frac{\epsilon_{sl}}{V_s} = \frac{\epsilon_s}{V_s} - \frac{\epsilon_l}{V_l} \tag{3}$$

where c_s and c are the saturation and equilibrium concentrations, ϵ_s and ϵ_l the adsorption potentials (at comparable volumes) of the solute and solvent, and V_s and V_l the corresponding molar volumes. (We shall omit the superscript bars wherever the subscript clearly indicates that we are dealing with a molar volume rather than an adsorbate volume.)

Since $\epsilon/\bar{V}$ is the abscissa of a correlation curve, eq 3 implies that the abscissa in the correlation curve for the adsorption of the liquid solute may be estimated as the difference between the abscissas of the corresponding curves for the solute and solvent. Since both of the latter are in turn derivable from the corresponding vapor-phase isotherms, eq 3 links liquid- to gas-phase adsorption for partially miscible liquids.

Manes and Hofer[7] have suggested that in the absence of experimental adsorption data for the components, the ratio of ϵ_i/V_i to ϵ_r/V_r (where the subscript i refers to a component and r to some reference substance) may be estimated from the refractive indices of the liquids by the equations

$$\gamma_i \equiv \frac{\epsilon_i/V_i}{\epsilon_r/V_r} = \frac{p_i}{p_r} \tag{4}$$

where p is defined as $(n^2 - 1)/(n^2 + 2)$ and n is the refractive index. The factor that relates the correlation curve for the adsorption to the hydrocarbon correlation curve (which Manes and Hofer used as their reference) then becomes

$$\gamma_{sl} = \gamma_s - \gamma_l = \frac{p_s - p_l}{p_h} \tag{5}$$

Wohleber and Manes[2] used these equations to estimate the adsorption of a number of partially miscible organic solutes from water solution. Although the adsorption of water was anomalously weak, most of the data could be successfully correlated by the use of a constant empirical value of γ for water, together with the hydrocarbon correlation curve for the carbon and the calculated values for the γ factors of the adsorbates.

For adsorption from miscible liquids, Hansen and Fackler[6] derived the equations[10]

$$-\epsilon_1/V_1 + \frac{RT}{V_1} \ln (x_{1\sigma}/x_{1B}) = -\epsilon_2/V_2 + \frac{RT}{V_2} \ln (x_{2\sigma}/x_{2B}) \tag{6}$$

and

$$V\Delta c_1 \, m = \int_0^{\sigma} \left(\frac{x_{1\sigma}}{V_\sigma} - \frac{x_{1B}}{V_B} \right) d\sigma \tag{7}$$

In eq 6 $x_{1\phi}$, x_{1B}, $x_{2\phi}$, x_{2B} refer to the mole fraction of each component in bulk and in the adsorbate, in any volume element $d\phi$, and the various values of ϵ refer to the same element of volume. Equation 6 is used to determine the composition of the adsorbate in each element of the adsorption space. Equation 7 is used to determine the experimentally determined adsorption. In this equation V_ϕ and V_B refer to the average volume per mole of the bulk and adsorbate mixtures; m is the mass of the adsorbent. V is the solution volume and Δc the reduction in concentration of component 1 in solution.

For miscible systems, as for partially miscible systems, one may either determine ϵ for each component as a function of the adsorbate volume from its vapor-phase isotherm or, alternately, one may estimate it by use of eq 5.

The treatment by Wohleber and Manes[2] of partially miscible liquid systems neglects any solubility of solvent in the solute adsorbate. We have derived equations to include this effect; the derivation applies the Hansen-Fackler[6] treatment to account for variations in the composition of the adsorbate within the adsorption space. The derived equations were applied to our data on partially miscible systems, but did not improve the correlation, presumably because of the relatively low solubility limits. The derivation, which may be useful for some systems, is given in the Appendix.[11]

Vapor pressures were calculated from the Antoine equation constants given by National Bureau of Standards[12] and by Hala, *et al.*[13] Solubility data for the hydrocarbon–methanol systems were obtained from the compilations by Stephen and Stephen[14] and by Kiser, *et al.*[15]

Experimental Section

All of the experiments described in this article and the earlier ones in this series were carried out with carbon samples from a single batch; this enables comparison of the reported results with the results of earlier experiments. The carbon, of 1140 m^2/g surface area (BET), was used as received except for oven drying at 110° for 24 hr. The batch was Pittsburgh Activated Carbon grade CAL.

The paraffins (C_6, C_7, C_8, C_9, C_{10}, and TMP), and benzene, toluene, and methanol were all reagent grade chemicals (Matheson Coleman and Bell) with a minimum purity of 99.5% as determined by gas chromatography; they were used as received. Where analysis was made by uv spectrophotometry (benzene and toluene) the adsorbate reagents were Spectroquality grade.

As in earlier articles, the weighed carbon samples were shaken with measured volumes of solutions of measured concentrations in 125-ml screw-capped erlenmeyer flasks for 16 hr in a water bath thermostated at 25°. Following equilibration the carbon was allowed to settle in the bath and samples of the supernatant liquid were either filtered through sintered glass or else centrifuged. Paraffinic adsorbates were analyzed by glc in a Victoreen Series 4000 gas chromatograph equipped with a dual flame ionization detector and electrometer interfaced to a Digital Equipment Corp. (DEC) Lab 8/E computer. The computer integrated the peak areas to a reproducibility of 0.2%. The column packing was Porapak Q (porous polymer beads of polystyrene–divinylbenzene), except for the analysis of C_{10} (from either C_8 or from TMP), where the column packing was Durapak (Carbowax bonded to a silicone base). Both packings were obtained from Waters Associates.

Spectrophotometric measurements were carried out in a Cary 14 spectrophotometer in the ultraviolet range.

Vapor-phase adsorption isotherms were determined on a McBain balance with quartz springs and buckets. Elevated temperatures were maintained around the sample by placing the sample tube in a dewar flask internally wound with heater tape. Temperatures were controlled by a variable voltage supply and measured by a thermocouple external to the sample tube.

Results and Discussion

Vapor Phase. Table 1[11] gives the experimental data for the vapor-phase adsorption of methanol, benzene, toluene, C_6, C_7, C_8, C_{10}, and TMP. In addition to the loading as a function of temperature and pressure, Table 1 gives the same data calculated in terms of the volume adsorbed and $T/\bar{V} \log p_s/p$ ($\epsilon/4.6\bar{V}$), following the notation of earlier articles.

Figure 1 shows the data for benzene and toluene; Figures 2 and 3 show similar data for methanol and for C_6, C_8, and C_{10}. In all cases the curves are calculated from the hydrocarbon (paraffin) correlation curve[7] for the carbon and the refractive index of the liquid phase.

Figure 1 illustrates that benzene and toluene are in good agreement with theory. Figure 2 shows good agreement of methanol adsorption with theory at the higher loadings, with positive deviations (high loading for a given adsorption potential or high adsorption potential for a given loading) at the lower loadings. Figure 3 shows good agreement at high capacities for the paraffins, with negative deviations that increase with reduced loading and with increasing molecular size of the adsorbate. Similar plots for C_7 and for TMP (not shown to save space) show C_7 to be intermediate between C_6 and C_8, and TMP to be somewhat more deviant than C_{10}.

The positive deviations for methanol at low loadings are consistent with earlier observations[16] that methanol tends to chemisorb on carbon, presumably by interaction with surface oxygenated groups. The downward deviations for the paraffins, since they are most pronounced at low loadings and for larger molecules, would appear to be consistent with some sort of molecular sieving. However, the presumed molecular sieving would have to be due to fine pores of limited depth rather than of limited cross section, since the limiting cross sections of the normal paraffins should be about the same. We shall see, however, that these considerations do not appear to apply when the same paraffins are solutes.

Consider now the validity of the generalized hydrocarbon (paraffin) correlation curves as reported, for example, by Grant, Manes, and Smith[9] and by Grant and Manes.[17] Whereas these curves were based on the adsorption of paraffins from methane to hexane, the authors noted that for experimental reasons the low capacity range was based only on the adsorption of methane and ethane, and therefore that there was no direct experimental verification of the validity of the paraffin correlation line for the higher paraffins at the low capacities. Having circumvented the earlier experimental limitations, we now find that the generalized correlation line does not in fact account for all of the vapor-phase adsorption of the higher paraffins. Nevertheless, we shall soon see that it is useful for predicting the adsorptive behavior of the higher paraffins as solvents.

Partially Miscible Liquids. Table 2[11] gives the experimental data for the adsorption of C_7, C_8, C_9, C_{10}, and TMP from methanol solution. Figure 4, which is typical of the results, shows the adsorption data for TMP from methanol,

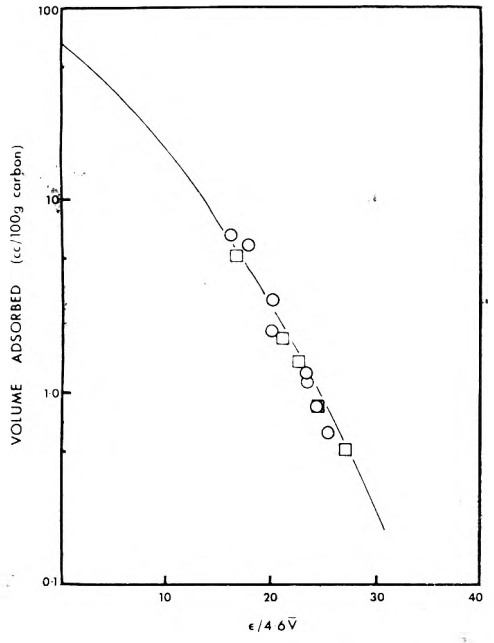

Figure 1. Vapor-phase adsorption of benzene (O) and toluene (□), plotted as volume adsorbed *vs.* $\epsilon/4.6\bar{V}$ (= $T/\bar{V}$ log p_s/p). The solid line was calculated from paraffin correlation line and refractive indices.

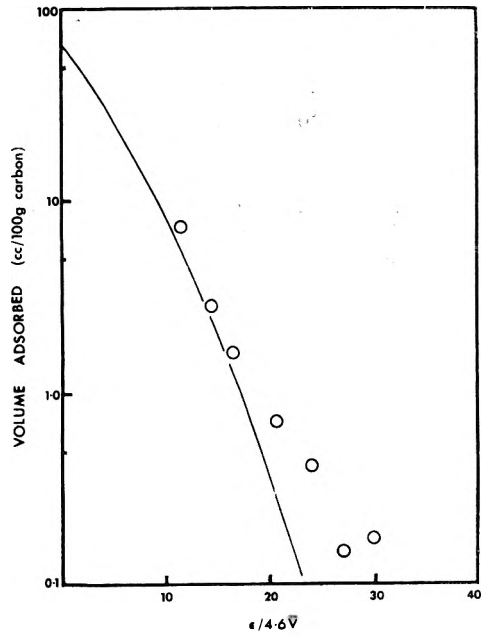

Figure 2. Vapor-phase adsorption of methanol, plotted as in Figure 1.

plotted as volume adsorbed *vs.* $T/\bar{V}$ log x_s/x, as compared with the predicted line based on the earlier work of Wohleber and Manes.[2] The predicted value of the abscissa at the lowest adsorption point overestimates the equilibrium solute concentration by about two orders of magnitude. However, the experimental data follow a curve that appears to differ from the predicted curve only by an abscissa scale factor, in analogy with the results of Wohleber and Manes on water solutions. Moreover, because the calculated γ values for methanol and the paraffins are rather close together (0.87 and 1.00), one would expect the adsorption data to be quite sensitive to any deviations from theory.

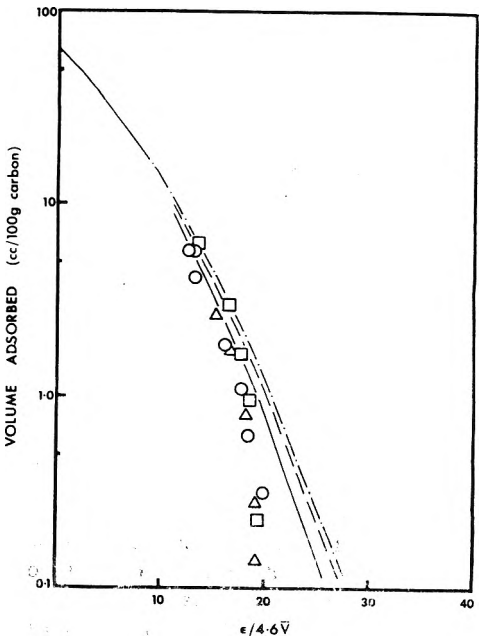

Figure 3. Vapor-phase adsorption of *n*-hexane (O), *n*-octane (□), and *n*-decane (Δ), plotted as in Figure 1. Calculated correlation curves are *n*-hexane (——), *n*-octane (– –), and *n*-decane (– · –).

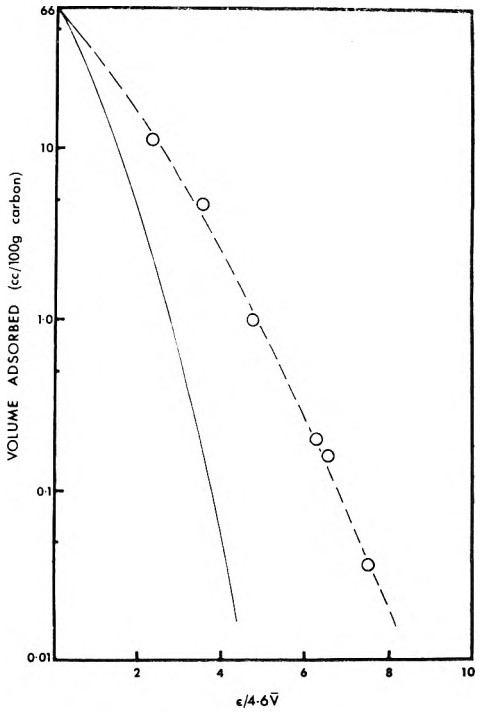

Figure 4. Adsorption of TMP from methanol, plotted as volume adsorbed *vs.* $\epsilon_{sl}/4.6\bar{V}$ (= $T/\bar{V}$ *log* x_s/x): calculated curve (—); experimental curve (- - - - -).

Empirical factors were determined for all of the adsorption data as follows: C_7, 0.70; C_8, 0.74; TMP, 0.76; C_9, 0.79; and C_{10}, 0.78, for a mean of 0.75. Thus the empirical scale factors are lower than the calculated factors by approximately 15%. With the application of the empirical scale factor, the results fall quite nicely into coincidence, over a wide range of concentrations.

The use of an empirical γ factor for methanol, together with the theoretical isotherms for the components as calcu-

lated from the paraffin correlation curve for the carbon, leads to considerably better correlation of the observations than does the use of the experimental vapor-phase isotherms. The ignoring, in effect, of the observed upward deviations of the methanol vapor-phase isotherm may be justified if these deviations are due to chemisorptive interactions with oxygenated groups on the carbon, since the chemisorptive binding sites probably differ from those of high energy physical adsorption. However, it is more difficult to justify an empirical factor for methanol as a solvent when that empirical factor differs significantly from the vapor-phase isotherm. Moreover, it is similarly difficult to justify ignoring the observed negative deviations of the vapor-phase isotherms of the paraffin solutes, which deviations are not at all reflected in the experimental observations on liquid mixtures. If one ascribes the vapor-phase deviations to structural or steric or molecular sieving effects, it is difficult to explain, on the basis of the Polanyi model, why these effects do not influence the adsorption of the same component when it is a solute. Finally, the validity of the observed deviations in the gas-phase isotherms is supported by the liquid-phase isotherms in which the paraffins are solvents. These we now consider.

Miscible Liquids. Table 3[11] gives the adsorption data for benzene in methanol, C_6, C_7, C_8, C_{10}, and TMP; toluene in methanol, C_6, and C_8; and C_{10} in C_8 and TMP. The data were reduced to volume adsorbed as a function of bulk mole fraction, using the method of Hansen and Fackler.[6] As input to this treatment we could use, for both solvent and solute, either the correlation curves derived from the paraffin correlation curve and the refractive index, or the experimental vapor-phase isotherm. For benzene and toluene in methanol the input data for the method were the correlation curve for the solute (for which the experimental and the calculated curves coincided) and the theoretical correlation curve for methanol (with an abscissa scale factor of 0.75 as was used for the partially miscible systems with methanol solvent). It turned out that the adsorption in methanol was well accounted for by this procedure; again it was better to ignore the positive deviations in the vapor-phase methanol isotherm. For the paraffin solvent systems, however, the data are best correlated by using the theoretical correlation curve for the solute (as in the previous section, where methanol was the solvent), and the experimental correlation curves for the solvents.

Figures 5–7 are plots of the adsorbate volume against the log of the solute mole fraction, as calculated by the Hansen–Fackler method. Figure 5 shows, for example, the adsorption of benzene from TMP, and Figure 6 the adsorption of toluene from hexane. In these figures the dotted line is calculated on the assumption of theoretical correlation curves for both solvent and solute, and the solid line is calculated by incorporating the experimental gas-phase isotherm for the solvent. The deviations of the solvent vapor-phase isotherms, which had previously shown no experimental consequences, have here made themselves manifest.

Up to this point a comparison of the adsorption of benzene from the paraffins and of the paraffins from methanol would suggest that downward deviations of the vapor-phase isotherms are reflected in the behavior of the solvent, but not of the solute. The possibility arises, however, that failure of the deviations in the solute vapor isotherms to be reflected in the corresponding liquid-phase isotherm may be peculiar to methanol solutions. We now consider the adsorption of C_{10} from TMP and from C_8. Figure 7

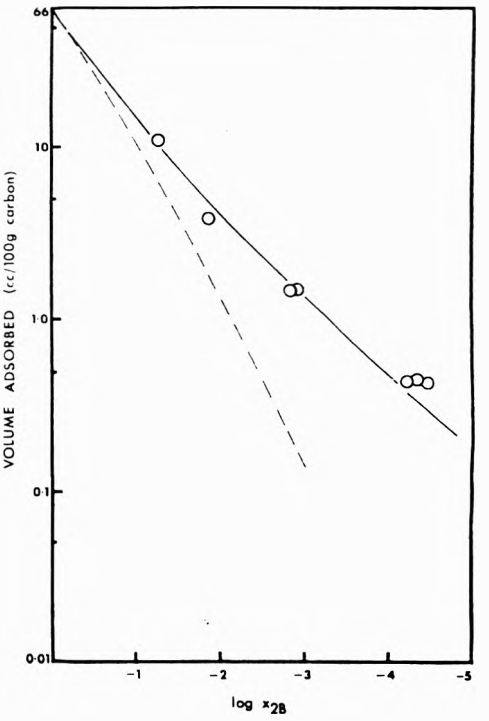

Figure 5. Adsorption of benzene from TMP plotted as volume adsorbed *vs.* log of solute (bulk) mole fraction: (—) calculated from experimental vapor phase isotherm of solvent; (- - -) calculated from refractive indices.

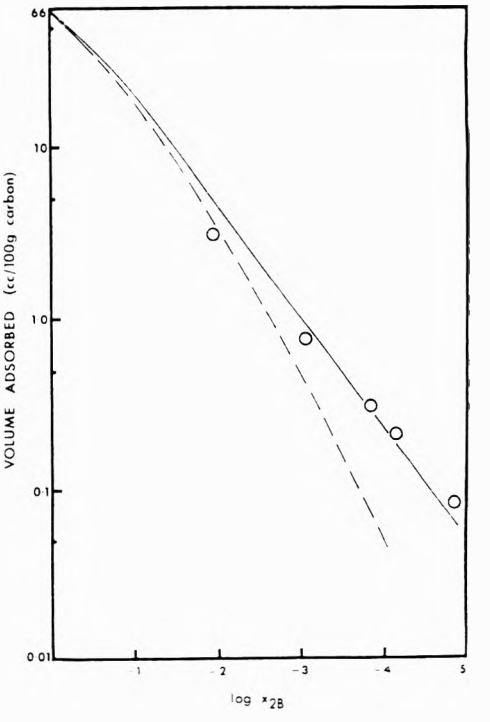

Figure 6. Adsorption of toluene from *n*-hexane. Plot and legend similar to Figure 5.

shows the plot of the adsorption of C_{10} from C_8 as compared with the theoretical curve calculated both from the experimental gas-phase isotherms of both components (dotted line) and from the experimental isotherm of the solvent and the theoretical isotherm of the solute. Again, the combination of the experimental solvent and theoreti-

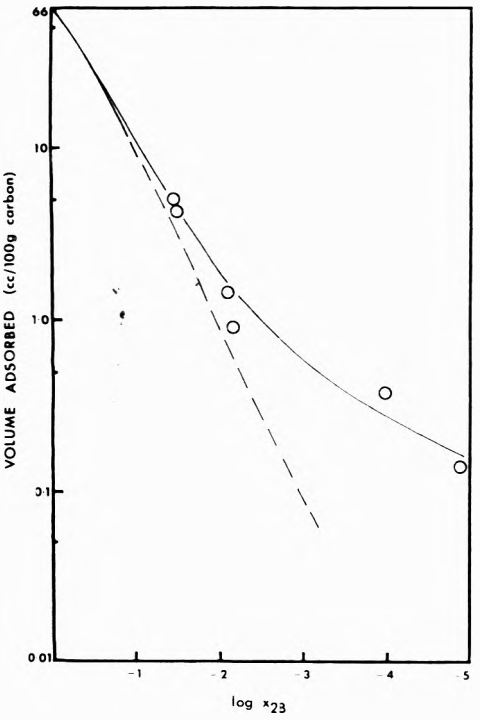

Figure 7. Adsorption of *n*-decane from *n*-octane. Plot and legend similar to Figure 6.

cal solute correlation curves accounts for the data. The plot for C_{10} from TMP (not shown) is quite similar.

Final Comments. Although the presumed structural effects on the vapor-phase isotherms have not here shown any effects on the liquid-phase adsorption of solutes, molecular sieving of solutes is well known in, for example, the removal of color bodies from sucrose. Moreover, Chiou and Manes[18] found steric effects to profoundly affect the adsorption of octahedral acetylacetonate complexes. We would therefore expect such effects to appear with larger or more hindered solutes than we have here observed.

Finally, the correlation methods that have been used here may well be applicable to at least a somewhat greater variety of binary mixtures than we have here been able to observe. Whereas the principal difficulty to further application would appear to be the necessity of determining the low-capacity adsorption isotherm of each new solvent, this apparent difficulty could be readily circumvented by determining the adsorption of a reference solute, such as benzene, in a new solvent. Any deviations due to the solvent should be the same for a wide variety of solutes and should be readily incorporated into the calculations by the methods described here.

Conclusions

(1) For benzene and toluene, the vapor-phase adsorption isotherms on activated carbon are in keeping with predictions from the Polanyi approach. For methanol, positive deviations appear, particularly at low capacities; these may be ascribed to adsorptive interaction with surface groups on the carbon. The paraffin hydrocarbons from hexane and above fit the theory at high capacities, but deviate downward at low capacities, the downward deviation increasing at lower capacities and with increasing molecular size of the paraffin. These deviations may be tentatively ascribed to structural or steric effects such as inability to be accommodated by shallow pores, rather than to molecular sieving in the usual sense of inability to enter fine pores of indefinite depth.

(2) For dilute solutions of benzene, toluene, and the paraffins in methanol solution, the liquid-phase adsorption isotherms are what one would predict from the theoretically derived isotherms (rather than the experimental ones), with the exception of a small empirical correction factor for the adsorption isotherm of methanol.

(3) For solutions of benzene in the paraffins, and for solutions of decane in octane and in TMP, the adsorption isotherms are what one would expect from using a Polanyi-based (Hansen–Fackler) treatment, using the experimental adsorption isotherms of the solvent and (where they differ from the experimental) the theoretical isotherms of the solutes.

(4) We have not found a satisfactory model to account for the observations that the downward deviations of adsorption isotherms, presumably due to structural effects, do not affect the adsorptive behavior of a component when it is a solute.

Acknowledgments. We thank the Goodyear Tire and Rubber Company for support of T.W.S. in the form of a Goodyear Fellowship.

Supplementary Material Available. Tables 1-3 and an Appendix will appear following these pages in the microfilm edition of this volume of the journal. Photocopies of the supplementary material from this paper only or microfiche (105 × 148 mm, 24× reduction, negatives) containing all of the supplementary material for the papers in this issue may be obtained from the Journals Department, American Chemical Society, 1155 16th St., N.W., Washington, D.C. 20036. Remit check or money order for $3.00 for photocopy or $2.00 for microfiche, referring to code number JPC-75-604.

References and Notes

(1) This article is based on the Ph.D. dissertation of T. W. Schenz, Kent State University, Dec 1973.
(2) D. A. Wohleber and M. Manes, *J. Phys. Chem.*, **75**, 61 (1971).
(3) D. A. Wohleber and M. Manes, *J. Phys. Chem.*, **77**, 809 (1973).
(4) M. Polanyi, *Verh. Deut. Phys. Ges.*, **16**, 1012 (1914); **18**, 55 (1916); *Z. Elektrochem.*, **26**, 370 (1920).
(5) J. J. Kipling, "Adsorption from Solution of Non-Electrolytes," Academic Press, New York, N.Y., 1965.
(6) R. S. Hansen and W. V. Fackler, *J. Phys. Chem.*, **57**, 634 (1953).
(7) M. Manes and L. J. E. Hofer, *J. Phys. Chem.*, **73**, 584 (1969).
(8) M. M. Dubinin and D. F. Timofeyev, *C. R. Acad. Sci. URSS*, **54** (8), 701 (1946).
(9) R. J. Grant, M. Manes, and S. B. Smith, *AIChE J.*, **8**, 403 (1962).
(10) The notation has been slightly changed for convenience. Attention is directed to typographical errors in eq 4 of ref 3, which is properly rendered in eq 7.
(11) See paragraph at end of text regarding supplementary material.
(12) National Bureau of Standards, "Selected Values of Properties of Hydrocarbons," Circular No. C461, Washington, D.C., 1947.
(13) Z. Hala, I. Wichterle, J. Polak, and T. Boublik, "Vapor-Liquid Equilibrium Data at Normal Pressures," Pergamon Press, Oxford, 1968.
(14) H. Stephen and T. Stephen, Ed., "Solubilities of Inorganic and Organic Compounds," Vol. 1, Part 2, MacMillan, New York, N.Y., 1963.
(15) R. W. Kiser, G. D. Johnson, and M. D. Shetlar, *J. Chem. Eng. Data.*, **6**, 338 (1961).
(16) Reference 5, p 173.
(17) R. J. Grant and M. Manes, *Ind. Eng. Chem., Fundam.*, **3**, 221 (1964).
(18) C. C. T. Chiou and M. Manes, *J. Phys. Chem.*, **77**, 809 (1973).

Reactions of Surface Isocyanate Groups with Selected Compounds

M. L. Unland

Corporate Research Department, Monsanto Company, St. Louis, Missouri 63166 *(Received August 30, 1974)*

Publication costs assisted by Monsanto Company

An infrared study was made of the reaction of –NCO groups on a Rh/Al_2O_3 surface with the following compounds: H_2, H_2O, D_2O, NH_3, n-$C_3H_7NH_2$, CH_3OH, C_2H_5OH, $(CH_3)_2CHOH$, HCHO, CH_3COOH, and HCl. Reactions of surface isocyanate groups are, for the most part, analogous to reactions of organic isocyanates with these same compounds. In the reaction of CH_3OH with –NCO, isotopic labeling of surface isocyanates showed that a new band observed in the 1680–1690-cm^{-1} region was due to a group containing both carbon and nitrogen atoms. This group is believed to be a surface urethane ($-NHCOOCH_3$). Further, prolonged pumping on the sample at room temperature or at slightly elevated temperatures was sufficient to cause reappearance of surface –NCO at the expense of $-NHCOOCH_3$. In other words, the surface-isocyanate + alcohol → surface-urethane reaction is reversible under fairly mild conditions.

Introduction

Recent infrared studies of the reduction of nitric oxide by carbon monoxide have led to the discovery of isocyanate species on the surface of both noble metal[1-3] and base metal[4] catalysts. The role of this surface isocyanate species in the NO + CO reaction is not clear. It may be an important factor in formation of NH_3 in auto exhaust or it may simply be the end result of a side reaction as the proposed mechanism of London and Bell[4] suggests. In any event, its presence does require the formation of a carbon–nitrogen bond on the catalyst surface and, therefore, could give insight into some interesting chemistry. The aim of the present study was to determine whether the reactions of the surface isocyanate species are analogous to the reactions of organic isocyanates. To this end, studies were made of the effect of treating the surface containing the –NCO group with various reactants at various temperatures. The extent of reaction was followed by observing changes in the infrared spectra of the samples.

Experimental Section

The infrared spectrometer and the sample cell have been described earlier.[1,2] The sample was prepared by air drying a dispersion of Baymal[5] and $Rh(NO_3)_3$ in distilled water on a CaF_2 disk. The resulting film was calcined in vacuo at 400° for ~4 hr after which it was oxidized in 100 Torr of O_2, evacuated, and reduced in 100 Torr of H_2, all at 400°. The nominal composition of the film was 5% Rh/Al_2O_3.[6] Before each experiment, the sample was "cleaned" at 400° by a similar evacuation–oxidation–evacuation–reduction–evacuation sequence. After cleaning the sample at 400°, the surface isocyanate was formed by dosing the hot sample with 100 Torr of a gas mixture containing (by volume) 10% CO, 5% NO, and 85% N_2. All materials were of reagent grade and used without further purification. The sample was cooled in this atmosphere and the pressure was reduced to ~1 Torr before scanning to check the –NCO band. After formation of –NCO, the sample was dosed with ~10 Torr of the desired reactant gas and allowed to equilibrate for ~15 min before further treatment. If the effects of temperature were to be examined, the sample was heated to the desired temperature and allowed to cool before the pressure was reduced to 1 Torr for examination. If temperature studies were not desired, the pressure was immediately reduced to 1 Torr and the scan started. All scans were made at or very close to room temperature.

Chemistry of Isocyanates. The preparation, uses, and chemistry of organic isocyanate compounds are detailed in the literature.[7-9] In general, reactions of isocyanates with compounds containing an active hydrogen are rapid and occur according to the general equation:

$$R{-}N{=}C{=}O + H{-}A \longrightarrow R{-}\underset{\displaystyle H}{\overset{\displaystyle |}{N}}{-}\overset{\displaystyle O}{\overset{\displaystyle ||}{C}}{-}A \qquad (1)$$

Perhaps the most important example of this is the reaction of isocyanates with alcohols to give urethane products:

$$R{-}NCO + R'OH \longrightarrow \underset{\text{urethane}}{RNH\overset{\displaystyle O}{\overset{\displaystyle ||}{C}}OR'} \qquad (2)$$

Other examples include reaction with water

$$RNCO + H_2O \longrightarrow \underset{\text{carbamic acid}}{RNHCOOH} \longrightarrow \underset{\text{amine}}{RNH_2} + CO_2 \qquad (3)$$

amines

$$RNCO + R'NH_2 \longrightarrow \underset{\text{urea}}{RNH\overset{\displaystyle O}{\overset{\displaystyle ||}{C}}{-}NHR'} \qquad (4)$$

carboxylic acids

$$RNCO + R'COOH \longrightarrow \underset{\text{anhydride}}{RNH\overset{\displaystyle O}{\overset{\displaystyle ||}{C}}{-}O{-}\overset{\displaystyle O}{\overset{\displaystyle ||}{C}}{-}R'} \longrightarrow \underset{\text{amide}}{RNH\overset{\displaystyle O}{\overset{\displaystyle ||}{C}}{-}R'} + CO_2 \qquad (5)$$

and halogen acids.

$$RNCO + HCl \rightleftharpoons \underset{\text{carbamyl halide}}{RNHCOCl} \qquad (6)$$

From the above, it can be seen that variations of general reaction 1 can lead to a number of interesting products.

Results and Discussion

A. Reaction of –NCO with Hydrogen. From extension of reaction 1, one might expect hydrogen to react with surface isocyanates according to eq 7. Thus, one might look for ad-

$$M\text{—}NCO + H_2 \longrightarrow M\text{—}N(H)\text{—}C(=O)\text{—}H \longrightarrow MNH_2 + CO \xrightarrow[?]{H_2} M\text{—}H + NH_3 \quad (7)$$

sorbed CO, adsorbed NH_3, or an $-NH_2$ deformation mode in the ir as evidence of reaction. Figure 1 shows results of a study of the interaction of H_2 and -NCO at various temperatures. Other experiments have shown that under 1 Torr of a 10% CO, 5% NO, 85% N_2 blend, -NCO and CO groups are stable at temperatures as high as 250° with only slight decreases in intensity being observed. Thus, decreased intensity of -NCO (~2256 cm^{-1}) and CO bands (~2100 and 2033 cm^{-1}) may be attributed to reaction with or displacement by the reactant gas. From Figure 1C, the -NCO species and H_2 apparently do not react at room temperature; however, at 150°, the -NCO band is considerably decreased in intensity while at 250°, the bands have almost completely disappeared. Unfortunately, the deformation bands of $-NH_2$ are in a region ~1600 cm^{-1} where the spectrum is already crowded. However, in Figure 1D and 1E, there does appear to be increased intensity at ~1610 and ~1458 cm^{-1}. These bands correspond to the bands at 1618 and 1458 cm^{-1} observed when NH_3 is adsorbed on the cleaned sample (see Figure 4B). Further, the band at 2015 cm^{-1} in Figure 1D is undoubtedly a CO species formed either by reaction 7 or by displacement of one of the CO's in the $-Rh(CO)_2$ group giving rise to the doublet observed in Figure 1B and 1C. The observed spectra in Figure 1 are therefore consistent with eq 7. Formation of NH_3 by reaction of H_2 with an -NCO group at elevated temperatures is consistent with the results of Shelef[10] who observed increased NH_3 in the effluent from the noble metal-catalyzed reaction of NO and H_2 upon addition of CO to the feedstream.

B. Reaction of -NCO with H_2O and D_2O. Hydrolysis of organic isocyanates by reaction 3 is well known. The analogous surface reactions would give $Rh\text{–}NH_2$ and CO_2 products. Inspection of Figure 2 shows no evidence of N–H stretching bands in the 3300–3400-cm^{-1} region and the 1631-cm^{-1} band due to adsorbed H_2O covers the region where one might expect to see any $-NH_2$ deformation mode. Thus, while H_2O appears to react with or displace the -NCO species at room temperature, there is no evidence for the expected products from the spectra in Figure 1.

The same experiment was tried with D_2O and the resulting spectra are presented in Figure 3. By using D_2O rather than H_2O, the 1631-cm^{-1} band of Figure 2B is moved out of our range of observation. Any ND_3 or $-ND_2$ deformation modes will also be out of range leaving only the hope of finding carbonate species from the adsorption of product CO_2. While assignment of the 1580- and 1450-cm^{-1} bands in Figure 3E is not conclusive, it is consistent with adsorption of product CO_2. Based on the above, it is felt that H_2O does react with surface isocyanate species even at room temperature but the final products cannot be determined from the present study.

C. Reaction of -NCO with NH_3 and n-$C_3H_7NH_2$. From reaction 4, one might expect the formation of mono- or disubstituted ureas on the surface when the -NCO is exposed to NH_3 or n-$C_3H_7NH_2$, respectively. The urea structure

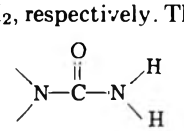

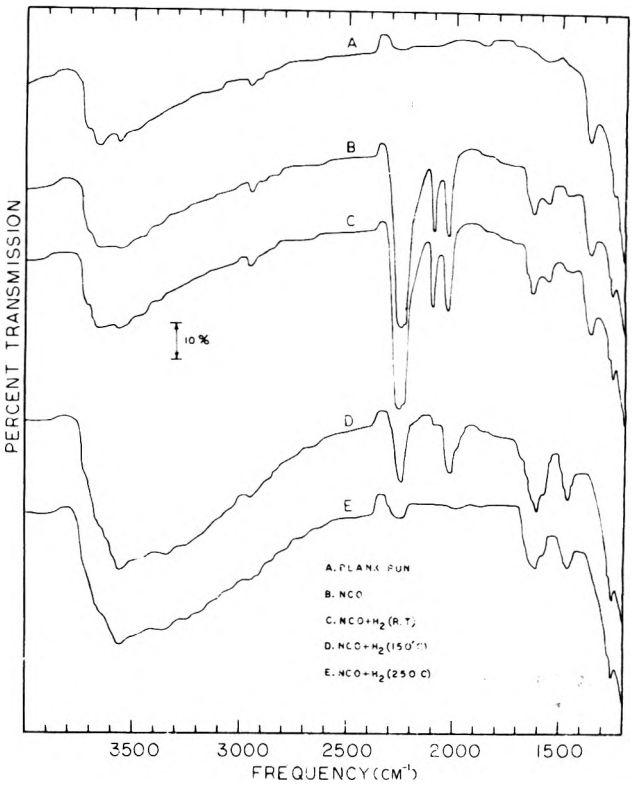

Figure 1. Spectra from interaction of H_2 with -NCO groups on the surface of Rh/Al_2O_3.

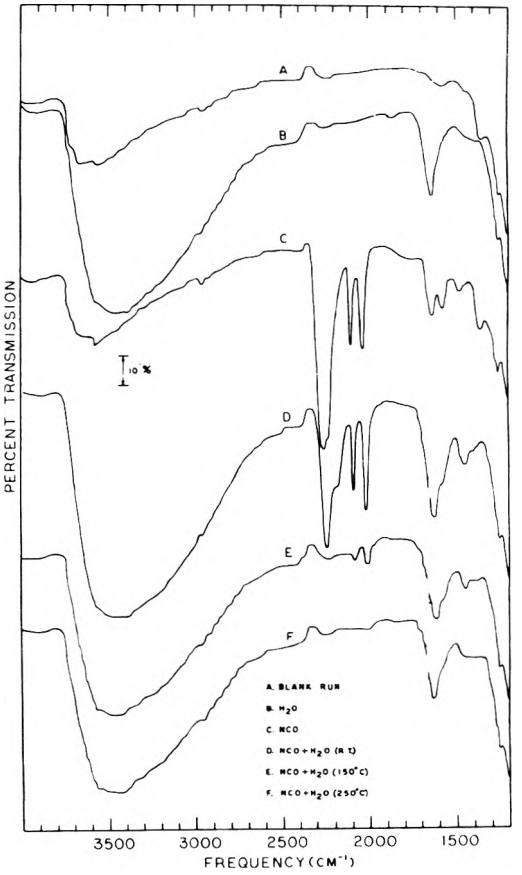

Figure 2. Spectra from interaction of H_2O with -NCO groups on the surface of Rh/Al_2O_3.

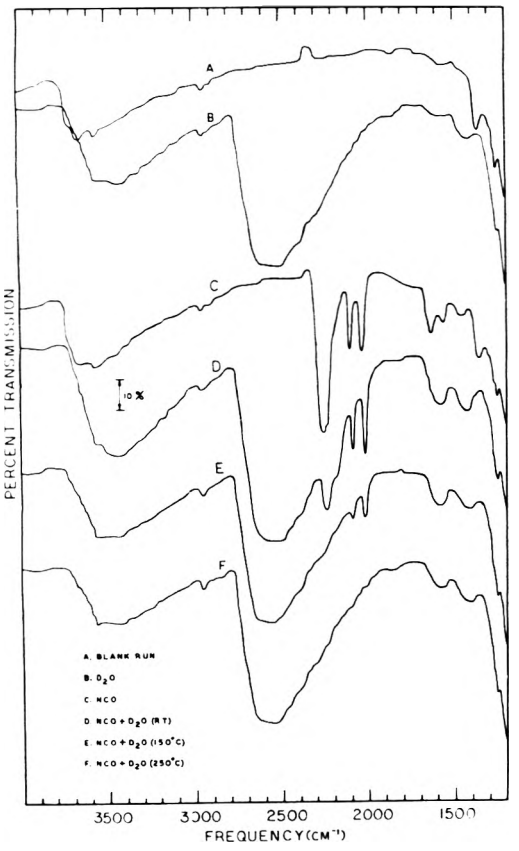

Figure 3. Spectra from interaction of D_2O with -NCO groups on the surface of Rh/Al_2O_3.

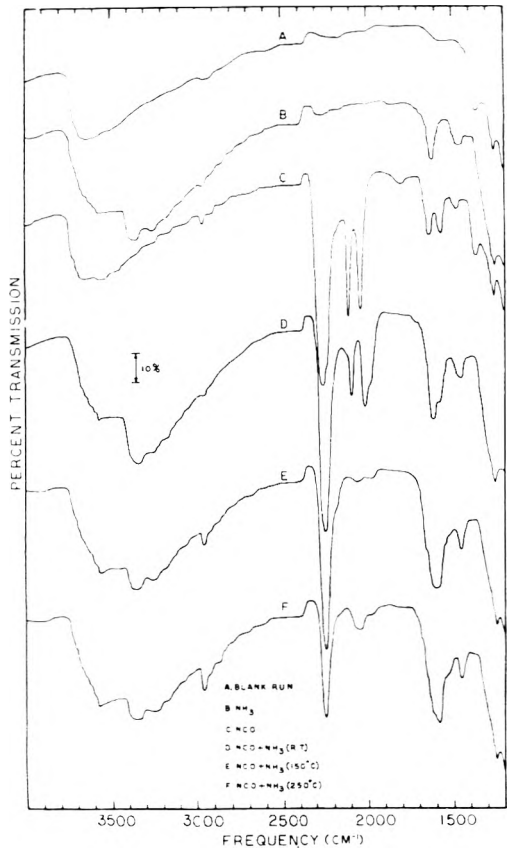

Figure 4. Spectra from interaction of NH_3 with -NCO groups on the surface of Rh/Al_2O_3.

is expected to have a C=O stretching band in the 1640–1695-cm^{-1} region and a $-NH_2$ deformation mode at ~1634 cm^{-1}. Again, the expected products have ir adsorptions in a crowded region making interpretation difficult and more speculative than one would like. The results are presented in Figures 4 and 5. Notice that -NCO remains observable even with heating of -NCO + NH_3 (or n-$C_3H_7NH_2$) to 250° in contrast to the behavior with H_2 or H_2O. From this, we conclude that the reaction of RNH_2 (R = H or alkyl group) with surface -NCO is not as facile as with H_2, H_2O, or R-OH (shown in Figure 6). This finding is contrary to normal organic chemistry experience where such reactions proceed with relative ease. Reactions on a surface probably encounter stereochemical restrictions not ordinarily present. From Figures 4 and 5, it appears that interaction of NH_3 and n-$C_3H_7NH_2$ involves the $-Rh(CO)_2$ species more than it does the -NCO group. There is essentially no evidence for the expected urea structure in Figures 4 and 5 since the 1300–1700-cm^{-1} regions in D, E, and F can be viewed as the addition of spectra B and C in each case.

D. Reactions of -NCO with Alcohols. As shown in eq 2, the expected product from reaction of an isocyanate with an alcohol is a urethane

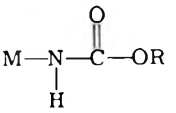

In this case, the C=O stretch should fall in the 1700–1734-cm^{-1} region and be somewhat higher than the 1635-cm^{-1} band normally found when NO and CO are allowed to react on the hot Rh surface. Thus, if a urethane group is formed, there is a chance of observing one of its characteristic bands. Results of experiments using CH_3OH are given in Figure 6. First, interaction of alcohol with -NCO seems quite extensive at room temperature and removal or displacement of the -NCO group is almost complete between 200 and 250°. Secondly, there is a strong new band between 1680 and 1690 cm^{-1}. Finally, a very weak band in the 1330–1360-cm^{-1} range is found in D and E of Figure 6 and appears to be related to the presence or absence of the stronger 1680–1690-cm^{-1} band. We speculate that the 1680–1690- and 1300–1360-cm^{-1} bands are due to a urethane-type structure caused by reaction of the alcohol with the surface -NCO group. It also seems reasonable to interpret bands at 2000–2020 and 1820–1830 cm^{-1} in the spectra after reaction at elevated temperatures (E and F of Figure 6) as adsorbed urethane decomposition products CO and NO, respectively.

In order to aid assignment of the 1691-cm^{-1} band in Figure 6D and 6E, isotope labeling experiments were carried out using ^{13}CO and ^{15}NO under the same conditions as for Figure 6D. Table I presents the observed isotope shifts. The main result is that the 1691-cm^{-1} band shifts down by 33 cm^{-1} upon ^{13}C labeling and by 7 cm^{-1} upon ^{15}N labeling showing that this surface structure contains carbon and nitrogen atoms which were originally part of the isocyanate group. A much larger shift upon carbon labeling is consistent with a urethane structure since the ir active mode should be almost entirely a -C=O stretch with only a minor influence from the nitrogen atom. Thus, labeling experiments confirm formation of $MNHC(=O)OCH_3$ from room temperature reaction of CH_3OH and an -NCO group on the Rh surface. The reaction is general since similar results were obtained with CH_3CH_2OH and $(CH_3)_2CHOH$.

TABLE I: Summary of ^{13}C and ^{15}N Labeling Experiments on the -NCO + CH_3OH Reaction over Rh/Al_2O_3 at Room Temperature

	-NCO	$[NCO^-]^a$	-CO	-CO	-C=N-H	CO_3^{2-}	$(CO_3^{2-})^b$
A. Observed shifts in bands after NO + CO reaction at 400°							
Unlabeled band, cm^{-1} [c]	2254	2232	2099	2031	1629	1564	1457
^{13}C (shift)	-59	-59	-51	-47	-19	-54	-32
^{15}N (shift)	-17	-17	-5	-1	-18	+6	-6
	-NCO	$[NCO^-]^a$	-CO	-CO	$-NHCOOCH_3$	-C=N-H	$(CO_3^{2-})^b$
B. Observed shifts in bands after subsequent treatment of A with CH_3OH at room temperature							
Unlabeled band, cm^{-1} [c]	2250	2178	2080	2010	1691	1606	1459
^{13}C (shift)	-59	-60	-58	-46	-33	-19	-14
^{15}N (shift)	-17	-8	-1	0	-7	-12	-1

[a] The band assigned as an $[NCO^-]$ group might also be due to a bridging -NCO group. See J. Nelson and S. M. Nelson, *J. Chem. Soc.*, 1597 (1969). [b] The assignments in parentheses are considered tenuous. [c] The accuracy of these bands is estimated as ±5 cm^{-1}.

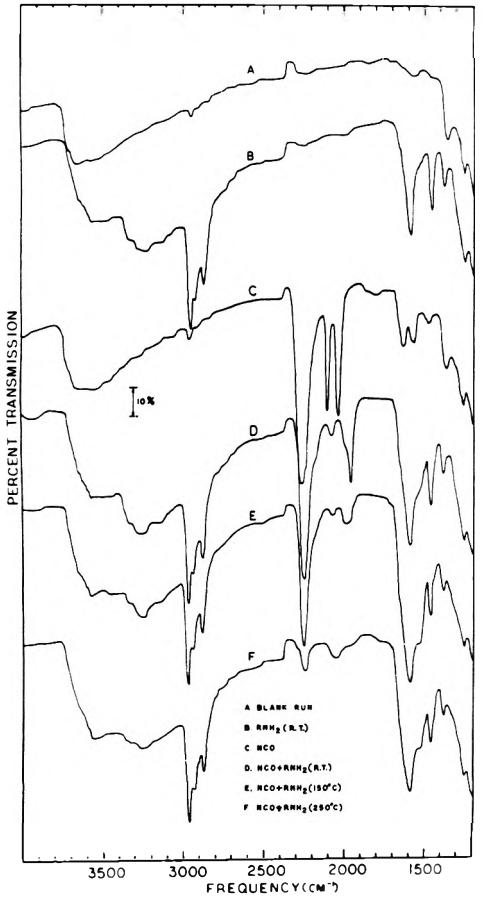

Figure 5. Spectra from interaction of n-$C_3H_7NH_2$ with -NCO groups on the surface of Rh/Al_2O_3.

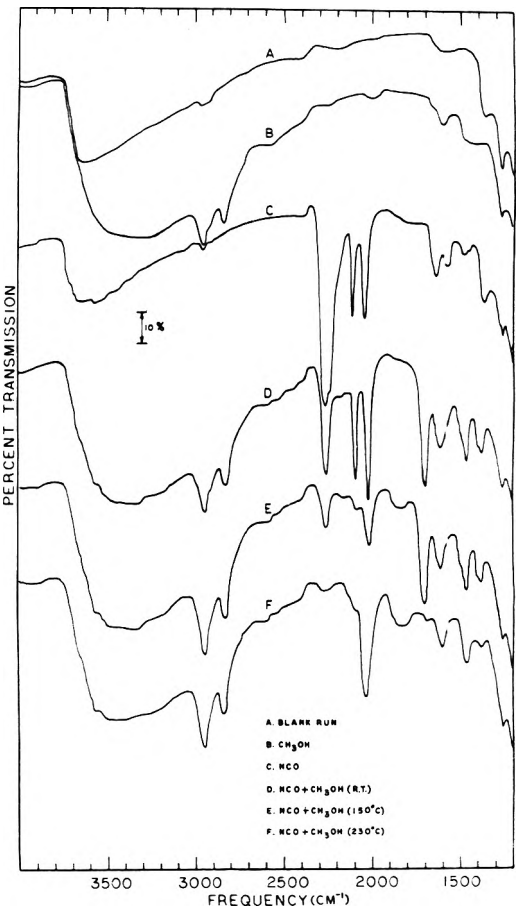

Figure 6. Spectra from interaction of CH_3OH with -NCO groups on the surface of Rh/Al_2O_3.

In other experiments it was noticed that after prolonged pumping on a sample which gave a spectrum such as in Figure 6D or E, the intensity of the -NCO band seemed to increase while the 1691-cm^{-1} urethane band decreased. It appears that the isocyanate + alcohol → urethane reaction on the surface is actually reversible and that alcohol can, in effect, be pumped out of a urethane structure. To further test this hypothesis, one of the samples having the urethane structure on its surface was heated to ~150° while pumping on the sample. After this treatment, the -NCO band returned to ~70–80% of its original intensity with a corresponding decrease in the intensity of the urethane band. This is taken as additional evidence of the reversibility of the isocyanate + alcohol reaction on the Rh/Al_2O_3 surface. While it was not convenient to monitor the products from the reaction in the infrared cell, several attempts were made to detect urethane products by passing NO + CO + CH_3OH over Rh/Al_2O_3 catalysts in a conventional fixed-bed reactor. The liquid products were condensed in a Dry Ice or liquid nitrogen trap and then injected into a chromatograph with flame ionization detection. No evi-

dence could be found for either urethane or –NCO surface species by this method.

E. Reaction of –NCO with HCHO. It is known that polyurethane structures can be formed by copolymerization of aldehydes and isocyanates.[11] If formaldehyde forms urethane or polyurethane structures with surface isocyanate groups, some features of the resulting spectra should be similar to those observed after interaction of alcohols with surface –NCO. A comparison of Figure 7E for HCHO with Figure 6E for CH_3OH shows definite similarities in the 1900–2300-cm^{-1} region. While no well-resolved band in the 1680–1690-cm^{-1} region can be observed for HCHO (as was found for alcohols), Figure 7E and F does show a slight increase in intensity of the shoulder (~1640 cm^{-1}) on a strong doublet centered at ~1600 cm^{-1}. This might be interpreted as evidence for a urethane band, however, other explanations (such as amines) are possible.

Formaldehyde adsorbed on a Rh/Al_2O_3 surface (Figure 7B) is of some interest. Formate ions with bands at 2800, 1580, and 1380 cm^{-1} are clearly present. In addition, CO bands (linear and bridged) at 2018 and 1838 cm^{-1} are observed and indicate that some of the HCHO is decomposing upon contact with the Rh surface even at room temperature. From Figure 7D it is apparent that when –NCO and $Rh(CO)_2$ groups are already present the decomposition of HCHO to CO does not occur to a very large extent, probably, because the Rh sites necessary for decomposition are blocked by these other species. While the spectra of Figure 7 show evidence for reaction of formaldehyde with the surface isocyanate groups, the case is much more tenuous than it was with the alcohols where surface reactions were clearly occurring and a product could be observed.

F. Reaction of –NCO with Acids. Interaction of a carboxylic acid and a surface isocyanate group as proposed in eq 5 could lead to either a surface anhydride or amide group. Evidence for anhydride or amide products could not be found. A surface anhydride species was clearly absent since the expected CO bands at 1800–1835 and 1740–1750 cm^{-1} would be in a relatively uncluttered region. Evidence against formation of an amide group was not as convincing since the 1630–1650-cm^{-1} region where the CO band was expected is strongly overlapped by the acetic acid spectra.

Reaction of surface –NCO groups with halogen acids should lead to a carbamyl halide structure as shown in reaction 6. By analogy with spectra of diphenylcarbamyl chloride, one would expect to find the C=O stretch in the 1730–1740-cm^{-1} region. In Figure 8D there does appear to be a new band at ~1722 cm^{-1} which would not be predicted from addition of Figure 8B and C. While 1722 cm^{-1} is lower than the 1730–1740-cm^{-1} region expected, a similar shift to lower frequency was observed in the reaction of alcohols with surface –NCO where the C=O stretch expected at 1700–1736 cm^{-1} actually appears in the 1680–1690-cm^{-1} region. In the present case, this 1722-cm^{-1} band is relatively weak so that its assignment as the C=O stretch of a carbamyl chloride is tenuous. The 1722-cm^{-1} band apparently arises from a structure which is fairly sensitive to heat since it is not observed in Figure 8E and F. Carbamyl halides are known[6] to be relatively stable at room temperatures, but dissociate at about 100°. The spectra in Figure 8E and F appear to reflect this instability.

Summary

All of the substances examined appear to react with or alter the surface –NCO group to some extent either at room

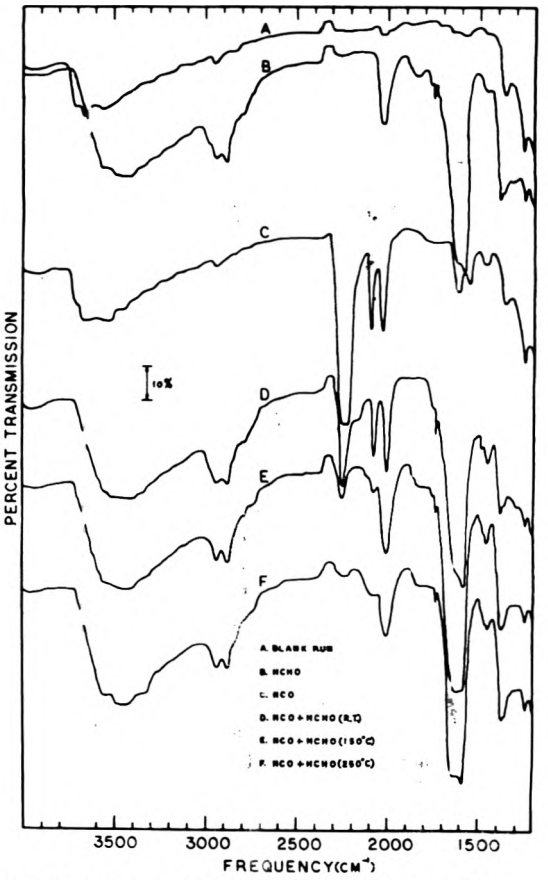

Figure 7. Spectra from interaction of HCHO with –NCO groups on the surface of Rh/Al_2O_3.

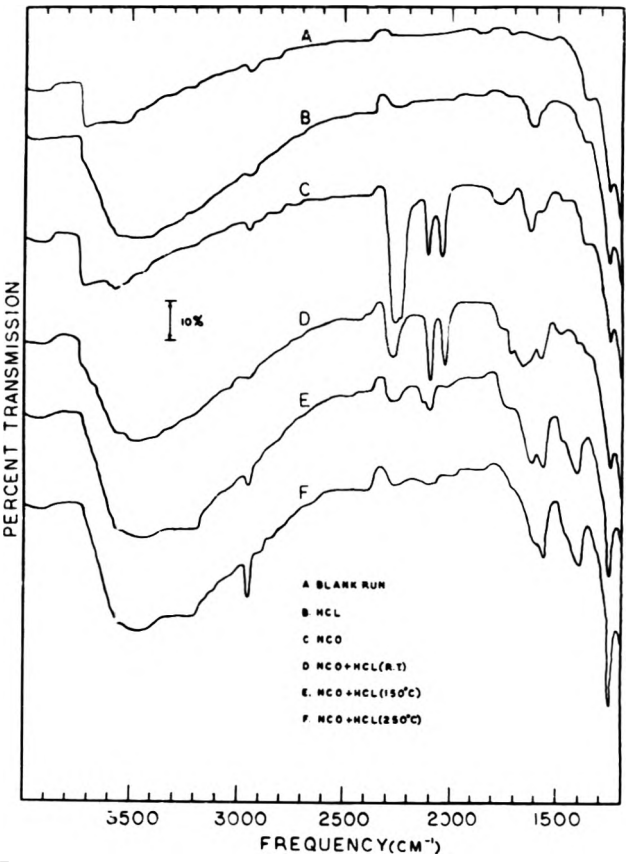

Figure 8. Spectra from interaction of HCl with –NCO groups on the surface of Rh/Al_2O_3.

temperature or at elevated temperatures. While it is not possible to order the substances in terms of their reactivity toward surface isocyanate groups, it does appear that H_2, NH_3, n-$C_3H_7NH_2$, and H_2O have less effect on –NCO at room temperature than the rest of the compounds. The acids seem to be the most reactive. The most reactive of the alcohols seemed to be CH_3OH. There was no apparent difference between CH_3CH_2OH and $(CH_3)_2CHOH$ as far as reactivity is concerned. Originally, it was thought that there might be steric effects between the primary and secondary alcohols, but other than a slight downward shift (~5 cm^{-1}) of the urethane C=O frequency, no real differences were observed. It could be argued from this that the Rh–NCO sites are well exposed and not buried in the pore structure, but the basis for such a conclusion needs more than spectral evidence.

One of the more interesting aspects of this study is the reversible nature of the alcohol + isocyanate → urethane reaction. It has been known for some time that addition reactions of isocyanate with various compounds having an active hydrogen are reversible when heat is applied. For example, urethanes from primary alcohols are known to regenerate isocyanates[12] when heated above 250°. Commercial advantage is taken of this regeneratability in the production of one-component systems for heat curable coatings. This study shows that the reversability of the reaction occurs even when the isocyanate group is attached to the surface of a noble metal.

In conclusion, the results suggest that the reactions of surface isocyanate species can be predicted by analogy with the reactions of organic isocyanates. Some differences are, of course, observed such as the reluctance of –NCO to react with ammonia and amines and the relative ease of reversing the isocyanate + alcohol → urethane reaction.

Acknowledgment. The author wishes to acknowledge the technical assistance of Mr. S.D. Koban in obtaining some of the spectra and also talks with Drs. D. Forster, G.M. Intille, and J.F. Roth concerning various aspects of this work.

References and Notes

(1) M. L. Unland, *Science*, **179**, 567 (1973).
(2) M. L. Unland, *J. Phys. Chem.*, **77**, 1952 (1973).
(3) M. L. Unland, *J. Catal.*, **31**, 459 (1973).
(4) J. W. London and A. T. Bell, *J. Catal.*, **31**, 96 (1973).
(5) J. Bugosh, *et al.*, *Ind. Eng. Chem., Prod. Res. Develop.*, **1**, 157 (1962).
(6) Transmission electron microscope photographs of films prepared in a similar fashion indicate that the Rh is highly dispersed with the majority of the Rh particles less than ~70 Å in diameter.
(7) Kirk-Othmer Encyclopedia of Chemical Technology, Vol. 12, p 45.
(8) M. J. Ostle, "Industrial Organic Nitrogen Compounds," Reinhold, New York, N.Y., 1961, p 284.
(9) S. Ozaki, *Chem. Rev.*, **72**, 457 (1972).
(10) M. Shelef and H. S. Gandhi, *Ind. Eng. Chem., Prod. Res. Develop.*, **11**, 393 (1972).
(11) H. Takida and T. Noro, *Kobunshi Kagaku*, **22**, 463 (1965); *Chem. Abstr.*, **64**, 2174*b* (1966).
(12) B. A. Dombrow, "Polyurethanes," Reinhold, New York, N.Y., 1957, p 26.

Matrix Isolation Studies of Hydrogen Bonding. The Vibrational Correlation Diagram

Bruce S. Ault, Eleanor Steinback, and George C. Pimentel*

Department of Chemistry, University of California, Berkeley, California 94720 *(Received August 16, 1974)*

Publication costs assisted by the U.S. Office of Naval Research

The infrared spectra have been obtained for a number of 1:1 hydrogen bonded complexes isolated in a nitrogen matrix at 15°K. The complexes studied and their absorptions (successively, ν_s and ν_b, given in cm^{-1}) are as follows: $(CH_3)_2O \cdot HCl$, 2280, 525; $(CH_3)_3N \cdot HCl$, 1595, 1370; $(CH_3)_3N \cdot HBr$, 1870, 1600; $H_3N \cdot HBr$, 1390, 1211; $(CH_3)_2CO \cdot HBr$, 1700; $H_2O \cdot HBr$, 2310, 410. For each acid, the value of ν_s in the complex depends systematically, though not monotonically, upon base strength, as measured by proton affinity. We define the normalized proton affinity difference, $\Delta = [PA(B) - PA(X^-)]/[PA(B) + PA(X^-)]$, and find that plots of both $\Delta\nu_s/\nu_s^0$ and ν_b against Δ correlate all of the systems studied (including $H_3N \cdot HCl$ and $H_2O \cdot HCl$). We call such a plot a *vibrational correlation diagram* and we associate the trends with an increasing extent of proton transfer as Δ and base strength increase. According to this interpretation, the proton is "completely shared" if Δ is near −0.23. Partial proton transfer occurs if Δ is less negative than −0.23, increasing progressively as base strength increases.

Introduction

The matrix isolation infrared spectra of the $H_2O \cdot HCl$ and $H_3N \cdot HCl$ complexes have been particularly informative.[1,2] They show that in neither of these hydrogen bonded complexes does proton transfer occur to form ion pairs. Moreover, the spectra differ markedly, suggesting that a concerted study of a variety of systems would display the systematics of proton transfer in hydrogen bonds as a function of acid and base strength. We present here such a study and we introduce a vibrational correlation diagram which gives coherence to the results.

Experimental Section

The apparatus and techniques were identical with those used earlier.[1,2] Except when noted, the two reactants were

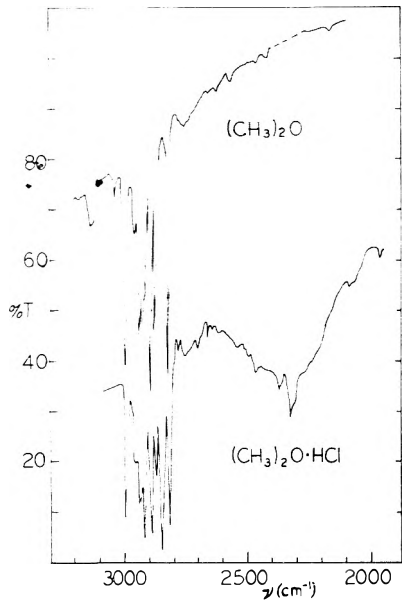

Figure 1. Infrared spectrum of HCl and dimethyl ether in nitrogen: upper curve, $(CH_3)_2O:N_2$ = 1:300, lower curve, $HCl:(CH_3)_2O:N_2$ = 1:1:300.

premixed with nitrogen in separate 3- or 5-l. bulbs and deposited simultaneously from separate jets onto a CsI window maintained at 15°K. The total amount deposited was generally 40–45 mmol at a final matrix composition of acid:base:matrix = 1:1:350. Deposition times ranged from 6 to 8 hr.

The infrared spectrum of each complex was recorded on a Perkin Elmer Model 225 infrared spectrophotometer over the spectral range 4000–350 cm^{-1}. Frequency accuracy was ± 1 cm^{-1} and the spectral slit width was roughly constant at 2 cm^{-1}.

The HCl (Matheson, 99%), HBr (Matheson, 99%), NH_3 (Matheson, 99%), $(CH_3)_2O$ (Liquid Carbonic), $(CH_3)_2CO$ (Fisher), $(CH_3)_3N$ (Matheson), DCl (Merck Sharp and Dohme, Ltd, Canada), and DBr (Merck Sharp and Dohme, Ltd, Canada) were each purified by condensation with liquid nitrogen to permit removal of volatile impurities followed by one or more thawing–recondensing cycles. Both H_2O and D_2O (ICN, 99.8%) were merely degassed by repeated freezing–thawing cycles.

Results

The spectra of the parent molecules isolated at a concentration of 1:300 in a nitrogen matrix have already been reported for HCl,[1] DCl,[1] H_2O,[1] D_2O,[1] NH_3,[2] and ND_3.[2] The spectrum of HBr, which resembles that of HCl,[1] consists of a simple doublet at 2540 (0.34) and 2495 cm^{-1} (0.04) (optical densities are given parenthetically). The matrix spectra of the other parent molecules will be presented here, along with those of their hydrogen bonded complexes.

HCl and $(CH_3)_2O$. The hydrochloric acid–dimethyl ether complex has been thoroughly studied in the gas[3,4] and solid[5] phases and its hydrogen bond energy has been measured to be 7.1 kcal/mol.[6] Hence it provides a valuable tie point.

The matrix spectrum of the parent base, $(CH_3)_2O$, is shown in the upper spectral curve of Figure 1. When HCl and $(CH_3)_2O$ are codeposited in a one-jet experiment, two new bands were observed, at 2280 (0.18) and 525 cm^{-1} (0.04). The band at 2280 cm^{-1}, shown in the lower curve of Figure 1, has a half-width near 300 cm^{-1}, while the less intense band at 525 cm^{-1} has a smaller half-width, about 85 cm^{-1}, and a shoulder at 575 cm^{-1}.

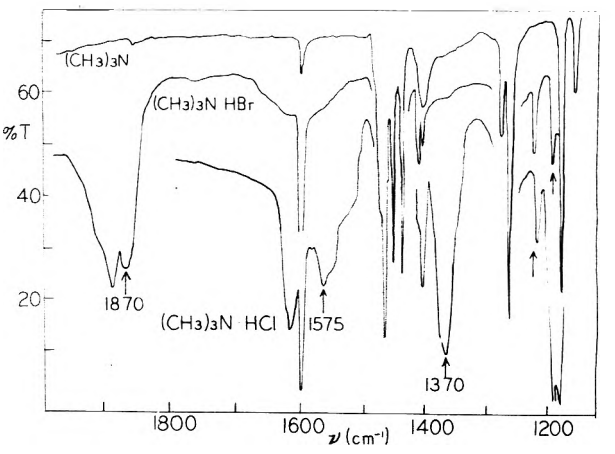

Figure 2. Infrared spectrum of HCl, HBr, and trimethylamine in nitrogen: top curve, $(CH_3)_3N:N_2$ = 1:350; middle curve, $HBr:(CH_3)_3N:N_2$ = 1:1:350; bottom curve, $HCl:(CH_3)_3N:N_2$ = 1:1:350.

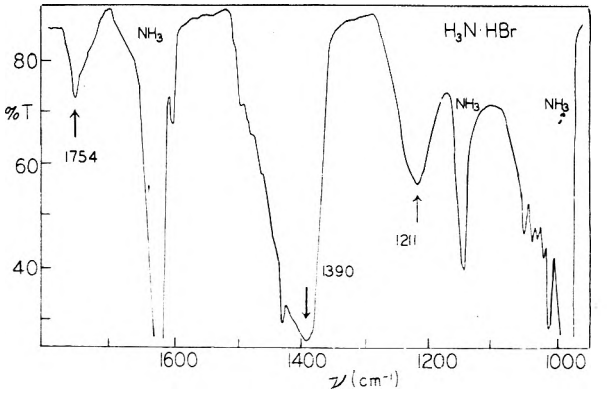

Figure 3. Infrared spectrum of HBr and ammonia in nitrogen: $HBr:NH_3:N_2$ = 1:1:350.

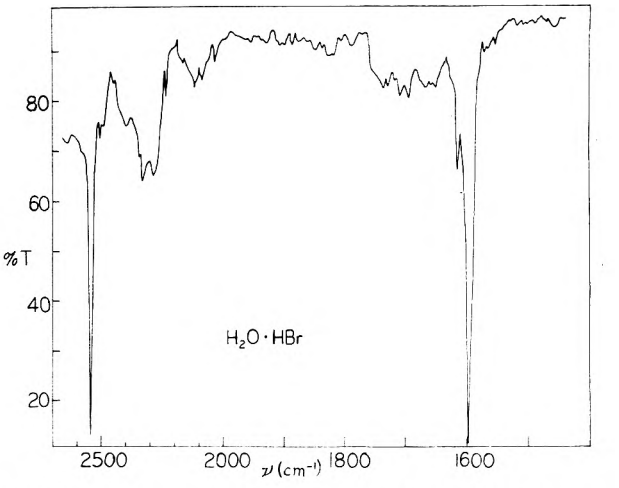

Figure 4. Infrared spectrum of HBr and water in nitrogen, 2600–1500 cm^{-1}: $HBr:H_2O:N_2$ = 1:1:350.

HCl and $N(CH_3)_3$. Figure 2 shows the spectrum of trimethylamine in nitrogen at a mole ratio of 1 to 350 (top curve). In the bottom curve is shown the spectrum obtained from a two-jet deposition to give a matrix mixture of $HCl:(CH_3)_3N:N_2$ = 1:1:350. Most obvious is the broad dou-

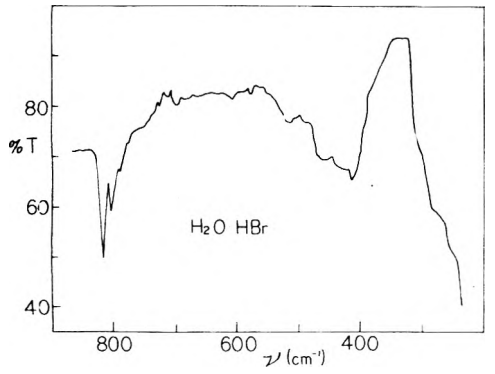

Figure 5. Infrared spectrum of HBr and water in nitrogen, 850–350 cm^{-1}: $HBr:H_2O:N_2$ = 1:1:350.

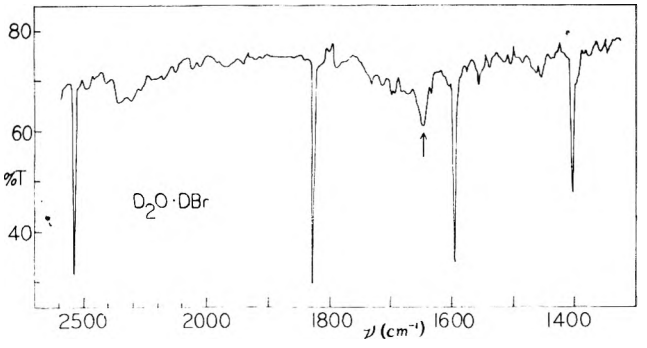

Figure 6. Infrared spectrum of DBr, HBr, and water in nitrogen, 2600–1350 cm^{-1}: $DBr:HBr:D_2O:N_2$ = ¾:¼:1:200.

blet at 1615 (0.23) and 1575 cm^{-1} (0.18), bracketing the sharp band of monomeric H_2O (an impurity) at 1597 cm^{-1}. Each of these two doublet features has a band width near 45 cm^{-1}. Another broad absorption appears at 1370 cm^{-1} (0.31), this time with a half-width near 30 cm^{-1}. Finally, there are bands at 1197 (0.55), 1004 (0.22), and 1220 cm^{-1} (0.09), the last two of which are quite sharp (half-width, about 5 and 10 cm^{-1}, respectively). When the matrix was warmed to 40°K to allow diffusion, all of these spectral features disappeared.

These two compounds were also deposited in a 1:1 ratio *without* a matrix gas to provide a reference spectrum of crystalline trimethylammonium chloride. The sample was deposited at 77°K, annealed for about 20 min at room temperature, recooled to 77°K, and finally, to 20°K. The spectrum of the crystal was recorded at each temperature. None of the absorptions mentioned above was present. Instead, the spectrum is dominated by a broad doublet in the range 2400–2700 cm^{-1} with peak absorptions (after annealing) at 2600 and 2490 cm^{-1}. There was, as well, a medium intensity band at 1230 cm^{-1} which shifted to 1245 cm^{-1} after annealing. All of the other bands were similar to those observed in the matrix spectrum of $(CH_3)_3N$.

HBr and $N(CH_3)_3$. The middle curve in Figure 2 shows the spectrum obtained from a two-jet deposition to give a matrix mixture of $HBr:(CH_3)_3N:N_2$ = 1:1:350. One prominent absorption appeared that is not in the parent spectrum, a broad, close doublet at 1870 (0.20) and 1890 cm^{-1} (0.24) with overall half-width near 80 cm^{-1}. A weaker and comparably broad band is seen at 1600 cm^{-1}, again with the 1597-cm^{-1} sharp absorption of isolated H_2O impurity superimposed. Finally, there are sharp bands at 1225 (0.10), 1196 (0.12), and 1000 cm^{-1} (0.05). The first two of these have half-widths of about 4 cm^{-1}.

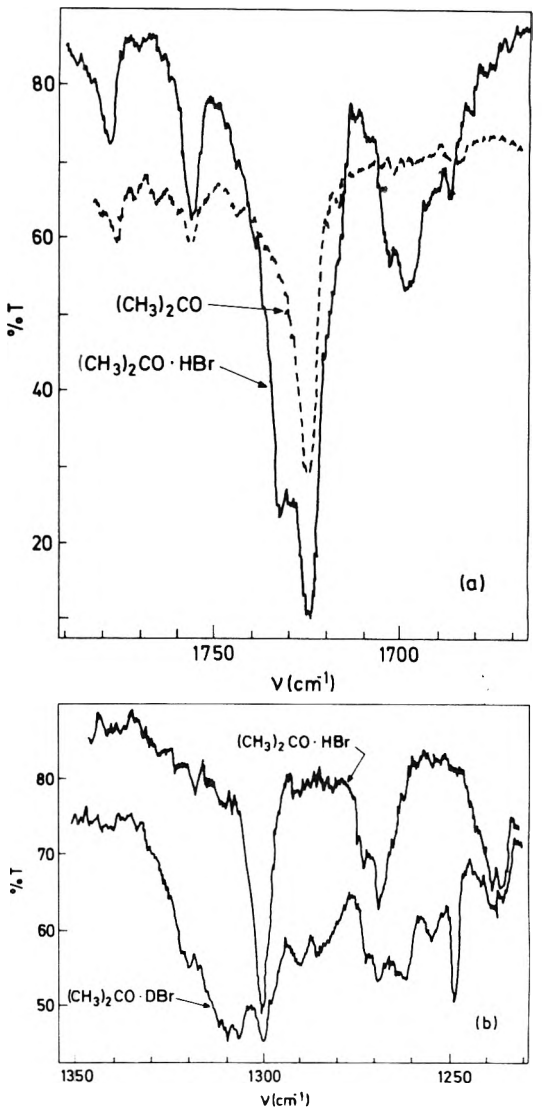

Figure 7. Infrared spectrum of HBr, DBr, and acetone in nitrogen: $(CH_3)_2CO:(HBr + DBr):N_2$ = 1:1:400; (a) 1670–1790 cm^{-1}; (b) 1230–1350 cm^{-1} (no parent absorptions appear in this region).

HBr and NH_3. Figure 3 shows the spectrum of a matrix mixture of $NH_3:HBr:N_2$ = 1:1:350. Four peaks appear that are not present in the spectra of the isolated parent compounds: at 300 (0.15), 1211 (0.20), 1390 (0.74), and 1754 cm^{-1} (0.08). The half-widths of these four features are, respectively, 10, 65, 60, and about 25 cm^{-1}. After diffusion at 40°K and recooling to 15°K, all of these new bands disappeared and strong bands at 1400 and 3100 cm^{-1} appeared. A second experiment at mole ratios 1:1:400 confirmed these results.

HBr and H_2O, *DBr and* D_2O. Figure 4 shows the spectrum of an $HBr:H_2O:N_2$ = 1:1:350 matrix mixture prepared in a single-jet deposition. One new feature appears, a broad band centered at 2310 cm^{-1} whose band center and apparent structure seemed to vary some somewhat from experiment to experiment, undoubtedly because of interference by atmospheric CO_2. A second broad band was observed at 410 cm^{-1}, with a shoulder at 460 cm^{-1}, as shown in Figure 5.

Figure 6 shows the spectrum obtained in a similar experiment using DBr and D_2O. Exchange had occurred in the vacuum line, to give a D/H ratio near 3 (as indicated by the

HCl and DCl parent bands). The band at 2310 cm^{-1} appears again, somewhat weakened, and a distinct new band is seen at 1644 cm^{-1}. Because of excessive scattering, no information was gained about the spectrum beyond 500 cm^{-1}.

HBr, DBr, and Acetone. One experiment was conducted with HBr and acetone and two with HBr–DBr mixtures and acetone. Figure 7a and 7b show the key spectral regions in these experiments, conducted with $(CH_3)_2CO$:(HBr + DBr):N_2 = 1:1:400. With HBr, new absorptions appeared at 1733 (shoulder), 1700 (0.37), 1300 (0.22), 1268 (0.11), 1182 (0.21), 1095 (0.22), 1069 (0.13), and 509 (0.30) cm^{-1}. The most intense of these bands, at 1700 cm^{-1}, is also distinctive in its 20-cm^{-1} band width, as is evident in Figure 7a. All of the other bands have normal widths of a few wave numbers.

In the HBr–DBr experiments, the H/D ratios were near unity, so all of the above absorptions were observed. In addition, a broad and intense absorption appeared at 1308 cm^{-1} (OD 0.23, band width about 24 cm^{-1}), as shown in Figure 7b. Again, new features with band widths of a few wave numbers were observed at 1248 (0.33), 1194 (0.05), and 484 (0.23) cm^{-1}.

Discussion

In the first two papers of this series,[1,2] the infrared spectra of the $H_2O \cdot HCl$ and $H_3N \cdot HCl$ complexes were compared to the expected spectra for a range of prototype complexes. This analysis helped us classify $H_2O \cdot HCl$ as a normal hydrogen bonded complex, type I, in which the proton is best considered to be still attached to the chlorine atom. In contrast, $H_3N \cdot HCl$ seems to contain a proton not attached preferentially to either the chlorine or the nitrogen atom. We call this a "completely shared" or type II hydrogen bond, to be differentiated from an ion pair structure, type III, in which proton transfer has occurred and the complex involves a hydrogen bond between an ammonium ion and a chloride ion.

Of course, as base strength is systematically varied, a continuum of hydrogen bond types is to be expected, in which types I, II, and III are merely the extreme and most readily characterized cases. These extreme types, with the two specific examples as tie points, provide guidance as we interpret the spectrum of each of the systems studied here. Then the entire array can be coherently related through a correlation diagram based upon the relative base strengths involved.

$(CH_3)_2O \cdot HCl$. The matrix-isolated complex shows two major absorptions, at 2280 and 525 cm^{-1}. These are sufficiently close to the gas-phase absorptions centered as 2574 and 475 cm^{-1} to be given the same assignments, respectively, ν_s and ν_b.

On the other hand, the frequency discrepancies are large enough to be of significant interest. In fact they lend authority to the recent reanalysis by Lassegues and Huong[7] and by Bertie and Falk[8] in which ν_s (for the gas-phase complex) is assigned at a lower frequency, at 2480 cm^{-1}. The central and most intense peak at 2574 cm^{-1} is then assigned as a combination of ν_s with ν_σ = 95 cm^{-1}, the latter mode being the heavy atom stretching frequency of the hydrogen bond. These conclusions were reached on the basis of the spectral temperature dependence, as measured by Bertie and Falk[8] between +34 and −30°, and by Lassegues and Huong[7] over the range +90 to −50°.

Since the spectrum of a matrix-isolated molecule usually relates simply to its gas-phase spectrum, the matrix spectra presented here can be considered to extend the observed temperature dependence down to 20°K. If this view is taken, then even at the lowest temperatures studied earlier,[7,8] there must have been significant excitation of low-frequency vibrations that tend to weaken the hydrogen bond and, hence, to shift ν_s to higher frequencies. An obvious possibility is the excitation of bending modes, which intrinsically distort the hydrogen bond from the most stable, linear geometry.

$(CH_3)_3N \cdot HCl$. Since the base strength of trimethylamine exceeds that of ammonia, proton transfer in the $(CH_3)_3N \cdot HCl$ complex can be expected to be more complete than in $H_3N \cdot HCl$, a type II complex. Hence the trimethylamine hydrochloride spectrum can be interpreted with a type III complex in mind.

Five new features are observed, the most prominent of which are the broad doublet at 1575/1615 cm^{-1} and the intense band at 1370 cm^{-1}. While there is no certain explanation for the 40-cm^{-1} splitting of the doublet, the breadth and intensity support its assignment to ν_s and to ν_s in combination with a low-frequency mode, possibly ν_σ, the heavy atom stretch. Similarly, the shape and strength of the band at 1370 cm^{-1} support its assignment to ν_b.

It is reasonable to presume that the remaining three bands, at 1220, 1197, and 1004 cm^{-1}, are due to vibrational modes of the base shifted somewhat from the nearby absorption frequencies of the isolated parent, 1270, 1187, and 1039 cm^{-1}. In assessing this possibility, we find useful guidance in the spectrum of the trimethylamine iodine complex, as studied by Yada, *et al.*[9] They found that three parent features shift most noticeably on complex formation, the gas-phase bands at 1272, 1183, and 1043 cm^{-1}. In a Nujol mull spectrum, the iodine complex has counterpart bands at 1250, 1206, and 1002 cm^{-1}. The similar pattern of shifts suggests that the hydrogen bond perturbs the vibrational motions of the trimethylamine base in the same manner as does the iodine complex.[10]

With this reassurance, it is of interest to examine which motions are the ones most affected. Unfortunately, the vibrational assignment of so complex a molecule as trimethylamine inevitably carries some uncertainty and, perhaps, some intrinsic ambiguity, as far as descriptive labels are concerned. Yada, *et al.*,[9] reference the available information and propose the following assignments for the bands of our interest: 1272 cm^{-1}, ν_{20}(E), C–N stretch; 1183 cm^{-1}, $\nu_5(A_1)$, CH_3 rock; 1043 cm^{-1}, ν_{19}(E), CH_3 rock.

$(CH_3)_3N \cdot HBr$. By far the most prominent feature in the spectrum of this complex, the 1870/1890-cm^{-1} doublet, displays the characteristics expected for ν_s: it is very intense, it is very broad, and its frequency is strongly shifted from the parent frequency, all of which are appropriate to a hydrogen bond formed between such a strong acid and a strong base. In a similar way, the broad and somewhat weaker band centered at 1600 cm^{-1} is readily assigned as ν_b. Again, the only interpretation we can offer for the doublet character of ν_s is that it is due to $\nu_s + \nu_\sigma$ with ν_σ = 20 cm^{-1}.

The remaining features, at 1225, 1196, and 1000 cm^{-1}, are remarkably close to the three absorptions of the $(CH_3)_3N \cdot HCl$ complex that were assigned as perturbed vibrations of the parent amine. The correspondence reassures that interpretation.

$H_3N \cdot HBr$. Once again, the most prominent band in the spectrum of the $H_3N \cdot HBr$ complex, at 1390 cm^{-1}, is a

TABLE I: Assigned Frequencies for ν_s, ν_b, and ν in Solid N_2 at 15°K (cm^{-1})

Complex	PA,[a] kcal/mol	ν_s	ν_b	ν_σ	$\Delta\nu_s/\nu_m$	Δ
HCl (monomer)	333[b]	2854				
H_2O·HCl[e]	163	2540	460	60	−0.110	−0.343
$(CH_3)_2O$·HCl	186	2280	525	95[c]	−0.201	−0.283
H_3N·HCl[f]	209	705	630		−0.753	−0.229
$(CH_3)_3N$·HCl	229	1595	1370	40(?)	−0.441	−0.189
HBr (monomer)	323[d]	2540				
H_2O·HBr	163	2310	410	50	−0.091	−0.329
$(CH_3)_2CO$·HBr	190	1700			−0.331	−0.259
H_3N·HBr	209	1390	1211	300	−0.453	−0.214
$(CH_3)_3N$·HBr	227	1870	1600	20(?)	−0.264	−0.175

[a] Proton affinities are those compiled in ref 12. [b] Proton affinity of Cl^-. [c] Gas phase frequency.[8] [d] Proton affinity of Br^-. [e] Reference 1. [f] Reference 2.

likely choice for ν_s. Its 80-cm^{-1} half-width and intensity are appropriate to this assignment. That it should not be assigned as the triply degenerate bending mode of the ammonium ion is attested by the absence of absorption near 3100 cm^{-1} attributable to the NH stretching vibration, which absorption is plainly evident after diffusion to form the ammonium chloride crystal.

If ν_s falls at 1390 cm^{-1}, then the second most intense band at 1211 cm^{-1} is a logical choice for ν_b. The band at 300 cm^{-1} is in a range appropriate to the heavy atom stretching motion, ν_σ. Three possible assignments of the weak band at 1754 cm^{-1} are to be considered: it could be a combination of ν_σ with either ν_s or ν_b or it could be the degenerate bending mode of the parent ammonia (ν = 1630 cm^{-1}) shifted by the quite strong hydrogen bond in this complex. Either combination would require rather large anharmonicity while the parent band choice would imply a rather large shift, so none of the explanations is readily preferred.

H_2O · HBr and D_2O · DBr. There is little ambiguity in assigning ν_s to the broad feature at 2310 cm^{-1}, which properly shifts on deuteration to 1644 cm^{-1}. This relatively modest shift from the monomeric HBr frequency (ν_s^0 = 2540 cm^{-1}) signals a rather weak hydrogen bond, so that assignment of ν_b to the low-frequency absorption at 410 cm^{-1} is quite reasonable.

If the shoulder at 460 cm^{-1} is attributed to a combination with ν_b, then the difference, 50 cm^{-1}, might be assigned as ν_σ. The analogous spacing in the H_2O · HCl complex at 60 cm^{-1} is in reasonable accord when reduced masses are considered.

$(CH_3)_2CO$ · HBr and $(CH_3)_2CO$ · DBr. The intense absorption in the HBr–$(CH_3)_2CO$ spectrum at 1700 cm^{-1} is distinctive in its band width and it has a broad counterpart in the DBr–$(CH_3)_2CO$ spectrum at 1308 cm^{-1}. The band width and isotopic shift, 1.30, identifies the 1700-cm^{-1} band as ν_s of the $(CH_3)_2CO$ · HBr complex. None of the other new features seems to be a suitable candidate for ν_b. Each of the new, sharp bands in the DBr–$(CH_3)_2CO$ spectrum has a similar HBr–$(CH_3)_2CO$ counterpart 4–6% higher in frequency. Hence, all of the additonal bands seem to be associated with shifted frequencies of the parent acetone molecule.

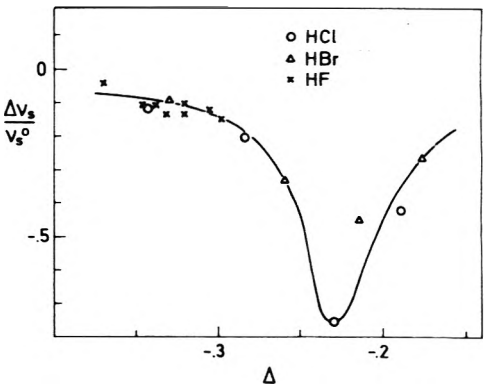

Figure 8. A plot of $\Delta\nu_s/\nu_s$ *vs.* Δ for a series of hydrogen bonds, Δ = (PA(B) − PA(A^-))/(PA(B) + PA(A^-)).

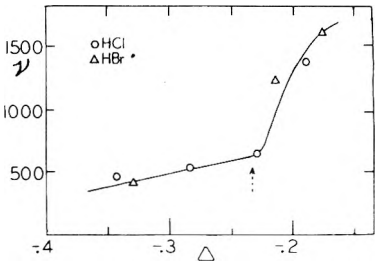

Figure 9. A plot of ν_b *vs.* Δ for a series of hydrogen bonds, A–H · · · B.

Vibrational Correlation Diagram. Table I compiles the observed frequencies and assignments, including those of H_2O · HCl[1] and H_3N · HCl.[2] For each of the two acids, HCl and HBr, the bases are arranged in order of increasing base strength, as measured by the proton affinity of the base, PA (given in the second column). In this sequence, the value of ν_s passes through a minimum for each acid. This behavior is consistent with the principles implicit in the designations of types I, II, and III complexes.[1,2] When an acid forms a hydrogen bond to a base, A–H · · · B, ν_s is lowered and the A–H distance increases relative tc the isolated A–H molecule. If the base strength is increased, the frequency continues to decrease and the A–H distance to increase until the proton can no longer be said to be preferentially associated with A (a type II complex). Further increase of base strength, then, will draw the proton close enough to become strongly associated with B, causing ν_s to rise again, approaching the limiting frequency of the isolated ion, HB^+. Of course, the base strength (proton affinity) of B needed for proton transfer from an acid A–H will also depend upon the base strength of the conjugate base, A^-. Hence, *proton transfer in a hydrogen bond should depend systematically upon the difference between the proton affinities of B and A^-.*

These ideas suggest that a continuum of hydrogen bond types is to be expected, of which types I and III are limiting cases and type II is a special case intermediate to them. They also suggest a convenient parameter with which to correlate the vibrational frequency trends within this continuum. We define the normalized proton affinity difference, Δ, as follows:

$$\Delta = \frac{\mathrm{PA(B)} - \mathrm{PA(A^-)}}{\mathrm{PA(B)} + \mathrm{PA(A^-)}}$$

TABLE II: Electrostatic Contributions to Proton Transfer in Hydrogen Bonds

	Type I	Type II	Type III
Neutral species	A–H····B	$^{-1/2}$A···H···B$^{+1/2}$	$^{-1}$A····H–B^{+1}
Bihalide ions	X_1–H····X_2^{-1}	$^{-1/2}X_1$···H···$X_2^{-1/2}$	$^{-1}X_1$····H–X_2

The limiting values of Δ are ± 1; $\Delta = -1$ corresponds to $PA(A^-) \gg PA(B)$ or, $PA(B) \to 0$, and $\Delta = +1$ corresponds to $PA(B) \gg PA(A^-)$ or, hypothetically, $PA(A^-) \to 0$. In the limit $\Delta \to -1$, ν_s and ν_b approach the hydrogen stretching and bending frequencies of the free A–H molecule and ν_σ approaches zero. (If A–H is diatomic, the bending motion becomes a rotation, so $\nu_b \to 0$.) In the limit $\Delta \to +1$, ν_s and ν_b approach the appropriate frequencies of the free HB^+ ion and, again, $\nu_\sigma \to 0$.

With these extremes in mind, we have plotted $\Delta\nu_s/\nu_s^0$ in Figure 8 (ν_s^0 is the value of ν_s for the matrix-isolated A–H molecule and $\Delta\nu = \nu_s - \nu_s^0$). Also included (the solid dots) are the gas-phase measurements for HF with a variety of bases,[13] as reported by Couzi, *et al.*[14] We see that the plot interleaves the HCl and HBr data and it accommodates the gas-phase HF data as well, showing that they are all consistent when viewed in this way. Furthermore, the plot displays the expected continuum of bond types; we shall call it a *vibrational correlation diagram.*

This type of diagram correlates, as well, the trend in ν_b, as shown in Figure 9. For large, negative values of Δ (type I complexes), ν_b should approach zero, as it seems to do. For less negative values of Δ (type III complexes), ν_b should rise toward ν_b of the ion HB^+. At this limit, there is some ambiguity, particularly when the isolated HB^+ contains equivalent hydrogens [as in H_3O^+ or NH_4^+, and in contrast to $HN(CH_3)_3^+$]. However, for the range of Δ studied, Figure 9 shows that the correlation is not impaired by this ambiguity, undoubtedly because the hydrogen bond interaction is still strong enough to maintain the uniqueness of the transferring proton.

Concerning the ν_σ trends seen in Table I, the doubt involved in the assignments permits only the observation that the strongest hydrogen bond is expected for type II complexes. Hence ν_σ is expected to display a maximum for intermediate values of Δ, as the data seem to indicate.

The position of the minimum in Figure 8, which we designate Δ_{II}, is a matter of some interest. According to our interpretation, this is the value of Δ that produces a "completely shared" proton, the heteronuclear counterpart of centrosymmetric hydrogen bonds such as those in HF_2^- and HCl_2^- (type II). For these prototype systems, $\Delta_{II} = 0$, whereas in Figure 8, Δ_{II} is near -0.23. The reason for this difference can be associated with the electrostatic asymmetry in the hydrogen bonds studied here, an asymmetry which is not present in the bihalide ions. This is illustrated in Table II in which the proton in assumed to carry all of its +1 charge with it as it transfers (zero order approximation). Plainly, there is an electrostatic attraction to be considered in the neutral species hydrogen bond of type III that is not present in type I. This implies that proton transfer will be aided somewhat, and will occur with a weaker base strength [lower PA(B)] than would be needed without this attraction. Hence, Δ_{II} will have a negative value.

Not unexpectedly, this qualitatively appealing electrostatic picture has quantitative inadequacies. The equally shared proton in the type II $H_3N \cdot HCl$ complex surely does not transfer a full unit charge, perhaps half a unit charge is a more reasonable guess, as pictured in Table II. The electrostatic energy implied would be -51 kcal/mol at a charge separation of 3.26 Å (the Cl · · · N distance found in crystalline ammonium chloride, NaCl lattice). This is much less than the proton affinity difference that corresponds to $\Delta_{II} = -0.23$, $PA(NH_3) - PA(Cl^-) = -124$ kcal/mol. The discrepancy, $124 - 51 = 73$ kcal/mol, is enhanced by the 19 kcal/mol energy of the hydrogen bond.[15,16] Thus, the electrostatic asymmetry does not provide quantitative predictability of the magnitude of Δ_{II} even though it rationally accounts for its nonzero and negative value.

Conclusions

Some years ago, Barrow and coworkers[17,18] found some spectroscopic evidence for proton transfer in hydrogen bonds, but only recently have there appeared promising avenues by which to advance this pioneering work. One avenue that can be cited is through theoretical calculations, in view of the successful predictions by Clementi, *et al.*,[15,16] concerning the $H_3N \cdot HCl$ complex. The present work introduces another powerful approach, the vibrational correlation diagram, which is made possible by access to proton affinities as quantitative measures of base strength.[12] With data provided by matrix isolation spectroscopy, the vibrational correlation diagram displays the relative base strength needed for proton transfer in a hydrogen bond and provides a criterion for deciding when a heteronuclear hydrogen bond will involve a completely shared proton. Both the concepts and the techniques are applicable to other systems, including those of biological interest, and further work is in progress.

Acknowledgment. We gratefully acknowledge support of this research by the U.S. Office of Naval Research under Grant No. N00014-A-0200-102.

References and Notes

(1) B. S. Ault and G. C. Pimentel, *J. Phys. Chem.*, **77**, 57 (1973).
(2) B. S. Ault and G. C. Pimentel, *J. Phys. Chem.*, **77**, 1649 (1973).
(3) J. E. Bertie and D. J. Millen, *J. Chem. Soc.*, 497, 514 (1965).
(4) J. Arnold and D. J. Millen, *J. Chem. Soc.* 503, 510 (1965).
(5) R. M. Seel and N. Sheppard, *Spectrochim. Acta, Sect. A*, **25**, 1287 (1969).
(6) G. Govile, A. D. H. Clague, and H. J. Bernstein, *J. Chem. Phys.*, **49**, 2821 (1968).
(7) J. G. Lassegues and P. V. Huong, *Chem. Phys. Lett.*, **17**, 444 (1972).
(8) J. E. Bertie and M. V. Falk, *Can. J. Chem.*, **51**, 1713 (1973).
(9) H. Yada, J. Tanaka, and S. Nagakura, *J. Mol. Spectrosc.*, **9**, 461 (1962).
(10) Part or all of the absorption at 1197 cm^{-1} could be due to aggregates of trimethylamine but it is not expected at the concentration used.
(11) G. C. Pimentel and A. L. McClellan, "The Hydrogen Bond," W. H. Freeman, San Francisco, Calif., 1960, pp 137–140.
(12) J. L. Beauchamp, *Annu. Rev. Phys. Chem.*, **22**, 527 (1971).
(13) The bases, listed in order of increasing Δ, are $(C_2H_5)_2O$ $(CH_3)_2S$, $(CH_3)_2CO$, $(CH_3)_2O$, CH_3CHO, CH_3OH, and CH_3I. The most intense feature in the absorption band was used for $\Delta\nu_s/\nu_s^0$ when shoulders or weaker satellite bands appeared.
(14) M. Couzi, J. Le Calvé, P. Van Huong, and J. Lascombe, *J. Mol. Struct.*, 5, 363 (1970).
(15) E. Clementi, *J. Chem. Phys.*, **46**, 3851 (1967); **47**, 2323 (1967).
(16) E. Clementi and J. N. Sayles, *J. Chem. Phys.*, **47**, 3837 (1967).
(17) E. A. Yerger and G. M. Barrow, *J. Amer. Chem. Soc.*, **77**, 4474 (1955).
(18) G. M. Barrow, *J. Amer. Chem. Soc.*, **78**, 5802 (1956).

Matrix Isolation Infrared Studies of Lithium Bonding

Bruce S. Ault and George C. Pimentel*

Department of Chemistry, University of California, Berkeley, California 94720 *(Received August 16, 1974)*

Publication costs assisted by the U.S. Office of Naval Research

Matrix isolation infrared spectra (15°K) have been obtained for complexes between LiX (X = Cl, Br) and a number of electron donor bases. The complexes studied and the absorption frequencies assigned as the Li–X stretching modes, ν_S, are as follows: $(CH_3)_3N \cdot {}^6LiCl$, 632; $H_3N \cdot {}^6LiCl$, 538; $(CH_3)_2O \cdot {}^6LiCl$, 524; $H_2O \cdot {}^6LiCl$, 553; $(CH_3)_3N \cdot {}^7LiBr$, 554; $H_3N \cdot {}^7LiBr$, 584, 479; $H_2O \cdot {}^7LiBr$, 460 cm^{-1}. The relative frequency shifts (referred to the average, isolated-monomer frequency, $\bar{\nu}_M$) depend in the same way as hydrogen bond shifts when plotted in a *vibrational correlation diagram*, a plot of $(\nu_S - \bar{\nu}_M)/\bar{\nu}_M$ against the normalized proton affinity difference, $\Delta = [PA(B) - PA(X^-)]/[PA(B) + PA(X^-)]$. The minimum value of $(\nu_S - \bar{\nu}_M)/\bar{\nu}_M$ is located near $\Delta = -0.28$, rather close to that of the hydrogen bonded HX(X = Cl, Br) complexes with the same bases ($\Delta = -0.23$ to -0.26). The evidence indicates that these complexes have geometries such as those found in hydrogen bonds, so that the interaction is reasonably called a "lithium bond."

Introduction

We have recently reported the systematic infrared study of a series of hydrohalide–base, hydrogen bonded complexes *via* the matrix isolation method.[1-3] In the last of these papers[3] (hereafter, called ASP), a *vibrational correlation diagram* was introduced that correlates the observed infrared absorptions and that reveals the base strength needed for proton transfer from the acid. Here we report similar studies and extend the same interpretive technique to lithium halide complexes with a series of bases.

It is often assumed that hydrogen is unique in its ability to form the bond called the hydrogen bond. There have, however, been some speculations that lithium atom might display a similar attractive interaction: by Shigorin[4] on the basis of spectroscopic study of organolithium compounds, by West and Glaze[5] (who disprove Shigorin's contention with ^6Li isotopic studies) on the basis of gas-phase association, and by Balasubramanian, *et al.*,[6] on the basis of infrared shifts observed between 300 and 600 cm^{-1} in the spectra of lithium halide–amide solutions. Relevant to this lithium bond possibility are the measurements by Dzidic and Kebarle[7] of the lithium ion affinity of water, 34 kcal/mol.

Theoretical calculations on lithium bonds have also been attempted, notably by Kollman and coworkers.[8] Using Hartree–Fock calculations, they concluded that LiF could bond to a suitable base. Lithium ion affinities have been calculated, too; for water using detailed Hartree–Fock calculations[9] and for strong bases using the CNDO/Z method.[10]

All of this background encourages the expectation that lithium bonding can occur, but decisive evidence is lacking. Such weak interactions are notoriously difficult to distinguish by conventional techniques, whereas the matrix isolation method is uniquely suited. We report here a systematic spectroscopic study, using the matrix method, of a series of lithium halide–base complexes. These spectra establish, we believe, the existence of lithium bonding.

Experimental Section

The apparatus was similar to that used in ASP except that a Knudsen cell was incorporated in the cold cell base, following the design by Andrews and Pimentel.[11] The heating wire was changed to 0.02-in. diameter tantalum wire (NRC), which permitted somewhat higher temperatures than accessible with chromel A. The oven temperature was measured with a chromel P *vs.* alumel thermocouple, but because of thermal contact difficulties, the temperatures are uncertain to ±20°. The oven orifice was aimed at 45° incidence to the cold window.

The lithium halides are quite hygroscopic, so they were stored in a drying oven at 125° prior to use. After the Knudsen cell was loaded, the sample was left under vacuum for several days in the cold cell, during part of which the oven temperature was raised to 200°. Despite this degassing procedure, a small amount of water was present in many of the matrix samples, as revealed by the absorption at 1600 cm^{-1} due to monomeric H_2O.

The matrix samples were prepared by depositing a premixed argon:base gas mixture at a mole ratio of 125:1 onto a CsI window held at 15°K. At the same time, the oven temperature was raised to the range 475–525° so as to codeposit the lithium halide in roughly stoichiometric ratio. Deposition rates were about 5 mmol of Ar/hr and deposition times fell in the range 5–8 hr. While the presence of the hot Knudsen cell reduced the cold cell refill time from 8 to 5 hr, the water impurity absorption spectrum showed that diffusion was not caused.

The infrared spectrum of each complex was recorded on a Perkin-Elmer Model 225 infrared spectrophotometer over the spectral range 4000–200 cm^{-1}. Frequency accuracy was ±0.5 cm^{-1} and the spectral slit width was roughly constant at 2 cm^{-1}.

The crystals used were as follows: LiCl (natural isotopic abundance, Mallinckrodt), ^6LiCl (99%, Oak Ridge National Labs), and LiBr (natural isotopic abundance, Mallinckrodt). The NH_3 (Matheson), $(CH_3)_2O$ (Liquid Carbonic), and $(CH_3)_3N$ (Matheson) were purified by condensation under vacuum with liquid nitrogen (to remove volatile impurities) followed by one or more thawing, recondensing cycles.

Results

The spectrum of lithium chloride was recorded in the presence of four bases [H_2O, NH_3, $N(CH_3)_3$, and $(CH_3)_2O$]

TABLE I: Spectral Observations Using ^6LiCl $\nu(cm^{-1})$ (Optical Densities Given Parenthetically)

Base					
None	H_2O	NH_3	$N(CH_3)_3$	$(CH_3)_2O$	Identn[a]
			632(0.04)		$(CH_3)_3N \cdot LiCl$
616(0.40)	616(0.96)	617(0.28)	617(0.21)	617(0.08)	M
607(0.50)	607(0.90)	606(0.33)	607(0.11)	607(0.03)	M
	576(0.02)	575(0.01)	576(0.02)	577–590(0.02)	?
553(0.02)	553(0.07)	554(0.03)		540–550(0.04)	$H_2O \cdot LiCl$
532(0.06)	532(0.06)	538(0.09)			$H_3N \cdot LiCl$
				524(0.16)	$(CH_3)_2O \cdot LiCl$
518(0.42)	518(1.2)	518(0.43)	518(0.50)	516(0.23)	D
510(0.87)	510(∞)	511(∞)	510(1.1)	510(0.31)	D
497(0.08)	497(0.16)	497(0.09)		499(0.05)	?

[a] M = monomer, D = dimer.

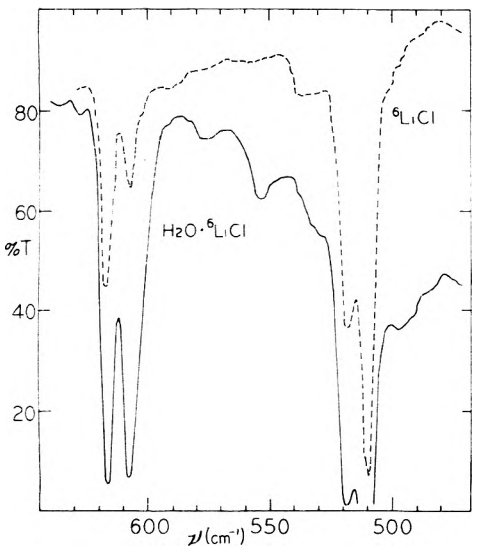

Figure 1. Infrared spectrum of ^6LiCl in argon (15°K): dashed spectrum, dry sample; solid spectrum, ^6LiCl with H_2O present.

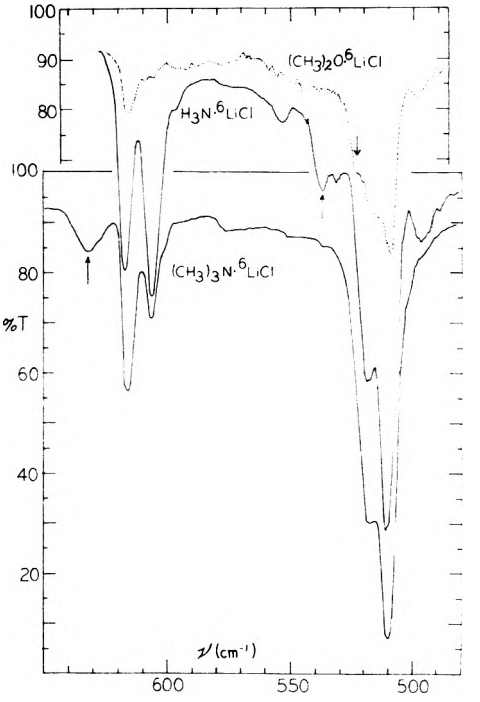

Figure 2. Infrared spectrum of ^6LiCl in argon with bases present (15°K): dashed spectrum, ^6LiCl with $(CH_3)_2O$:Ar = 1:125; upper solid spectrum, ^6LiCl with NH_3:Ar = 1:150; lower solid spectrum, ^6LiCl with $(CH_3)_3N$:Ar = 1:100.

and for some of these both with LiCl containing natural lithium isotopic abundance (93% ^7Li, 7% ^6Li) and with 99% ^6LiCl. These results are presented first. The spectrum of lithium bromide was recorded in the presence of two bases [NH_3 and $N(CH_3)_3$] but only with natural abundance LiBr.

LiCl. The dashed curve in Figure 1 shows the spectrum of carefully dried ^6LiCl. Two doublets are seen, one at 616 and 607 cm^{-1} and the other at 518 and 510 cm^{-1}. Also, there is a weak band at 553 cm^{-1} and a shoulder at 532 cm^{-1}. The prominent features are in accord with spectra published earlier by Snelson and Pitzer[12] and by Schick and Schnepp.[13] The high-frequency pair of bands is rather clearly associated with monomeric ^6LiCl, the doublet structure being commonly ascribed to site splitting in the matrix. The relative intensities of the doublet components varied from experiment to experiment. The low-frequency pair of bands has been assigned to ^6LiCl dimers[12,13] which is in qualitative agreement with vapor composition measurements[14] that show a monomer/dimer ratio near 0.56 at a temperature of 642°. The shoulder at 532 cm^{-1} could be due to higher polymers.

In the spectrum of LiCl with natural isotopic abundance (which we designate ^nLiCl), the two monomer features are found shifted to 580 and 565 cm^{-1}. The isotopic shifts $\nu(^6LiCl)/\nu(^7LiCl)$ are 1.062 and 1.074. The dimer features at 488 and 480 cm^{-1} also duplicate reasonably their ^6LiCl counterparts. A rather prominent shoulder at 500 cm^{-1} can be assigned as a $^6LiCl \cdot {}^7LiCl$ dimer.[12]

Table I lists the frequencies and optical densities for a typical experiment using ^6LiCl, along with similar data for the depositions that included bases (to be described).

LiCl and H_2O. Water was often present as an impurity, particularly in the first experiments conducted after the Knudsen cell was recharged. Of course, the presence of H_2O is unequivocally signalled by sharp features near 1600 cm^{-1}. As well, when H_2O was present, a new band occurs near 553 cm^{-1} as seen in the solid curve of Figure 1. With ^nLiCl, H_2O impurity produces a counterpart absorption at 518 cm^{-1}, with an isotopic shift of 1.068.

These features, due to the $H_2O \cdot LiCl$ complex, are occasionally present in the spectra of other complexes, so their recognition is of some importance.

TABLE II: Spectral Observations Using ^{n}LiBr ν(cm^{-1}) (Optical Densities Given Parenthetically)

Base			
None	NH_3	$N(CH_3)_3$	Identn[a]
	584(0.06)		$H_3N\cdot{}^{7}$LiBr
554(0.02)	553(0.04)	554(0.08)	^{6}LiBr, M, $(CH_3)_3N\cdot{}^{7}$LiBr
539(0.03)	532–539(~0.06)	539(0.03)	^{6}LiBr, M
521(0.18)	521(0.22)	520(0.25)	^{7}LiBr, M
502(0.22)	502(0.37)	502(0.49)	^{7}LiBr, M
	479(0.13)		$H_3N\cdot{}^{7}$LiBr
466(0.07)	464(0.10)	469(0.09)	^{6}LiBr, D
457(0.11)	458(0.11)	458(0.13)	^{6}LiBr, D, $H_2O\cdot{}^{7}$LiBr
438(0.50)	438(0.62)	438(∞)	^{7}LiBr, D
432(0.47)		432(0.68)	^{7}LiBr, D
421(0.09)			

[a] M = monomer, D = dimer.

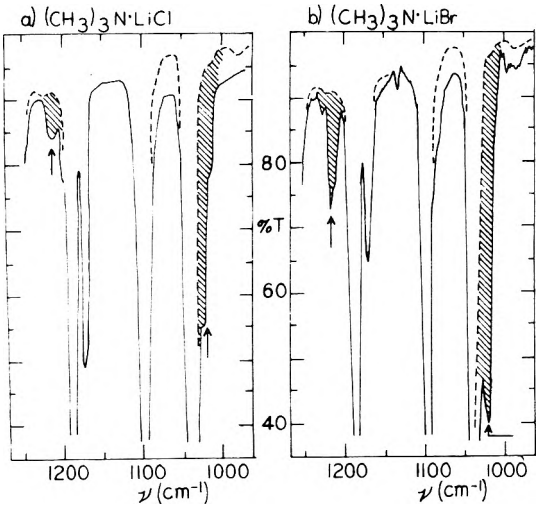

Figure 3. Infrared spectrum of trimethylamine in argon, 1000–1300 cm^{-1}: dashed curve, $(CH_3)_3N$:Ar = 1:100; solid curves, lithium halide present (a) ^{6}LiCl, (b) ^{n}LiBr; shaded area shows absorption due to $(CH_3)_3N\cdot LiX$ complex.

LiCl and NH_3. The upper solid curve in Figure 2 shows the spectrum of a 150:1 argon:NH_3 mixture codeposited with ^{6}LiCl. There are features at 554, 538, and 497 cm^{-1} that are not present in the ^{6}LiCl spectrum. The first of these is assigned to the $H_2O\cdot{}^{6}$LiCl complex. Since ammonia has no absorptions in this spectral range, either of the other two features, 538 or 497 cm^{-1}, might be assigned to the $H_3N\cdot{}^{6}$LiCl complex. The band width is 4 cm^{-1}.

In the counterpart experiment using ^{n}LiCl (argon:NH_3 = 175:1) absorptions consistently appear at 510 and at 462 cm^{-1}. The latter band might be the ^{7}Li counterpart to the unassigned ^{6}LiCl absorption at 497 cm^{-1}, with an isotopic shift of 1.076. The other feature, at 510 cm^{-1}, coincides with one of the ^{6}LiCl dimer absorptions, but the intensity (typically, with optical density between 0.1 and 0.2) far exceeds that expected for the natural abundance mixture. We believe that 510 cm^{-1} is due, in part, to $H_3N\cdot{}^{7}$LiCl, which implies an isotopic shift of 1.055.

Thus, we have two possible assignments for the LiCl stretching mode in the $H_3N\cdot{}^{6}$LiCl complex, 538 and 497 cm^{-1}, each with reasonable lithium isotopic shifts. We favor the 538 cm^{-1} choice because the lower frequency of the two $H_3N\cdot{}^{7}$LiCl counterpart bands, 510 and 462 cm^{-1}, was variable and sometimes seemed to be present in spectra of samples involving other bases.

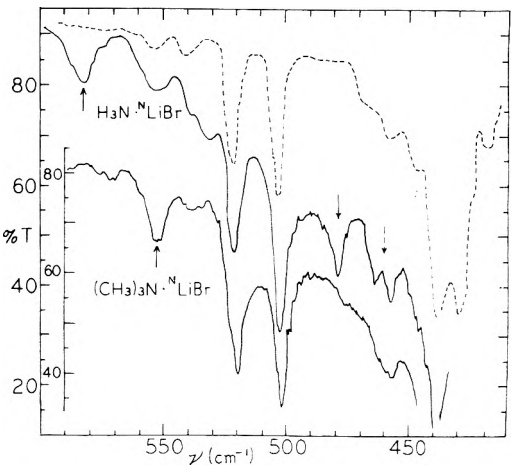

Figure 4. Infrared spectrum of ^{n}LiBr in argon with bases present (15°K): dashed spectrum, ^{n}LiBr alone; upper solid spectrum, ^{n}LiBr with NH_3:Ar = 1:125; lower solid spectrum, ^{n}LiBr with $(CH_3)_3N$:Ar = 1:125.

LiCl and $N(CH_3)_3$. In three experiments conducted with ^{6}LiCl and $N(CH_3)_3$, no new features were detected at a frequency below the monomer LiCl bands. However, the lower solid curve in Figure 2 shows that a new band does appear at higher frequency, at 632 cm^{-1}. In agreement, the spectrum obtained with ^{n}LiCl reveals a corresponding feature at 592 cm^{-1}, again just above the monomer bands of ^{7}LiCl and shifted from 632 cm^{-1} by a factor of 1.068. These features are attributed to the $(CH_3)_3N\cdot$LiCl complex.

The frequency range 1000–1300 cm^{-1}, which furnishes a part of the "fingerprint" region of the base, $N(CH_3)_3$, is shown in Figure 3a for the ^{6}LiCl experiment. The dashed curve indicates the spectrum of the base alone in solid nitrogen. In the argon matrix, with ^{6}LiCl present, there is weak absorption at 1212 cm^{-1} and also a rather pronounced shoulder at 1025 cm^{-1}, neither of which is present without ^{6}LiCl. These features, which were also present in the ^{7}LiCl · $N(CH_3)_3$ experiment, correspond closely to similar absorptions of $N(CH_3)_3$ in hydrogen bonded complexes with HCl and HBr (see ASP).

LiCl and $(CH_3)_2O$. Codeposition of ^{6}LiCl and a 125:1 = argon:$(CH_3)_2O$ mixture was carried out three times, but only with prolonged deposition (24 hr) was a new band observed. The dotted curve in Figure 2 shows the spectrum recorded in this experiment. There is a quite distinct shoulder at 524 cm^{-1} alongside the high-frequency component of the dimer doublet at 518 cm^{-1}. This shoulder is far more intense than the weak feature at 532 cm^{-1} noted in Figure 1; we believe that the 524 cm^{-1} band is due to the $(CH_3)_2O\cdot{}^{6}$LiCl complex.

LiBr. The dashed curve in Figure 4 shows the spectrum of ^{n}LiBr in Ar, which closely resembles that in the literature.[13] This sample, evaporated at an oven temperature near 475°, displays monomer absorptions at 521 and 502 cm^{-1} due to ^{7}LiBr, and weak counterparts at 554 and 539 cm^{-1} due to ^{6}LiBr. A doublet attributable to dimer absorption is seen at 438 and 432 cm^{-1} and there are shoulders on either side, at 421 cm^{-1} and over the region 450–470 cm^{-1} in which ^{6}LiBr dimers would absorb. The observed bands and their optical densities are given in Table II.

LiBr and H_2O. As in the LiCl experiments, complete removal of water from the samples was a problem, so recognition of the $H_2O \cdot$ LiBr absorption was important. From the spectra of samples that had not been thoroughly dried, the absorption due to this complex was deduced to be at 460 cm^{-1}. The frequency uncertainty is large, about ± 5 cm^{-1}, because this spectral region also contains absorptions due to ^{6}LiBr dimers and isotopically mixed ^{6}LiBr $\cdot$ ^{7}LiBr dimers.

LiBr and NH_3. Argon and ammonia at 125:1 were codeposited with ^{7}LiBr to give the spectrum shown in the top solid curve in Figure 4. Two distinct new bands are evident at 584 and at 479 cm^{-1}. The band widths are, respectively, about 10 cm^{-1} and about 4 cm^{-1}. The experiment was repeated with deuterated ammonia (D/H was about 4, which implies that the sample contains about 50% ND_3 and 38% NHD_2). Unfortunately, the experiment was indecisive because of poor photometry below 475 cm^{-1}; no absorption near 479 cm^{-1} was discernable. A band was observed at 580 cm^{-1}, shifted only small amount from the 584-cm^{-1} NH_3 counterpart.

LiBr and $N(CH_3)_3$. The lower solid curve in Figure 4 shows the spectrum of an Ar:$N(CH_3)_3$ mixture at 125:1 with ^{7}LiBr. One new band was observed below 1000 cm^{-1} at 554 cm^{-1}. The weakness of the absorption at 539 cm^{-1}, due to monomeric ^{6}LiBr, shows that the band at 554 cm^{-1} cannot be wholly due to ^{6}LiBr. Hence it can be attributed to the $(CH_3)_3N \cdot$ LiBr complex.

Again, new spectral features were seen in the region 1000–1350 cm^{-1}. Figure 3b shows this region and two absorptions are clearly resolved at 1215 and at 1022 cm^{-1}. The half-width of the first band is about 10 cm^{-1}.

Discussion

Lithium Bond Stretching Motions. For each of the LiX base systems studied, it was possible to identify a new absorption feature in the general spectral region of the LiX monomeric absorption. These new bands are listed in the second column of Table III. There are three opportunities to determine the dependence upon the lithium isotopic mass, in the complexes of LiCl with bases H_2O, NH_3, and $N(CH_3)_3$. The frequency ratios, $\nu(^6Li)/\nu(^7Li)$, are, respectively, 1.068, 1.055, and 1.068. These are all quite close to the observed isotopic shifts of the monomeric LiCl doublet frequencies, 1.062 and 1.074. Clearly, each of these bands is due to a vibration of lithium in the complex. Its proximity to the monomeric LiCl absorption identifies the mode as a perturbed LiCl stretching frequency, ν_s.

Although isotopic verification is not available for the other complexes, we believe that ν_s for each of them has been observed, as listed in Table III.

Perturbed Modes of the Base. Only for the trimethylamine complexes was it possible to discern perturbed modes of the base. As shown in Figure 3, there are two rather indistinct bands in the spectrum of $(CH_3)_3N \cdot$ LiCl, a weak band at 1212 cm^{-1}, and a pronounced shoulder at 1025 cm^{-1}. More clearly resolved counterparts are seen in the spectrum of the $(CH_3)_3N \cdot$ ^{7}LiBr complex, in this case at 1215 cm^{-1} and at 1022 cm^{-1}. These new features are reminiscent of the spectra of the corresponding trimethylamine complexes with HCl and HBr, as reported in ASP. With HCl, bands were observed at 1220, 1197, and 1004 cm^{-1} whereas HBr produced new bands at 1225, 1196, and 1000 cm^{-1}. The conclusions and discussion in ASP are again applicable: the 1212- and 1215-cm^{-1} bands are due to the perturbed trimethylamine vibration that appears at 1272 cm^{-1} for the gas. The 1025- and 1022-cm^{-1} bands are due to the perturbed 1043-cm^{-1} gas-phase vibration.

TABLE III: Vibrational Frequencies and Relative Shifts for Lithium Halide–Base Complexes

Complex	ν_s, cm^{-1}	$(\nu_s - \nu_M)/\nu_M$	Δ_H[b]
$H_2O \cdot {}^6$LiCl	553	−0.096	−0.343
$H_2O \cdot {}^7$LiCl	518	−0.095	−0.343
$(CH_3)_2O \cdot {}^6$LiCl	524	−0.143	−0.283
$H_3N \cdot {}^6$LiCl	538	−0.120	−0.229
$H_3N \cdot {}^7$LiCl	510(?)	−0.109	−0.229
$(CH_3)_3N \cdot {}^6$NiCl	632	+0.034	−0.189
$(CH_3)_3N \cdot {}^7$LiCl	592	+0.034	−0.189
$H_2O \cdot {}^7$LiBr	460	−0.101	−0.329
$H_3N \cdot {}^7$LiBr	584	+0.142	−0.214
	479	−0.064	
$(CH_3)_3N \cdot {}^7$LiBr	554	+0.083	−0.175

[a] ν_M is taken as the average of the two unperturbed monomer frequencies: ν_M(LiCl) = 611.5 cm^{-1}; $\bar{\nu}_M(^7LiCl)$ = 572.5 cm^{-1}; $\bar{\nu}_M(^7LiBr)$ = 511.5 cm^{-1}. [b] Δ_H = [PA(B) − PA(X^-)]/[PA(B) + PA(X^-)]. Proton affinities are taken from ref 15.

We believe that the correspondence between the LiX and HX perturbations of the trimethylamine vibrations indicates that the lithium halide–base complexes are structurally related to their hydrogen bonded counterpart complexes. This encourages us to explore the ν_s frequency shifts in the same way that was so successful for the hydrogen bond systems, *i.e.*, using the vibrational correlation diagram.

Vibrational Correlation Diagram. If the LiX–base complexes are like their hydrogen bonded counterparts, we can expect for weak bases that the LiX stretching frequency will be progressively lowered as base strength increases. This lowering of ν_s will be accompanied by an increase in the X–Li bond length and a decrease in the Li $\cdots$ B distance. If base strength is steadily increased, there will come a point at which the X–Li distance will be sufficiently long and the Li $\cdots$ B distance sufficiently short that the lithium can be said to be transferred, presumably as Li^+. For such high base strengths, the value of ν_s can be expected to rise again, approaching the limiting frequency of the isolated LiB^+ ion. Between the extremes, there will be a base strength at which ν_s is a minimum, which corresponds to a "completely shared" lithium ion, in which the lithium ion cannot be said to be preferentially bonded either to X^- nor to B.

If this analogy to hydrogen bonding is valid, it should be manifested by a systematic dependence of ν_s upon the difference in the lithium ion affinities of X^- and B. Unfortunately, most lithium ion affinities are, as yet, either unknown or quite uncertain. However, internal consistency requires that if the analogy to hydrogen bonding is legitimate, then lithium ion affinities ought to be monotonically related to proton affinities. Hence, we can explore the systematic dependence of ν_s upon base strength by examining how ν_s changes as a function of Δ, where Δ is defined in terms of proton affinities, just as used in ASP:

$$\Delta = \frac{PA(B) - PA(X^-)}{PA(B) + PA(X^-)}$$

For this purpose, Table III lists the appropriate values of Δ and the relative frequency shifts, $\Delta\nu_s/\nu_s^0 = (\nu_s - \bar{\nu}_M)/\bar{\nu}_M$.

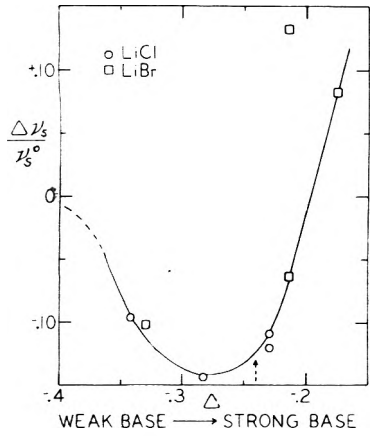

Figure 5. A plot of $\Delta\nu_s/\nu_s^0$ *vs.* Δ for a series of LiX complexes X–Li···B: $\Delta\nu_s/\nu_s^0 = (\nu_s - \bar{\nu}_M)/\bar{\nu}_M$; $\Delta = [PA(B) - PA(X^-)]/[PA(B) + PA(X^-)]$.

For the lithium halides, it is necessary to use as a reference frequency, ν_s^0, one of the two components of the monomer doublet or, having no criterion for preference, the average of the two. We take the latter path, $\nu_s^0 = \bar{\nu}_M$. Figure 5 shows the values of $\Delta\nu_s/\nu_s^0$ plotted *vs.* Δ. There are two observed bands for the $H_3N \cdot LiBr$ complex, so both are shown. The lower frequency correlates smoothly with the other data. This suggests that ν_s is at 479 cm^{-1} and that the higher frequency, 584 cm^{-1}, is a perturbed vibration of the base.

The obvious systematization of the data in Figure 5 is convincing, and it tends to substantiate the lithium ion transfer interpretation of the ν_s frequency shifts. The shape of the curve suggests that there is a continuum of bond types in these complexes. While the extreme bond type at weak base strength (highly negative values of Δ) might be described as a dipole-polarizability bond and that at high base strength as an ion pair, there is no sudden transition from one type to the other. Instead, the curve suggests that at $\Delta \approx -0.28$, the lithium ion is "completely shared" in a bond that is best likened to a type II hydrogen bond (see ASP). Clearly such a bond would not be adequately described by either of the extreme models derived from an electrostatic point of view.

The relationship to hydrogen bonding is further elucidated by comparing the values of Δ at which $\Delta\nu_s/\nu_s^0$ is a minimum (which we call Δ_{II}). In Figure 5, Δ_{II} is near -0.28 for the lithium halide complexes, rather close to the value -0.23, which was determined for the hydrohalide complexes (see ASP). The difference is in the direction that indicates lithium ion transfer occurs with a somewhat weaker base than needed for proton transfer. To make a specific comparison, a base with proton affinity near 187 kcal/mol will form a type II ("completely shared") lithium bond with LiCl whereas a proton affinity near 206 kcal/mol is needed to form a type II hydrogen bond with HCl. This difference seems to be intuitively agreeable on the basis of the high charge separation existing in the lithium halides (as indicated by the molecular dipole moments). On the other hand, it is not what would be expected from a naive inspection of bond energies, since the bond energy of LiCl, 112 kcal/mol, *exceeds* that of HCl by 9 kcal/mol. In fact, a more complete thermodynamic analysis is necessary, based upon lithium ion affinities.

Thermodynamic Considerations. Unfortunately, only one neutral molecule lithium ion affinity has been measured, that of water:

$$Li^+(g) + H_2O(g) \rightarrow H_2OLi^+(g) \qquad \Delta H = -34.0 \text{ kcal/mol}$$

With this value, we can calculate the energy needed to form an ion pair at infinite separation from gaseous LiCl and H_2O molecules, to be compared to comparable calculations for HCl.

$$LiCl(g) + H_2O(g) \longrightarrow H_2OLi^+(g) + Cl^-(g) \qquad H = +119 \text{ kcal/mol}$$

$$HCl(g) + H_2O(g) \longrightarrow H_3O^+(g) + Cl^-(g) \qquad H = +168 \text{ kcal/mol}$$

$$HCl(g) + NH_3(g) \longrightarrow NH_4^+(g) + Cl^-(g) \qquad H = +124 \text{ kcal/mol}$$

Thus, lithium ion transfer from Cl^- to H_2O requires about the same energy as proton transfer from Cl^- to the stronger base, NH_3. This is consistent with the conclusion based on Figure 5, that lithium ion transfer will occur with a weaker base than is needed for proton transfer.

Of course, the consideration is not complete until the two ions are brought into proximity. Regarding Cl^- and H_2OLi^+ as point charges, they would have to be placed at a separation 2.8 Å to make ion pair formation thermoneutral. This separation should be compared to the expected Cl···O distance if it is assumed that the charge on H_2OLi^+ is lodged on the central oxygen atom. That distance must exceed the sum of the equilibrium bond distances in LiCl(g), 2.02 Å, and Li_2O, estimated to be about 1.6 Å (r_0 = 1.52 Å in LiF(g)). This sum, 3.6 Å, is much larger than 2.8 Å and suggests that charge transfer will not occur, consistent with the implications of the vibrational correlation diagram.

Spectral Characteristics of Lithium Bonds. Hydrogen bonding produces unique and obvious spectral perturbations in ν_s: large frequency shifts, increase in intensity, and increase in band width. These effects are muted or absent in the spectra of the lithium halide–base complexes. Figure 5 shows changes in $\Delta\nu_s/\nu_s^0$ that qualitatively resemble those caused by hydrogen bonding, but much smaller in magnitude. The minimum in the $\Delta\nu_s/\nu_s^0$ curve is about -0.14 in the lithium complexes, whereas it reaches -0.76 for hydrogen bonded complexes (see Figure 8, ASP).

Even less similar are the intensity and band width behaviors. All of the new features recorded for lithium halide complexes are relatively weak and their band widths are increased, but only modestly over the band widths observed for the isolated monomer. The low intensity could, of course, be due to a low concentration (rather than to a low absorption coefficient) but there is evidence to the contrary. The 1215-cm^{-1} band in the $(CH_3)_3N \cdot LiBr$ spectrum is almost as intense as the comparable band at 1225 cm^{-1} in the $(CH_3)_3N \cdot HBr$ spectrum. This suggests that there are comparable amounts of complex, so the low intensity of ν_s in $(CH_3)_3N \cdot LiBr$ must be due to low absorption coefficient.

The absence of intensity enhancement may be connected with the fact that the lithium halide bond is extremely polar before bond formation, so that the possibility for significant enhancement is lessened. Nevertheless, neither the intensity nor the band width behavioral differences between hydrogen bonded complexes and their lithium counterparts is readily rationalized. This contrast adds a dimension to a subject that remains unsettled; perhaps it may

ultimately contribute to a clearer understanding of the behavior of both systems.

Conclusions

We believe that the present data provide strong evidence for the formation of complexes in which two molecules are linked by a lithium atom in a geometry such as that found in hydrogen bonds. Furthermore, the vibrational correlation diagram indicates a continuum of such complexes can be formed by varying the base strength, again in close analogy to hydrogen bonding behavior. We believe that in this continuum, there is a progressive transfer of the lithium ion and that for appropriate base strength, the lithium occupies an intermediate position in which it is not bonded to either adjacent atom preferentially, *i.e.*, it is "completely shared." While the data suggest that a lithium ion transfer occurs with a weaker base for lithium halides than for hydrohalides, the difference is perhaps not as significant as is the fact that it is a rather small difference. The only striking absence of similarity to the hydrogen bond lies in the fact that neither the intensity nor the band width of ν_s is dramatically affected in these lithium complexes. Despite this one discordance, we feel that the likenesses warrant the conclusion that these lithium halide–base complexes involve bonding such as that in hydrogen bonds, that is, they contain *lithium bonds*.

Acknowledgment. We gratefully acknowledge support of this research by the U.S. Office of Naval Research, under Grant No. N00014-69-0200-102.

References and Notes

(1) B. S. Ault and G. C. Pimentel, *J. Phys. Chem.*, **77**, 57 (1973).
(2) B. S. Ault and G. C. Pimentel, *J. Phys. Chem.*, **77**, 1649 (1973).
(3) B. S. Ault, E. Steinback, and G. C. Pimentel, *J. Phys. Chem.*, preceding paper. (This reference is called ASP in the text of this paper.)
(4) D. N. Shigorin, *Spectrochim. Acta*, **14**, 198 (1959).
(5) F. West and W. Glaze, *J. Amer. Chem. Soc.*, **83**, 3581 (1961).
(6) D. Balasubramanian, A. Goel, and C. N. R. Rao, *Chem. Phys. Lett.*, **17**, 482 (1972).
(7) I. Dzidic and P. Kebarle, *J. Phys. Chem.*, **74**, 1466 (1970).
(8) P. A. Kollman, J. F. Liebman, and L. C. Allen, *J. Amer. Chem. Soc.*, **92**, 1142 (1970).
(9) E. Clementi and H. Popkie, *J. Chem. Phys.*, **57**, 1077 (1972).
(10) P. Schuster, *Chem. Phys. Lett.*, **3**, 433 (1969).
(11) W. L. S. Andrews and G. C. Pimentel, *J. Chem. Phys.*, **44**, 2361 (1966).
(12) A. Snelson and K. S. Pitzer, *J. Phys. Chem.*, **67**, 882 (1963).
(13) S. Schick and O. Schnepp, *J. Chem. Phys.*, **41**, 463 (1964).
(14) R. C. Miller and P. Kusch, *J. Chem. Phys.*, **25**, 860 (1956).
(15) J. L. Beauchamp, *Annu. Rev. Phys. Chem.*, **22**, 527 (1971).

Photorotamerism of Aromatic α-Dicarbonyls[1]

J. F. Arnett and S. P. McGlynn*

Coates Chemical Laboratories, The Louisiana State University, Baton Rouge, Louisiana 70803 *(Received November 8, 1974)*

Publication costs assisted by the U.S. Atomic Energy Commission Biomedical and Environmental Research Physics Program

Absorption and emission spectra are reported for five aromatic α-dicarbonyls in fluid solutions at room temperature. All emissions proceed from relaxed excited states, both S_1 and T_1, which possess coplanar or nearly coplanar dicarbonyl geometries, whereas absorption initiates in relaxed ground states, S_0, which exhibit widely different values of the CO/CO dihedral angle in different molecules. It is argued that low-energy $\pi^* \leftarrow$ n transitions in these molecules are heavily localized on the dicarbonyl moiety.

Introduction

Our previous studies of the emissive characteristics of nonaromatic α-dicarbonyl systems (e.g., pyruvic acid,[2a] oxalic acid,[2b] oxamide,[3] parabanic acid[4]) evolved, in part, into a consideration of the geometric differences between the relaxed, absorbing ground state and the relaxed, emitting excited states. In this work, we extend these geometric concerns to mono- and diaromatic α-dicarbonyl systems.

Prior work[5-11] on mono- and diaromatic α-dicarbonyl systems is sparse and has been limited, largely, to the diaromatic benzil (I). In the most cogent discussion of such luminescence properties which is available, Morantz and Wright[5] postulated that photoexcitation of the skewed ground state of compound I leads to relaxed, emitting S_1 and T_1 states in which the α-dicarbonyl system is planar. One consequence of this supposition is that if I were "frozen" into a ground state conformation in which the α-dicarbonyl subsystem was maintained planar, or nearly so, all geometric relaxation processes in the S_1 and T_1 states would be evaded. An examination of molecular models indicated that the molecules phenyl mesityl diketone (II) and mesitil (III) might satisfy the requirements of a planar α-dicarbonyl S_0 geometry. In particular, such models for the ground state of compound III suggest that the intercarbonyl dihedral angle, θ, should be $\sim$180° and the "mesityl/adjacent carbonyl" dihedral angle, Φ, should lie in the 45–90° range.

The extent to which coplanarity of the aromatic and carbonyl moieties affects the luminescence properties (i.e., contributes to the large Stokes shift of the fluorescence observed in many aromatic α-dicarbonyls) is largely unknown. A study of the excited state properties of 1-phenyl-1,2-propanedione (IV), 3,3-dimethyl-1,2-indanedione (V), and 3,3,5,5-tetramethylcyclopentanedione (VI) might provide information on this point. Examination of molecular models indicates that coplanarity of the aromatic and car-

bonyl fragments is sterically hindered, to a slight extent, in the S_0 state of IV, is sterically enforced in all states of V, and is absent in VI, since this last molecule possesses no

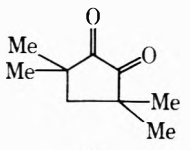

VI

aryl parts; in addition, coplanarity of the α-dicarbonyl systems is enforced cisoid in all states of V and VI and is probably transoid in the S_1 and T_1 states of IV.

Finally, much of the prior work[5-11] consisted of a correspondence of absorption spectra obtained in liquid solutions at room temperature with emission data obtained in glassy solutions at low-temperatures (usually 77°K). In view of the fact that glassification may itself induce structural changes in the solute species, it seemed appropriate to confine all measurements to fluid media at ~300°K.

Since the observed emission spectra of the fluid systems contain both phosphorescence and fluorescence components, some means of distinguishing them is required. The technique of extensive degassing coupled with that of air saturation provides apt discrimination. Phosphorescence is either diminished or completely quenched in the air-saturated solutions whereas fluorescence is usually not much affected.

Experimental Section

Benzil (Baker) and 1-phenyl-1,2-propanedione (Eastman) were purchased commercially. Mesitil and phenyl mesityl diketone were prepared by an air oxidation of the corresponding benzoins.[12] 3,3-Dimethyl-1,2-indanedione was prepared by standard methods.[13] All solids were purified immediately prior to use by sublimation, recrystallization, and/or thin layer chromatography. The liquid 1-phenyl-1,2-propanedione was purified by vacuum distillation.

Instrumentation and techniques have been decribed previously.[2a,3] Total emission spectra were recorded at ambient temperatures (~300°K) on samples previously submitted to an extensive freeze–evacuate–thaw degassing procedure and on samples subjected to aeration procedures; the fluorescence and phosphorescence components were determined by simple comparison of the degassed and the aerated solution spectra.

Results

Absorption and emission spectra of compounds I–V are presented in Figures 1–5. Pertinent data for compound VI are available elsewhere.[14] The absorption spectra are characterized by a low-energy $^1\Gamma_{n\pi^*} \leftarrow {}^1\Gamma_1$ transition of weak intensity and a higher energy $^1\Gamma_{\pi\pi^*} \leftarrow {}^1\Gamma_1$ transition of variable (i.e., moderate to strong) intensity. The total luminescence spectra comprise both $^1\Gamma_{n\pi^*} \rightarrow {}^1\Gamma_1$ and $^3\Gamma_{n\pi^*} \rightarrow {}^1\Gamma_1$ processes.

Salient features of the absorption and emission spectra are given in Table I. Data are given for only one $^1\Gamma_{\pi\pi^*} \leftarrow {}^1\Gamma_1$ transition: the most intense such transition at $\bar{\nu} < 45{,}000$ cm^{-1}. Other $^1\Gamma_{\pi\pi^*} \leftarrow {}^1\Gamma_1$ transitions are observable (e.g., in Figures 1, 3, 4, and 5) but are not distinct in some compounds and not detectable in others.

The $^1\Gamma_{n\pi^*} \leftarrow {}^1\Gamma_1$ absorption is broad and structureless in compounds I, II, and IV but exhibits distinct vibrational structure in compounds III and V. A vibrational analysis of

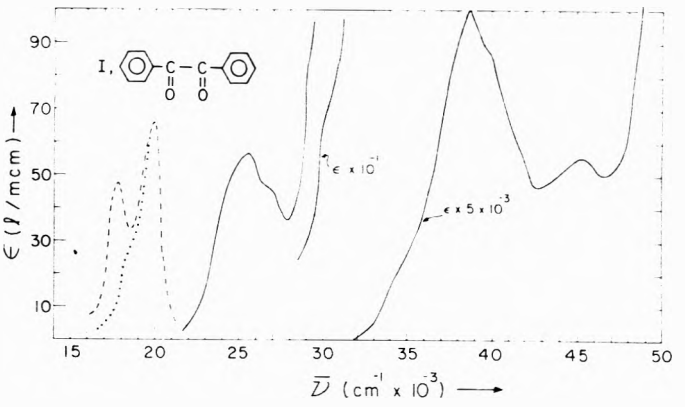

Figure 1. Absorption and emission spectra of benzil (I) in 3-methylpentane at ~300°K. The scale of emission intensities is linear: (- - - -) total luminescence of degassed solution; (· · · ·) total luminescence of aerated solution.

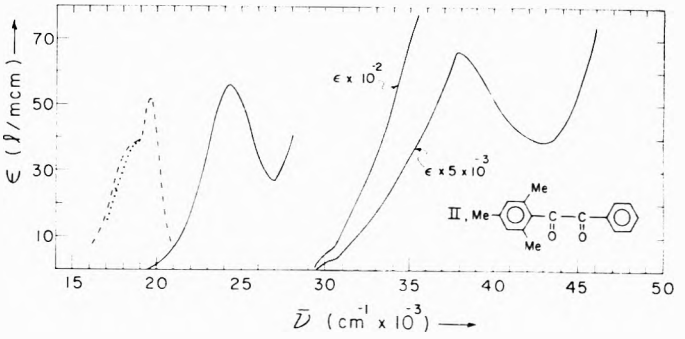

Figure 2. Absorption (in 3-methylpentane) and emission (in methylcyclohexane) spectra of phenyl mesityl diketone (II) at ~300°K. The scale of emission intensities is linear: (- - - -) total luminescence of degassed solution; (· · · ·) total luminescence of aerated solution.

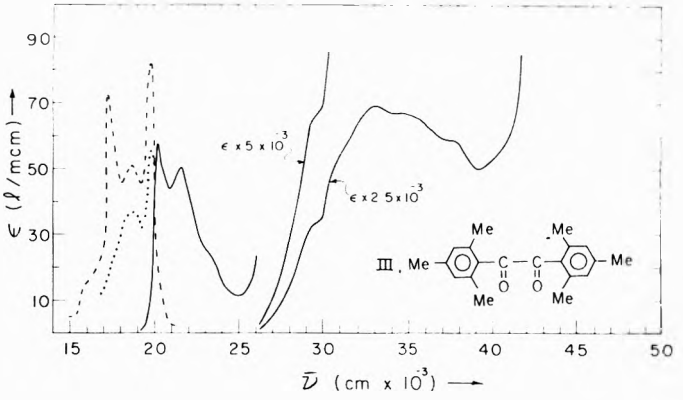

Figure 3. Absorption and emission spectra of mesitil (III) in 3-methylpentane at ~300°K. The scale of emission intensities is linear: (- - - -) total luminescence of degassed solution; (· · · ·) total luminescence of aerated solution.

this absorption for the indanedione V is give in Table II; considerable activity in a symmetric carbonyl stretching mode, $\bar{\nu} = 1450$ cm^{-1}, is evident. The corresponding frequency observed in mesitil (III) is ~1350 cm^{-1}. The $^1\Gamma_{n\pi^*} \leftarrow {}^1\Gamma_1$ absorption band of compound IV is somewhat different from the others. It exhibits a poorly resolved structure on the long wavelength edge but is structureless at higher energies; in addition, the half-width of this band, 5400 cm^{-1}, appears to be larger than that of any other compound studied here. Indeed, analogy to the corresponding

TABLE I: Absorption and Emission Characteristics of Some α-Dicarbonyls[a]

Compd	$^1\Gamma_{n\pi^*} \leftarrow {}^1\Gamma_1$ $\bar{\nu}_{max}$, cm^{-1}	ϵ, M^{-1} cm^{-1}	$^1\Gamma_{n\pi^*} \rightarrow {}^1\Gamma_1$ $\bar{\nu}_{max}$, cm^{-1}	$^3\Gamma_{n\pi^*} \rightarrow {}^1\Gamma_1$ $\bar{\nu}_{max}$, cm^{-1}	Stokes shift ΔF, cm^{-1}	ST split ΔST, cm^{-1}	$^1\Gamma_{\pi\pi^*} \leftarrow {}^1\Gamma_1$ $\bar{\nu}_{max}$, cm^{-1}	ϵ, M^{-1} cm^{-1}	Dihedral Angles θ, deg	Φ, deg
I	25,600	56	19,950	17,800	5650	2150	38,700	20,250	~90	0–10
II	24,300	52	19,450	*b*	4850	*b*	37,800	13,300	90–180	0; 45–90
III	20,200	57	19,800	17,330	400	2470	33,000	2,750	~180	45–90
IV	24,550	28	20,700	18,300	3850	2400	38,500	8,150	70–110	0–10
V	18,900	36	18,700	16,760	200	1940	36,600	8,870	0–10	0–10
VI	18,870[c]	31[c]							~0	

[a] All data refer to band maxima observed in solutions in 3-methylpentane at ~300°K. [b] Although II does phosphoresce, the difference of total luminescence spectra of degassed and aerated solutions (see Figure 2) is insufficient to locate λ_{max} of the phosphorescence with any degree of accuracy. [c] In cyclohexane solutions; as reported in ref 14 of text.

TABLE II: Vibronic Analysis of the $^1\Gamma_{n\pi^*} \leftarrow {}^1\Gamma_1$ Absorption Band of Indanedione (V)

λ, mμ	$\bar{\nu}$, cm^{-1}	$\Delta\bar{\nu}$, cm^{-1}		Assignment ν_1, ν_2
528	18,940	0	0	0,0
510	19,610	670		1,0
490	20,410		1470	0,1
475	21,050	1440		1,1
458	21,830		1420	0,2

$\nu_1 = 670\ cm^{-1}$
$\nu_2 = 1440\ cm^{-1}$

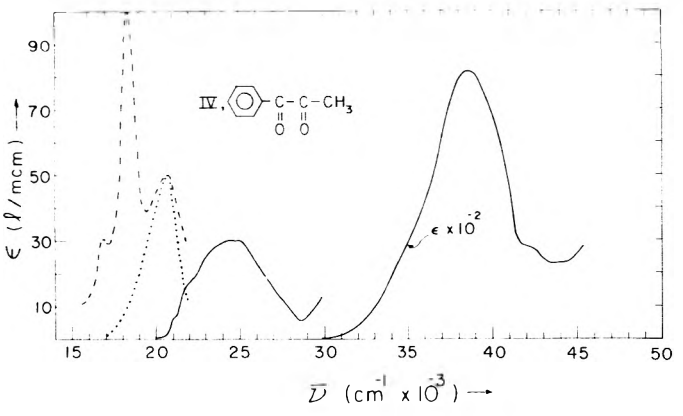

Figure 4. The absorption and emission spectra of 1-phenyl-1,2-propanedione (IV) in 3-methylpentane at 300°K. The scale of emission intensities is linear: (- - - -) total luminescence of degassed solution; (· · · ·) total luminescence of aerated solution.

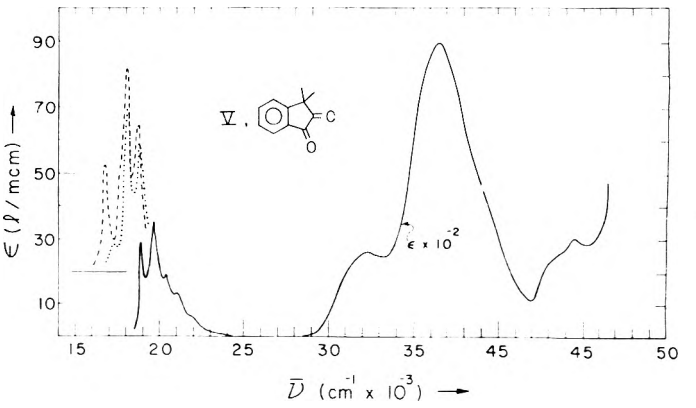

Figure 5. Absorption and emission spectra of 3,3-dimethyl-1,2-indanedione (V) in 3-methylpentane at ~300°K. The scale of emission intensities is linear. The emission spectra are displaced vertically for greater clarity: (- - - -) total luminescence of degassed solution; (· · · ·) total luminescence of aerated solution.

absorption band of pyruvic acid and various of its esters[2a] leads one to conclude that compound IV samples a variety of ground state geometries, including the planar situation where $\theta = 180°$. Nonetheless, it is the contention here that the dominant entities present in IV have dihedral angles such that $70 < \theta < 110°$. Intercarbonyl dihedral angles which have been inferred or deduced for the other compounds are listed in Table I. Comparison of Table I and Figures 1–5 indicates that the presence of vibrational structure in the $^1\Gamma_{n\pi^*} \leftarrow {}^1\Gamma_1$ absorption band is an indicator of CO/CO coplanarity in both the ground and excited states.

The fluorescence origin band in compounds III and V is almost coincident with the 0,0 band of the $^1\Gamma_{n\pi^*} \leftarrow {}^1\Gamma_1$ absorption band. A similar coincidence is also evident in compound IV, if one supposes the absorption 0,0 to lie at 21,000 cm^{-1} (i.e., in the structured red edge). The Stokes shifts of the measurable "vibrationless" origins lie, then, in the range 300–200 cm^{-1} and their smallness indicates a complementarity of emission and absorption processes. The fluorescence of compounds III, IV, and V is, therefore, of $^1\Gamma_{n\pi^*} \rightarrow {}^1\Gamma_1$ nature. The fluorescence band maxima of compounds I, II, and IV exhibit large Stokes shifts relative to the unstructured $^1\Gamma_{n\pi^*} \leftarrow {}^1\Gamma_1$ absorption maxima. By analogy with IV, where a nascent structure is detectable in the red edge of the $^1\Gamma_{n\pi^*} \leftarrow {}^1\Gamma_1$ absorption band, it follows that the fluorescence of compounds I and II is also of $^1\Gamma_{n\pi^*} \rightarrow {}^1\Gamma_1$ nature.

Given that the fluorescence is of $^1\Gamma_{n\pi^*} \rightarrow {}^1\Gamma_1$ nature, the characteristic singlet–triplet split of 1900–2500 cm^{-1} evidenced by all compounds indicates[15] that the phosphorescence is always of $^3\Gamma_{n\pi^*} \rightarrow {}^1\Gamma_1$ type. This conclusion is also in accord with the 77°K data for phosphorescence lifetimes and with vibronic analysis of these $T_1 \rightarrow S_0$ emission spectra.

It is probable that much of the fluorescence observed here (i.e., in fluid nonpolar systems at ~300°K) is of a thermally activated $S_1 \leftarrow T_1$ nature.[16]

Discussion

The ground state geometry of I has received considerable attention.[17] It has been established that the benzoyl sub-

units are planar and aligned at $70 \leq \theta \leq 90°$. No crystallographic data are available for II and III. Steric effects induced by ortho substitution on the phenyl ring suggest that $90 \leq \theta \leq 180°$ for II and that $\theta \simeq 180°$ for III. Moreover, the same effects suggest that the "phenyl/adjacent carbonyl" dihedral angle, Φ should increase toward 90° as one proceeds from I toward III. These suppositions concerning ground state geometries of I, II, and III have been used by Leonard and Blout[18] to rationalize the decrease of energy of the $^1\Gamma_{n\pi^*} \leftarrow {}^1\Gamma_1$ transition and the decrease of intensity of the $^1\Gamma_{\pi\pi^*} \leftarrow {}^1\Gamma_1$ transition which occur on proceeding from I toward III (see Table I). Straightforward application of the Leonard–Blout principles[18] to the monoaromatic α-dicarbonyls, IV and V, establishes the most probable geometry of IV relative to that which is sterically enforced on V. These geometries, consistent from the point of view of steric considerations and absorption spectroscopic data, are listed in Table I under θ and Φ.

The $^1\Gamma_{n\pi^*} \leftarrow {}^1\Gamma_1$ energies of the diaromatic α-dicarbonyls vary over a broad range of 5400 cm^{-1}. The $^1\Gamma_{n\pi^*} \rightarrow {}^1\Gamma_1$ and $^3\Gamma_{n\pi^*} \rightarrow {}^1\Gamma_1$ energies, by contrast, span a very narrow range of ~500 cm^{-1}. This near-constancy of emission energies suggests that the three diaromatics decay radiatively from a common, well-defined geometry. In turn, the observed differences of Stokes shifts, which vary over a range of 5250 cm^{-1}, must then be associated with ground state geometric differences and the effects which these differences exert on $^1\Gamma_{n\pi^*} \leftarrow {}^1\Gamma_1$ absorption energies. As a result, we conclude, in agreement with Morantz and Wright,[5] that the geometry of the ground state is categorized by a CO/CO dihedral angle which varies from molecule to molecule whereas the S_1 state exhibits CO/CO coplanarity in all molecules. This conclusion is vindicated by the negligible Stokes shift and by the mirror-image relationship of fluorescence and absorption spectra in V where the CO/CO coplanarity is sterically enforced.

This common α-dicarbonyl coplanarity of all S_1 geometries must be extended also to all T_1 state geometries because of the relative constancy of all ΔST splittings of Table I. Thus, for mesitil, we conclude that $\theta(S_1) = \theta(T_1) = \theta(S_0) \simeq 180°$; for indanedione, we conclude that $\theta(S_1) = \theta(T_1) = \theta(S_0) = 0°$; for I, we conclude that $\theta(S_1) = \theta(T_1) = 180°$, whereas $\theta(S_0) \simeq 90°$; and, for II, we conclude that $\theta(S_1) = \theta(T_1) = 180°$, whereas $90 \leq \theta(S_0) \leq 180°$.

The similarity of the absorption and emission properties of compounds I, II, and IV, the previously mentioned red-edge structure of the lowest-energy absorption band of IV being disregarded, indicates that the S_0, T_1, and S_1 geometries found in IV are similar[19] to those of the corresponding states in I and II. All of these compounds possess "phenyl/adjacent carbonyl" near-coplanarity and CO/CO noncoplanarity in their S_0 states.[19] On the other hand, the S_1 and T_1 geometries of compound IV are identical with those listed for S_1 and T_1 states of III; in this manner, the large Stokes shift, $\Delta F = 3850$ cm^{-1}, of compound IV finds a ready interpretation.

Only one facet of the data of Table I, namely, the decrease of $^{1,3}\Gamma_{n,\pi^*} \leftrightarrow {}^1\Gamma_1$ energies in V relative to III, remains to be interpreted. One might suspect that these decreases are in some way associated with the coplanarity of the "phenyl/adjacent carbonyl" which is sterically enforced in V. This, however, is not the case: Sandris and Ourisson[14] have shown that compound VI has $^1\Gamma_{n\pi^*} \leftarrow {}^1\Gamma_1$ absorption peaks at 538 and 508 mμ, in good correspondence with the related peaks of V at 528 and 510 mμ, respectively. Since compound VI contains no aryl attachments whatsoever, it seems clear that the low values of $^{1,3}\Gamma_{n\pi^*} \leftrightarrow {}^1\Gamma_1$ energies in V are not attributable to phenyl–carbonyl interaction effects (i.e., are independent of Φ). Consequently, we are forced to seek an alternative interpretation of this effect. The transoid geometry of the α-dicarbonyl subunit of III in all three states (i.e., S_0, S_1, and T_1) as opposed to the cisoid geometry of V and VI in the same states provides an apt explanation.

First, the $^1\Gamma_{n\pi^*} \leftarrow {}^1\Gamma_1$ transition, as indicated by a comparison of the absorption spectra of V and VI, is not very sensitive to aryl substitution. Consequently, we can assert that the $^{1,3}\Gamma_{n,\pi^*} \leftrightarrow {}^1\Gamma_1$ processes in aromatic α-dicarbonyls are highly localized on the dicarbonyl group.[20] In view of this, we can presume to compare the absorption and emission properties of III and V with those of glyoxal. Now, the difference of the absorption origin bands (i.e., 0,0 bands) of compounds III and V is ~1300 cm^{-1}, in very good accord with the corresponding difference of fluorescence origin bands of ~1100 cm^{-1}. The same differences[21] for *trans*- and *cis*-glyoxal are, in both instances, 1465 cm^{-1} (the *trans*-glyoxal S_1 state being of higher energy than the *cis*-glyoxal). The near-identity of these two sets of separations suggests that the energy differences of the $^{1,3}\Gamma_{n\pi^*} \leftrightarrow {}^1\Gamma_1$ processes of III and V are almost wholly attributable to the transoid nature of III and the cis nature of V and that the variance of the angle Φ in these two compounds has little or no effect on $^1\Gamma_{n\pi^*} \leftrightarrow {}^1\Gamma_1$ energies.

References and Notes

(1) This work was supported by contract between the United States Atomic Energy Commission Biomedical and Environmental Research Physics Program and The Louisiana State University.
(2) (a) J. F. Arnett, D. B. Larson, and S. P. McGlynn, *J. Amer. Chem. Soc.*, **95,** 7599 (1973); (b) H. J. Maria and S. P. McGlynn, *J. Mol. Spectrosc.*, **42,** 296, 1776 (1972).
(3) D. B. Larson and S. P. McGlynn, *J. Mol. Spectrosc.*, **47,** 469 (1973).
(4) D. B. Larson, J. F. Arnett, and S. P. McGlynn, *J. Amer. Chem. Soc.*, **95,** 6928 (1973).
(5) D. J. Morantz and A. J. C. Wright, *J. Chem. Phys.*, **53,** 1522 (1970); **54,** 692 (1971).
(6) S. C. Bera, R. K. Mukherjee, P. Mukherjee, and M. Chowdhury, *J. Chem. Phys.*, **55,** 5826 (1971).
(7) M. Almgren, *Photochem. Photobiol.*, **9,** 1 (1969).
(8) S. C. Bera, R. Mukherjee, and M. Chowdhury, *J. Chem. Phys.*, **51,** 754 (1969).
(9) T. R. Evans and P. A. Leermakers, *J. Amer. Chem. Soc.*, **89,** 4380 (1967).
(10) N. K. Chaudhuri and M. A. El-Sayed, *J. Chem. Phys.*, **47,** 1133 (1967).
(11) A. Kuboyama and S. Yabe, *Bull. Chem. Soc., Jap.*, **40,** 2475 (1967).
(12) (a) "Organic Synthesis," Collect. Vol. II, p 509, 1948; (b) "Organic Reactions," Vol. 4, p 269; (c) "Organic Synthesis," Collect. Vol. I, p 87, 1948.
(13) C. F. Koelsch and C. D. LeClaire, *J. Org. Chem.*, **6,** 516 (1941).
(14) C. Sandris and G. Ourisson, *Bull. Chim. Soc. Fr.*, **23,** 958 (1956).
(15) S. P. McGlynn, T. Azumi, and M. Kinoshita, "Molecular Spectroscopy of the Triplet State," Prentice-Hall, Englewood Cliffs, N.J., 1969.
(16) C. A. Parker and T. A. Joyce, *J. Chem. Soc. D,* 1421 (1968).
(17) (a) N. C. B. Allen, *Phil. Mag.*, **3,** 1037 (1927); (b) K. Banerjee and F. L. Sinha, *Indian J. Phys.*, **11,** 409 (1949); (c) C. J. Brown and R. Sardanaga, *Acta. Crystallogr.*, **18,** 158 (1965).
(18) N. J. Leonard and E. R. Blout, *J. Amer. Chem. Soc.*, **72,** 484 (1950).
(19) Note that this conclusion pertains only to the dominant (i.e., majority) structure of the S_0 state of molecule IV. As previously concluded, the geometry of the S_0 state of this molecule samples a variable range of θ; a small population of molecules for which $\theta \simeq 180°$ is, in fact, suggested by the red-edge structure of the $^1\Gamma_{n,\pi} \leftarrow {}^1\Gamma_1$ absorption band of Figure 4.
(20) J. F. Arnett, G. Newkome, W. L. Mattice, and S. P. McGlynn, *J. Amer. Chem. Soc.*, **96,** 4385 (1974).
(21) (a) W. Holzer and D. A. Ramsay, *Can. J. Phys.*, **48,** 1759 (1970); (b) G. N. Currie and D. A. Ramsay, *ibid.*, **49,** 317 (1970); (c) R. Y. Dong and D. A. Ramsay, *ibid.*, **51,** 1491 (1973).

Charge Transfer Spectroscopy, Redox Energetics, and Photoredox Behavior of Transition Metal Ammine Complexes. A Critical Comparison of Observations with Mechanisms and Models[1]

John F. Endicott,* Guillermo J. Ferraudi, and John R. Barber

Department of Chemistry, Wayne State University, Detroit, Michigan 48202
(Received May 10, 1974; Revised Manuscript Received November 10, 1974)

Publication costs assisted by the National Science Foundation

Information is considered which bears on the nature of CTTM transitions and on the mechanisms of photoredox decompositions in transition metal complexes. The shifts of CTTM absorption bands in various solvent media and models for solvent perturbation of the CTTM excited state potential energy surfaces are presented. The absorption spectroscopy, the thermodynamics of CTTM transitions of outer sphere (ion pair) and inner sphere complexes of cobalt(III) and ruthenium(III), and the photoredox behavior of these systems are compared in some detail. It is inferred that an excited state Jahn-Teller distortion leads to a greater Franck–Condon contribution to the transition energies in the cobalt(III) complexes than in the ruthenium(III) complexes. Marcus' theory of solvent repolarization is used to estimate Franck–Condon contributions. Appreciable metal–ligand covalent bonding is inferred to be important in CTTM excited states of ruthenium complexes. Various radical pair models, which have been proposed to describe the photoredox chemistry of cobalt(III) complexes, are compared to photochemical data for $Co(NH_3)_5X^{2+}$ (X = Cl, Br, NSC, N_3, NO_2). These comparisons indicate that, although radical pair species appear to be the primary photoredox products, photophysical processes occurring in the CTTM excited states are important in determining net product yields, with the overall quantum yield being a function of both excited state and radical pair processes. Approaches to excited state models are discussed.

Introduction

Mechanistic discussions of photoredox reactions of cobalt(III) complexes are commonly formulated around "radical pair" or "excited state" models.[2] Despite the importance of the evolution of useful mechanistic models to a coherent understanding of the photoredox chemistry of transition metal complexes, neither the radical pair nor the excited state approach has yielded useful models of established applicability. At least two different radical pair models have been proposed,[3–5] but these models have been subjected to few critical appraisals.[5a] Even approaches to the formulation of specific excited state models are rare in the published literature. It is the aim of the present paper to (1) present some approaches to the formulation of useful excited state models for the photochemistry of coordination complexes; (2) to examine the complementarity of excited state and radical pair models; and (3) to present experimental observations, some original with this report, some previously published, which bear critically on the validity of various models. These aims will require a consideration of the energetics of charge transfer to metal (CTTM) electronic transitions, some observations on CTTM spectra, and some careful formulations of radical pair models. New photochemical studies are reported in the present paper, and additional photochemical studies pertaining to more detailed considerations of some of the problems posed will be reported elsewhere.[6]

Photoredox decompositions are a characteristic result of direct irradiation of CTTM absorption bands of cobalt(III) and other complexes.[2] For purposes of organizing our approaches to the mechanistic questions it is useful to distinguish and discuss separately, the likely principal events in the photoredox reaction sequence: (A) excitation; (B) photophysical processes possible for the initial CTTM excited state; (C) fragmentation of the reactive CTTM excited state to form solvent trapped radical species; (D) separation of these radical fragments to form independent radical species in bulk solution; and (E) the formation of final products. In this report we will concern ourselves with steps A–C in this sequence.

Experimental Section

All spectroscopic studies were performed on a Cary 14 spectrophotometer. Reference solutions were prepared without the coordination complex substrate, but otherwise of the same composition as the sample solutions.

Photochemical apparatus and techniques have been described elsewhere.[6–10] Quantum yield determinations were based on cobalt(II) analyses,[9–11] changes of absorbance of photolyte solutions, and, for specific complexes, on analyses of N_3^- NH_3, NCS^-, or chromatographically separated complexes. Chemical actinometers were Reineckate,[12] ferrioxalate,[13] or uranyl oxalate[14] solutions for the lowest energy visible, visible–ultraviolet, and deep-ultraviolet irradiations, respectively.

Although we have not relied on substrate absorption changes as the single measurement on which quantum yields were based, we have found such absorption changes to be useful as a check on the validity of yields based on other determinations. We did not work out a quantitative chromatographic separation of the cobalt(III) products which result from ultraviolet irradiations of $Co(NH_3)_5Br^{2+}$; however, absorption changes were consistent with aquation yields reported by Adamson and Sporer[3] and the redox yields reported by those authors and confirmed by us for near-ultraviolet excitations; for most ultraviolet excitations

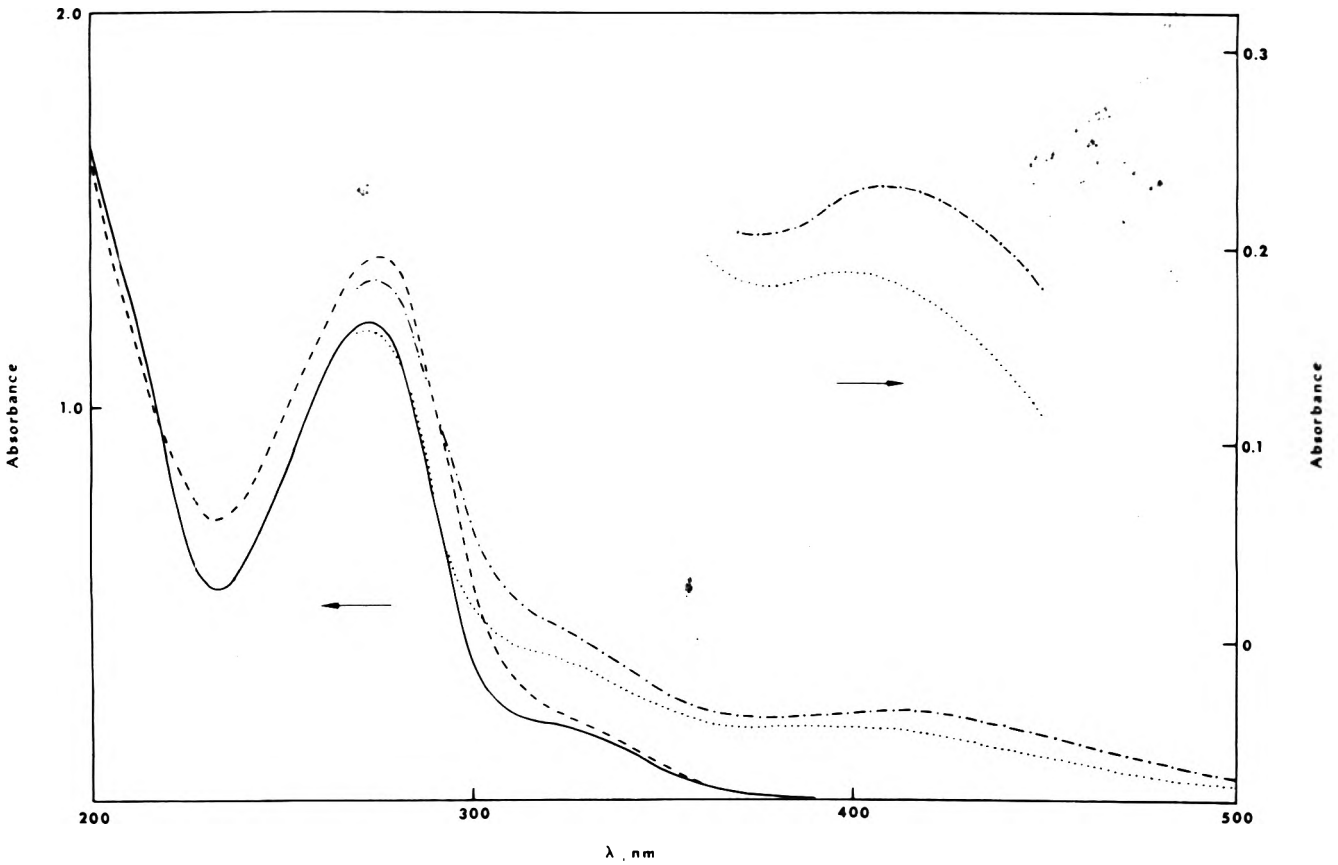

Figure 1. Absorption spectrum of 2.5×10^{-3} *M* $[Ru(NH_3)_6](ClO_4)_3$ in various media: (—) H_2O; (- - -) 50% glycerol; (· · · ·) 0.2 *M* NaI in H_2O; (- · - · -) 0.2 *M* NaI in 50% glycerol. Curves on upper right are ion pair spectra on expanded absorbance scale.

the observed absorbance changes were compatible with photoredox as the only detectable process, as reported previously at 254 nm.[2a,7a] We have had similar experiences with $Co(NH_3)_5Cl^{2+}$; Balzani and coworkers[15] have reported an ammonia aquation process for this complex, but no yield for this process has been reported and we have been unable to separate a $Co(NH_3)_4OH_2Cl^{2+}$ product chromatographically (see also ref 7b).

For $Co(NH_3)_5N_3^{2+}$ and $Co(NH_3)_5NCS^{2+}$ we have determined NH_3 by a colorimetric procedure[16] following chromatographic removal of cobalt(III) and cobalt(II) species. Azide analyses are described elsewhere;[8] NCS^- was determined per the procedure of Adamson, *et al.*,[12] following similar chromatographic separations.

The chromatographic separations were accomplished with about 1 ml of Bio-Rad AG 50-W-X2 cation exchange resin, pretreated by washing with 25 ml of a solution 1 *M* in $NaClO_4$ and 10^{-3} *M* in $HClO_4$. A 3-ml aliquot of photolyte (or of a blank solution) was passed slowly through the column, then washed with 4 ml of 10^{-3} *M* $HClO_4$. Effluents were collected in about 5-ml aliquots and analyzed per the noted procedures. Similar treatments were performed on blank solutions or on solutions containing known $[NH_4^+]$ or $[NCS^-]$, to calibrate the analytical procedure.

Results

This study has involved the careful examination of CTTM absorption spectra and the determination of photoredox yields of several $Co(NH_3)_5X^{2+}$ complexes over an extended range of ultraviolet excitation energies. The spectroscopic observations for $Ru(NH_3)_6^{3+}$ and $Co(NH_3)_5Br^{2+}$ are presented in Figures 1 and 2, respectively, and summarized in Table I. The photochemical results are summarized in Figures 3 and 4 and are tabulated in Table III.[17]

Discussion

A. Excitation. Concerning Charge Transfer Spectra. One would hope that approaches which have proved useful for understanding CTTM spectra would provide insight into charge transfer photochemistry or even provide a basis for models describing important features of photoredox chemistry. The early analyses of $Fe(OH_2)_5X^{2+}$ (X = OH, Cl, Br) did relate photochemical and spectroscopic observations,[18-20] and the approach we have evolved below is to a significant extent an extension and specific application of some of those ideas. Jørgensen's more recent and remarkably successful semiempirical correlation (1) of the

$$\tilde{\nu} = 30(\chi_L - \chi_M) + 10Dq + \delta S + \cdots \quad (1)$$

frequencies, $\tilde{\nu}$ in kK, of the absorption maxima of CTTM transitions[21-23] has not yet led to useful approaches to photochemical models, but some of the arguments employed in the Jørgensen treatment are important components of our discussion of the behavior of CTTM excited states.

One may formally describe CTTM excitation in a $M^{III}L_5(X^-)$ complex as indicated in (2). The dominant physical features of this type of transition are: (1) a net increase in electronic charge density near the center of the molecule in the CTTM excited state, $*[M^{II}L_5(\cdot X)]$, compared to the ground state, and (2) a significantly smaller molecular dipole moment in the excited state than in the ground state.

It is important to note that all of the photochemical studies considered here and most of the spectroscopic stud-

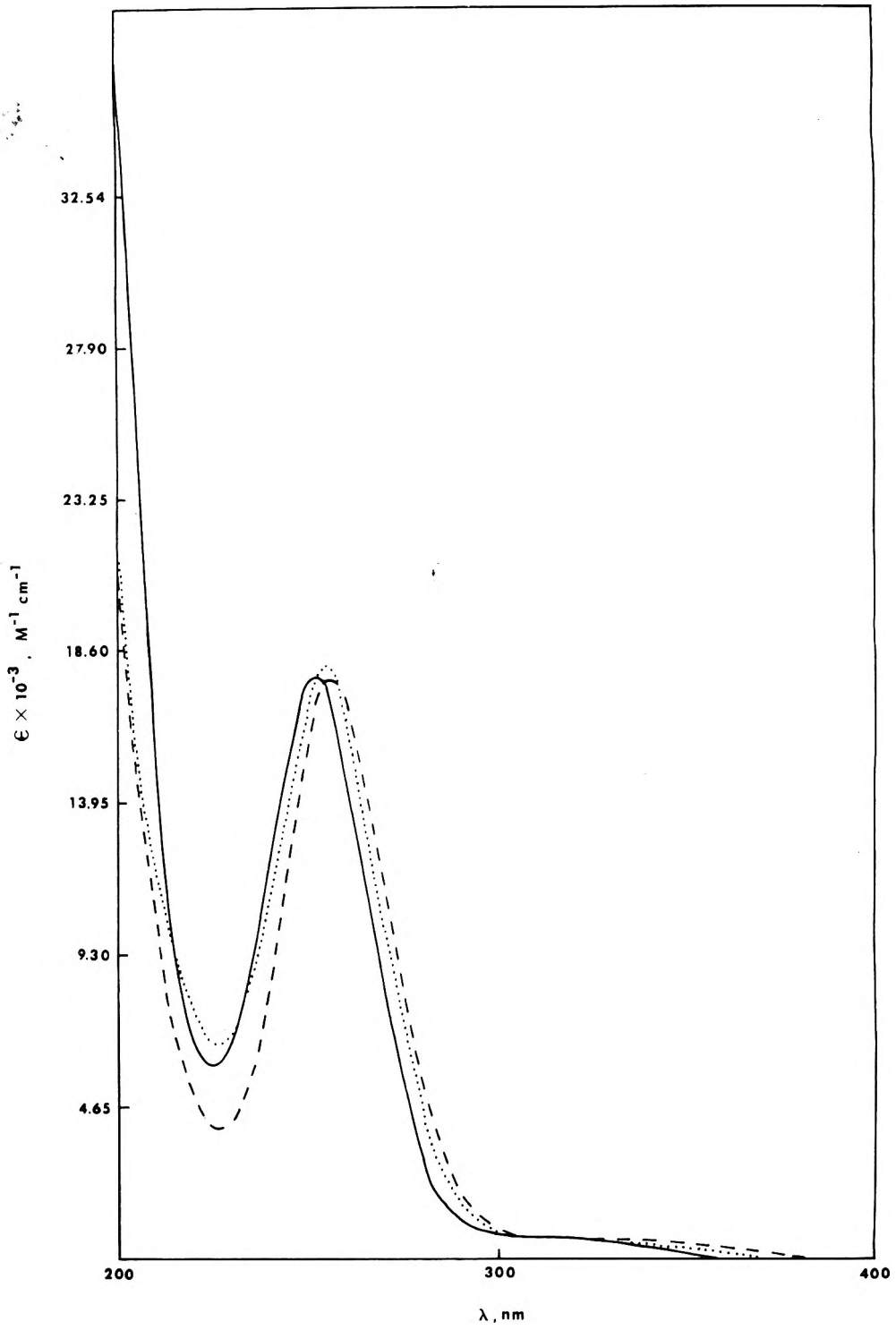

Figure 2. Absorption spectrum of $Co(NH_3)_5Br^{2+}$ in various media: (—) H_2O; (· · · · ·) 90% glycerol; (- - -) 85% H_3PO_4.

ies have been performed in solutions of very polar solvents, and that the ionic species must be considered to be strongly solvated. A change in charge density and in molecular dipole moment must change the energetics of interaction between the complex substrate and the solvent medium. For cationic complexes, CTTM excitation as in (2) should ultimately result in some electrostrictive relaxation of solvent molecules as a result of the change in charge separation. Two limiting cases may be considered in discussing various

$$M^{III}L_5(X^{-}) + h\nu \longrightarrow {}^{*}\{M^{II}L_5(\cdot X)\} \qquad (2)$$

systems: (1) a simple reorientation of solvent molecules to accommodate the change in dipole moment and charge density; and (2) oxidation of the solvent in the charge transfer process. The first limiting case describes behavior usually to be expected in aqueous solution (solvent oxidized with difficulty).[24] Some similarities in the role of the solvent in CTTM spectroscopy and photochemistry and in the spectroscopy and photochemistry of charge transfer complexes[25] might be anticipated, although the excited state dipole moment is generally smaller than the ground state dipole moment in the former transitions and larger in

TABLE I: Solvent Effects on the CTTM Spectra of Some Transition Metal Complexes[a]

Complex	$\tilde{\nu}_{max}$, kK	$\Delta\tilde{\nu}_{max}$, kK[b]	$^1/_2\nu$, kK[c]	$10^3\epsilon_{max}$[d]	Solvent conditions[e]
$Co(NH_3)_5Cl^{2+}$	44.05		3.0	20	Water
	43.48	0.57	2.9	19.5	90% glycerol
$Co(NH_3)_5Br^{2+}$	39.68		2.5	17.8	Water
	39.22	0.46	2.5	18.0	90% glycerol
	39.06	0.62	2.6	17.7	85% H_3PO_4
$Co(NH_3)_5N_3^{2+}$	33.45		3.0	8.8	Water
	32.90	0.55	2.5	9.0	90% glycerol
$Co(NH_3)_5NCS^{2+}$	32.79		4.0	1.09	Water
	32.52	0.27	3.3	1.13	60% glycerol
$\{Co(NH_3)_6^{3+}, I^-\}$	~ 33	~ 0.40[f]			50% glycerol
$\{Ru(NH_3)_6^{3+}, I^-\}$	25.00				Water
	24.39	0.60			50% glycerol

[a] All spectra at 25°; lowest energy CTTM maximum listed (unresolved maxima or shoulders are not listed). [b] Shift to the red with respect to ν_{max} in water. [c] Half-band width at half-height. [d] M^{-1} cm^{-1}. [e] Volume percentages. [f] Based on the red shift of the low-energy edge of the CTTM band.

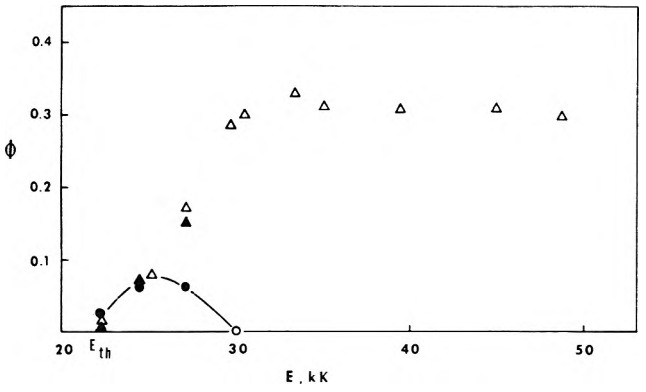

Figure 3. Variation of redox and labilization quantum yields with excitation energy for irradiations of $Co(NH_3)_5Br^{2+}$: △, $\phi_{Co^{2+}}$ (this work, see ref 17); ▲, $\phi_{Co^{2+}}$ (ref 3); O, quantum yield of $Co(NH_3)_5OH_2^{3+}$ (this work, see ref 17); ●, quantum yield of $Co(NH_3)_5OH_2^{3+}$ (ref 3).

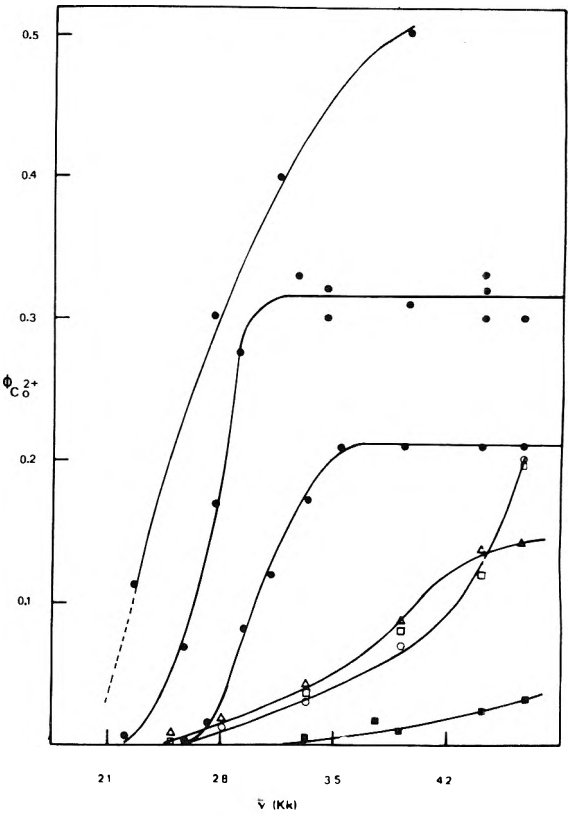

Figure 4. Excitation energy dependence of the quantum yields for photoreduction of several cobalt(III) complexes in acidic aqueous solution. From the top curves are for: $Co(NH_3)_5NO_2^{2+}$ (ref 4); $Co(NH_3)_5Br^{2+}$ (ref 3, 31, and this work); $Co(NH_3)_5Cl^{2+}$ (ref 3, 30–32, and this work); $Co(HEDTA)NO_2^-$ (□, 35a); $Co(HEDTA)Br^-$ (O, ref 35a); $Co(HEDTA)Cl^-$ (△, ref 35a); and $Co(EDTA)^-$ (■, ref 35b).

the latter. The second limiting case is analogous to the charge transfer to solvent (CTTS) spectroscopy[18,19,26] and photochemistry[18,19,27] of halide ions, but with the opposite sense of flow of charge; i.e., in this limit one would expect a net transfer of positive charge to the solvent nearest neighbors. These considerations suggest that models of CTTM spectra and photochemistry should incorporate many of the features which have been found useful in models of CTTS and charge-transfer (donor–acceptor) complexes. Further to our more immediate concerns these considerations have led us to carefully examine CTTM spectra of several coordination complexes in different solvent media.

1. $Ru(NH_3)_6^{3+}$. The dominant absorption feature of this complex is a transition at 274 nm which is very likely CTTM in nature (assignment based on eq 1 and comparison with $Co(NH_3)_6^{3+}$).[22] This band is increased in intensity and red shifted about 1 kK in a 50% glycerol–water medium[28] (Figure 1). This sensitivity to the solvent environment is common for CTTM transitions (see sections 2 and 3). It is important that the solvent sensitivity is not found to increase with increasing energy, no new absorption feature is observed, and it therefore seems most implausible that these spectroscopic features result from the onset of a glycerol → Ru(III) CTTM transitions. It is far more likely that the red shift and the intensity enhancement are manifestations of the role of the solvent environment in the photophysics of a characteristic CTTM transition.

Jørgensen has attributed similar spectral shifts in CTTM absorption maxima of hexahalo complexes to variations in M–X bond distances.[21d] While such variations in bond length may well account for the pressure dependence of CTTM absorption maxima, the limiting models mentioned in the preceeding section have more immediate photochemical implications and seem to provide more plausible accounts of the solvent perturbations of CTTM spectra we have observed; for example, in our studies the complex cations are no doubt preferentially solvated by water in the mixed solvent media so that the observed perturbations must be the result of changes in the competitive interac-

tions of water molecules with the cations and with the bulk solvent environment.

The $NH_3 \rightarrow Ru(III)$ charge transfer transition can be described formally as generating a metal center with a t_{2g}^6 electron configuration, the source of additional charge being a ligand centered p-type orbital;[29] i.e., the spin allowed transition generates a doublet excited state with T_{1u} symmetry properties. The weak symmetry forbiddeness of a $^2T_{2g} \rightarrow {}^2T_{1u}$ transition[30] probably contributes to the small molar absorptivity[29] ($\epsilon \simeq 500\ M^{-1}\ cm^{-1}$) of the observed transition. Since the molecule contains six identical ligands, the excited state wave function would be expected to contain a separate, but equal, contribution from each of the ammine ligands.[21] Therefore, the Franck–Condon CTTM excited state of $M(NH_3)_6^{3+}$ should be regarded as containing six fractionally oxidized ligands.[21d] Thus the CTTM transition for complexes of O_h microsymmetry does not involve a net change of molecular dipole moment and any solvent perturbation of this transition must involve something other than the interactions mentioned in the first limiting case of the preceding section.

The other limiting model mentioned above, transfer of positive charge to solvent, has not received much attention. An insightful approach to this limit is suggested by Fox's[27,31] modification of the Mulliken charge-transfer complex theory[32] for application to CTTS spectra. This approach suggests that the solvent contribution to eq 1 could take the form of eq 3, where I_{solv} is the ionization potential

$$\Delta(h\nu)_{solv} = \delta(I_{solv} - E_{complex}) + \frac{\sigma^2}{I_{solv} - E_{complex}}\left(\frac{1}{r_i^2}\right) \quad (3)$$

of the solvent, $E_{complex}$ is the electron affinity of the coordination complex, σ is an overlap term which depends on the overlap integral and polarization terms,[27,32] and δ is a constant, $\delta \leq 1$. We have written eq 3 with a smaller contribution from the first term than that in the corresponding CTTS theory since the principal component of the CTTM transition must be due to first coordination sphere ligands. We may then represent the solvent shift of the CTTM transition of any specific complex as in (4). This reduces to (5) for small values of the overlap parameter and values of

$$\Delta(h\nu)_{solv\text{-}a} - \Delta(h\nu)_{solv\text{-}b} = \Delta\Delta(h\nu) = \delta\Delta I_{solv} + \left[\frac{\sigma_a^2}{I_{solv\text{-}a} - E_{complex}} - \frac{\sigma_b^2}{I_{solv\text{-}b} - E_{complex}}\right]\left(\frac{1}{r_i^2}\right) \quad (4)$$

$$\Delta\Delta(h\nu) \simeq \delta\Delta I_{solv} \simeq \delta'\Delta E^\circ_{solv} \quad (5)$$

$|I_{solv} - E_{complex}| \gg 0$; the ionization potential of the solvent may be assumed proportional to the standard reduction potential of the solvent, E°_{solv}. Thus the magnitude of the solvent shift, compared to aqueous solutions, should increase in proportion to the ease of oxidizing the solvent, all other factors being equal. In mixed solvent media, one would expect the solvent shifts to reflect variations in the composition immediate solvent environment; more specifically, one would expect highly charged cationic species to be preferentially solvated by water and that molecules of solvents such as glycerol would become statistically significant in the solvation environment only at relatively large concentrations. We have only observed solvent shifts in solutions more concentrated than 1 M in the nonaqueous component. For example, glycerol is more easily oxidized than water (by approximately 1 V), and we observed a shift of the $NH_3 \rightarrow Ru$ CTTM transition to lower energies in 50% glycerol.

We have observed qualitatively similar solvent shifts of the CTTM absorption of $Co(NH_3)_6^{3+}$. For this complex the CTTM maximum occurs at relatively high energies (~50 kK) so that the spectroscopic resolution of effects could not be as clear as for the ruthenium analog. The CTTM transition for this complex should be described in terms similar to those used for $Ru(NH_3)_6^{3+}$, with the principal difference being the strongly allowed $^1A_{2g} \rightarrow {}^1T_{1u}$ component ($\epsilon \sim 2 \times 10^4\ M^{-1}\ cm^{-1}$) of the transition for the cobalt complex.

The nature of the Franck–Condon excited states is important in developing useful mechanistic models for CTTM photochemistry, since these are the initial points on the photoreaction coordinates. For an octahedral complex irradiated at the CTTM absorption maximum, this initial "point" corresponds to a species with a unit of positive charge distributed equally over the ligands, and with nuclear coordinates constrained to be the same as for the ground state species. As the system moves along the photoreaction coordinate the excited system will relax until thermally equilibrated, primary photoproducts are formed. These primary photoproducts will have the positive charge localized on a single molecular (or radical) species. For $Co(NH_3)_6^{3+}$, the $t_{2g}^6e_g$ excited state electronic configuration of the metal would require a Jahn-Teller distortion, probably axial, as the system relaxes along the photoreaction coordinate; such a distortion would tend to facilitate the localization of charge by lowering the molecular symmetry. No such distortion is expected of $Ru(NH_3)_6^{3+}$ and this may be a factor in the greater photoreactivity of the cobalt complex.[6,33]

The observation and analysis of solvent perturbations of CTTM transitions in $M(NH_3)_6^{3+}$ complexes suggests that primary photooxidation of solvent could be a possibility for high-energy excitations. Primary photooxidation of solvent has been proposed in photoredox studies of metallophenanthroline complexes in methanol.[34] Siegel and Armor very recently reported that the efficient 184.9-nm stimulated photoreduction of $Ru(NH_3)_6^{3+}$ did involve oxidation of solvent species.[33] The discussion above points out a mechanism for the delocalization of some positive charge over solvent species, and we would estimate a threshold energy of about 45 kK[35] for the appearance of such a process in the presence of $Ru(NH_3)_6^{3+}$. We believe this mechanism provides a much more plausible account of the high efficiency of the 184.9-nm photoredox process than the scavenging mechanism proposed by Siegel and Armor.

2. Dipolar CTTM Transitions. Ion Pair Charge Transfer Spectra. It is instructive to begin our consideration of the effect of solvent on the more dipolar transitions by considering those charge transfer transitions which have the largest change in dipole moment and the weakest metal–ligand covalent bond, charge transfer transitions in ion pair species. As illustrated in Figure 1 and reported previously,[36] the $\{Ru(NH_3)_6^{3+}, I^-\}$ ion pair exhibits a charge transfer absorption band in a spectral region where neither $Ru(NH_3)_6^{3+}$ nor I^- has detectable absorption. Since the I^- is constrained to remain outside the first coordination sphere, the CTTM transition for this system may be represented as in eq 6 where the Franck–Condon allowed transi-

$$\{Ru(NH_3)_6^{3+}, I^-\} + h\nu \longrightarrow {}^*\{Ru(NH_3)_6^{2+}, \cdot I\} \quad (6)$$

tion produces an excited state, $^*\{Ru(NH_3)_6^{2+}, \cdot I\}$, which resembles a radical pair species, but with the ground state

solvent environment and bond lengths. The CTTM band of $\{Ru(NH_3)_6^{3+},I^-\}$ is red shifted about 0.6 kK in 50% glycerol–water compared to aqueous solution. It is to be noted that our discussion of the $\{Ru(NH_3)_6^{3+},I^-\}$ ion pair is very similar to Rabinowitch's discussion of $Fe^{III}X^-$ species,[18] but in the ion pair system there is much less ambiguity regarding the nature of the M–X chemical bond in either the ground state or the excited state.

Although the CTTM absorption band is less well defined,[37] this transition in the $\{Co(NH_3)_6^{3+},I^-\}$ ion pair is similarly altered by changes in solvent composition.

3. Dipolar CTTM Transitions. $M^{III}L_5(X^-)$ Complexes. The $M^{III}L_5(X^-)$ complexes exhibit solvent shifts of their $X^- \rightarrow Co$ CTTM transitions comparable to those observed for ion pair species (Figure 2, Table I). In addition to the complexes in Table I we have found that the lowest energy CTTM maxima of $Ru(NH_3)_5Br^{2+}$ and $Co(HEDTA)NO_2^-$ vary differently with solvent composition. Our salts of these complexes had limited solubility in anhydrous solvents, but they were reasonably soluble in "wet" (5–10% water) solvents. Solutions of either complex in such mixed solvents had lower energy CTTM absorption maxima than the corresponding aqueous solutions; these red shifts were largest (1 kK) in methanol for $Ru(NH_3)_5Br^{2+}$ and (0.7 kK) in dimethyl sulfoxide for $Co(HEDTA)NO_2^-$. In order of decreasing energy of the lowest energy CTTM absorption maximum we found for $Ru(NH_3)_5Br^{2+}$, $H_2O \sim DMSO > AN > CH_3OH$; and for $Co(HEDTA)NO_2^-$, $H_2O \sim CH_3OH > AN > DMSO$ (AN = acetonitrile, DMSO = dimethyl sulfoxide). Since these solutions all contain water, the observed red shifts most likely represent variations in the complex ion–water dipole interactions as perturbed by the organic solvents; e.g., different orderings of the spectral shift induced by various solvents for $Ru(NH_3)_5Br^{2+}$ and $Co(HEDTA)NO_2^-$ no doubt occur because the CTTM transition involves a decrease of dipole moment in the former complex and an increase of dipole moment in the latter.

4. Inferences from CTTM Spectra. (a) The energies of CTTM transition have been found to be perturbed by the solvent environment. This implies that solvent significantly affects the excited state potential energy manifold and suggests that the solvent environment should be considered in any description of the photoredox reaction coordinate. (b) It is possible to identify systems which approach the limiting cases in which spectroscopic solvation effects are attributable to (i) different ground state and excited state dipolar interactions (ion pair systems), or (ii) delocalization of charge over the solvent environment ($M(NH_3)_6^{3+}$ complexes); however, most cases probably fall between these limits.

5. Photochemical Implications. If the CTTM excited state were very short lived, then the rate of dielectric relaxation of the solvent could become a significant feature of the reaction coordinate describing the relaxation of the excited system from the initial Franck-Condon excited state to the primary photoproducts. In order to come to terms with the problems posed, we need to arrive at some sort of estimate of the energy of solvent repolarization along the photoreaction coordinate, to establish the nature of the primary photoproducts, to arrive at a means of estimating the energy of these products, and to find a means of estimating the energy associated with any change of metal–ligand bond lengths. These quantities must then be compared to experimentally observed CTTM transition energies and photoredox excitation energies. Approaches to each of these problems will be considered below. However, the problems as posed assume a smooth relaxation along a single photoreaction coordinate. Gross kinetic features of such a relaxation process and of complications involving alternative relaxation pathways are considered in the following section.

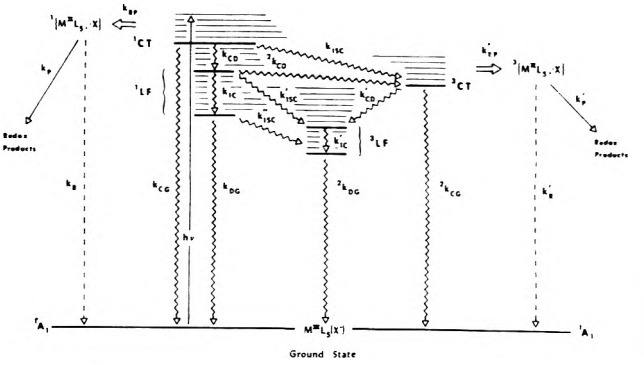

Figure 5. Kinetic scheme indicating excited states and intermediates which may in principle play a role in the photoredox chemistry of cobalt complexes.

B. Excited State Processes of Possible Mechanistic Importance. A somewhat simplified diagram representing processes which might occur following CTTM excitation is shown in Figure 5. The overall quantum yield of redox products, ϕ_P, is given in terms of these processes by

$$\phi_P = \Phi_{RP}\frac{k_P}{k_R + k_P} + \Phi_{RP}'\frac{k_P'}{k_R' + k_P'} \qquad (7)$$

where

$$\Phi_{RP} = \frac{k_{RP}}{k_{RP} + k_{CG} + k_{CD} + k_{isc}}$$

$$\Phi_{RP}' = \Phi_{isc}\frac{k_{RP}'}{{}^2k_{CG} + k_{CD}' + k_{RP}'}$$

$$\Phi_{isc} = \frac{k_{isc}}{k_{RP} + k_{CG} + k_{CD} + k_{isc}} + \frac{k_{CD}}{k_{RP} + k_{CG} + k_{CD} + k_{isc}}\frac{{}^2k_{DC}}{k_{ic} + k_{isc}' + {}^2k_{CD}}$$

It is instructive to consider several limiting cases.

1. The Photodissociative Limit. For $k_{RP} \gg (k_{CG} + k_{CD} + k_{isc} + \ldots)$, $\Phi_{RP} \rightarrow 1$ and $\Phi_P \rightarrow [k_P/(k_P + k_R)]$. It is in this limiting case that photophysical processes in the CTTM excited states play no role in determination of the yields of photoproducts.[38] In order to compare this limit to experimental observations, some additional considerations on the nature of radical pair species, $\{M^{II}L_5, \cdot X\}$ and the nature of the rate constants, k_P and k_R, are required; such considerations are presented in section C.

2. The Limit of Efficient Electronic Relaxation. For $k_{CD} \gg k_{RP}$, k_{isc}, and for $k_{ic} \gg {}^2k_{DC}$, $\phi_P \sim 0$, and the observed photochemical products will tend to be those characteristic of population of ligand field excited states. This limit may be appropriate to the excitation of the low-energy CTTM bands of ruthenium(III) complexes,[6] but seems less applicable to the photochemistry of cobalt(III) and rhodium(III) complexes.[2]

3. Limiting Triplet State Contributions. Charge transfer triplet states will make the predominant contribution to formation of products if the following conditions hold: (a)

$\Phi_{RP} \gg \Phi_{RP'}$ and/or (b) $[k_P/(k_R + k_P)] \ll [k_{P'}/(k_{R'} + k_{P'})]$. Condition a holds for cases that $k_{isc} > (k_{RP} + k_{CD} + k_{CG})$; but in addition some solvent relaxation would be expected to occur on the time scale for intersystem crossing so that one would also expect $k_{RP'} > k_{RP}$ to contribute to this condition. Since the time scale for geminate radical recombination is very short, the spin forbiddeness of $^3\{M^{III}L_5, \cdot X\} \rightarrow M^{III}L_5(X^-)$[39] suggests that $k_{R'} < k_R$ might be generally expected to be valid. Thus a, and more specifically $k_{isc} \gg (k_{RP} + k_{CD} + k_{CG} + \ldots)$, seems likely to be the most critical condition for contributions of the triplet charge transfer pathway to photoredox decomposition of $M^{III}L_5(X^-)$ complexes.[40]

C. Solvent Trapped Metallo-Fragment-Radical Species. Models and Experimental Comparisons. The primary products of decomposition CTTM excited states should be regarded as solvent trapped radical pair species.[2-5,18,19] Experimental and theoretical studies of radical pair species have been reviewed elsewhere.[18,19,41,42] In the present section we consider radical pair models specifically applicable to the photochemistry of transition metal complexes and compare inferences based on these models to observed photochemical behavior. With radical pair species presumed to be the primary photoproducts, then the net photochemical information depends on both (a) any photophysical processes which compete with radical pair formation from CTTM excited states, and (b) the chemical behavior of radical pair species. While we consider radical pair models as a necessary complement to models for excited state behavior, at least some of these models were originally proposed[3,18] excluding any role for CTTM excited states and should thus be regarded as models for limiting photodissociative behavior (see section B1).

1. The Adamson Radical Pair Model(s). Approximately 15 years ago Adamson[3] proposed that a simple radical pair model could account for all the features of the photoredox chemistry of cobalt complexes.[2a-d,3,43] The Adamson model is described in eq 8–12,[2a,b,3a,b] where $\{Co^{II}L_5, \cdot X\}$ and

$$Co^{III}L_5(X^-) + h\nu \longrightarrow \{Co^{II}L_5, \cdot X\} + \Delta \quad (8)$$

$$\{Co^{II}L_5, \cdot X\} \xrightarrow{\text{small } \Delta} Co^{III}L_5(X^-) \quad (9)$$

$$\{Co^{II}L_5, \cdot X\} \xrightarrow{\text{large } \Delta} \{Co^{II}L_5S, \cdot X\} \quad (10)$$

$$\{Co^{II}L_5S, \cdot X\} \xrightarrow{k_{11}, \phi_R} Co^{II}L_5S + \cdot X \quad (11)$$

$$\{Co^{II}L_5S, \cdot X\} \xrightarrow{k_{12}, \phi_L} Co^{III}L_5S + X^- \quad (12)$$

$\{Co^{II}L_5S, \cdot X\}$ are geminate and secondary (or solvent separated) radical pair species respectively and where Δ is the energy difference between the energy of the absorbed photon and the minimum energy[44] required for homolytic Co^{III}–X^- bond cleavage. This excess energy Δ is postulated to appear in the separating radical fragments as linear momentum and to contribute to the formation of the secondary radical pair species. In the earliest version of this model[3] (ARPM-1), it was further postulated that some of this excess energy still contributed to the linear momentum of the separating radical fragments in the secondary radical pair species so that the ratio k_{11}/k_{12} was expected to increase with Δ. A more recent restatement of this model[2d] (ARPM-2) treats the secondary radical pair as if the linear momentum has been dissipated in (10) so that the ratio of k_{11}/k_{12} should be a constant; this latter modification (ARPM-2) appears to be somewhat more consistent with current thinking about geminate and secondary radical pair species.[42]

Some definite inferences may be made on the basis of the Adamson model(s).

(a) *Only the secondary radical pairs lead to products.* Since the ratio of yields of secondary to geminate radical pairs is postulated to depend only on Δ, the total yield of photochemical products, $(\phi_L + \phi_R)$, is predicted to increase monotonically with Δ.

(b) From ARPM-1, *the yield of solvated product ($M^{III}L_5S$) should pass through a maximum with increasing* Δ.

(b′) From ARPM-2, *the ratio of the yields of photosolvation of photoredox should stand in a constant ratio; i.e.,* ϕ_L/ϕ_R = *constant.*

(c) *The photosolvation process involves only the ligand photooxidized.*

(d) *Increasing the solvent viscosity, for constant* Δ, *should favor (9) over (10) and (12) over (11).*

Predictions a–c may be compared with experimental data available for $Co^{III}(NH_3)_5(X^-)$ (X = Cl, Br, NCS, N_3, NO_2) complexes. For these complexes X^- aquation is observed only for relatively low-energy irradiations of $Co(NH_3)_5Cl^{2+}$,[2,3,17] $Co(NH_3)_5Br^{2+}$,[2,3,17] and $Co(NH_3)_5NCS^{2+}$,[2,3,17] and photoaquation of the X^- ligand has not been detected (i.e., ϕ_L is generally less than $\sim 10^{-3}$) for irradiations of "pure" CTTM absorption bands of these complexes (i.e., for irradiations with $\lambda < 350$ nm).[2,15,17] For $Co(NH_3)_5N_3^{2+}$, ammonia aquation, but no azide aquation, has been found to result from irradiations over the range 580 nm $\geq \lambda \geq$ 214 nm;[9] for irradiations of $Co(NH_3)_5NO_2^{2+}$ photoredox decomposition has been found to be accompanied by linkage isomerization of NO_2^- but not by aquation.[2a,4,5] Thus inference c and reaction 12 do not appear to have universal validity.

If X^- aquation, ammonia aquation, and linkage isomerization all are considered examples of ligand labilization reactions accompanying the formation of a cobalt(II) fragment in the radical pair products, then some modification of (12) could still lead to inferences a, b, or b′, and d. Figure 6 examines the inference that $(\phi_L + \phi_R)$ should increase monotonically (presumably to unity) with Δ: for irradiations of $Co(NH_3)_5Br^{2+}$ and $Co(NH_3)_5Cl^{2+}$ in aqueous solutions well-defined limiting quantum yields of much less than unity are observed for large Δ; for $Co(NH_3)_5NCS^{2+}$, the variation of $(\phi_L + \phi_R)$ is far more complex than predicted, while for $Co(NH_3)_5NO_2^{2+}$, $(\phi_L + \phi_R)$ may monotonically approach a limiting unitary value. The labilization yields from excitations of $Co(NH_3)_5Cl^{2-}$, $Co(NH_3)_5Br^{2+}$ (Figure 3), and $Co(NH_3)_5NCS^{2+}$ do reach a maximum value; *in each case this maximum is observed in the near ultraviolet region exhibiting significant spectral overlap of ligand field and CTTM absorption bands.*

Figure 7 analyzes the constancy of observed values of the ratio of ϕ_L/ϕ_R. Among these five complexes we find two kinds of limiting behavior of the ϕ_L/ϕ_R ratios. For one complex, $Co(NH_3)_5NO_2^{2+}$, prediction b′ (of ARPM-2) is observed; this observation was previously made and interpreted by Balzani and coworkers.[4] For $Co(NH_3)_5Br^{2+}$ and probably $Co(NH_3)_5Cl^{2+}$, the ϕ_L/ϕ_R ratio[45] decreases nearly monotonically with increasing excitation energy. Both types of behavior are found over limited ranges of excitation of $Co(NH_3)_5N_3^{2+}$ [46] and $Co(NH_3)_5NCS^{2+}$.[45] It seems unlikely that any single radical pair model can by itself accommodate all the variations in ϕ_L/ϕ_R ratios.

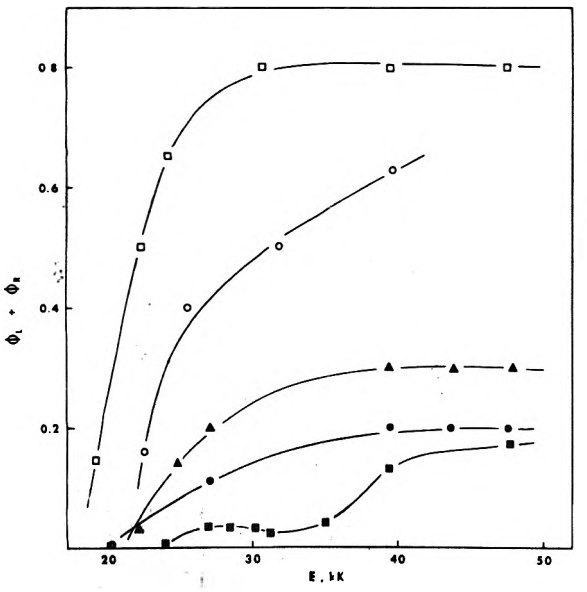

Figure 6. Dependence of the sum of quantum yields for labilization and redox ($\phi_L + \phi_R$) on excitation energy for several acidopentamminecobalt(III) complexes: □, $Co(NH_3)_5N_3^{2+}$ (ref 9); ○, $Co(NH_3)_5NO_2^{2+}$ (ref 4); ▲, $Co(NH_3)_5Br^{2+}$ (this work, ref 17; see also ref 3a, 3b, and 7a); ●, $Co(NH_3)_5Cl^{2+}$ (this work, ref 17; see also ref 3, 7a, and 15); ■, $Co(NH_3)_5NCS^{2+}$ (this work, ref 17; see also ref 3a, 3b, and 35). ϕ_L refers to NH_3 aquation for $Co(NH_3)_5N_3^{2+}$, linkage isomerization for $Co(NH_3)_5NO_2^{2+}$, Br^- aquation for $Co(NH_3)_5Br^{2+}$, Cl^- and NH_3 aquation for $Co(NH_3)_5Cl^{2+}$, and NCS^- aquation for $Co(NH_3)_5NCS^{2+}$.

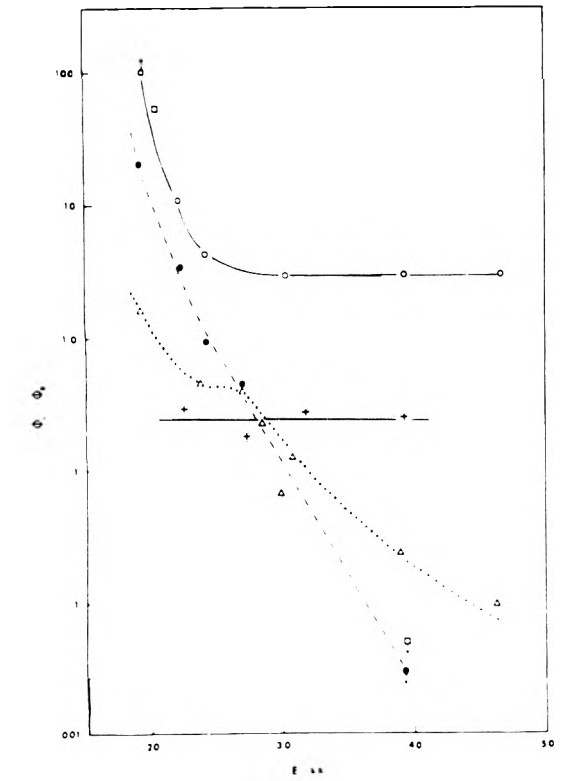

Figure 7. Variation with excitation energy of the ratio of labilization and redox yields, ϕ_L/ϕ_R, for several acidopentamminecobalt(III) complexes: ○, $Co(NH_3)_5N_3^{2+}$; ■, $Co(NH_3)_5Cl^{2+}$; ●, $Co(NH_3)_5Br^{2+}$; +, $Co(NH_3)_5NO_2^{2+}$. Arrows directed upward indicate that entry is for a lower limit; arrows directed downward indicate that entry is for an upper limit. See caption to Figure 6 for references and processes considered in ϕ_L.

Although one may legitimately question whether the observed labilization yields derive from only the charge transfer component of the excitations, prediction b of ARPM-1 is more successful (3 out of 5) than prediction b′ of ARPM-2 (1 out of 5).

The final inference, d, drawn from the Adamson model(s) has received little attention in the literature. In a study of $Co(NH_3)_5NO_2^{2+}$ in glycerol–water mixtures, Scandola and coworkers have found that the yield of linkage isomer increased and the redox yield decreased with increasing solvent viscosity,[5a] in agreement with the last part of inference d; i.e., increasing solvent viscosity apparently favored a radical recombination reaction over diffusive separation of metallo fragment and radical species. Similar studies of $Co(NH_3)_5X^{2+}$ (X = Cl, Br, N_3, NCS) complexes in this laboratory[6,35] have indicated that the variations of ϕ_R with solvent composition depend on X and on the excitation energy; for most of these complexes it has been possible to find excitation wavelengths for which ϕ_R increases with percentage glycerol in the solvent. Despite the complexity of the several "solvent effects" observed, each of the $Co(NH_3)_5X^{2+}$ complexes does seem to exhibit behavior consistent with d over some range of excitation energies.

From the above considerations there can be little doubt that the photoredox chemistry of $Co(NH_3)_5X^{2+}$ complexes is generally more complex than the Adamson model(s) would permit. Despite the apparent inadequacies of these radical pair models, and despite the exaggerated claims occasionally made for these models,[2b] these models do have a number of useful features. For example, with the elimination of (12) one would have an instructive and simple model for limiting photodissociative behavior; some complexes do seem to approach this kind of behavior under some conditions. Furthermore, this is useful as the simplest limiting model for radical pair behavior in systems with nearly limitless potential for radical pair complexity.

2. A Model Allowing for Secondary Radical Pair Recombination. Balzani and coworkers[4] suggested that the linkage isomerization observed to result from excitation of $Co(NH_3)_5NO_2^{2+}$ was the result of the recombination of solvent separated, $\{Co(NH_3)_5OH_2^{2+}, \cdot NO_2\}$, radical pairs. This suggests an alternative to the Adamson mechanism(s) in which reaction 12 is replaced by 13. This mechanism re-

$$\{Co^{II}L_5S, \cdot X\} \xrightarrow{k_{13}, \phi_L} Co^{III}L_5X + S \qquad (13)$$

quires appreciable lability of the solvent, but is plausible for low spin, Jahn-Teller distorted cobalt(II) fragments.[47] Provided that the secondary radical pair is thermally "cool," the ratio of product yields, ϕ_L/ϕ_R, should be constant, as observed for $Co(NH_3)_5NO_2$[4,5] and as observed over limited ranges of excitation of $Co(NH_3)_5N_3^{2+}$ [9b] and $Co(NH_3)_5NCS^{2+}$. Furthermore, this model would allow for secondary radical pair recombination reactions which regenerate the original substrate, and thus for limiting values of $\phi_R < 1$ for very large Δ. Despite the greater flexibility, this model is not adequate to describe all the details of all the photoredox chemistry of cobalt complexes; for example, this model cannot account for the complex wavelength dependence of quantum yields for $Co(NH_3)_5NCS^{2+}$, the sensitivity of photoredox behavior to the composition of the solvent medium,[6] or electronic relaxation processes which occur, even for $Co(NH_3)_5NO_2^{2+}$, prior to formation of radical pair species.[5a,48,49]

3. Other Possible Variations on Radical Pair Models.

There is of course no *a priori* reason to expect that very similar radical pair species should be formed in the photoredox decompositions of different cobalt complexes irradiated at different wavelengths or in different solvent media. However if qualitatively different kinds of radical pairs are formed in different systems, their formation must be dictated by the nature of their excited state precursors.

Since the CTTM transition is spin allowed, and since the final cobalt(II) products are most commonly high-spin d^7 species, it seems surprising to us that questions of spin multiplicity have played so small a role in previous discussions of radical pair models. There are four possible spin combinations of the cobalt(II) and radical fragments trapped in solvent cages: the cobalt(II) fragment may be high spin or low spin, and the spin moments of the cobalt and radical fragments may be either aligned or opposed. This gives rise to possible geminate and secondary radical pairs of singlet (low spin cobalt), triplet (low spin or high spin cobalt), and quintet (high spin cobalt) spin multiplicities. The radical pairs with singlet spin multiplicity are correlated with the original electronic transition, while radical pairs with high spin cobalt(II) are correlated with the final products. While the rate constant for spin relaxation of cobalt is expected to be large,[39] it is not clear that it is significantly larger than the rate constant for dissociation of radical pair species ($>10^9$ sec^{-1}). One likely influence of the difference in recombination kinetics for the spin allowed and spin forbidden processes (i.e., that $k_R > k_R'$) was a feature of our discussion in section B3. Such a spin restriction on radical recombination reactions could make diffusive separation of *geminate* radical pairs competitive with geminate recombination, and should be an especially important consideration when the cobalt(II) fragment is high spin rather than low spin.

Finally we wish to observe that the radical pairs containing a low-spin cobalt(II) fragment will necessarily be formed at an energy greater than the energy of radical pairs containing high-spin cobalt(II); the difference in energy should be similar to the energy difference ΔH_{spin} between the thermally equilibrated lowest energy doublet excited state of cobalt(II) and the high-spin ground state.

Although none of the radical pair models discussed above can be regarded as well established, the weight of evidence as well as considerations of logic strongly support the view that the primary products of excited state decomposition are radical pair species. Clearly additional probing of the nature and behavior of radical pair species is necessary.

D. Some Observations on the Photoredox Behavior of Cobalt Complexes. Figure 4 demonstrates that for $Co(NH_3)_5X^{2+}$ and $Co(HEDTA)X^-$ (X = Cl, Br, NO_2) complexes the variation of the quantum yield of cobalt(II) with excitation energy depends very strongly on the ligand which is photooxidized: for the pentammine complexes the X^- ligand is photooxidized (with the possibility of both Cl^- and NH_3 oxidation for $Co(NH_3)_5Cl^{2+}$ [7b]). It is important to observe that for each complex represented in Figure 4, the energy region over which $\phi_{Co^{2+}}$ increases rapidly to significant values corresponds to the lowest energy region in which CTTM absorbances (assignments per ref 21 and 22) begin to make significant contributions.

Whereas Figure 4 demonstrates that the ligand photooxidized is a major factor in determining the quantum yield profile, this figure also demonstrates that other factors contribute significantly since the $Co(HEDTA)X^-$ and $Co(EDTA)^-$ complexes differ in their behavior despite the fact that the EDTA ligand is oxidized in each case.

It is convenient to define certain experimental parameters in terms of data such as in Figures 3 or 4. Since the rise of the photoredox quantum yield is generally very rapid with increasing energy, the resulting curves of $\phi_{Co^{2+}}$ vs. excitation energy may be approximately extrapolated to $\phi_{Co^{2+}} \rightarrow 0$; alternatively, the energy corresponding to $\phi_{Co^{2+}} \rightarrow 0$ may be approximated by the largest excitation energy for which $\phi_{Co^{2+}}$ is 1% of the maximum observed quantum yield. The excitation energy corresponding to this onset of significant photoredox behavior will be designated the "photoredox threshold energy," E_{th}. For high-energy excitations many of the photoredox yields approach well-defined limiting values, $\phi^l_{Co^{2+}}$ (e.g., see Figure 3). It is then seen that the photoredox behaviors of $Co(NH_3)_5X^{2+}$ complexes generally differ in that values of E_{th} tend to increase as the reduction potentials of the ($\cdot X + e^- \rightleftharpoons X^-$) couples[50-52] become more positive, while values of $\phi^l_{Co^{2+}}$ vary in a complex manner with X; i.e., values of $\phi^l_{Co^{2+}}$ decrease in the following order with changes in X, $NO_2 > Br > Cl \geq N_3 \sim NCS$. With the exception of $Co(NH_3)_5NCS^{2+}$, the approach to $\phi^l_{Co^{2+}}$ is smooth for the pentammine complexes investigated, with the curvature varying somewhat from complex to complex. The $Co(HEDTA)X^-$ complexes are seen to be similar in their (relatively poorly defined) E_{th} values, but to differ appreciably in values of $\phi^l_{Co^{2+}}$.

E. Considerations of Redox Energetics. Several authors have made comparisons of thermodynamic quantities and CTTM spectroscopy.[18,19,53,54] The present approach differs from those previous comparisons in that (a) we allow for some effects of covalent bonding, (b) we estimate the energies of the Franck–Condon contributions, (c) the specific substrates selected for discussion here are more appropriate to our main purpose, and (d) we use the comparisons developed to gain insight into the nature of the CTTM excited states.

1. Ion Pair Systems. The thermodynamic parameters are more easily defined for ion pair species, so these serve as a useful point of departure in this discussion. The $\{Ru(NH_3)_6^{3+},I^-\}$ ion pair exhibits a CTTM absorption maximum at the blue end of the spectrum where the absorptivities of the free cation and anion are negligible (see Figure 1). The standard reduction potentials (SRP) of the $Ru(NH_3)_6^{3+}|Ru(NH_3)_6^{2+}$ and $\cdot I|I^-$ couples are 0.1[55] and 1.42 V,[50-52] respectively; the respective entropies for these couples are estimated to be $\Delta S^\circ = +39$[56,57] and 9.1 eu.[24,50] From these parameters we estimate that $\Delta H^\circ = 15.6$ kK/mol for reaction 14. While the formation constants for the

$$Ru(NH_3)_6^{3+} + I^- \rightleftharpoons Ru(NH_3)_6^{2+} + \cdot I \qquad (14)$$

respective ion pair and radical pair species are of the order of 10 and 0.1 M^{-1},[37,58] the enthalpies of formation probably are 0 ± 1 kK.[37b] We therefore estimate that $\Delta H^\circ_{IP} = 16$ kK/mol for reaction 15; this is in reasonable agreement

$$\{Ru(NH_3)_6^{3+},I^-\} \longrightarrow \{Ru(NH_3)_6^{2+},\cdot I\} \qquad (15)$$

with the value of $E_{th}' = 18$ kK/mol estimated for the onset of CTTM absorbance in the $\{Ru(NH_3)_6^{3-},I^-\}$ ion pair.

The thermodynamic parameters for the $\{Co(NH_3)_6^{3+},X^-\}$ and $\{Ru(NH_3)_6^{3+},X^-\}$ ion pairs are very similar[24,55,56] yet E_{th}' is larger by about 8 kK/mol for the cobalt than for the ruthenium ion pairs (Table II). There seem two likely sources of the observed dependence of E_{th}' on the metal: (1) the CTTM transitions are spin allowed

TABLE II: Energy Quantities Pertinent to CTTM Transitions in Several Coordination Complexes

Complex	E_{th}[a,b]	E_{th}'[a,c]	$\lambda/4$[a,d]	E_{max}(obsd)[a,e]	E_{max}(calcd)[a,f]	$\Delta H°_{IP}$[g]	$\Delta H^{\ddagger}$[h]	$\Delta H°_{C}$[i]
$\{Co(NH_3)_6^{3+},I^-\}$		26	14	~33	33[j](40)	15		15
$\{Co(NH_3)_6^{3+},Br^-\}$		29	15		40[j](44)	21		21
$Co(NH_3)_5I^{2+}$		17	8	26	26(25)	11	~7[k]	~18
$Co(NH_3)_5Br^{2+}$	22	22	10	32.0	34(32)	16	8	24
$Co(NH_3)_5Cl^{2+}$	26	28	11	36.5	40(39)	21	7.7	29
$Co(NH_3)_5NCS^{2+}$	24	~22				14	11.5	26
$Co(NH_3)_5N_3^{2+}$	22[l]	23[l]				15	11.5	27
$\{Ru(NH_3)_6^{3+},I^-\}$		17	5.8	25	22(23)	16		16
$\{Ru(NH_3)_6^{3+},Br^-\}$		22	6.7	~32	28(29)	21		21
$Ru(NH_3)_5I^{2+}$		14[m]	5.8	18.6	(19.8)	13	8.5	21
$Ru(NH_3)_5Br^{2+}$		19[m]	6.4	25.1	(25.4)	19	7.7	27
$Ru(NH_3)_5Cl^{2+}$		24[m]	7	31.0	(31)	23	9.6	34

[a] All energies in kK/mol. [b] Extrapolated low-energy limit for the onset of appreciable photoredox behavior; this study except as indicated. See also ref 3. [c] Extrapolated low-energy limit for the onset of appreciable CTTM absorption; this study except as indicated. [d] $\lambda = \lambda_o + \lambda_i$; reorganizational parameters estimated per discussion in section E2c; see ref 66. [e] Observed energy of lowest energy CTTM absorption maximum. [f] $E_{max}(calcd) = \Delta H°_C + \lambda/4$. Values in parentheses are for $E_{max}(calcd) = E_{th}' + \lambda/4$. [g] Estimated per procedure in text. [h] Data from ref 58a. [i] For ion pairs $\Delta H°_C = \Delta H°_{IP}$; for $M^{III}L_5X$ complexes $\Delta H°_C = \Delta H°_{IP} + \Delta H^{\ddagger}$. [j] E_{max} (calcd) = $\Delta H°_{spin}$; $\Delta H°_{spin}$ = 4 kK/mol. [k] Estimate based on values for $Co(NH_3)_5Cl^{2+}$ and $Co(NH_3)_5Br^{2+}$. [l] Reference 9b. [m] Estimated from data in H. Hartmann and C. Bushbeck, *Z. Phys. Chem. (Frankfurt am Main)*, 11, 120 (1957).

leaving the cobalt with a $t_{2g}^6e_g$ electronic configuration, while the ruthenium excited state would be t_{2g}^6—the ground state of $Co(NH_3)_6^{2+}$ has a $t_{2g}^5e_g^2$ configuration, with a minimum energy of $\Delta H°_{spin}$ between the low- and high-spin states; (2) a $t_{2g}^6e_g$ electronic configuration should result in a large Jahn-Teller distortion[47] thus shifting the excited state potential energy surface of the cobalt system along the photoreaction coordinate with respect to the similar surface for the ruthenium system. This would result in a larger Franck–Condon contribution, $\Delta H°_{FC}$, to the CTTM transition for cobalt than for ruthenium. Thus we may attribute the difference between E_{th}'(Co) and E_{th}'(Ru) to the sum of Franck–Condon and spin contributions; i.e., $E_{th}'(Co) - E_{th}'(Ru) = \Delta H°_{spin} + \Delta H°_{FC} \simeq 8$ kK.

2. Pentammine Systems. In order to apply this approach to $M^{III}L_5X$ complexes, some additional considerations are necessary. Consistent with the discussion in sections B and C we assume that the primary photoredox products are radical pairs; and at the threshold for photoredox behavior these are geminate $\{M^{III}L_5,X^-\}$ radical pairs. The corresponding ion pairs, $\{M^{III}L_5,X^-\}$, are unknown as ground state species, but are the presumed transition states[59] for thermal hydrolysis reactions of the complexes discussed here. We may thus approximate the thermodynamic analog of reaction 16 in the stepwise manner of reaction 17, where

$$M^{III}L_5(X^-) \xrightarrow{\Delta H°_C} \{M^{III}L_5, \cdot X\} \quad (16)$$

$$M^{III}L_5(X^-) \xrightarrow{\Delta H^{\ddagger}} \{M^{III}L_5, X^-\} \xrightarrow{\Delta H°_{IP}} \{M^{II}L_5, \cdot X\} \quad (17)$$

$\Delta H^{\ddagger}$ is the enthalpy of activation for the corresponding thermal aquation reactions.

A final quantity which must be taken into account is the possibility of some metallo-radical bonding in the excited state. If the metallo-radical bond energy is E_B, then the observed absorption threshold should be related to the other energy quantities by (18). In eq 18, $\Delta H°_{IP}$ contains a contribution, $\Delta H°_M$, from the $M(NH_3)_5^{3+}|M(NH_3)_5^{2+}$ couple and a contribution, $\Delta H°_X$, from the $\cdot X|X^-$ couple. The sum $(\Delta H°_X + \Delta H^{\ddagger})$ is available from literature data, while the remaining terms on the right hand side of (18), $(\Delta H°_M + \Delta H°_{FC} - E_B)$, are not. This suggests two levels of approach to the use of eq 18: (a) to establish empirical correlations of the type (19), where α is an experimentally determined

$$E_{th}' = \Delta H°_X + \Delta H^{\ddagger} + \alpha \quad (19)$$

quantity which is a function of metal, radical, solvent, etc.; and (b) to find a means of estimating the unknown energy quantities. We believe both approaches will prove useful and they are developed below to the limit of information presently available

$$E_{th}' = \Delta H°_{IP} + \Delta H^{\ddagger} + \Delta H°_{FC} - E_B \quad (18)$$

(*a*) *Empirical Correlations Involving Threshold Energies.* For $Co(NH_3)_5X^{2+}$ (X = Cl, Br, N_3, NCS, and NO_2[60]) we estimate from parameters in Table II or tabulated elsewhere[22,50-52] that $\alpha(av) = -2.8 \pm 0.9$ kK/mol. Among the halopentammines, $\alpha = -1.9$, -2.7, and -0.6 kK/mol for Cl, Br, and I, respectively.

For $Ru(NH_3)_5X^{2+}$ (X = Cl, Br, and I) we estimate that $\alpha = -6.8$, -5.4, and -5.1 kK/mol, respectively, or that $\alpha(av) = -5.8 \pm 0.7$ kK/mol.

Although the insensitivity of α to the acido ligand may be a fortuitious result of cancellation of radical dependent terms, with appropriate caution (19) can be used as a basis for assignment of CTTM transitions, and, since E_{th}' and E_{th} are generally about equal ($Co(NH_3)_5NO_2^{2+}$ is one exception to this[49]), the empirical correlation can be used as a basis for predicting excitation energies for which photoredox should become significant in cobalt(III) complexes.

(*b*) *Estimates of* $\Delta H°_M$. An approach to estimating the contributions to $\Delta H°_{IP}$ from the $M^{III}(NH_3)_5|M^{II}(NH_3)_5$ couples is available if we assume the entropy contributions differ little from those of the hexammine couples and if we use correlations of standard potentials of cobalt(III)|cobalt(II) couples with variations in crystal field stabilization energy.[56,61]

For cobalt complexes of the type *trans*-$Co(N_4)X_2$ (N_4 = cyclic nitrogen donor ligand), the cobalt(II) ground state is low spin[62,63] and the potentials of the $Co^{III}(N_4)X_2|Co^{II}(N_4)X_2$ couples have been found to increase with decreasing crystal field strengths of the axial ligands.[61] On the basis of this correlation we would expect the $Co(NH_3)_5^{3+}|Co(NH_3)_5^{2+}$ couple to have a SRP value about

1 V more positive than the SRP of the $Co(NH_3)_6^{3+}|Co(NH_3)_6^{2+}$ couple,[64] for low-spin cobalt(II) products; assuming $\Delta H^\circ_{spin} \sim 4$ kK/mol[65] for $Co(NH_3)_6^{2+}$, the SRP of $Co(NH_3)_5^{3+}|Co(NH_3)_5^{2+}$ (low spin) would be about 0.5 V more positive than the SRP of $Co(NH_3)_6^{3+}|Co(NH_3)_6^{2+}$ (high spin).

The potentials for the corresponding ruthenium couples vary less[55,57,66] than those of cobalt with changes in ligation; this may be presumed to be mostly a consequence of the greater ligand field stabilization energy of six coordinate ruthenium(II) compared to six coordinate cobalt(II).[59a] On the basis of the estimated differences in ligand field stabilization energy of five and six coordinate ruthenium, we would estimate a difference of about 0.2 V for the $Ru(NH_3)_5^{3+}|Ru(NH_3)_5^{2+}$ and $Ru(NH_3)_6^{3+}|Ru(NH_3)_6^{2+}$ couples.

Estimates of ΔH°_{IP} based on the above approximations are included in Table II. For the $Co^{III}(NH_3)_5X$ complexes $E_{th} \simeq E_{th}'$ and $\Delta H^\circ_C - E_{th}' = (2 \pm 1)$ kK/mol.

Two points merit additional consideration: (1) ΔH°_C for the $Ru^{III}(NH_3)_5X$ complexes is significantly larger (by 8 ± 2 kK) than E_{th}'; and (2) while $E_{th}' \leq \Delta H^\circ_C$ for the $Co^{III}(NH_3)_5X$ complexes, $E_{th}' > \Delta H^\circ_{IP}$ for the $\{Co(NH_3)_6^{3+},X^-\}$ ion pairs.

A significant portion of ΔH°_C for the $Ru^{III}(NH_3)_5X$ complexes must come from the generation of pentacoordinate ruthenium(II) in the hypothetical $\{Ru(NH_3)_5^{2+}, \cdot X\}$ radical pair product. There are likely to be two contributions to the endoergicity of the excited state reaction, $^*\{Ru^{II}(NH_3)_5(\cdot X)\} \rightarrow \{Ru(NH_3)_5^{2+}, \cdot X\}$: (1) residual Ru(II)–(·X) bonding in the excited state; and (2) the related difference in LFSE of hexa- and pentacoordinate ruthenium(II) species. In support of these arguments for an endoergic dissociation of the thermally equilibrated CTTM excited states of $Ru^{III}(NH_3)_5X$ complexes, we note that irradiations in the lowest energy CTTM bands in these complexes have not been found to produce significant photoredox decompositions.[6,33]

We would expect similar contributions of ΔH°_{spin} and somewhat smaller Franck–Condon contributions to the CTTM transitions of $Co^{III}(NH_3)_5X$ complexes compared to CTTM transitions in $\{Co(NH_3)_6^{3+},X^-\}$ ion pairs; we estimated $\Delta H^\circ_{FC} \simeq 8$ kK for the latter complexes. It is therefore somewhat surprising that E_{th}' should be found approximately equal to ΔH°_C for $Co^{III}(NH_3)_5X$ complexes. This may imply some residual Co(II)–(·X) bonding in the CTTM excited state, analogous to the ruthenium case, *i.e.*, $\Delta H^\circ_C - E_{th}' = \Delta H^\circ_{FC} - E_B$ where the bond energy and Franck–Condon contributions have opposite signs and our estimates have already taken some account of ΔH°_{spin}.

(c) *Franck–Condon Contributions.* There is an approach to estimating Franck–Condon contributions which appears to be useful for CTTM transitions. In reconstructing the initial Franck–Condon excited state from the radical pair products, we may consider the total energy associated with the changes in internuclear distances to fall into two categories: (i) energy changes associated with compression to ground state bond lengths of the metal–ligand distances in the reduced metallo fragment, and (ii) energy changes associated with the reorientation of solvent molecules until the solvent environment of the ground state is regenerated. Such a reconstruction of the ground state nuclear geometries is very similar to processes postulated to be generally involved in bimolecular, condensed phase electron transfer reactions.[67] Thus we may represent the reorganizational energy as $\lambda/4$ where $\lambda = \lambda_i + \lambda_0$, λ_i is the first coordination sphere contribution due to the M^{II}–L compression, and λ_0 is given by (20).[68] Using such an approach we could estimate the energy difference between relaxed radical pair species and any other species with different nuclear coordinates. For the present discussion we consider only the difference in energy between the radical pair products and the Franck–Condon excited state with nuclear coordinates identical with those of the ground state.

$$\lambda_0 = e^2\left(\frac{1}{2a_1} + \frac{1}{2a_2} - \frac{1}{r}\right)\left(\frac{1}{D_{op}} - \frac{1}{D_{el}}\right) \quad (20)$$

In the estimates of $\lambda/4$ which are reported in Table II, we have neglected contributions of λ_i for ruthenium complexes since there are only small differences in the bond lengths of ruthenium(II) and ruthenium(III) complexes.[69] For the cobalt complexes we have treated the low-spin cobalt(II) fragments of the radical pair products as axially distorted with a final distortion of 0.5 Å per bond;[47] in the acidopentammines we have assumed the distortion to be localized along the C_4 axis. This distortion is also the basis for values of a_1 used in the actual calculations. We have based the M–X distances in $\{M(NH_3)_6^{3+},I^-\}$ systems on the Ru(II)–I^- distance in $[Ru(NH_3)_6]I_2$.[69]

For the $\{M(NH_3)_6^{3+},X^-\}$ ion pairs the sum, $(\Delta H^\circ_{IP} + (\lambda/4 + \Delta H^\circ_{spin})$, seems to provide a reasonable estimate of the energy of the CTTM absorption maximum; in these estimates ΔH°_{spin} is taken to be 4 kK/mol for the cobalt complexes (see Table II).

For the halopentammineruthenium(III) complexes, the sum, $(\Delta H^\circ_C + \lambda/4)$, is considerably greater than the energy of the absorption maximum consistent with Ru(II)–(·X) covalent bond energy in the range of 8–15 kK/mol for the thermally equilibrated CTTM excited state. If the values of E_{th}' are taken as estimates of the energy of the vibrationally relaxed CTTM excited state, then the energy of the absorption maximum, E_{max}, is very closely estimated by the sum, $(E_{th}' + \lambda_0/4)$, for each ruthenium complex in Table II (note that values of λ_0 are determined predominately by the ·X radius, a_2, and are relatively insensitive to a reasonable range of choices of r).

The above observations argue strongly that the Franck–Condon excited state generated by absorption of radiation with $h\nu = E_{max}$ has an arrangement of nuclei identical with that of the ground state. Furthermore absorption at E_{th}' must be Franck–Condon "forbidden," hence the low intensity; such excitations would presumably generate highly distorted Franck–Condon excited states. *However the distortions of these CTTM excited states of $Ru(NH_3)_5X^{2+}$ complexes must occur principally in their solvation environments.* In fact eq 2 provides a means of analyzing some of the solvent shifts discussed in section A; however, for ionic species in mixed solvent media specific solvation effects are probably important, and bulk solution values of D_{op} and D_{el} are most likely inappropriate.

While the above approach to the analysis of CTTM spectra seems to indicate an appreciable contribution of Franck–Condon terms of E_{th}' for $\{Co(NH_3)_6^{3+},X^-\}$ ion pair complexes (probably arising from the very large inner sphere Co–N distortions; $\lambda_i/4 \sim 9$ kK/mol), there appear to be no significant Franck–Condon contributions to E_{th}' for the halopentamminecobalt(III) complexes. The excellent agreement of E_{max}(calcd) and E_{max}(obsd) tends to confirm the various approximations we have employed, and suggests that for these complexes E_B may not be greater

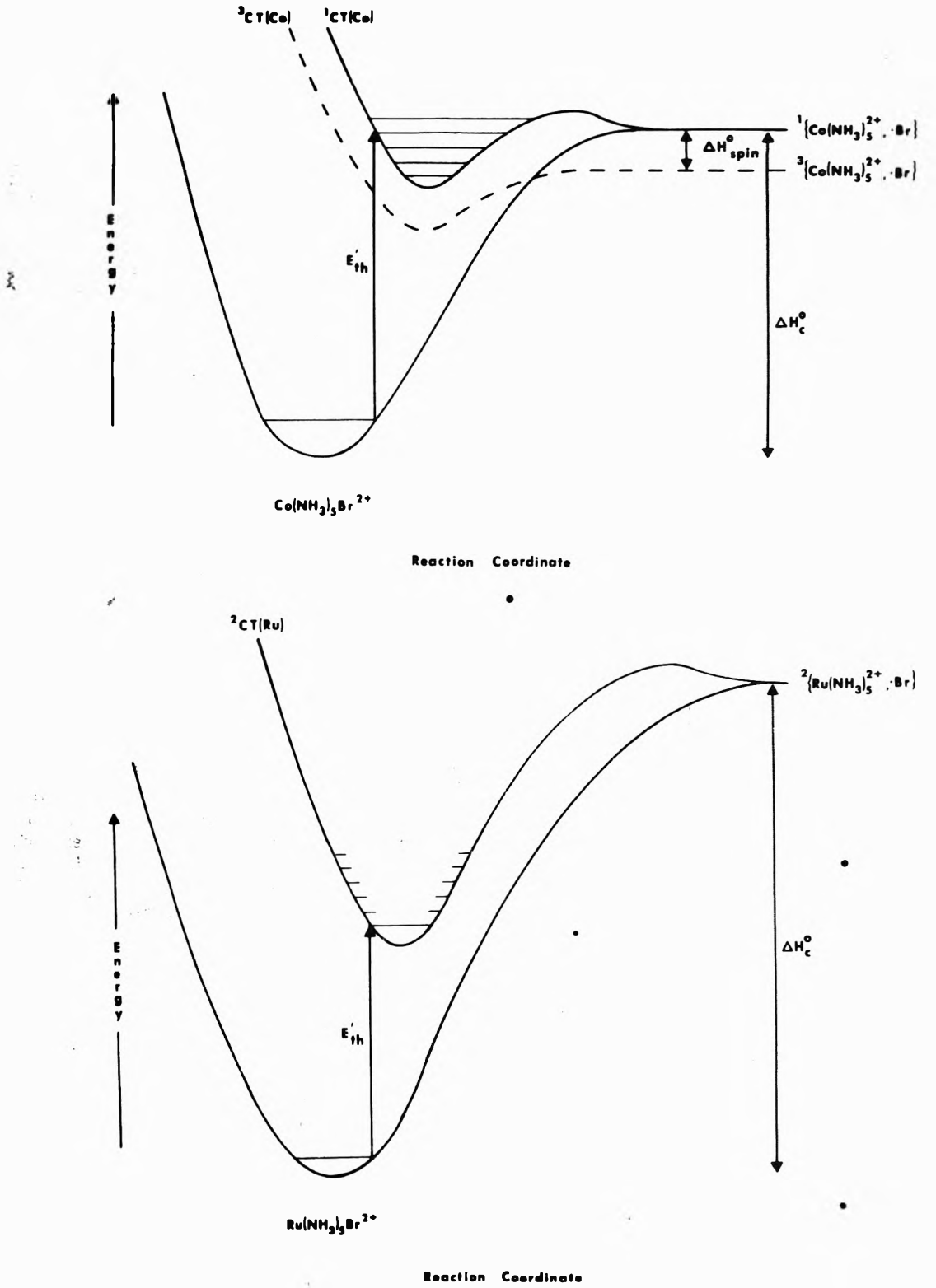

Figure 8. Hypothetical potential energy surfaces describing photoredox decompositions of bromopentamminecobalt(III) and -ruthenium(III) complexes.

than 2 or 3 kK/mol. If for these complexes $E_R \sim 0$, then the observation of $\phi^l_{Co^{2+}} < 1$ would be best accounted for if vibrational relaxation and/or electronic relaxation within the Franck–Condon excited state occurred more rapidly than dielectric relaxation of the solvent environment. At the present time this seems a plausible inference, and this inference leads us to two additional predictions: (i) at least the spectroscopic CTTM excited states in the halopentamminecobalt(III) complexes probably have lifetimes shorter than or approximately equal to the lifetime for dielectric relaxation of the immediate solvent environment (i.e., probably less than 10^{-11} sec); and (ii) photoredox behavior in these complexes could be a very sensitive function of the rate of dielectric relaxation of the solvation sheath. The

latter inference may well account for the dramatic variations of $\phi_{Co^{2+}}$ found for irradiations of $Co(NH_3)_5Br^{2+}$ in different solvent media.[6a] Since some dielectric relaxation would likely occur on the time scale for intersystem crossing, and since covalent bonding in a triplet CTTM state would not be expected to be greater than that found in the singlet states, we surmise that all CTTM excited states of these cobalt(III) complexes must be very short lived. Neither present information nor the above considerations provide a sound basis for ascribing the observed photoreactions to either a singlet channel or a triplet channel. However in either case we would predict Φ_{RP} (and Φ_{RP}') to be a function of the dielectric relaxation time of the solvent shell.

Finally we note that the argument employed above requires that there be an appreciable reorganizational barrier to radical recombination. The significance of such kinetic barriers in determining values of k_R and product distributions will be explored elsewhere.[35,49]

F. Summary. In this manuscript we have developed a systematic analysis of the energetics of the photoredox behavior of transition metal complexes. The energy, E_{max}, of a CTTM absorption maximum has been shown to be the sum of the enthalpy change associated with electron transfer within an ion pair complex, ΔH°_{IP}, the enthalpy of ion pair formation, $\Delta H^\ddagger$; the enthalpy of activation for aquation of acidopentammine complexes, a Franck–Condon contribution, $\lambda/4$, and a contribution arising from metal-radical covalent bonding in the excited state, E_B; thus $E_{max} = \Delta H^\circ_{IP} + \Delta H^\ddagger + (\lambda/4) - E_B$. In this analysis the Franck–Condon contribution is attributed to M–X bond compression (λ_i) and solvent reorientation (λ_0), where λ is Marcus' reorganizational parameter and $\lambda = \lambda_i + \lambda_0$. The threshold energy for CTTM absorption, $E_{th}' = E_{max} - \lambda/4$.

For several $Co(NH_3)_5X^{2+}$ complexes (i.e., for X = Cl, Br, NCS, N_3) we find that E_{th}' is approximately equal to the threshold energy for photoredox behavior, E_{th}, and that $E_{th}' \simeq E_{th} \simeq \Delta H^\circ_{IP} + \Delta H^\ddagger$. The net barrier to excited state dissociation in such systems is inferred to be small, but it is also inferred that the excitation energy dependence of redox quantum yields does require some electronic and/or vibrational relaxation of the Franck–Condon excited states; these processes are inferred to occur at rates more rapid than or in competition with the rates of dielectric relaxation of the solvent. As a consequence, this approach implies that CTTM excited states are very short lived in these systems and that photoredox yields should be a sensitive function of the dielectric relaxation time of the immediate solvent environment.

The approach employed thus requires that the solvent participate actively in the processes occurring along the photoreaction coordinates describing relaxation of the Franck–Condon excited state to the primary radical pair products. In addition to an intimate role in the dynamics of excited state and radical pair processes, the solvent affects the energetics of the CTTM transitions, through $\lambda/4$ terms and the contributions of solvation energies to ΔH°_{IP} and $\Delta H^\ddagger$ in systems whose CTTM transitions result in large changes in dipole moment. It also seems likely that some charge delocalization over the solvent contributes to CTTM energetics, especially for complexes with O_h microsymmetry.

A qualitative representation of the above mechanistic picture for $Ru(NH_3)_5Br^{2+}$ and $Co(NH_3)_5Br^{2+}$ is shown in Figure 8. This figure qualitatively represents a more strongly bond CTTM excited state for ruthenium, CTTM(Ru), than for cobalt, CTTM(Co); a large Jahn-Teller distortion of CTTM(Co); a barrier to solvent reorganization (affecting radical recombination as well as excited state dissociation); and low lying triplet CTTM state of the cobalt complex, ^3CT, which correlates with the high-spin cobalt(II) products through a radical pair species of triplet spin multiplicity. While we are not in a position at the present time to present a rigorous quantitative theory of photoredox reactions, we believe that the above considerations will be very useful in organizing significant mechanistic studies and in developing empirical photochemical models. The above considerations do allow for great sensitivity of photoredox processes to the composition of the solvent medium; studies of medium effects in photoredox reactions will be reported elsewhere.[6]

Acknowledgments. The authors are grateful to Professor V. Balzani for a careful reading of the manuscript and for his many critical comments and useful discussions on many of the key issues. The authors are also indebted to Professor F. Scandola for a thorough and critical review of the manuscript. Finally, some discussions with Professor E. C. Lim have been stimulating and insightful and Dr. P. Natarajan provided several helpful comments and suggestions.

Supplementary Material Available. Tabulated quantum yield data (Table III) will appear following these pages in the microfilm edition of this volume of the journal. Photocopies of the supplementary material from this paper only or microfiche (105 × 148 mm, 24× reduction, negatives) containing all of the supplementary material for papers in this issue may be obtained from the Journals Department, American Chemical Society, 1155 16th Street, N.W., Washington, D.C. 20036. Remit check or money order for $3.00 for photocopy or $2.00 for microfiche, referring to code number JPC-75-630.

References and Notes

(1) (a) Partial support of this research by the National Science Foundation (Grant No. GP 38888X) is gratefully acknowledged. (b) Additional support of this research by means of a fellowship for G. J. Ferraudi from the Faculty of Science, University of Chile, is also gratefully acknowledged.
(2) For pertinent reviews see: (a) V. Balzani and V. Carassiti, "Photochemistry of Coordination Compounds," Academic Press, New York, N.Y., 1970; (b) P. D. Fleischauer, A. W. Adamson, and G. Sartori, *Progr. Inorg. Chem.*, **17**, 1 (1972); (c) D. W. Watts, *MTP (Med. Tech. Publ. Co.) Int. Rev. Sci., Inorg. Chem., Ser. One*, **9**, 52 (1972); (d) A. W. Adamson, W. L. Waltz, E. Zinato, D. W. Watts, P. D. Fleischauer, and R. D. Lindholm, *Chem. Rev.*, **68**, 541 (1968); (e) D. R. Eaton, *Spectrosc. Inorg. Chem.*, [1], **9**, 29 (1970).
(3) (a) A. W. Adamson and A. H. Sporer, *J. Amer. Chem. Soc.*, **80**, 3865 (1958); (b) A. W. Adamson, *Discuss. Faraday Soc.*, **29**, 163 (1960); (c) R. A. Pribush, C. K. Poon, C. M. Bruce, and A. W. Adamson, *J. Amer. Chem. Soc.*, **96**, 3027 (1974).
(4) V. Balzani, R. Ballardini, N. Sabbatini, and L. Moggi, *Inorg. Chem.*, 7, 1398 (1968).
(5) (a) F. Scandola, C. Bartocci, and M. A. Scandola, *J. Amer. Chem. Soc.*, **95**, 7898 (1973); (b) F. Scandola, C. Bartocci, and M. A. Scandola, *J. Phys. Chem.*, **78**, 572 (1974).
(6) (a) J. F. Endicott, G. J. Ferraudi, and J. R. Barber, *J. Amer. Chem. Soc.*, **97**, 219 (1975); (b) J. F. Endicott and G. J. Ferraudi, *ibid.*, **96**, 3681 (1974).
(7) (a) J. F. Endicott and M. Z. Hoffman, *J. Amer. Chem. Soc.*, **87**, 3348 (1965); (b) G. Caspari, R. G. Hughes, J. F. Endicott, and M. Z. Hoffman, *ibid.*, **92**, 6801 (1970).
(8) W. L. Wells and J. F. Endicott, *J. Phys. Chem.*, **75**, 3075 (1971).
(9) (a) J. F. Endicott, M. Z. Hoffman, and L. S. Beres, *J. Phys. Chem.*, **74**, 1021 (1970); (b) G. J. Ferraudi and J. F. Endicott, *J. Amer. Chem. Soc.*, submitted for publication; (c) G. Ferraudi and J. F. Endicott, *J. Chem. Soc., Chem. Commun.*, 674 (1973).
(10) (a) P. Natarajan and J. F. Endicott, *J. Amer. Chem. Soc.*, **95**, 2470 (1973); (b) *J. Phys. Chem.*, **77**, 2049 (1973).
(11) R. E. Kitson, *Anal. Chem.*, **22**, 664 (1959).

(12) (a) E. Wegner and A. W. Adamson, *J. Amer. Chem. Soc.*, **88,** 394 (1966); (b) E. Zinato, R. D. Lindholm, and A. W. Adamson, *ibid.*, **91,** 1076 (1969).
(13) G. A. Parker and G. C. Hatchard, *Proc. Roy. Soc., Ser. A,* **234,** 518 (1956).
(14) (a) J. G. Calvert and J. N. Pitts, Jr., "Photochemistry," Wiley, New York, N.Y., 1966; (b) J. N. Pitts, Jr., *J. Amer. Chem. Soc.*, **77,** 5499 (1955).
(15) L. Moggi, N. Sabbatini, and V. Balzani, *Gazz. Chim. Ital.*, **97,** 980 (1967).
(16) W. Bollester, C. Bushman, and P. Tidwell, *Anal Chem.*, **33,** 592 (1961).
(17) Quantum yield data obtained for the present study are collected in Table III. See paragraph at end of paper regarding supplementary material.
(18) E. Rabinowitch, *Rev. Mod. Phys.*, **14,** 112 (1942).
(19) N. Uri, *Chem. Rev.*, **50,** 375 (1952).
(20) See also ref 2a, pp 174–178.
(21) (a) C. K. Jorgensen, *Progr. Inorg. Chem.*, **4,** 73 (1962); (b) "Orbitals in Atoms and Molecules," Academic Press, New York, N.Y., 1962; (c) "Absorption Spectra and Chemical Bonding in Complexes," Oxford University Press, Oxford, 1962; (d) "Oxidation Numbers and Oxidation States," Springer, New York, N.Y., 1969.
(22) A parameterized application of (1) to the CTTM absorption bands of $M^{III}L_5X$ complexes is presented in J. F. Endicott, "Concepts of Inorganic Photochemistry," A. W. Adamson and P. D. Fleischauer, Ed., Wiley-Interscience, in press, Chapter 3.
(23) In eq 1 χ_L and χ_M are optical electronegativities of metal and ligand, respectively, in ML_6 complexes; $10Dq$ is the crystal field splitting in the octahedral complex, and the higher terms account for differences in electron pairing energies (δS) and Racah parameters. See also H. H. Schmidtke, "Physical Methods in Advanced Inorganic Chemistry," H. A. O. Hill and P. Day, Ed., Interscience, New York, N.Y., 1968, Chapter 4.
(24) W. M. Latimer, "Oxidation Potentials," 2nd ed, Prentice Hall, Englewood Cliffs, N.J., 1952.
(25) For a recent review see M. Ottolenghi, *Accounts Chem. Res.*, **6,** 153 (1973).
(26) For a review see M. J. Blandamer and M. F. Fox, *Chem. Rev.*, **70,** 59 (1970).
(27) For a review see M. F. Fox, *Quart. Rev. Chem. Soc.*, **24,** 565 (1970).
(28) This may be compared to a 5-kK blue shift of the CTTS band of I^- in neat glycerol compared to water.[29]
(29) For some useful commentation symmetry species and on the effects of orbital overlap on charge transfer transitions see (a) A. B. P. Lever, *J. Chem. Educ.*, **9,** 612 (1974); (b) W. Byers, B. FaChun Chow, A. B. P. Lever, and R. V. Parish, *J. Amer. Chem. Soc.*, **91,** 1329 (1969).
(30) F. A. Cotton, "Chemical Applications of Group Theory," Wiley, 1972.
(31) M. F. Fox and T. F. Hunter, *Nature (London)*, **223,** 177 (1968).
(32) R. S. Mulliken and W. B. Person, "Molecular Complexes," Interscience, New York, N.Y., 1968.
(33) J. Siegel and J. N. Armor, *J. Amer. Chem. Soc.*, **96,** 4102 (1974).
(34) (a) S. Sundarajan and E. L. Wehry, *J. Phys. Chem.*, **76,** 1528 (1972); (b) E. L. Wehry and R. A. Ward, *Inorg. Chem.*, **10,** 2660 (1971).
(35) G. J. Ferraudi and J. F. Endicott, manuscript in preparation.
(36) H. Elsgernd and J. K. Beattie, *Inorg. Chem.*, **7,** 2468 (1968).
(37) (a) M. G. Evans and G. H. Nancollas, *Trans. Faraday Soc.*, **49,** 363 (1949); (b) M. T. Beck, *Coord. Chem. Rev.*, **3,** 91 (1968).
(38) See section C1 below and ref 2 and 3.
(39) Note however that spin relaxation rates appear to be rapid in transition metal complexes; see (a) J. T. Yardley and J. K. Beattie, *J. Amer. Chem. Soc.*, **94,** 8925 (1972); (b) J. K. Beattie, N. Sutin, D. H. Turner, and G. W. Flynn, *ibid.*, **95,** 2052 (1973).
(40) This is a limiting argument, analyzing conditions for population of photoactive triplet states in systems where the spin labels are at least useful approximations. Some of the limitations on assignment of spin labels in coordination complexes have been recently discussed by G. A. Crosby, K. W. Hipps, and W. H. Elfring, Jr., *J. Amer. Chem. Soc.*, **96,** 629 (1974).
(41) R. M. Noyes, *Progr. React. Kinet.*, **1,** 128 (1961).
(42) J. P. Lorand, *Progr. Inorg. Chem.*, **17,** 207 (1972).
(43) To simplify our discussion we have adopted the relatively recent modification (A. Vogler and A. W. Adamson, *J. Phys. Chem.*, **74,** 67 (1970)) that this model is applicable only to the charge transfer photochemistry of cobalt complexes.
(44) It is convenient to associate this "minimum energy" with E_{th} as defined below.
(45) The only photoaquation data available for ultraviolet excitation of these complexes pertains to Br^- and Cl^- aquation respectively; for excitations at $\lambda \leq 300$ nm, ammonia aquation has not been detected and an upper limit of $\phi_{NH_3} \leq \phi_{Co^{2+}}$ may be estimated.
(46) For this complex ammonia aquation predominates and azide aquation is not of major importance.
(47) Axially distorted (Co–OH_2 bond lengths of 2.3–2.5 Å) low spin *trans*-$Co(N_4)(OH_2)_2^{2+}$ complexes with macrocyclic nitrogen donor N_4 ligands may be taken as models of Jahn-Teller distortions in low spin cobalt(II) species: M. D. Glick, J. M. Kuszaj, and J. F. Endicott, *J. Amer. Chem. Soc.*, **95,** 5097 (1973); M. D. Glick, W. G. Schmonsees, and J. F. Endicott, *ibid.*, **96,** 5661 (1974).
(48) V. Balzani, private communication to J.F.E. (1974). The regeneration of substrate $Co(NH_3)_5NO_2^{2+}$ is not kinetically competitive with processes leading to observed products.
(49) J. F. Endicott, *Inorg. Chem.*, in press.
(50) W. H. Woodruff and D. W. Margerum, *Inorg. Chem.*, **12,** 962 (1973).
(51) S. D. Malone and J. F. Endicott, *J. Phys. Chem.*, **76,** 2223 (1972).
(52) A. T. Thornton and A. S. Laurence, *J. Chem. Soc.*, 1632 (1973).
(53) G. Stein, J. Jortner, and A. Treinin, *J. Chem. Phys.*, **30,** 1110 (1959).
(54) M. G. Evans, N. S. Hush, and N. Uri, *Quart. Rev., Chem. Soc.*, **6,** 186 (1952).
(55) T. J. Meyer and H. Taube, *Inorg. Chem.*, **7,** 2369 (1968).
(56) P. A. Rock, *Inorg. Chem.*, **7,** 837 (1968); actually this reference discusses only the $Co(NH_3)_3^{3+}|Co(NH_3)_6^{2+}$ couple and we have assumed similar enthalpic and entropic contributions for the ruthenium couple. Lavallee *et al.*[43] have reported $\Delta S^\circ = -4.1$ for the ruthenium couple; however, this value appears to have been determined for an ionic strength of 0.5, not extrapolated to zero ionic strength. Use of the more negative value of ΔS° would reduce all our estimated values of ΔH°_{IP} for ruthenium couples by about 4 kK. The relatively good agreement between ΔH°_{IP} and E_{th}' for the ion pair complexes, $\{Ru(NH_3)_6^{3+},X^-\}$, suggests that the larger value of ΔS° is reasonably correct.
(57) D. K. Lavalle, C. Lavalle, J. C. Sullivan, and E. Deutsch, *Inorg. Chem.*, **12,** 570 (1973).
(58) R. G. Wilkins, *Accounts Chem. Res.*, 3, 408 (1970).
(59) For reviews see (a) F. Basolo and R. G. Pearson, "Mechanisms of Inorganic Reactions," 2nd ed, Wiley, New York, N.Y., 1967; (b) V. S. Sastri and C. H. Langford, *MTP (Med. Tech. Publ. Co.) Int. Rev. Sci., Inorg. Chem., Ser. One,* **9,** 203 (1970).
(60) For this complex we have had to substitute a value of $E_{th} = 19$ kK, the photoredox threshold, for the absorbance threshold energy (see ref 48).
(61) D. P. Rillema, J. F. Endicott, and E. Papaconstantinou, *Inorg. Chem.*, **10,** 1739 (1971); see especially Figure 3.
(62) (a) D. P. Rillema, J. F. Endicott, and N. A. P. Kane-Maquire, *J. Chem. Soc., Chem. Commun.*, 495 (1972); (b) unpublished observations.
(63) L. Warner, Ph.D. Dissertation, The Ohio State University, 1968.
(64) In this estimate we have taken the average axial ligand field strength of the pentacoordinate complexes as the appropriate quantity to use in Figure 3 of ref 61.
(65) Estimated from parameters in ref 56.
(66) H. S. Lim, D. J. Barelay, and F. C. Anson, *Inorg. Chem.*, **11,** 1460 (1972).
(67) (a) R. A. Marcus, *J. Phys. Chem.*, **72,** 891 (1968); (b) **56,** 854 (1963); (c) *Annu. Rev. Phys. Chem.*, **15,** 155 (1964).
(68) We take the parameters in (20) to be: a_1, the radius of the reduced metallo fragment; a_2, the radius of the ·X radical (covalent radius); r, the distance of separation of the fragments in the particular Franck–Condon state being considered; D_{op} is the square of the index of refraction of the medium; D_s is the dielectric constant of the medium; e is the charge on the electron. For the Franck–Condon state with nuclear coordinates identical with those of the ground state we take $r = a_1' + a_2$ (a_1' the covalent radius of the one electron oxidized metal) when the ground state is $M(NH_3)_5X$; for ion pairs we take a_1 to be the radius of the $M(NH_3)_6^{2+}$ complex, a_2 the covalent radius of ·X and, r to be the sum of the radius of $M(NH_3)_6^{3+}$ and the ionic radius of X^-. In our estimates of λ_0 for ion pair complexes we did not take account of reorganization of ionic atmospheres, which in the 0.1 *M* solutions should contribute a few kK.
(69) H. C. Stynes and J. A. Ibers, *Inorg. Chem.*, **10,** 2304 (1971).
(70) J. E. Huheey, "Inorganic Chemistry," Harper and Row, New York, N.Y., 1972, pp 73 and 184.

Photochemistry of the Nitro Group in Aromatic Heterocyclic Molecules

A. Cu and A. C. Testa*

Department of Chemistry, St. John's University, Jamaica, New York 11439
(Received May 13, 1974; Revised Manuscript Received December 13, 1974)

The 313-nm photolysis of 5-nitroquinoline in 50% isopropyl alcohol and water with varying concentrations of hydrochloric acid results in photoreduction with formation of 5-amino-6,8-dichloroquinoline. The photoreduction to an amine is similar to that observed for nitrobenzene and 1-nitronaphthalene and appears to proceed via the anion of the nitro compound to the hydroxylamine. The quantum yield for photoreduction increases with increasing HCl concentration and reaches an upper limit of $5.44 \pm 0.16 \times 10^{-2}$ when (HCl) ≥ 1 *M*. Comparison of the behavior in HCl and H_2SO_4 and previously reported results for nitrobenzene, 1-nitronaphthalene, and 4-nitropyridine indicate that the primary process involves an electron transfer from the chloride ion to the triplet state of the nitro compound.

Introduction

The photochemistry and excited state behavior of aromatic nitro compounds has been a subject of continuing interest in our laboratory. Following our initial studies on nitrobenzene[1-3] and nitronaphthalenes,[4] we recently reported that the 4-nitropyridinium ion undergoes photoreduction via the $^3n,\pi^*$ state to form 4-hydroxylaminopyridine as the only primary photoproduct.[5] In that study a limiting quantum yield of 0.65 ± 0.05 was measured for the acid concentration range 0.5–2.0 *M* HCl. The primary photochemical event was shown to involve electron transfer from the chloride ion and evidence for the anions of 4-nitropyridine and nitrobenzene were obtained from flash photolysis studies.[6] As an extension of our photochemical studies of 1-nitronaphthalene into heterocyclic systems we have undertaken a photochemical study of 5-nitroquinoline in aqueous alcohol solutions containing HCl. In addition to identifying the reactive excited state and the photoproduct, the importance of electron transfer as a primary process was worthy of investigation. Triplet yields of nitro compounds are known for nitrobenzene (0.67)[3] and 1- and 2-nitronaphthalene (0.63 and 0.83, respectively)[3] and are probably comparable in 4-nitropyridine and 5-nitroquinoline. Although the triplet yield of pyridine may be small,[7,8] the large photochemical quantum yields for 4-nitropyridine observed in alcohol–aqueous HCl solutions indicate that at least in some cases the triplet yields of substituted pyridines can be substantial, i.e., >0.5.

Results and Discussion

The 313-nm irradiation of degassed 0.5×10^{-4} *M* 5-nitroquinoline in aqueous alcohol solutions containing HCl results in the decrease of its absorption band at 315 nm with an increasing absorption in the region 240–265 nm. Upon prolonged photolysis a three peaked structure typical of aminoquinoline hydrochlorides appears at 248, 255, and 265 nm. It is thus evident that photoreduction to 5-aminoquinoline is occurring. The absorption increases at 240 and 265 nm during the early stages of the photoreduction suggesting that the corresponding hydroxylaminoquinoline is the primary photoproduct. The photoproduct was identified from its spectra (uv, ir, nmr) and by comparison with a sample of 5-aminoquinoline to be 5-amino-6,8-dichloroquinoline. The overall process occurring is

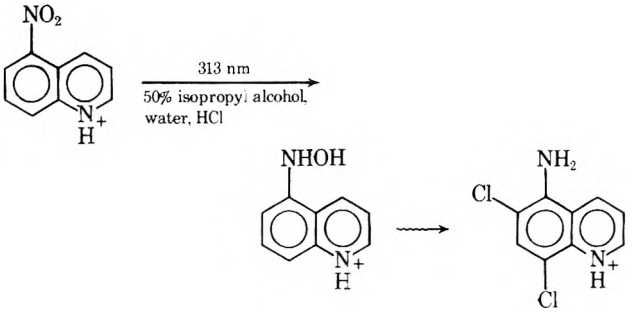

By comparison of our results with those for 1-nitronaphthalene it seems reasonable to assign the reactive state as $^3\pi,\pi^*$.

The quantum yield for the photoreduction is observed to increase with increasing HCl concentration and a summary of degassed data is presented in Figure 1. The increasing quantum yield observed in the lower acidity range is due to increasing protonation of the ring nitrogen, while in the higher acidity range the limiting quantum yield indicates complete protonation. The limiting quantum yield of $5.44 \pm 0.16 \times 10^{-2}$ is observed for (HCl) ≥ 1 *M*, at which concentration the ring nitrogen is totally protonated. In order to establish whether or not the small quantum yield observed is due to a small triplet yield, the phosphorescence yield was measured at 77°K in EPA. The phosphorescence yield of 5-nitroquinoline relative to the value of 0.051 for naphthalene in EPA[9] was determined to be 0.27; consequently, it is clear that not all the available triplets are reacting. Photochemical depletion of 5-nitroquinoline was determined by polarographic analysis in acetic acid–sodium acetate buffers. The photoreduction yields for air-saturated solutions are approximately 25% lower, however, the acid dependence is similar to that shown in Figure 1. The importance of chloride in the primary process is reflected in the observation that the photochemical disappearance is significantly lower in H_2SO_4. In 6 *M* HCl, when the ring proton is totally protonated, $\Phi = 5.9 \times 10^{-2}$, which decreases to a value of $0.23 \pm 0.02 \times 10^{-2}$ in pure isopropyl alcohol. A similar effect is observed in the photochemistry of 4-nitropyridine where the photoreduction quantum yield in pure isopropyl alcohol is only $1.3 \pm 0.03 \times 10^{-2}$, and significantly smaller than the quantum yields measured in the presence of HCl. Since the major impetus of this study was to investigate the importance of the chloride ion as an elec-

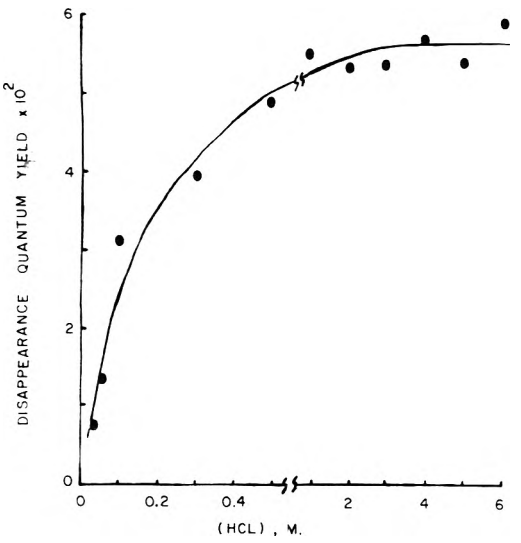

Figure 1. Photoreduction quantum yields for 1×10^{-2} *M* 5-nitroquinoline in degassed 50% isopropyl alcohol–water *vs.* HCl concentration (λ_{exc} 313 nm; $I_a \sim 2.5 \times 10^{15}$ quanta/sec).

tron donor to the triplet state of the aromatic nitro compound no analysis of photoproducts was performed for isopropyl alcohol solutions. The photoreduction of aromatic nitro compounds with alcohols is generally a very inefficient process.[1,3,4] In 50% isopropyl alcohol–water, 6 *N* in H_2SO_4, the disappearance quantum yield of 5-nitroquinoline is only $0.99 \pm 0.02 \times 10^{-2}$ due to the absence of the chloride ion. In the absence of chloride ions and protons hydrogen abstraction from the alcohol is the only contributing photochemical process. By comparison of our results for 5-nitroquinoline with those for 4-nitropyridine, nitrobenzene, and 1-nitronaphthalene it seems very likely that electron transfer to the $^3\pi,\pi^*$ state, producing the anion, is the primary process, which is then followed by a rapid protonation. A representation for the photoreduction of 5-nitroquinoline, $ArNO_2$, is given in Scheme I.

Scheme I

$$ArNO_2 \xrightarrow{h\nu} ArNO_2^{*1} \xrightarrow{k_{isc}} ArNO_2^{*3} \quad (1)$$

$$ArNO_2^{*3} \longrightarrow ArNO_2 \quad (2)$$

$$ArNO_2^{*3} + Cl^- \rightleftharpoons ArNO_2^{\cdot -} + Cl\cdot \quad (3)$$

$$ArNO_2^{\cdot -} + H^+ \longrightarrow ArNO_2H^{\cdot} \quad (4)$$

$$ArNO_2H^{\cdot} + (CH_3)_2CHOH \longrightarrow ArNHOH \longrightarrow ArNH_2 \quad (5)$$

(chlorinated aromatic amines)

The results demonstrate the involvement of chloride ion as an electron donor, since a sixfold decrease in photochemical disappearance is observed when 6 *N* HCl is replaced with 6 *N* H_2SO_4. Wubbels et al.[10] have shown a similar effect in nitrobenzene. A summary of the photoreduction quantum yields for 5-nitroquinoline obtained in this study with those for previously studied aromatic nitro compounds in 50% isopropyl alcohol–water with varying concentration of HCl is presented in Table I for nitrobenzene (NB), 4-nitropyridine (4-NP), 1-nitronaphthalene (1-NN), and 5-nitroquinoline (5-NQ) in 2, 3, and 6 *M* HCl.

Photolysis of 10^{-2} and 10^{-4} *M* 5-nitroquinoline did not exhibit any measurable differences. Previous results with

TABLE I: Photoreduction Quantum Yields (Degassed Solutions) for Aromatic Nitro Compounds in 50% Isopropyl Alcohol–Water with Varying HCl Concentration

(HCl), *M*	NB[a,c]	4-NP[b,d]	1-NN[a,e]	5-NQ[b,f]
2	1.8×10^{-2}	0.59	3.4×10^{-3}	5.3×10^{-2}
3	2.6×10^{-2}	0.16	5.7×10^{-3}	5.3×10^{-2}
6	0.14	0.06	12.8×10^{-3}	5.9×10^{-2}

[a] 366-nm excitation. [b] 313-nm excitation. [c] Reference 2. [d] Reference 5. [e] Reference 4. [f] This study.

nitrobenzene and 4-nitropyridine indicate that there is no concentration or intensity dependence on the photoreduction quantum yield of aromatic nitro compounds.[1,5] Photolysis with 313 and 366 nm produces the same electronic state and thus the same photoreduction quantum yield. The primary photoproduct does not effectively absorb either of these wavelengths so that the quantum yield measurements are not affected by secondary events. No dark reactions were observed when the degassed cells, after photolysis, were left in the dark for 2 days.

The data tabulated in Table I indicate that the photoreduction quantum yield of the nitro group in heterocyclics is generally higher than in the carbocyclic aromatic, and that the quantum yields for 1-nitronaphthalene and 5-nitroquinoline are an order of magnitude smaller than in the case of nitrobenzene and 4-nitropyridine, respectively. A similar behavior has been observed in the photoreduction quantum yields for phenyl ketones relative to naphthyl ketones.[11] Porter and Suppan[12] have concluded that triplet π,π^* states are ~10% as reactive as triplet n,π^* states in aromatic ketones. Similarly, in the case of aromatic nitro compounds the $^3\pi,\pi^*$ states (1-nitronaphthalene and 5-nitroquinoline) generally live longer than $^3n,\pi^*$ (nitrobenzene and 4-nitropyridine), both in solution and in frozen glasses,[3] and exhibit lower reactivity as seen in the quantum yield results summarized in Table I. In the π,π^* triplets of 1-nitronaphthalene and 5-nitroquinoline the excitation is localized primarily in the aromatic nucleus. In such cases the NO_2 group is probably electron rich rather than electron poor as is the case in n,π^* states. Consequently, radical-like reactivity at oxygen may be considerably diminished. Thus, one possible interpretation for the above data is that anion formation for 1-nitronaphthalene and 5-nitroquinoline is less facile than for phenyl or pyridine type anions, i.e., electron transfer to a $^3n,\pi^*$ state is favored over transfer to a $^3\pi,\pi^*$ state. A referee has suggested the possibility that the energy of the triplet state may be significant in the electron transfer from Cl^- and the conversion of the triplet to the anion; however, we believe that electron deficiency is more important than energy of the triplet state. It is very unlikely that variation of triplet yields in the four molecules is an important consideration in accounting for differences in the observed photochemical quantum yields.

There is a decreasing quantum yield exhibited by 4-nitropyridine when (HCl) > 2 *M*, which is an exception to the trend shown in Table I. Nitrobenzene, 1-nitronaphthalene, and 5-nitroquinoline, on the other hand, show a general increasing quantum yield with increasing HCl concentration. It appears that an acid-catalyzed process decreases the photochemical efficiency in this molecule; however, a satisfactory explanation for this behavior is still lacking.

Experimental Section

Materials. 5-Nitroquinoline and 5-aminoquinoline were obtained from Aldrich Chemical Co. and recrystallized twice from pentane and once from benzene before using. Spectrograde isopropyl alcohol and EPA were used as received. Glass distilled water and reagent grade HCl and H_2SO_4 were used for aqueous solutions.

Equipment. All quantitative photolysis experiments were performed with 313-nm excitation in 50% isopropyl alcohol–water with varying acid concentrations, employing 1-cm spectrophotometric quartz cells. Other experimental procedures have been described elsewhere.[5] Light intensities were typically 2.5×10^{15} quanta/sec as determined with the potassium ferrioxalate actinometer.[13]

The disappearance of 5-nitroquinoline was determined by polarographic analysis of buffered acetic acid–sodium acetate solutions (pH 4.7) before and after photolysis. There were no interfering waves associated with photoproducts generated during the photolysis. The polarographic potential was scanned from 0 to −0.8 V, and the half-wave potential appears at approximately −0.34 V vs. sce. Experiments were designed to keep the disappearance of 5-nitroquinoline at ≤15%.

Large-scale photolyses were performed through a Pyrex sleeve with an Hanovia 450-W medium-pressure mercury immersion lamp (Type 679A-36). In a typical experiment, 1.50 g of 5-nitroquinoline was dissolved in 800 ml of 50% isopropyl alcohol–water, 0.15 *M* in HCl, and irradiating under nitrogen for approximately 9 hr. The originally colorless solution was red at the end of the experiment. The solution was then concentrated by evaporation in vacuo and separation of the product was achieved with silica gel preparative TLC plates. The isolated photoproduct was established to be 6,8-dichloro-5-aminoquinoline by comparing its uv (Cary 14), nmr (Varian A60A), and ir (Beckman IR-8) spectra with that for 5-aminoquinoline. The photoproduct exhibits an amine band at 2.8 μ and the amine protons, which appear at 4.2 δ in 5-aminoquinoline, are shifted to 5.2 δ due to chlorine substitution. The ring protons in the photoproduct appear between 7.5 and 9.0 δ.

Phosphorescence measurements of 4×10^{-5} *M* 5-nitroquinoline at 77°K were made in EPA and in 50% isopropyl alcohol–water with varying amounts of HCl. The phosphorescence yields, using 313-nm excitation, for 5-nitroquinoline in EPA was determined relative to a value of 0.051 for naphthalene, which phosphoresces in the same wavelength region.

References and Notes

(1) R. Hurley and A. C. Testa, *J. Amer. Chem. Soc.*, **88**, 4330 (1966).
(2) R. Hurley and A. C. Testa, *J. Amer. Chem. Soc.*, **89**, 6917 (1967).
(3) R. Hurley and A. C. Testa, *J. Amer. Chem. Soc.*, **90**, 1949 (1968).
(4) W. Trotter and A. C. Testa, *J. Phys. Chem.*, **74**, 845 (1970).
(5) A. Cu and A. C. Testa, *J. Phys. Chem.*, **77**, 1487 (1973).
(6) A. Cu and A. C. Testa, *J. Amer. Chem. Soc.*, **96**, 1963 (1974).
(7) J. Lemaire, *J. Phys. Chem.*, **71**, 612 (1967).
(8) R. B. Cundall, S. Davies, and K. Dunnicliff in "The Triplet State," A. B. Zahlan, Ed., Cambridge University Press, New York, N.Y., 1967, p 183.
(9) S. P. McGlynn, T. Azumi, and M. Kinoshita in "Molecular Spectroscopy of the Triplet-State," Prentice-Hall, Englewood Cliff, N.J., 1969, p 272.
(10) G. G. Wubbels, J. W. Jordan, and N. S. Mills, *J. Amer. Chem. Soc.*, **95**, 1281 (1973).
(11) P. J. Wagner and G. S. Hammond, *Advan. Photochem.*, **5**, 99 (1968).
(12) G. Porter and P. Suppan, *Trans. Faraday Soc.*, **61**, 1664 (1965).
(13) C. G. Hatchard and C. A. Parker, *Proc. Roy. Soc., Ser. A*, **235**, 518 (1956).

Electron Spin Resonance Study of the α-Keto Iminoxy Radicals of Some Bicyclic Ketones

H. Căldăraru, A. Caragheorgheopol, M. Moraru,[1] and V. E. Sahini*

Department of Quantum Chemistry, Institute of Physical Chemistry, Bucharest 13, Romania (*Received August 12, 1974*)

α-Keto iminoxy radicals from some cyclic and bicyclic ketones were studied by esr. Using properly substituted compounds of known conformation and configuration the proton hfs's have been assigned and their dependence on molecular geometry could be followed. For the α-anti proton hfs a $\cos^2\theta$ type dependence involving hyperconjugation with the iminoxy carbon $2p_\pi$ orbital was found. This is an indication of π–σ polarization contributing to the spin density transmission in this class of σ radicals.

Introduction

For some years the iminoxy radicals ($R_1R_2C{=}NO\cdot$) have been the subject of interest, the aim being to understand the hyperfine interaction mechanism in this class of σ-type radicals. From a large amount of data Norman and Gilbert[2] found evidence for a preferential syn interaction which is most efficient in the plane of σ bonds and is highly favored by a W geometry. Our preliminary data on α-keto iminoxy radicals[3] showed however the unexpected feature that significant hfs from anti protons was involved. The same type of interaction was described in a recent work of Russell and Mackor[4] who have undertaken a systematic study of cyclohexanone iminoxy radicals with new and important conclusions regarding the hyperfine interaction mechanism.

We have studied a series of substituted bicyclic compounds with known configurations and conformations, and

have obtained relevant information regarding the positional and angular dependence of the hyperfine interaction in α-keto iminoxy radicals. Our results agree with Russell and Mackor's conclusions which thus appear to have a more general significance.

Results

Fox, McRae, and Symons[5] were the first to synthesize α-keto iminoxy radicals by allowing gaseous nitrogen dioxide to react with ketones having a free active methylene group. The radicals studied in this work have been obtained by the same method starting from the ketones derived from cyclohexanone (I–V), cycloheptanone (VI), bicyclo[3.3.1]nonan-2-one (VII–XI), bicyclo[3.2.1]octan-2-one (XII–XIV), bicyclo[3.3.1]nonan-3-one (XV–XVII), bicyclo-[4.2.1]nonan-2-one (XVIII), bicyclo[4.2.1]nonan-3-one (XIX), and bicyclo[3.2.2]nonan-6-one (XX). The parameters of their esr spectra are summarized in Table I.

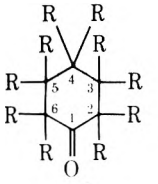

I–V

VI

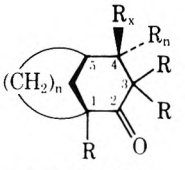

n = 3, VII–XI
n = 2, XII–XIV

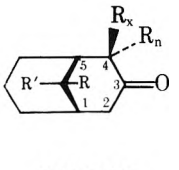

XV–XVII

I. $R_2 - R_6 = H$
II. $R_2, R_6 = D$; $R_3 - R_5 = H$
III. R_{4eq} = t-Butyl; $R_2, R_3, R_{4ax}, R_5, R_6 = H$
IV. R_{2eq}, R_{4eq} = t-Butyl; $R_{2ax}, R_3, R_{4ax}, R_5, R_6 = H$
V. $R_4 = O$
VII. $R_1 = R_3 = R_{4n} = R_{4x} = H$
VIII. $R_1 = R_3 = D$; $R_{4n} = R_{4x} = H$
IX. $R_1 = R_3 = R_{4n} = H$; R_{4x} = Ph
X. $R_1 = R_3 = D$; $R_{4n} = H$; R_{4x} = Ph
XI. $R_1 = R_3 = R_{4x} = H$; R_{4n} = Ph
XII. $R_1 = R_3 = R_{4n} = R_{4x} = H$
XIII. $R_1 = R_3 = R_{4n} = H$; R_{4x} = Ph
XIV. $R_1 = R_3 = R_{4x} = H$; R_{4n} = Ph
XV. $R_{4n} = R_{4x} = R = R' = H$
XVI. $R_{4n} = H$; R_{4x} = Ph; R, R' = O
XVII. $R_{4n} = R = H$; R_{4x} = Ph; R' = OH

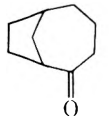

XVIII

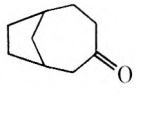

XIX

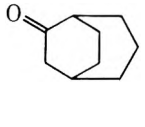

XX

The α-keto iminoxy radicals have the general formula R_1–CO–CNO–R_2 with two possible stereoisomers:

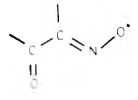

E

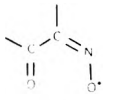

Z

Sites lying on the same side of the C=N double bond as the iminoxy oxygen will be referred to as syn, the opposite ones as anti.

The significant difference between the a_N values of the two isomers is characteristic of α-keto iminoxy radicals. Previous authors[5,6] have assigned the lower values to the *Z* and the higher ones to the *E* isomers. In our series the *Z* isomers all have $a_N \sim 27$ G and the *E* isomers have $a_N \sim 32$ G. This effect of the α-carbonyl group is well accounted for by an EH calculation[7] on some adequate simple model compounds.

The cyclohexane-1,4-dione (V) has four active methylene sites, so a large number of iminoxy radicals can result in the reaction with nitrogen dioxide. Actually we have seen four different iminoxy radicals. Radical i has a second nitrogen splitting of ~11 G and no proton hfs. So we propose a structure of the type:

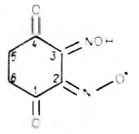

The other three radicals have no secondary hfs, which leads to the formula:

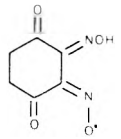

The three radicals probably differ by the presence of additional oxime groups in the 5 and/or 6 positions, or by the syn–anti isomerism of the adjacent oxime.

From bicyclo[4.2.1]nonan-3-one (XIX), with two distinct active sites (four possible radicals) three radicals have been obtained. Radical ii with $a_N \sim 29$ G having no proton hfs was ascribed to the *Z* isomer of the 2-oximino derivative. It follows that radical iii with $a_N \sim 27$ G corresponds to the 4-oximino *Z* isomer. Radical i is of an *E* type. On the basis of the proton hfs it is not possible to decide between the two substitution isomers which can be predicted.

Assignment of Proton Hfs. In all spectra the proton hfs could be easily distinguished on the side lines of the main nitrogen triplet, as these lines do not overlap.

Using cyclohexanone-2,2,6,6-d_4 (II), we were able to establish[3] the proton hfs assignments for radicals *E*-I, *E*-II and *Z*-I, *Z*-II as follows:

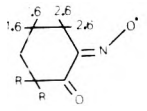

E-I, R = H
E-II, R = D

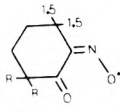

Z-I, R = H
Z-II, R = D

The hfs in the structurally related radicals VII–XIV clearly demands the following assignments:[8]

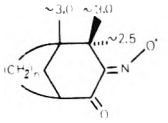

E

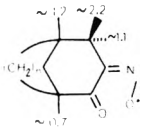

Z

We feel that the quasi-identity of the hfs on the α position justifies the extension of this description for radicals III and IV of the fixed cyclohexanone:

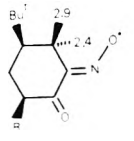

E-III, R = H
E-IV, R = Bu^t

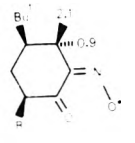

Z-III, R = H
Z-IV, R = Bu^t

TABLE I: Hfs Constants (Gauss) and g Factors of the α-Keto Iminoxy Radicals Measured at Room Temperature

Parent ketone	Iminoxy radicals	a_N	a_H	g
I[a]	*E*-I	32.8	2.6(2) 1.6(2)	2.00_{53}
	Z-I	26.6	1.5(2)	2.00_{53}
II[b]	*E*-II	32.9	2.6(2) 1.6(2)	2.00_{52}
	Z-II	26.8	1.5(2)	2.00_{52}
III[b]	*E*-III	32.9	2.9(1) 2.4(1)	2.00_{51}
	Z-III	26.8	2.1(1) 0.9(1)	2.00_{53}
IV[b]	*E*-IV	32.7	2.9(1) 2.5(1)	2.00_{52}
	Z-IV	26.4	2.1(1) 0.9(1)	2.005_{2}
V[a]	i	28.2	11.4(1)[d]	2.004_{4}
	ii	27.5		2.005_{5}
	iii	28.1		2.004_{2}
	iv	32.0		2.004_{2}
VI[a]	*E*-VI	33.1	Line-width effects[e]	2.005_{0}
	Z-VI	27.3		2.005_{0}
VII[a]	*E*-VII	33.0	3.1(2) 2.5(1)	2.005_{0}
	Z-VII	26.6	2.2(1) 1.2(1) 0.9(1) 0.7(1) 0.2(1)	2.005_{2}
VIII[c]	*E*-VIII	33.1	3.1(2) 2.5(1)	2.005_{0}
	Z-VIII	26.7	2.2(1) 1.2(1) 1.0(1)	2.005_{2}
IX[b]	*E*-IX	32.3	2.5(2)	2.005_{0}
	Z-IX	26.7	1.2(1) 1.0(1) 0.7(1) 0.3(1)	2.005_{2}
X[a]	*E*-X	32.4	2.5(2)	2.005_{0}
	Z-X	26.7	1.2(1) 1.1(1)	2.005_{2}
XI[b]	*E*-XI	32.0	3.0(2)	2.004_{9}
	Z-XI	27.4	2.2(1) 1.1(1) 0.7(1) 0.3(1)	2.005_{1}
XII[a]	*E*-XII	32.7	3.1(2) 2.5(1)	2.005_{0}
	Z-XII	26.8	2.2(1) 1.2(2)	2.005_{2}
XIII[b]	*E*-XIII	32.2	2.9(1) 2.6(1)	2.005_{0}
	Z-XIII	26.9	1.4(1) 1.2(1)	2.005_{2}
XIV[b]	*E*-XIV	31.9	2.9(2)	2.005_{0}
	Z-XIV	27.2	2.0(1) 1.2(1) 0.2(1)	2.005_{2}
XV[a]	*E*-XV	32.6	2.9(1) 2.0(1) 1.6(1) 0.6(1)	2.005_{1}
	Z-XV	26.0		2.005_{3}
XVI[b]	*E*-XVI	32.6	1.9(2) 0.8(1)	2.005_{0}
	Z-XVI	27.2	0.5(2)	2.005_{2}
XVII[b]	*E*-XVII	32.8	1.9(2) 0.8(1)	2.005_{0}
	Z-XVII	27.2	0.5(2)	2.005_{2}
XVIII[a]	*E*-XVIII	32.5	2.9(1) 1.7(1) 1.3(1) 0.3(1)	2.005_{0}
	Z-XVIII	26.4	1.8(1) 0.8(1) 0.4(1) 0.2(4)	2.005_{2}
XIX[a]	i	32.5	2.8(1) 1.9(2)	2.005_{0}
	ii	28.8		2.004_{6}
	iii	26.6	Spectrum of eight lines separated by 0.6 G	2.005_{2}
XX[a]	*E*-XX	32.3	Spectrum of weak lines	2.005_{0}
	Z-XX	27.0	2.2(1)	2.005_{2}

[a] From these ketones the radicals were obtained by method 1 (see Experimental Section). [b] From these ketones the radicals were obtained by method 2 (see Experimental Section). [c] The same radicals were obtained by Fox, McRae, and Symons.[5] [d] This splitting is on a nitrogen atom. [e] See Discussion.

As compared to the analogous bicyclic radicals, the ~3-G hfs is missing in the *E* isomers and the ~1 G one in the *Z* isomers, because of C-4 substitution.

The following assignments are reasonable in the series of radicals *E*-XV–*E*-XVII:

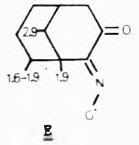

E

The spectra of the corresponding *Z* isomers have no major proton hfs.

We could not ascribe the hfs to actual protons in the bicyclo[4.2.1]nonane systems as the available data do not lead to unequivocal assignments.

The 2.2-G hfs in the radical *Z*-XX is assigned to the C-5 proton:

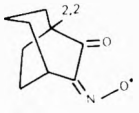

Z-XX

This results from the already proved assignments in the *Z* radical of isonitrosocamphor.[9]

Discussion

The hfs on geminal protons provide information regarding the mobility of the implied ring.

As indicated by the equivalence of the hfs of their geminal protons radicals *E*-I and *Z*-I are rapidly interconverting between limiting structures. In the bicyclic radicals VII–XIV this flipping is frozen, and a preferred conformation is adopted as indicated by the nonequivalence of the α-geminal protons in both *E* and *Z* isomers. The preferred conformation is the same for all members of this series as implied from the consistency of the proton hfs at *endo*- and *exo*-phenyl substitution. This conformation proved to be a chair-like one as established by Lee, Seymour, and Burgstahler[10] by X-ray and CD analysis in both solid and solution for the closely related 4,4-dimethylbicyclo[3.2.1]octane-2,3-dione. The hfs of about 3 G for the β proton in the *E* isomers as compared to a value close to zero for the corresponding proton in a boat-shaped ring (as established on the iminoxy radicals of *exo*-2-(*N*-morpholinyl)- and *exo,exo*-2,4-(*N*-morpholinyl)phenylbicyclo[3.3.1]nonan-9-one oximes[11]) is an independent indication of the chair conformation of the radicals themselves. The quasi-identity of the observed hfs in the whole series of substituted compounds (III, IV, VII–XIV) seems to justify the extension of this conclusion to radicals III and IV in spite of their apparent greater mobility.

The arithmetical mean rule holds for the splittings in the flipping radicals, as expected when the limiting conformations are equally probable. So, $a_H(\alpha\text{-syn}) = 2.6 \simeq \frac{1}{2}(2.4 + 2.9)$, $a_H(\alpha\text{-anti}) = 1.5 \simeq \frac{1}{2}(2.1 + 0.9)$, and $a_H(\beta\text{-syn}) = 1.6 \simeq \frac{1}{2}(3.0 + 0)$.

The spectrum of radical *E*-VI from cycloheptanone presents important line width effects. From −25 (below this temperature the radicals dimerize) to +60° (above this temperature the radicals decompose) the spectrum undergoes essential changes (which are reversible) approaching an imperfect 1:4:6:4:1 quintet (a_H = 1.5 G) at the high-temperature limit (Figure 1). Although the observed changes could not be reduced to some model of molecular motion, we find it important to notice the effect in contrast to cycloheptene systems (semidiones)[12] which are conformationally stable in this temperature range (−80° to +60°). The mobility of the seven-membered ring is drastically reduced in bicyclic compounds as illustrated by radicals *E*-XVIII and *Z*-XVIII in which the hfs of geminal protons are not averaged and the spectra do not change at temperatures up to +60°.

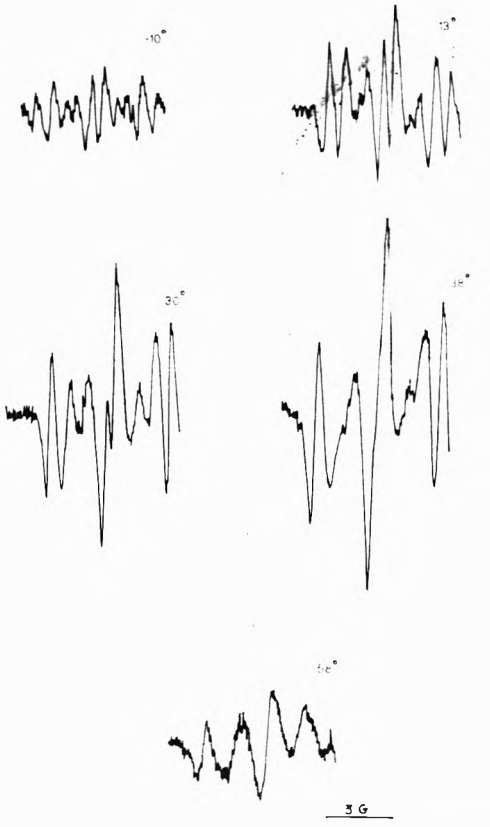

Figure 1. The low-field line of the nitrogen triplet in the esr spectrum of *E*-VI radical at different temperatures.

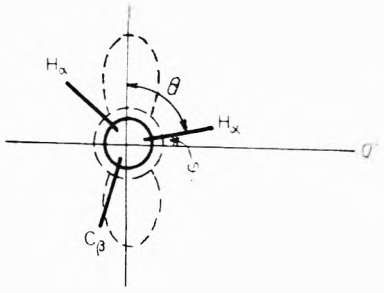

Figure 2. End-on-view of the p_π-like orbital on the minoxy C atom and the α-methylene group; σ represents the plane containing the C=NO· group.

Inspection of the proton hfs assignments leads to certain conclusions regarding the hfs-molecular geometry correlation. (i) α-anti protons show a hyperfine interaction which is essentially angularly dependent varying from 0 for protons in the σ plane to 1.8 G for a dihedral angle of 60° and to still higher values at greater angles (Table II and Figure 2).

Using C-4 phenyl compounds with firmly established configuration and assuming for the six-membered ring the

TABLE II: Hfs and Dihedral Angles (Figure 2) of the α-Anti Protons in Radicals with Known Geometry

φ, deg	a_H	Radical and the proton involved
0	0.4[a]	*Z*-XX, the C-1 proton; the iminoxy radicals of a series of bicyclo[3.3.1]nonan-9-one oximes, the bridgehead proton[c]
4	0.7	Iminoxy radical of bicyclo[3.3.1]nonan-3-one oxime, the equatorial proton[d]
~25[b]	1.1	*Z*-IX, *Z*-X, *Z*-XIII, the *endo*-C-4 proton
60	1.8	*Z* isomer of cyclopentanone, the C-3 protons[e]
~95[b]	2.2	*Z*-XI, *Z*-XIV, the *exo*-C-4 proton
113	2.0	Iminoxy radical of bicyclo[3.3.1]nonan-3-one oxime, the axial proton[d]

[a] The 0.4 value represents the line width. [b] Measured on Dreiding model of bicyclo[3.2.1]octan-2-on-3-iminoxy with a torsional angle between the keto and iminoxy groups of ~34°.[10] [c] Reference 11. [d] Reference 4. [e] Reference 5.

previously argued chair conformation, it was possible to determine that the higher hfs value (2.2 G) is due to the axial proton, the lower one (1.1 G) to its equatorial pair. This assignment is in agreement with the data showing that the hfs approaches zero for protons lying in the plane. It should be noted that α-anti nitrogen hfs have not been either observed when in the σ-bonds plane.[13]

The hfs-angle dependence in Table II seems to obey a $\cos^2\theta$ type relationship characteristic for hyperconjugative coupling with β protons in alkyl-type radicals:

$$a_H = B_0 + B_1 \cos^2\theta$$

where θ is the angle between the iminoxy carbon $2p_\pi$ orbital and the plane containing the C_{im}–C_α–H bonds (complementary to φ). A least-squares fit for the data in Table II leads to $B_0 = 0.6$ and $B_1 = 1.6$. The hfs of *anti*-methyl group observed[2,14] in a series of iminoxy radicals can be now calculated. For a free rotating methyl group $a_H = B_0 + B_1\langle\cos^2\theta\rangle_{av} = B_0 + \frac{1}{2}B_1 = 1.4$ G, a value in very good agreement with the experimental one.[2,14]

(ii) α-syn proton hfs vary much less with dihedral angle because the hfs value for the in-plane proton is also important. In our radicals the stronger interaction involves the axial position. This was proved in the same way as for anti protons.

(iii) A W-type geometry is favorable for efficient long-range coupling. Values of about 3 G were observed for β-syn protons when this condition is achieved in the *E* isomers (*E*-VII, *E*-VIII, *E*-XI–*E*-XV). In the *Z* isomers these values are lower and range between 2.2 G for *Z*-XX and 0.7 G for *Z*-VII, *Z*-IX, and *Z*-XI depending on the planarity of the fragment involved. Even β-anti protons were observed with about 1 G in the *Z*-VII–*Z*-XIV radicals.

All these data strongly support Russell and Mackor's conclusions[4] that "the hfs at the *anti*-position mainly comes from π-spin density at the unsaturated C atom." This mechanism, which also contributes to the hfs of out-of-plane α-syn protons, explains the observed angular dependence, which is reversed to what would be expected for electrons in σ orbitals. A recent INDO calculation on a model iminoxy radical ($CH_2NO\cdot$) supports this conclusion;[15] negative spin density was found in a p_π-like "orbital" on the unsaturated C atom.

So at present it appears that all observed esr data on iminoxy radicals can be accounted for by three types of interaction: (a) long-range spin delocalization which is asymmetric, preferential in syn, and more efficient in a planar W-shaped framework; (b) direct overlap sometimes having a significant magnitude for substituents in α-syn, in the σ plane; (c) π–σ spin polarization, by which the spin density in the σ orbital induces a negative π spin density at the iminoxy C atom. By hyperconjugation α protons are involved in the interaction, their hfs being zero in the nodal plane of the π orbital (the σ plane) and reaching the maximum when the CH bond is parallel to the π orbital.

Experimental Section

Materials. Cyclohexanone (I), 4-*tert*-butylcyclohexanone (III), cyclohexane-1,4-dione (V), and cycloheptanone (VI) were commercially available and used without purification.

Bicyclo[3.3.1]nonan-2-one (VII),[16] 4-*exo*- and 4-*endo*-phenylbicyclo[3.3.1]nonan-2-ones (IX and XI),[17] bicyclo[3.2.1]octan-2-one (XII),[18] 4-*exo*- and 4-*endo*-phenylbicyclo[3.2.1]octan-2-ones (XIII and XIV),[19] bicyclo[3.3.1]nonan-3-one (XV),[20] 4-*exo*-phenylbicyclo[3.3.1]nonane-3,9-dione (XVI),[21] and 4-*exo*-phenylbicyclo[3.3.1]nonan-9-*anti*-ol-3-one (XVII)[21] have been synthesized as described in the literature. The stereochemistry at C-4 position was firmly established by nmr and chemical methods.

The cyclohexanone-2,2,4,4-d_4 (II), bicyclo[3.3.1]nonan-2-one-1,3,3-d_3 (VIII), and 4-*exo*-phenylbicyclo[3.3.1]nonan-2-one-1,3,3-d_3 (X) have been prepared from the undeuterated ketones as described in the literature.[3,22] For the last two compounds the exchange time was 6 weeks. Their nmr spectra indicated more than 2.7 deuterium per molecule.

Benzene was dried on sodium wires and distilled. Dimethylformamide was dried on potassium carbonate and distilled. Nitrogen dioxide was prepared according to the literature[23] and dried before use by passing it over phosphoric acid.

Radicals. The α-keto iminoxy radicals were prepared in one of the following two ways: (1) passing gaseous nitrogen dioxide over a benzene solution of the ketone (or the ketone itself when liquid) in an esr sample tube; (2) adding a saturated solution of nitrogen dioxide in dimethylformamide over the ketone in the esr sample tube.

Esr Spectra. The esr spectra were recorded at room temperature on a JES-3BX (JEOL) spectrometer with 100-kHz modulation. The hfs constants and *g* factors were measured in comparison with potassium peroxylaminedisulfonate ($a_N = 13.0$ G, $g = 2.0055$). For measurements at low and high temperatures the variable temperature cavity and the corresponding units were used.

Acknowledgments. We are very much indebted to Dr. Eliza Avram for a sample of *cis*-2,4-di-*tert*-butylcyclohexanone (IV), and to Professor M. Hartmann for bicyclo[4.2.1]nonan-2-one (XVIII), bicyclo[4.2.1]nonan-3-one (XIX), and bicyclo[3.2.2]nonan-6-one (XX) samples received as gifts.

References and Notes

(1) Department of Organic Chemistry, University, Bucharest.
(2) R. O. C. Norman and B. C. Gilbert, *J. Phys. Chem.*, **71**, 14 (1967).
(3) A. Caragheorgheopol, H. Căldăraru, and V. E. Sahini, *Rev. Roum. Chim.*, **18**, 1497 (1973).
(4) G. A. Russell and A. Mackor, *J. Amer. Chem. Soc.*, **96**, 145 (1974).
(5) W. M. Fox, J. A. McRae, and M. C. R. Symons, *J. Chem. Soc. A*, 1773 (1967).
(6) W. M. Fox and M. C. R. Symons, *J. Chem. Soc. A*, 1503 (1966).

(7) A. Caragheorgheopol, H. Căldăraru, and V. E. Sahini, in press.
(8) The 2.5-G hfs of the β proton in the E4X radical as compared to the expected 3-G value seems to indicate a slight distorsion of this radical.
(9) B. C. Gilbert and R. O. C. Norman, *J. Chem. Soc. B*, 86 (1966).
(10) B. Lee, J. P. Seymour, and A. W. Burgstahler, *Chem. Commun.*, 235 (1974).
(11) H. Căldăraru and M. Moraru, *J. Amer. Chem. Soc.*, **96**, 149 (1974).
(12) G. A. Russell, G. R. Underwood, and D. C. Lini, *J. Amer. Chem. Soc.*, **89**, 6636 (1967).
(13) H. Căldăraru, A. Caragheorgheopol, and V. E. Sahini, *J. Magn. Resonance*, **11**, 335 (1973).
(14) B. C. Gilbert and R. O. C. Norman, *J. Chem. Soc. B*, 123 (1968).
(15) M. F. Chiu, B. C. Gilbert, and B. T. Sutcliffe, *J. Phys. Chem.*, **76**, 553 (1972).
(16) M. Hartmann, *Z. Chem.*, **6**, 182 (1966).
(17) V. Dressler and K. Bodendorf, *Justus Liebigs Ann. Chem.*, **720**, 71 (1968).
(18) W. Kraus, *Justus Liebigs Ann. Chem.*, **685**, 97 (1965).
(19) N. Bărbulescu and M. Moraru, *Rev. Chim. (Bucharest)*, **23**, 457 (1972).
(20) J. P. Schaefer, J. C. Lark, C. A. Flegal, and L. M. Honig, *J. Org. Chem.*, **32**, 1327 (1967).
(21) N. Bărbulescu, M. Moraru, and D. Sotcă, *Rev. Roum Chim.*, **18**, 873 (1973).
(22) J. P. Schaefer and J. C. Lark, *J. Org. Chem.*, **30**, 1337 (1965).
(23) "Handbook of Preparative Inorganic Chemistry," G. Erauer, Ed., Academic Press, New York, N.Y., 1963, p 488.

Electron Spin Resonance Spectra of the Phosphoranyl Radicals $ROPF_3$[1]

A. J. Colussi,[2] J. R. Morton,* and K. F. Preston

Division of Chemistry, National Research Council of Canada, Ottawa, Canada *(Received August 26, 1974)*

Publication costs assisted by the National Research Council of Canada

Esr spectra recorded during the liquid-phase photolysis of solutions of PF_3 and F_2O or certain peroxides ROOR are attributed to the phosphoranyl radicals PF_4 and $ROPF_3$. The magnitudes of the observed ^{31}P and ^{19}F hyperfine interactions in these radicals are indicative of a totally symmetric half-filled molecular orbital in a trigonal bipyramidal framework. With the exception of the *tert*-butoxy group, the oxyl groups in $ROPF_3$ invariably occupy an apical position. Variations in the hyperfine interactions of the latter radicals with changes in RO are essentially restricted to those of the ^{31}P nucleus and the apical ^{19}F nucleus, an effect reminiscent of the trans influence of ligands in metal complexes. INDO MO calculations reproduce qualitatively some of the experimental observations.

Introduction

It is now well established[3-6] that valence-shell expansion of elements of groups V–VII may take place by way of free-radical addition and that under certain conditions intermediate, short-lived valence states are detectable by the method of electron spin resonance spectroscopy (esr). Hyperfine interactions provide a ready means of identification of these species and also a sensitive probe of the unpaired electron spin density at the various magnetic nuclei present in the intermediates. Phosphorus-centered radicals have proved particularly informative because of the large magnetogyric ratio of the normal phosphorus isotope ^{31}P (I = ½). Of particular interest was the recent discovery of esr spectra of certain phosphoranyl radicals, formed by the addition of *tert*-butoxy radicals to various phosphines.[3] These radicals are derived from the prototype PH_4 and possess distorted trigonal bipyramidal geometry, with the *tert*-butoxy ligand invariably occupying an apical site.

These results, and our recent success[4,7] in observing intermediates during the addition of F atoms and various alkoxy and fluoroxy radicals to SF_4 led us to attempt similar experiments with PF_3 as the acceptor molecule. Radicals of the type .$ROPF_3$ are derived from the prototype[8] PF_4, and a comparison of their geometries with those of radicals derived from PH_4 would be of great interest in connection with recent theories of bonding in pentacoordinate phosphorus compounds.[9]

Results and Discussion

Esr spectra were observed during the photolysis of solutions of PF_3 and F_2O or a peroxide in an appropriate Freon. The experimental conditions are summarized in Table I, together with the spectral parameters obtained from the experimental data by exact diagonalization of the appropriate spin Hamiltonian.

The observed esr spectra were all characterized by a single large ^{31}P (I = ½) hyperfine interaction and by smaller interactions with three or more ^{19}F (I = ½) nuclei. In the case of the spectrum obtained during the photolysis of F_2O–PF_3 solutions the latter consisted of two pairs of equivalent ^{19}F interactions, the data being very similar to those ascribed[8] to PF_4 trapped in an SF_6 matrix.[10] Accordingly, we identify the spectrum observed during the photolysis of F_2O–PF_3 solutions with the radical PF_4; it is presumably formed by the addition of photolytically generated fluorine atoms to PF_3. Theoretical considerations suggest[13] that the larger (291 G) of the two ^{19}F hyperfine interactions be assigned to fluorine nuclei in the apical positions, the smaller (58 G) interactions to the equatorial fluorine nuclei in the pseudotrigonal configuration of the PF_4 radical.

Spectra observed during the photolysis of PF_3–peroxide solutions were attributed to $ROPF_3$ radicals. Apart from small hyperfine interactions (Table I, column 7) originating in the fluoroxyl ligands, the ^{31}P and ^{19}F interactions of

TABLE I: Esr Parameters of PF_4 and $ROPF_3$ Radicals

Radical	Solvent and temp, °C	g factor[a]	Hyperfine interactions[b]			
			^{31}P, G	^{19}F, G		
				Apical	Equatorial	In RO
PF_4	Freon 13	2.0002	1344	291	58	
	−160		(1)	(2)	(2)	
FSO_2PF_2	Freon 11	2.0020	1364.5	245.5	45.0	c
	−75		(1)	(1)	(2)	
FCO_2PF_2	Freon 11	2.0014	1306.1	262.0	42.1	23.3
	−90		(1)	(1)	(2)	(1)
CF_3OPF_2	CF_3OOCF_3	2.0018	1232.0	275.0	43.8	7.0
	−120		(1)	(1)	(2)	(3)
$(CF_3)_2COPF_2$	Freon 13	2.0017	1225.3	276.5	44.3	9.1
	−120		(1)	(1)	(2)	(6)
$(CH_3)_3COPF_2$	Freon 13	2.0015	1263.9	289.6	59.2	
	−120		(1)	(2)	(1)	

[a] Esr parameters were obtained from the experimental data using exact diagonalization procedures; g factors are accurate to ±0.0002, hfs to ±0.5G for $ROPF_3$ and to ±1 G for PF_4. [b] The numbers in parentheses beneath each hfs value indicate the number of equivalent interactions of that value. [c] Not resolved; maximum-slope line widths were ~3 G throughout.

these radicals were very similar to their analogs in PF_4 itself. We conclude that these radicals arise from the addition of oxyl radicals to PF_3 and may be regarded as derived from PF_4 by the substitution of an oxyl group for a fluorine atom. The data in Table I are therefore interpreted in terms of an equatorially substituted derivative of PF_4 in the case of $(CH_3)_3COPF_3$ and in terms of apically substituted derivatives in the remaining cases. Thus, in the case of CF_3OPF_3, for example, the CF_3O ligand occupies an apical position and reveals itself by the 7.0-G hyperfine interaction of its three equivalent ^{19}F nuclei. The fluorine nucleus in the other apical position has a 275-G hyperfine interaction, and the two equivalent equatorial fluorine nuclei show 43.8-G hyperfine interactions.

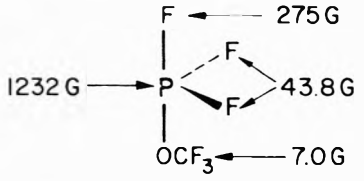

This picture of the structure of CF_3OPF_3 is consistent not only with the data on PF_4, but also with data on phosphoranyl radicals[3] derived from the prototype species PH_4. Thus the two equatorial protons in the radical $(CH_3)_3COPH_3$ had hyperfine interactions of 10.8 G, and the lone apical proton had an interaction of 139.6 G. It is noteworthy, however, that the ^{31}P hyperfine interaction in PF_4 and its derivatives is over twice that found in radicals derived from the prototype PH_4.

Of the five $ROPF_3$ radicals listed in Table I, four (RO = FSO_3, FCO_2, CF_3O, and $(CF_3)_3CO$) have the RO ligand in an apical position. The fifth species, $(CH_3)_3COPF_3$, has its RO ligand in an equatorial position, as demonstrated by the presence of two ^{19}F hyperfine interactions of 289.6 G (apical) and only one (equatorial) at 59.2 G. This configuration is in direct contrast to that of radicals formed by the addition of *tert*-butoxy radicals to phosphine and to a variety of alkyl phosphines, where the $(CH_3)_3CO$ ligand invariably occupied an apical position.[3]

Comparison of the hyperfine interactions associated with magnetic nuclei originating in the fluoroxy ligands (Table I, column 7) with the corresponding interactions in the sulfuranyl radicals[4,7] $ROSF_4$ leaves little doubt that the correct formulation is $ROPF_3$, rather than RPF_3, for the phosphoranyl radicals reported here. Indeed, attempts to prepare radicals of the latter type, for example, by photolysis of CF_3I containing dissolved PF_3, were not successful. The value (23 G) of the ^{19}F interaction of the FCO_2 ligand in FCO_2PF_3 is unexpectedly high and suggests that rotation about the C–O single bond is not free.[14] A similar conclusion may be drawn from the observation of six (rather than nine) equivalent ^{19}F hyperfine interactions from the $(CF_3)_3CO$ ligand in the radical $(CF_3)_3COPF_3$.

It is of interest to note that there appears to be a linear correlation between the ^{31}P hyperfine interaction and the apical ^{19}F hyperfine interaction in the four radicals $(RO)_{ap}PF_3$, whereas the two equivalent (equatorial) ^{19}F interactions appear to be unaffected by changes in the RO ligand (Figure 1). The common factor affecting both the ^{31}P hyperfine interaction and the $^{19}F_{ap}$ hyperfine interaction in these species is probably the electronegativity of the RO ligand. Moreover, since FSO_3 is indubitably more electronegative than $(CF_3)_3CO$ we conclude that Figure 1 demonstrates that with increasing electronegativity in RO (a) the ^{31}P hyperfine interaction increases, (b) the $^{19}F_{ap}$ interaction decreases, and (c) the $^{19}F_{eq}$ interactions are unaffected. The change in the ^{31}P hyperfine interaction is readily explained as follows: increasing the electronegativity in RO results in an increased contribution by the atomic orbitals of phosphorus to the molecular orbital occupied by the unpaired electron.[16] The increase in the ^{31}P hyperfine interaction simply reflects an increase in the phosphorus 3s contribution.

Changes in the ^{19}F interactions, on the other hand, are probably due to more subtle effects involving the bonding orbitals. It is well established that ligands in metal complexes exert a "trans influence," such that with increasing electronegativity of a ligand the bond trans to that ligand decreases in length, while cis bonds remain unaffected.[17,18] We believe that such an effect is operative in these phosphoranyl radicals (and in certain sulfuranyl radicals[7]) and

TABLE II: Summary of INDO Calculations

	Bond length[a], Å		Bond angle,[a] deg		Net unpaired s orbital spin density			Charge[b]		
	r_{eq}	r_{ap}	ϕ	θ	P	X_{eq}	X_{ap}	P	X_{eq}	X_{ap}
PH_4	1.45	1.53	98	150	0.185	0.00303	0.483	−0.384	0.041	0.151
PF_4	1.80	1.89	96	158	0.156	0.000251	0.00418	−1.126	0.321	0.242
PH_5	1.48	1.51	120	180				−0.916	0.137	0.252
PF_5	1.80	1.81	120	180				−1.748	0.335	0.372

[a] Values for the energy-optimized (C_{2v}) geometries; θ and ϕ are the angles between the two apical and the two equatorial bonds, respectively; angle $X_{eq}PX_{ap} > 90°$ in both PH_4 and PF_4. [b] Expressed as a fraction of the charge on the electron.

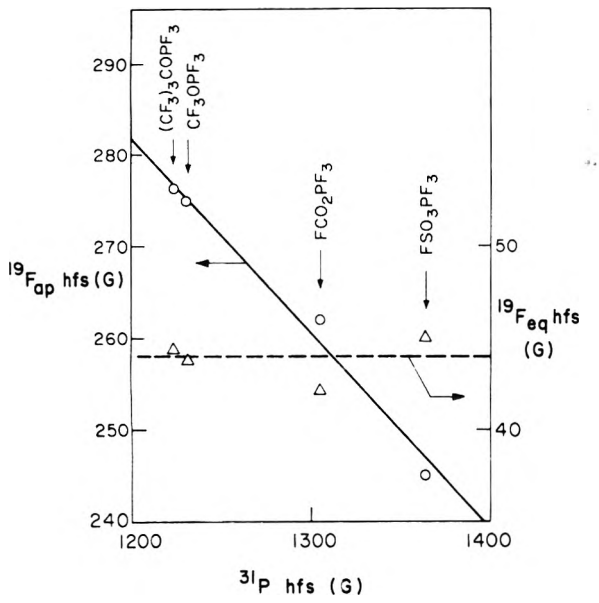

Figure 1. Correlation between ^{31}P hyperfine interaction in $(RO)_{ap}PF_3$ radicals and (a) the $^{19}F_{ap}$ hyperfine interaction O, (b) the $^{19}F_{eq}$ hyperfine interactions Δ.

that it accounts for the directional selectivity of the effect of ligand changes on the net unpaired s orbital spin densities. A decrease in the P–F_{ap} bond length will result in reduced absolute values for the σ–π parameters[19] Q_{SF}^F and Q_{FS}^F associated with the bond. Since both Q_{SF}^F and S^F, the core-polarization parameter for fluorine, are probably negative, while Q_{FS}^F is positive,[20] our observation that the $^{19}F_{ap}$ hyperfine interaction decreases with increasing electronegativity in RO implies that unpaired spin density in the apical fluorine 2p orbitals makes the dominant spin-polarization contribution to the isotropic hyperfine interaction at this nucleus. The invariance of the $^{19}F_{eq}$ hyperfine interactions, on the other hand, is the result of (a) smaller absolute values of the polarization parameters due to the shorter equatorial P–F bonds and (b) the fact that these bond lengths are essentially unaffected by changes in electronegativity at RO.

We have attempted to rationalize some of our observations on the configurations of phosphoranyl radicals in terms of the charge distributions predicted by INDO MO calculations for the prototype radicals PH_4 and PF_4. Using the INDO I (K = 1) parameterization[21] and a minimal basis set of s and p atomic orbitals these calculations were energy optimized within the constraints of an imposed C_{2v} symmetry. For comparison purposes we carried out similar calculations for the trigonal molecular configurations PH_5 and PF_5. The results of all INDO calculations appear in Table II. For PH_4, PH_5, and PF_5 the apical ligands have an appreciably greater charge density than the equatorial ligands. This result accounts for the apical substitution of *tert*-butoxy ligand(s) in radicals derived from PH_4,[3] since the more electronegative (than H) *tert*-butoxy ligand(s) will prefer sites of higher charge density. Similar results for PH_5 and PF_5 offer a simple rationalization of "Muetterties' rule" that in a trigonal bipyramidal configuration the more electronegative ligands will occupy the apical positions.[9,22]

The INDO calculation for PF_4, however, predicts the equatorial positions to possess the larger charge density, thus providing a satisfying rationale of our observation that oxyl groups (being less electronegative than fluorine) prefer to occupy apical positions in $ROPF_3$ radicals. The greater stability of the equatorial configuration of $(CH_3)_3COPF_3$ is not, of course, accounted for by this simplistic hypothesis. Other factors, such as π donor capability,[9] may well override electronegativity effects in determining the preferred configuration of that radical.[22]

The INDO method also enjoyed a certain measure of success in predicting net unpaired s orbital spin densities for the radicals PH_4 and PF_4 (Table II) in qualitative accord with the experimental observations on phosphoranyl radicals. Quantitatively, however, the results of the calculations in the INDO approximation were disappointing. In particular, the prediction of a larger ^{31}P hyperfine interaction in PH_4 compared to PF_4 is in direct conflict with experimental observations.[23] We did note, however, that the spin densities predicted at the Hückel level of approximation (for the INDO-optimized geometries) were more realistic, yielding a ratio of ^{31}P hyperfine interactions for PH_4 and PF_4 of 0.64. This has been a feature of many of our MO computations for σ radicals and suggests that the INDO method overemphasizes spin polarization contributions to the net unpaired s orbital spin densities.

The composition of the semioccupied orbital of PF_4 predicted by our MO calculations at both Hückel and INDO levels of approximation closely resembles that deduced by Gillbro and Williams[24] for the 33 valence-electron species $POCl_3^-$. The principal atomic orbital components are phosphorus 3s and $3p_\sigma$ combined (in antibonding fashion) with apical fluorine $2p_\sigma$ orbitals. Contributions to the half-filled orbital from atomic orbitals on the equatorial fluorines are small. A similar composition was predicted for the half-filled orbital of PH_4 where the contributions from the apical protons were necessarily restricted to H 1s orbitals.

Experimental Section

Bis(fluorocarbonyl) peroxide $(FCO)_2O_2$ was prepared[25] by the photolysis of a mixture of F_2O, CO, and O_2, perflu-

orodi-*tert*-butyl peroxide $(CF_3)_3CO_2C(CF_3)_3$ by the method of Gould, *et al.*,[26] and peroxydisulfuryl difluoride $F_2S_2O_6$ by the procedure of Staricco, *et al.*[27] PF_3 and CF_3OOCF_3 were purchased from PCR Inc., Gainesville, Fla., F_2O from Ozark-Mahoning Inc., Tulsa, Okla.

Esr spectra of $ROPF_3$ radicals were obtained by the photolysis in the cavity of the spectrometer of solutions of PF_3 and a peroxide in an appropriate Freon. The photolysis lamp was a 1000-W Schoeffel Hg–Xe high-pressure lamp, and the spectrometer was a Varian E-12 spectrometer equipped with an F-8A proton fluxmeter. The frequency of the latter and the frequency of the microwave resonant cavity were measured with a Systron-Donner Model 6057 frequency counter. The conditions under which the spectra were recorded and measured are given in Table I.

The spectrum of PF_4 was obtained by photolysis at −160° of a solution of 15 mol % each of PF_3 and F_2O in Freon 13.

Caution. Under no circumstances should these concentrations be exceeded, otherwise violent detonations may occur upon photolysis. (Solutions containing PF_3 and any of the hypofluorites CF_3OF, SF_5OF, or FSO_2OF tend to detonate spontaneously.)

References and Notes

(1) NRCC No. 14463.
(2) NRC Postdoctorate Fellow 1974.
(3) P. J. Krusic, W. Mahler, and J. K. Kochi, *J. Amer. Chem. Soc.*, **94**, 6033 (1972).
(4) J. R. Morton and K. F. Preston, *Chem. Phys. Lett.*, **18**, 98 (1973).
(5) J. R. Morton and K. F. Preston, *J. Chem. Phys.*, **58**, 2657 (1973).
(6) J. R. Morton and K. F. Preston, *J. Chem. Phys.*, **58**, 3112 (1973).
(7) A. R. Gregory, S. Karavelas, J. R. Morton, and K. F. Preston, *J. Amer. Chem. Soc.*, in press.
(8) R. W. Fessenden and R. H. Schuler, *J. Chem. Phys.*, **45**, 1845 (1966).
(9) R. Hoffmann, J. M. Howell, and E. L. Muetterties *J. Amer. Chem. Soc.*, **94**, 3047 (1972).
(10) It has recently been suggested[11] that an earlier spectrum, claimed by one of us[12] to be that of PF_4, was in fact that of PF_5^-.
(11) S. P. Mishra and M. C. R. Symons, *Chem. Commun.*, 279 (1974).
(12) J. R. Morton, *Can. J. Phys.*, **41**, 706 (1963).
(13) J. Higuchi, *J. Chem. Phys.*, **50**, 1001 (1969).
(14) Unfortunately, the corresponding sulfuranyl radical FCO_2SF_4 is unknown, although the radical FCO_2SO_2 also shows an anomalously large ^{19}F interaction (12 G)[15] when compared with those in CF_3OSO_2 (2.8 G).[5]
(15) J. R. Morton and K. F. Preston, unpublished data.
(16) P. W. Atkins and M. C. R. Symons, "The Structure of Inorganic Radicals," Elsevier, Amsterdam, 1967, p 103.
(17) T. G. Appleton, H. C. Clark, and L. E. Manzer, *Coord. Chem. Rev.*, **10**, 335 (1973).
(18) F. R. Hartley, *Chem. Soc. Rev.*, **2**, 163 (1973).
(19) M. Karplus and G. K. Fraenkel, *J. Chem. Phys.*, **35**, 1312 (1961).
(20) J. E. Wertz and J. R. Bolton, "Electron Spin Resonance," McGraw-Hill, New York, N.Y., 1972, Chapter 6.
(21) A. R. Gregory, *J. Chem. Phys.*, **60**, 3713 (1974).
(22) E. L. Muetterties, W. Mahler, and R. Schmutzler, *Inorg. Chem.*, **2**, 613 (1963).
(23) The isotropic ^{31}P hyperfine interaction in PH_4 is 519 G, A. J. Colussi, J. R. Morton, and K. F. Preston, *J. Chem. Phys.*, in press.
(24) T. Gillbro and F. Williams, *J. Amer. Chem. Soc.*, **96**, 5032 (1974).
(25) A. H. Jubert, J. E. Sicre, and H. J. Schumacher, *An. Assoc. Quim. Argent.*, **58**, 79 (1970).
(26) D. E. Gould, C. T. Ratcliffe, L. R. Anderson, and W. B. Fox, *Chem. Commun.*, 216 (1970).
(27) E. H. Staricco, J. E. Sicre, and H. J. Schumacher, *Z. Phys. Chem. (Frankfurt am Main)*, **35**, 122 (1962).

Application of the Partitioning of Electronic Energy in the CNDO Method to Heteronuclear Bonds. I. C—N, C=N, and C≡N

J. B. Moffat* and K. F. Tang

Department of Chemistry, University of Waterloo, Waterloo, Ontario, Canada N2L 3G1

(Received April 5, 1974)

Publication costs assisted by the National Research Council of Canada

The method of partitioning of total electronic energies within the CNDO/2 theory as suggested and applied to hydrocarbons by Fischer and Kollmar has been employed with a variety of molecules each containing one or more of C–N, C=N, and C≡N bonds. The two-center $E_{AB}{}^R$ terms appear to be characteristic of the AB bond, as anticipated, and good internal self-consistency of these values is obtained. The σ and π components in general reflect the usual qualitative picture of the nature of these three types of bonds.

1. Introduction

The interpretation of solutions, both nonempirical and semiempirical, of the Schrödinger equation for molecules is an important aspect of quantum chemistry. While the solutions themselves are both valuable and interesting, nevertheless, the chemist is in many instances more interested in relating the results to physical concepts commonly used in chemistry. One of these concepts is that of the bond. Methods of interpretation of wave functions and electronic energies of molecules which would assist in elucidating the nature of a chemical bond are therefore of paramount importance to the chemist. Further, it would be anticipated that if such methods were valid, quantities characteristic of a given bond in the molecule would emerge and could be related to measurable properties of the bond and reactivities of the molecule.

One approach to this problem was given by Ruedenberg[1] who devised a method for the partitioning of both the electron density and electronic energy of a molecule. This method was applied in this laboratory to the results of nonempirical calculations on diatomic molecules and small nitriles,[2] and it was shown that the intrabond interference

energy for a given bond was characteristic of that bond from molecule to molecule.[3]

The development of approximate self-consistent molecular orbital methods such as the CNDO technique of Pople, Santry, and Segal[4] has provided means of performing calculations on much larger molecules than may conveniently be done by more exact methods. A method for partitioning the energies obtained from such calculations has been suggested by Fischer and Kollmar[5] and applied to hydrocarbons.

The present work was initiated in an effort to determine the applicability of the Fischer–Kollmar (FK) method to heteronuclear bonds and in particular to those containing the CN single, double, or triple bond. In addition it is hoped that further information concerning the nature of the CN bond, and bonds in general, may result.

2. Theory

The ith molecular orbital is written as

$$\Psi_i = \sum_\mu C_{i\mu}\phi_\mu \tag{1}$$

with the summation being taken over all atomic orbitals ϕ_μ. Elements of the bond order matrix are given as

$$P_{\mu\nu} = \sum_i n_i C_{i\mu} C_{i\nu} \tag{2}$$

where n_i is the occupation number of the ith molecular orbital. The diagonal terms of the bond order matrix are grouped according to their atomic centers as

$$P_A = \sum_{\mu \epsilon A} P_{\mu\mu} \tag{3}$$

Within the Born–Oppenheimer approximation, the total electronic energy of a molecule is given by

$$E = 2\sum_i H_i + 2\sum_{i,j} J_{ij} - \sum_{i,j} K_{ij} + \sum_{A<B} \frac{Z_A Z_B}{R_{AB}} \tag{4}$$

where the terms, in order, represent the one-electron energy, the electronic repulsion energy, the electronic exchange energy, and the nuclear repulsion energy. The terms of eq 4 can be regrouped as one-center and two-center expressions.

$$E = \sum_A E_A + \sum_{A<B} E_{AB} \tag{5}$$

where

$$E_A = E_A{}^U + E_A{}^J + E_A{}^K \tag{6}$$

and

$$E_{AB} = E_{AB}{}^R + E_{AB}{}^V + E_{AB}{}^J + E_{AB}{}^K + E_{AB}{}^N \tag{7}$$

The individual terms in eq 6 are

$$E_A{}^U = \sum_{\mu \epsilon A} P_{\mu\mu} U_{\mu\mu} \tag{8}$$

where $U_{\mu\mu}$ is the one-electron energy of an electron in AO μ in the isolated atom, and $E_A{}^U$ is the total (one center) AO energy of the electrons on atom A

$$E_A{}^J = \tfrac{1}{2} P_A{}^2 \gamma_{AA} \tag{9}$$

where $E_A{}^J$ is the electronic repulsion of the electrons on atom A, and

$$E_A{}^K = \tfrac{1}{4}\gamma_{AA} \sum_{\substack{\mu\nu \\ \epsilon A}} = p_{\mu\nu}{}^2 \tag{10}$$

is the electronic exchange interaction of the electrons on atom A.

In eq 7, the two-center terms are

$$E_{AB}{}^R = 2 \sum_{\substack{\mu \epsilon A \\ \nu \epsilon B}} P_{\mu\nu}\beta_{\mu\nu}{}^0 S_{\mu\nu} \tag{11}$$

$$E_{AB}{}^V = -P_A V_{AB} - P_B V_{BA} \tag{12}$$

$$E_{AB}{}^J = P_A P_B \gamma_{AB} \tag{13}$$

$$E_{AB}{}^K = -\frac{1}{2}\gamma_{AB} \sum_{\substack{\mu \epsilon A \\ \nu \epsilon B}} p_{\mu\nu}{}^2 \tag{14}$$

$$E_{AB}{}^N = Z_A Z_B / R_{AB} \tag{15}$$

which represent the contribution of the resonance integrals to the energy of the A–B bond, the potential energy of the electrons on atom A in the field of nucleus B and vice versa, the repulsion of the electrons on atoms A and B, the electronic exchange interactions of the electrons on atoms A and B, and the nuclear repulsion energy of the nuclei A and B, respectively.

In Ruedenberg's original work[1] the concept of interference was introduced and was considered by him to be the "primordial source for the positive or negative stabilization energy which leads to chemical binding and antibinding." Interference contributions were obtained through the partitioning of electronic densities into quasiclassical and interference terms so that

$$\rho(x) = \rho^{CL}(x) + \rho^I(x) \tag{16}$$

where $\rho^{CL}(x)$ is the sum of atomic contributions, and the interference density, $\rho^I(x)$, has zero total population, that is

$$\rho^I(x)\, dV = 0 \tag{17}$$

One of the most convenient and interesting aspects of the Ruedenberg theory is that constructive interference ($\rho^I > 0$) leads to covalent bonding, while destructive interference ($\rho^I < 0$) leads to anticovalent bonding.

Within the framework of the LCAO–MO scheme and, in particular, the CNDO approximation for a closed shell molecule, the one-electron quasiclassical CNDO energy contains two parts, the one-center energies for a given atom A

$$E_A{}^U = \sum_\mu{}^A P_{\mu\mu} U_{\mu\mu}$$

$$= \sum_\mu{}^A 2 \sum_i^{occ} |C_{\mu i}|^2 \left(\mu \left| -\frac{1}{2}\nabla^2 - V_A \right| \mu \right) \tag{18}$$

and the two-center electron-nucleus attraction energy for the pair of atoms AB

$$E_{AB}{}^V = -P_{AA} V_{AB} - P_{BB} V_{BA}$$

$$= -\sum_\mu{}^A P_{\mu\mu} (\mu | V_B | \mu) - \sum_\nu{}^B P_{\nu\nu} (\nu | V_A | \nu)$$

$$= -2\sum_\mu{}^A \sum_i^{occ} |C_{\mu i}|^2 (\mu | V_B | \mu) -$$

$$2\sum_\nu{}^B \sum_i^{occ} |C_{\nu i}|^2 (\nu | V_A | \nu) \tag{19}$$

The one-electron interference energy for the pair of atoms AB is then

$$E_{AB}{}^R = 2\sum_\mu{}^A \sum_\nu{}^B P_{\mu\nu}\beta_{\mu\nu}$$

$$= 2\sum_\mu{}^A \sum_\nu{}^B 2 \sum_i^{occ} C_{\mu i}{}^* \beta_{AB}{}^0 S_{\mu\nu}$$

$$= 4\beta_{AB}{}^0 \sum_\mu{}^A \sum_\nu{}^B \sum_i^{occ} C_{\mu i}{}^* C_{\nu i} S_{\mu\nu} \tag{20}$$

TABLE I: Partitioned Two-Center Energies[a] of C–C Bonds in Nitriles

Molecule	R	E_{cc}^{V}	E_{cc}^{J}	E_{cc}^{K}	E_{cc}^{N}	E_{σ}^{R}	E_{π}^{R}	E_{cc}^{R}	E_{cc}	E_{cc}^{R}/E_{cc}
$(C_2H_5)CN$	2.925[b]	−10.532	5.253	−0.168	5.470			−1.081	−1.058	1.023
	2.785[b]	−10.815	5.323	−0.183	5.746			−1.232	−1.161	1.061
$NC(CH_3)CN$	2.759[b]	−10.849	5.317	−0.182	5.789	−1.097	−0.1464	−1.244	−1.160	1.072
CH_3CN	2.756[b]	−10.955	5.417	−0.189	5.806			−1.269	−1.191	1.065
$CH_3C{\equiv}CCN$	2.756[b]	−11.036	5.497	−0.191	5.807	−1.118	−0.1610	−1.279	−1.202	1.064
CH_2CHCN	2.698[c]	−11.098	5.468	−0.194	5.930			−1.325	−1.219	1.087
	2.694[b]	−11.112	5.476	−0.194	5.939			−1.327	−1.218	1.084
HC_3CN	2.612[d]	−11.356	5.585	−0.207	6.127	−1.212	−0.2198	−1.432	−1.283	1.116
$NCCN$	2.607[b]	−11.227	5.454	−0.207	6.135	−1.216	−0.2198	−1.436	−1.281	1.121
$CH_3C{\equiv}CCN$	2.606[b]	−11.525	5.743	−0.209	6.139	−1.215	−0.2288	−1.444	−1.296	1.114
$CH{\equiv}CCN$	2.603[b]	−11.381	5.597	−0.208	6.146	−1.216	−0.2236	−1.440	−1.286	1.120
$NCC{\equiv}CC{\equiv}CCN$	2.589[e]	−11.455	5.646	−0.211	6.180	−1.224	−0.2352	−1.458	−1.298	1.123
	2.589[e]	−11.545	5.737	−0.215	6.180	−1.221	−0.2452	−1.466	−1.309	1.120
$NCC{\equiv}CCN$	2.588[b]	−11.438	5.630	−0.211	6.180	−1.223	−0.2330	−1.456	−1.295	1.124
									mean	1.093 ± 0.070

[a] Bond distances and energies in au except where otherwise specified. [b] L. E. Sutton, "Tables of Interatomic Distances and Configuration in Molecules and Ions," (and supplement) The Chemical Society, London, 1965, 1958. [c] J. B. Moffat and R. J. Collins, *J. Mol. Spectrosc.*, 27, 252 (1968). [d] J. K. Tyler and J. Sheridan, *Trans. Faraday Soc.*, 59, 2661 (1963). [e] J. B. Moffat, *J. Chem. Eng. Data*, 14, 215 (1969). [f] J. B. Moffat, *Can. J. Chem.*, 48, 1820 (1970).

It is apparent from eq 20 that the bond orders $P_{\mu\nu}$ are related to the E_{AB}^{R} terms. In fact, when the bond order between two atoms is nonzero the interference energy will also be nonzero. However the interference energy between a given pair of atoms has the possibility to be either constructive or destructive, that is, positive or negative and is an energy term as opposed to a dimensionless quantity. As Ruedenberg[1] points out the interference density should not be in general interpreted as an overlap distribution. Fischer and Kollmar[5] have described such an analysis as a population analysis in which the individual terms are weighted with an energy factor $\beta_{\mu\nu}$.

Hence the E_{AB}^{R} term obtained from CNDO theory is directly related to the interference energy and should be a characteristic of the AB bond.

The calculations were performed on an IBM 360/75 computer using the CNDO/2 program of Pople and Segal[6] modified to permit calculation of the various energy terms in the partitioning method. The original methods for calculation of integrals as well as values of the parameters have been retained.

Results and Discussion

The energy terms of eq 6 and 7 are displayed in Tables I–V for a series of molecules each containing the nitrile bond. To facilitate comparison of the results, Table I gives the partitioned energies for the C–C bond, where the nitrile contains such a bond, Table II gives the terms for the C–H bond, if present, Table III shows the terms for the C≡C bond, where present, and Table IV contains the terms for the C≡N bond. The molecules are arranged in each table in decreasing order of the length of the bond being considered.

TABLE II: Partitioned Two-Center Energies of C–H Bonds in Nitriles

Molecule	R^a	E_{CH}^{R}	E_{C-H}	E_{CH}^{R}/E_{CH}
CH_3CCCN	2.092[b]	−0.7250	−0.7388	0.9813
CH_3CN	2.083[b]	−0.7297	−0.7417	0.9838
$(C_2H_5)CN$	2.063[b]	−0.7420	−0.7500	0.9893
$NC(CH_2)CN$	2.060[b]	−0.7195	−0.7145	1.007
CH_2CHCN	2.054[b]	−0.7540	−0.7570	0.9960
	2.053[c]	−0.7540	−0.7570	0.9960
HCN	2.014[d]	−0.7910	−0.7810	1.0128
	2.009[b]	−0.7930	−0.7815	1.0147
	2.000[f]	−0.7960	−0.7800	1.0205
$CHCCN$	1.998[b]	−0.7978	−0.7863	1.0170
				mean 1.0018 ± 0.0205

[a] See Table I for references.

TABLE III: Partitioned Two-Center Energies of C≡C Bonds in Nitriles

Molecule	R^a	E_{cc}^{V}	E_{cc}^{J}	E_{cc}^{K}	E_{cc}^{N}	E_{σ}^{R}	E_{π}^{R}	E_{cc}^{R}	E_{cc}	E_{cc}^{R}/E_{cc}
HC_2CN	2.278[b]	−12.766	6.419	−0.562	7.024	−1.361	−0.9904	−2.351	−2.236	1.051
	2.273[d]	−12.783	6.428	−0.564	7.038	−1.362	−0.9950	−2.357	−2.238	1.053
CH_3C_2CN	2.273[b]	−12.764	6.408	−0.541	7.038	−1.361	−0.9644	−2.326	−2.185	1.065
NCC_2CN	2.251[e]	−12.751	6.356	−0.535	7.109	−1.367	−0.9698	−2.337	−2.158	1.083
	2.249[b]	−12.758	6.359	−0.536	7.115	−1.369	−0.9700	−2.339	−2.159	1.083
NCC_2C_2CN	2.249[e]	−12.766	6.408	−0.541	7.033	−1.369	−0.9640	−2.333	−2.185	1.068
									mean	1.067 ± 0.016

[a] See Table I for references.

TABLE IV: Partitioned Two-Center Energies of C≡N Bonds in Nitriles

Molecule	R^a	E_{CN}^V	E_{CN}^J	E_{CN}^K	E_{CN}^N	E_σ^R	E_π^R	E_{CN}^R	E_{CN}	E_{CN}^R/E_{CN}
CH_2CHCN	2.204[c]	−16.961	8.399	−0.594	9.074	−1.362	−0.9483	−2.309	−2.171	1.064
CH_2CHCN	2.198[b]	−16.774	8.415	−0.595	9.100	−1.365	−0.9537	−2.319	−2.173	1.067
HC_2CN	2.189[b]	−16.744	8.363	−0.592	9.135	−1.365	−0.9620	−2.327	−2.165	1.075
$NC(CH_2)CN$	2.188[b]	−16.794	8.408	−0.603	9.139			−2.345	−2.195	1.068
HCN	2.187[f]	−16.865	8.483	−0.627	9.145	−1.367	−1.0076	−2.373	−2.237	1.061
CH_3CN	2.1866[b]	−16.839	8.451	−0.603	9.146	−1.367	−0.9655	−2.342	−2.187	1.071
HC_2CN	2.1864[d]	−16.759	8.371	−0.593	9.147			−2.332	−2.166	1.077
CH_3C_2CN	2.1864[b]	−16.784	8.398	−0.591	9.147	−1.369	−0.9634	−2.332	−2.162	1.079
NCCN	2.1864[b]	−16.715	8.328	−0.594	9.147	−1.370	−0.9676	−2.337	−2.171	1.076
	2.186[e]	−16.718	8.330	−0.594	9.149	−1.370	−0.9679	−2.338	−2.171	1.077
C_2H_5CN	2.1858[b]	−16.861	8.469	−0.605	9.150			−2.349	−2.195	1.071
HCN	2.183[b]	−16.885	8.494	−0.628	9.160	−1.369	−1.0100	−2.379	−2.238	1.063
HCN	2.179[d]	−16.908	8.506	−0.629	9.178	−1.374	−1.0153	−2.389	−2.242	1.066
NCC_2C_2CN	2.154[e]	−16.914	8.442	−0.596	9.284	−1.383	−0.9893	−2.372	−2.156	1.100
NCC_2CN	2.154[b]	−16.903	8.433	−0.597	9.284	−1.383	−0.9907	−2.374	−2.156	1.101
	2.154[e]	−16.903	8.426	−0.597	9.284	−1.386	−0.9920	−2.378	−2.168	1.097
										mean 1.071 ± 0.030

[a] See Table I for references.

TABLE V: Partitioned One-Center Energies of C and N in Nitriles

Molecule	E_C^U	E_C^J	E_C^K	E_N^U	E_N^J	E_N^K
$(C_2H_5)CN$	−9.401	4.728	−0.592	−18.639	9.517	−1.306
	−9.335	4.670	−0.585			
	−9.182	4.485	−0.563			
$NC(CH_2)CN$	−9.132	4.429	−0.556	−18.638	9.515	−1.306
	−9.309	4.650	−0.582			
	−9.131	4.428	−0.556			
CH_3CN	−9.438	4.765	−0.597	−18.620	9.497	−1.304
	−9.182	4.478	−0.562			
$CH_3C{\equiv}CCN$	−9.392	4.718	−0.590	−18.421	9.288	−1.282
	−9.349	4.656	−0.583			
	−9.545	4.871	−0.609			
$CH_2{=}CHCN$	−9.442	4.754	−0.596	−18.574	9.446	−1.299
	−9.352	4.681	−0.586			
	−9.199	4.495	−0.564			
$CH{\vdots}CCN$	−9.149	4.453	−0.558	−18.497	9.367	−1.290
	−9.375	4.692	−0.587			
	−9.562	4.863	−0.610			
NCCN	−9.154	4.459	−0.559	−18.397	9.261	−1.279
	−9.154	4.459	−0.559			
$NCC{\equiv}CC{\equiv}CCN$	−9.146	4.452	−0.558	−18.469	9.341	−1.287
	−9.414	4.734	−0.592			
	−9.348	4.665	−0.583			
$NCC{\equiv}CCN$	−9.159	4.465	−0.559	−18.424	9.293	−1.282
	−9.376	4.693	−0.587			

In each table it may be seen that the E_{AB}^R values for a given bond remain reasonably constant but there is, not unexpectedly, an increase in the value of E_{AB}^R as the internuclear distance decreases. There are some discrepancies, notably for $NCCH_2CN$ in Table II, for which no explanation, except that of an error in the nuclear configuration, can be offered at this time. Of course, each of the other two-center energy values in a given table display, in general, relatively constant values from molecule to molecule. It is not suggested that such quantities display no characteristics of the particular bond. Rather it is contended that the E_{AB}^R values may display more characteristics, and particularly those which are of most interest, of a chemical bond.

Both Fischer and Kollmar[5] and Dewar[7] have suggested that, in hydrocarbons, the partitioned quantity E_{AB}^R correlates well with E_{AB}, the total two-center energy for a given bond. To indicate such a correlation the last column of the tables for the C–C, C–H, C≡C, and C≡N bonds shows the ratio of E_{AB}^R to E_{AB} for the given bond. In all cases the ratio is constant to better than ±7%. Indeed, cancellation among the other terms contained in E_{AB} produces a correlation which is approximately one-to-one.

The relationship between E_{AB}^R and the internuclear dis-

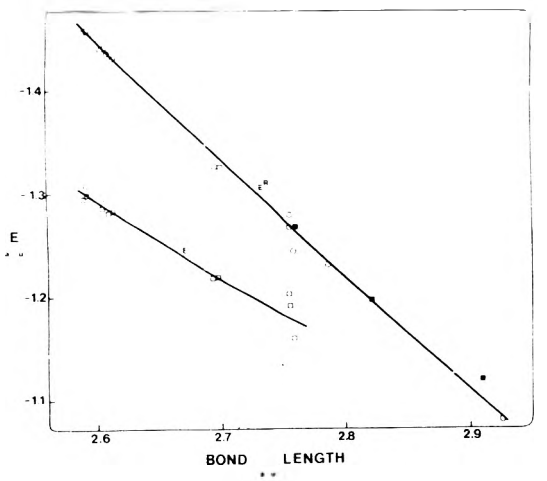

Figure 1. Dependence of E_{CC}^R and E_{CC} of C–C bond in nitriles on C–C internuclear distance; (O) E_{CC}^R, (□) E_{CC}, (■) E_{CC}^R of methylacetylene, propylene, and ethane.

tance is shown in Figure 1 for the C–C bond of the nitriles of Table I. For purposes of comparison E_{AB}^R values for the C–C bond in methylacetylene, propylene, and ethane are indicated in this figure. The almost linear correlation between E_{AB}^R and bond length provides further support for the use of E_{AB}^R as a measure of bond strength and bond characteristics. Similar correlations are found for C–H and C≡N values.

For completeness as well as purposes of comparison, the one-center energies (eq 6) for C and N in some of the nitriles are given in Table V. For a given atom the values of E^I, E^J, and E^K are quite constant over the set of molecules given.

It is of interest to compare values of E_{AB}^R for each of the three types of CN bonds, namely C–N, C=N, and C≡N. Unfortunately accurate experimental information on the nuclear configurations of molecules containing the CN single and double bonds is less available than for those containing the nitrile bond. Tables VI and VII give the values of E_{AB}^R, together with the σ and π components for some molecules containing CN single and double bonds, respectively. In the CN single bond compounds there is a small, but nonvanishing, contribution to the E_{AB}^R terms from molecular orbitals having only p-type atomic orbitals in the plane of the bond in question. For purposes of internal consistency these are classified as π components. In most cases such contributions are small except, of course, in the case where other π bonds are present in the molecule and some delocalization results. As indicated, with many of these compounds only geometries in the solid state were available. In some cases, the geometries were estimated from those of similar compounds. The E_{CN}^R values for the molecules containing either the amine or imine bond are much smaller than those for the nitrile bond, but again, as with those containing the latter bond, the values obtained for E_{CN}^R of a given type are relatively constant. In Table VI there are, however, some notable exceptions. These occur with dicyanodiamide and with pyridine. In the case of dicyanodiamide the are three apparent CN single bonds. However in the case of all of these bonds the π component of E_{CN}^R is substantially higher than for the case of ethylamine, for example. This suggests, not unexpectedly, that in the case of dicyanodiamide (and also with pyridine), there is sufficient π-electron delocalization from the imine and

TABLE VI: E_{AB}^R for Molecules Containing C–N Bond

Molecule	C–N bond length, Å	$-E_{CN}^R$, hartrees σ	π	Total
CH_3NH_2	1.474[a]			1.1037
$(CH_3)_2NH$	1.465[b]			1.1075
$(CH_3)_3N$	1.451[c]			1.1116
$C_2H_5NH_2$	1.47[d]	1.0444	0.0995	1.1439
CH_3NCH_2	1.44[e]	1.0470	0.1194	1.1664
$(NH_2)_2CNCN$	1.37[f]	1.0582	0.2835	1.3417
	1.28[f]	1.2618	0.2698	1.5316
	1.37[f]	1.0208	0.3200	1.3408
$(CH_3)_2NNH_2$	1.47[g]	1.0781	0.0683	1.1464
	1.47[g]	0.8213	0.3074	1.1287
C_5H_5N	1.34[h]	1.0808	0.3669	1.4477
H_2NCN (planar)	1.349[i]			1.3881
H_2NCN (nonplanar)	1.348[j]			1.3715
Pyrazine	1.334[k]			1.4500
Tetramethylpyrazine	1.30[l]	1.1071	0.3947	1.5018
Tetramethylpyrazine	1.32[l]	1.1065	0.3943	1.5009
Ethyleneimine	1.489[m]			0.9440

[a] D. R. Lide, Jr., *J. Chem. Phys.*, **27**, 343 (1957). [b] J. E. Wollrab and V. W. Laurie, *J. Chem. Phys.*, **48**, 5058 (1963). [c] J. E. Wollrab, *J. Chem. Phys.*, **52**, 1580 (1969). [d] P. W. Allen and L. E. Sutton, *Acta Crystallogr.*, **3**, 46 (1950). [e] K. V. L. N. Sastry and R. F. Curl, Jr., *J. Chem. Phys.*, **41**, 77 (1964). [f] E. W. Hughes, *J. Amer. Chem. Soc.*, **62**, 1258 (1940). [g] W. Beamer, *ibid.*, **70**, 2979 (1948). [h] B. Bak, L. Hansen-Nygaard and J. Rastrup-Anderson, *J. Mol. Spectrosc.*, **2**, 361 (1958). [i] D. R. Lide, Jr., *ibid.*, **8**, 153 (1962). [j] J. N. MacDonald, D. Taylor, and J. Sheridan, *ibid.*, **26**, 285 (1968). [k] M. Hackmeyer and J. L. Whitlen, *J. Chem. Phys.*, **54**, 3739 (1971). [l] D. T. Cromer, A. J. Hyde, and H. L. Ritter, *J. Amer. Chem. Soc.*, **73**, 5587 (1951). [m] R. Bonaccorsi, E. Scrocco, and J. Tomasi, *J. Chem. Phys.*, **52**, 5271 (1970).

TABLE VII: E_{AB}^R for Molecules Containing C=N Bond

Molecule	C=N bond length, A	$-E_{CN}^R$, hartrees σ	π	Total
$HNCH_2$	1.3[a]	1.0619	0.5392	1.6011
$H_2NCH_2^+$	1.36[b]	1.1630	0.3748	1.5378
NCH_2^-	1.36[b]	1.0458	0.4449	1.5907
$(NH_2)_2CNCN$	1.36[c]	1.1113	0.3134	1.4247
H_2CNN	1.32[d]	1.1741	0.3532	1.5273
CH_3NCH_2	1.3[e]	1.1293	0.5457	1.6750
Pyrazine	1.334[f]			1.4500
Tetramethylpyrazine	1.30[g]	1.1071	0.3947	1.5018
Tetramethylpyrazine	1.32[g]	1.1065	0.3943	1.5008
Pyridine	1.340[h]	1.0808	0.3669	1.4477

[a] J. M. Lehn and B. Munsch, *Theor. Chim. Acta*, **12**, 91 (1968). [b] R. D. Brown and A. Penfold, *Trans. Faraday Soc.*, **53**, 397 (1957). [c] E. W. Hughes, *J. Amer. Chem. Soc.*, **62**, 1258 (1940). [d] A. P. Cox, L. F. Thomas, and J. Sheridan, *Nature (London)*, **181**, 1000 (1958). [e] K. V. L. N. Sastry and R. F. Curl, Jr., *J. Chem. Phys.*, **41**, 77 (1964). [f] M. Hackmeyer and J. L. Whitlen, *J. Chem. Phys.*, **54**, 3739 (1971). [g] D. T. Cromer, A. J. Hyde, and H. L. Ritter, *J. Amer. Chem. Soc.*, **73**, 5587 (1951). [h] B. Bak, L. Hansen-Nygaard, and J. Rastrup-Anderson, *J. Mol. Spectrosc.*, **2**, 361 (1958).

cyano bonds which are present to alter the character of the CN bonds which are classically represented as single bonds. In the case of those molecules containing C=N bonds (Table VII) the total E_{CN}^R values are again reasonably constant from molecule to molecule. It is to be noticed that the

TABLE VIII: $E_{AB}{}^{R}$ of C_3HN and C_3H_5N[a]

	$C_1H{\equiv}C_2{-}C_3N$			
	C_1	C_2	C_3	N
C_2	*−2.351*			
C_3	0.036	*−1.446*		
N	0.000	0.011	*−2.327*	
H	*−0.798*	0.012	−0.001	0.000

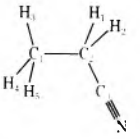

	C_1	C_2	C_3	N	H_1	H_2	H_3	H_4
C_2	*−1.081*							
C_3	−0.025	*−1.232*						
N	0.001	0.015	*−2.349*					
H_1	−0.003	*−0.729*	−0.008	0.001				
H_2	−0.003	*−0.729*	−0.008	0.001	0.003			
H_3	*−0.743*	−0.001	−0.002	0.000	0.002	0.002		
H_4	*−0.744*	−0.002	0.002	−0.000	0.002	0.002	0.003	
H_5	*−0.744*	−0.002	0.002	−0.000	−0.002	0.002	0.003	0.003

[a] Italicized terms correspond to $E_{AB}{}^{R}$ values between bonding atoms.

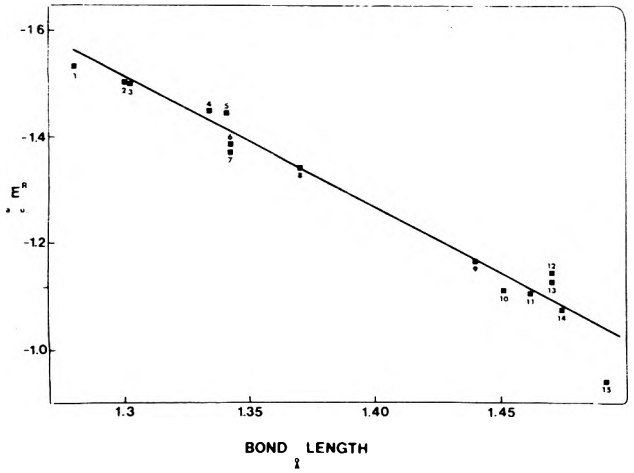

Figure 2. Variation of E^R with C–N bond length: (1) $(NH_2)_2CNCN$, (2) tetramethylpyrazine, (3) tetramethylpyrazine, (4) pyrazine, (5) pyridine, (6) H_2NCN (planar), (7) H_2NCN (nonplanar), (8) $(NH_2)_2CNCN$, (9) CH_3NCH_2, (10) $(CH_3)_3N$, (11) $(CH_3)_2NH$, (12) $C_2H_5NH_2$, $(CH_3)_2NNH_2$, (13) $(CH_3)_2NNH_2$, (14) CH_3NH_2, (15) CH_2CH_2N.

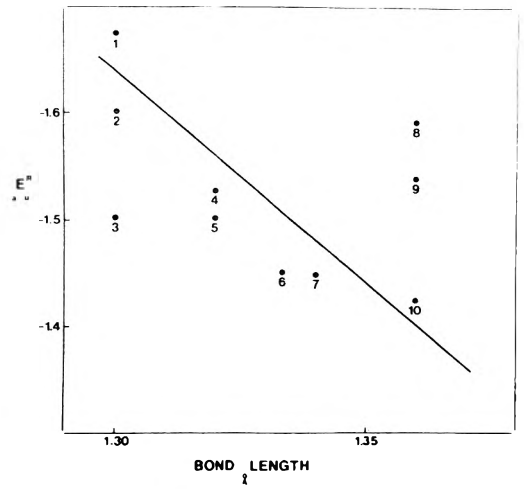

Figure 3. Variation of E^R with C=N bond length: (1) CH_3NCH_2, (2) $HNCH_2$, (3) tetramethylpyrazine, (4) H_2CNN, (5) tetramethylpyrazine, (6) pyrazine, (7) pyridine, (8) NCH_2^-, (9) $H_2NCH_2^+$, (10) $(NH_2)_2CNCN$.

$E_{CN}{}^{R}$ values for some of the C–N bonds in dicyanodiamide and the C–N bond in pyridine are similar to those found for C=N bonds as given in Table VII.

As is to be expected the E^R values increase in absolute magnitude as one passes from the C–N single bond through the double bond to the nitrile bond. In addition the absolute magnitude of the π contributions to E^R increase, in general, in the same manner. However the σ contributions are approximately the same for the C–N and C=N bonds while they are somewhat higher for the C≡N bond. Figures 2 and 3 show the correlation of E^R values with bond lengths for C–N and C=N bonds, respectively. As has been mentioned previously, some uncertainty as to the geometry exists in many of these examples, so it is difficult to determine the extent to which the deviations in these figures can be attributed to characteristics of the bond itself.

Comparison of the E^R values for the C≡C bond (Table III) with those for the C≡N bond (Table IV) reveals a strong similarity not only in the total values but also in the σ and π components. However, it is somewhat more difficult to extend such a comparison to the C–C and C–N bonds since the range of character of such bonds appears to be much greater than in the case of the triple bonds. However if the C–C bond most remote from the nitrile bond in ethyl cyanide is assumed to be a reasonably "pure" single bond, and similarly the C–N bond in methylamine, then it is seen that the E^R values are in good agreement as might be expected.

Finally, Table VIII provides the total $E_{AB}{}^{R}$ values of two

typical molecules for all atomic pairs in the molecules. The values for the directly bonded pairs are italicized. It may readily be seen that E^R values for pairs of atoms not directly bonded to each other are much smaller than those for the directly bonded pairs. This provides additional support for the use of $E_{AB}{}^R$ as characteristic of the bond. While in many cases $E_{AB}{}^R$ values for pairs of nonbonded atoms can be neglected, such values of $E_{AB}{}^R$ can be quite useful in elucidating the mechanism of chemical reactions.

The results of the present work provide reasonable evidence to support the extension of the scheme of Fischer and Kollmar[5] for the partitioning of total electronic energy to molecules other than hydrocarbons. In addition, the present and future use of such partitioned quantities, particularly that of $E_{AB}{}^R$, in elucidating the nature and characteristics of a chemical bond have been demonstrated. Finally, as England and Gordon[8] have pointed out, E^R is in fact directly related to Ruedenberg's interference energy, so that the fact that intraatomic interference energies calculated by semiempirical methods show the same behavior as those obtained with *ab initio* methods is gratifying. More work needs to be done in relating the partitioned quantities from semiempirical calculations with those from purely theoretical ones. Indeed, the existence of a relationship between the two for quantities such as $E_{AB}{}^R$ opens up the possibility of the development of a semiempirical method based on pairs of atoms, *i.e.*, bonds, and calibrated by means of the results of *ab initio* calculations.

Acknowledgments. Financial support from the National Research Council of Canada is gratefully acknowledged. One of us (K.F.T.) wishes to acknowledge with thanks a fellowship (1969–1970) received from the Province of Ontario and a bursary (1970–1971) from the National Research Council of Canada.

References and Notes

(1) K. Ruedenberg, *Rev. Mod. Phys.*, **34**, 326 (1962).
(2) J. B. Moffat and H. E. Popkie, *Int. J. Quantum Chem.*, **2**, 565 (1968).
(3) J. B. Moffat and H. E. Popkie, *Chem. Phys. Lett.*, **5**, 331 (1970).
(4) J. A. Pople, D. P. Santry, and G. A. Segal, *J. Chem. Phys.*, **43**, S129 (1965).
(5) H. Fischer and H. Kollmar, *Theor. Chim. Acta*, **16**, 163 (1970).
(6) Quantum Chemistry Program Exchange No. 142.
(7) M. J. S. Dewar and D. H. Lo, *J. Amer. Chem. Soc.*, **93**, 7201 (1971).
(8) W. England and M. S. Gordon, *J. Amer. Chem. Soc.*, **94**, 5168 (1972), and preceding papers.

Dielectric Studies of Molecular Association. Concentration Dependence of Dipole Moment of 1-Octanol in Solution

Colin Campbell, George Brink, and Leslie Glasser*

Department of Chemistry, Rhodes University, Grahamstown, 6140, South Africa

(Received January 24, 1974; Revised Manuscript Received November 4, 1974)

Publication costs assisted by Rhodes University

The permittivities at 2 MHz and 25° for 1-octanol in carbon tetrachloride, benzene, and cyclohexane solutions have been measured over the entire alcohol concentration range, with particular attention being paid to the range below 0.1 *M*. By use of the Kirkwood–Fröhlich equation the apparent dipole moment of the alcohol as a function of concentration has been evaluated; using this concentration dependence and infrared absorption results, the natures of the proposed associated species are considered. Equilibrium constants have been determined for a monomer–dimer–trimer equilibrium model of the alcohol self-association at low concentrations; the association follows a general pattern: monomer–small, high dipole moment polymer–low dipole moment cyclic polymer–high dipole moment polymers.

Introduction

The manner in which solute molecules in solution associate with one another and with solvent molecules has a marked effect on the physical properties of solutions. In this study we are concerned with the intermolecular behavior of alcohols in nonaqueous solvents. 1-Octanol was selected as being representative of medium length, straight chain, primary alcohols. Branched chain alcohols may have different properties in solutions as a result of possible steric interference in intermolecular interactions; some results relating to branched chain alcohols will appear in a later communication.

Many physical techniques may be used to study intermolecular behavior in solution. However, it is clear that no single method gives a complete understanding of the nature of the intermolecular interactions. In particular, infrared and nmr spectroscopies, which are commonly used, give little information concerning the *alignment* of neighboring solute molecules. Such information is vital for full understanding of the solution physical properties since, although it is accepted that hydrogen-bonded polymers of varying size are formed, little is known about the size and configuration of such species. To examine such parameters, we have measured the permittivities of the solution and, by

use of a generalized form of the Kirkwood–Fröhlich[1] equation, have calculated the apparent (bulk) dipole moment as a function of concentration; this gives information on the relative alignment of the molecular dipoles in associated species. Infrared spectroscopy has been used in conjunction with dielectric measurements to provide qualitative, but unambiguous, information on the appearance of new, small-polymer species with increasing concentration. The application of the two techniques in this complementary fashion has been invaluable in clarifying the data analysis.

Carbon tetrachloride, benzene, and cyclohexane have been chosen as representative nonpolar solvents. Although there can be no specific molecular interactions between the alcohol and these solvent molecules, their different electronic polarizabilities lead to different solvent behavior.

Dielectric data for normal alcohols in various solvents have previously been given by Ibbitson and Moore;[2] however, their data cover a limited concentration range and were not fully analyzed. Recently, further data for 1-heptanol in carbon tetrachloride at varying temperatures were published by Bordewijk, Kunst, and Rip.[3] We have used the model developed by Bordewijk, *et al.*, to obtain rough values for dipole moments of associated species and equilibrium constants for their formation from the concentration dependence of the apparent static dipole moment. An interesting nondielectric method for extracting the same information has been given by Tucker and Becker[4] for *tert*-butyl alcohol in hexadecane; this involves the use of vapor pressure measurements. Many investigators have used nuclear magnetic resonance chemical shifts in studying alcohol association and a comprehensive review on this subject has been given by Brodskii, *et al.*,[5] and by Davis and Deb.[6] However, in general, the concentration dependence of the chemical shift in the alcohols gives such a featureless curve compared, *e.g.*, with that of carboxylic acids[7] that little useful information can be extracted, except in special cases where only a single associated species can be assumed to be present.

Experimental Section

The solvents used were of spectroscopic grade. They were refluxed over P_2O_5 prior to distillation, and stored over molecular sieve (type 4A) for a short period before use. The 1-octanol (Aldrich Chemical Co., puriss grade) was predried over molecular sieve and fractionally distilled over CaH_2 using a spinning-band column; this removed the small amount of carbonyl impurity, as observed in infrared absorption analysis. The solvents and alcohol were checked for purity using gas chromatography, infrared spectroscopy, and refractive index measurements.

Static permittivity measurements (at 2 MHz, well below the dielectric absorption frequency range) were made using a W.T.W. dipolmeter (Model DM 01), with a DFL 1 cell for concentrations up to about 0.1 *M*, and a DFL 2 cell for higher concentrations. The permittivity of the pure alcohol was checked in the DFL 2 cell using a General Radio 716C bridge at 10 kHz. The cells were thermostatted through the outer water jacket using a water bath controlled to ±0.02°. The two cells were calibrated using carbon tetrachloride, benzene, and cyclohexane; and carbon tetrachloride, cyclohexane, and butyl ether, respectively, against published permittivities.[8]

Infrared spectra were recorded on a Beckman IR-8 spectrophotometer; frequencies are accurate to ±5 cm^{-1} for the –OH stretching vibrations. A variable path-length cell was used to compensate for solvent absorption, and the solvent cell was thermostatted at 25.0°.

Results

The low-frequency permittivities for 1-octanol in carbon tetrachloride, in benzene, and in cyclohexane at 25.0° are deposited as supplementary material.[9] The precision of the permittivity measurements is better than 0.0001 units at the lower concentrations (DFL 1 cell) and about 0.0004 units at the higher concentrations (DFL 2 cell).

The apparent dipole moments are calculated using a generalized form of the Kirkwood–Fröhlich equation[1] which, for the case of a dipolar material in a nonpolar medium, may be written (in cgs units):

$$\mu_{app}^2 \equiv g\mu_0^2 = \frac{9kT}{4\pi L}\frac{M_2}{\rho w_2}\frac{(\epsilon - \epsilon_\infty)(2\epsilon + \epsilon_\infty)}{\epsilon(\epsilon_\infty + 2)^2} \quad (1)$$

where k, L, T, M, ρ, and ϵ have their usual meanings, w refers to mass fraction, and subscript 2 refers to the solute. ϵ_∞ is the limiting high-frequency permittivity of the solution and is often taken as n_D^2 (Maxwell's relationship) or as mn_D^2, to include an approximation for the atomic polarization where m has a value from 1.05 to 1.15. The apparent dipole moment, μ_{app}, and the gas-phase value μ_0, are related through the factor g. A value of g greater than unity is interpreted as being due to a parallel alignment of near-neighbor dipoles, and a value of g less than unity is ascribed to an antiparallel arrangement.

The choice of a value for ϵ_∞ presents a problem since, if we select $\epsilon_\infty = n_D^2$ for each solution, we find that the calculated values of g are quite meaningless. We have therefore proceeded as follows. The specific refraction

$$R_i = (n_i n_i^2 - 1)/(n_i n_i^2 + 2)\rho_i \quad (2)$$

is, to a good approximation, an additive quantity,[10] therefore, for a solution we may write

$$R = w_1 R_1 + w_2 R_2 \quad (3)$$

For the pure 1-octanol, n_2^2 was taken to be $1.05\ n_D^2 = 2.1396$; for the solvents n_1^2 was taken as the intercept obtained from a least-squares fit of the low concentration permittivity data.

Figure 1 shows the concentration dependence of μ_{app}^2 of 1-octanol in the three solvents, with a logarithmic scale along the abscissa. This scale permits a condensation into a single graph of the interesting behavior of μ_{app}^2 over the whole concentration range. For the purposes of the graph only μ_{app}^2 at the lowest concentrations has been calculated from values of ϵ smoothed using a cubic polynomial; this was done because of the extreme sensitivity of the term $(\epsilon - \epsilon_\infty)$ in eq 1 to small errors in ϵ. The values of μ_{app}^2 in the low concentration range, calculated from *unsmoothed* experimental values of ϵ, are shown in Figures 2–4, using a linear concentration scale on the graphs. The solid lines in Figures 2–4 represent least-squares fits for monomer–dimer–trimer models; these are discussed below.

The arrows in Figures 1–4 indicate the concentrations at which the infrared spectra depicted in Figure 5 were recorded; these spectra lie in the fundamental –OH stretching region.

Discussion

In the infrared spectra of the alcohol solutions at the lowest concentration in each of the three solvents (Figure

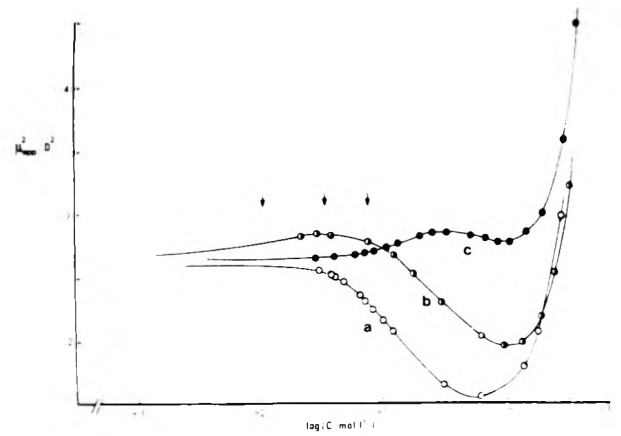

Figure 1. μ_{app}^2 *vs.* the logarithm of solute concentrations in *M* for 1-octanol in (a) cyclohexane, (b) carbon tetrachloride, and (c) benzene solutions at 25.0°. At the lowest concentrations, where data points are not given, μ_{app}^2 is calculated from smoothed values of ϵ. The arrows indicate the concentrations at which the infrared spectra in Figure 5 were recorded.

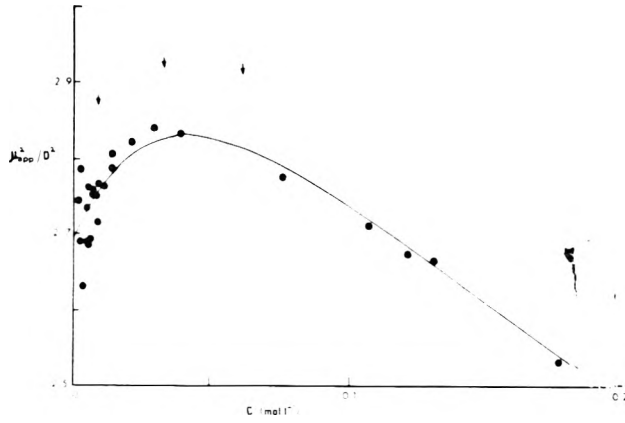

Figure 2. μ_{app}^2 *vs.* concentration in *M* for 1-octanol in carbon tetrachloride at low concentrations. Discrete points are experimental values; the continuous line is a least-squares fit assuming a monomer–dimer–trimer model. The arrows indicate the concentrations at which the infrared spectra in Figure 5 were recorded.

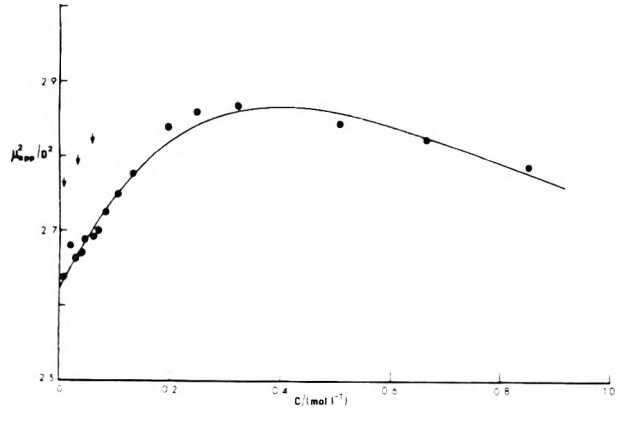

Figure 3. μ_{app}^2 *vs.* concentration in *M* for 1-octano in benzene at low concentrations. See legend to Figure 2 for other details.

5), only a single –OH stretching vibration (3650 cm^{-1}) is observed when a 1-mm sample cell is used; this is the nonbonded –OH stretching vibration. This does not mean that associated species are entirely absent, but rather that their

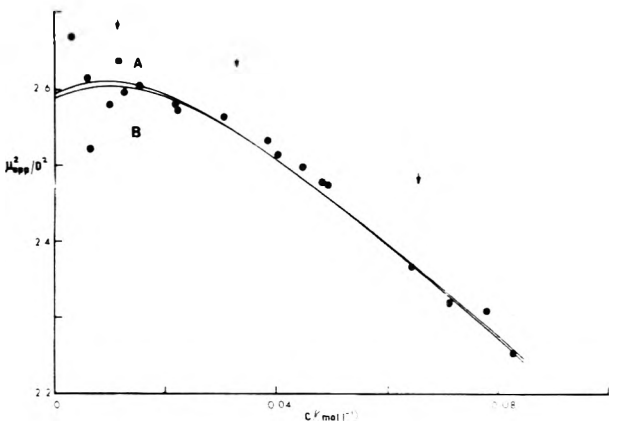

Figure 4. μ_{app}^2 *vs.* concentration in *M* for 1-octanol in cyclohexane at low concentrations. See legend to Figure 2 for other details; lines A and B represent two different least-squares fits to the data (see text).

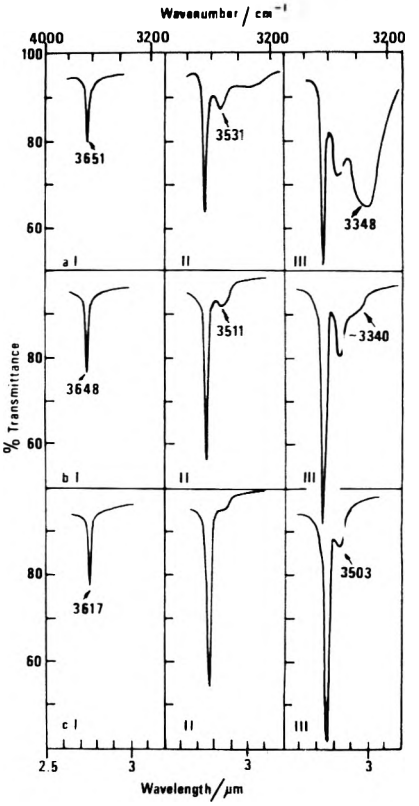

Figure 5. Infrared spectra at 25.0° of 1-octanol in (a) cyclohexane, (b) carbon tetrachloride, and (c) benzene at concentrations: (I) 0.0107 *M*, (II) 0.0339 *M*, and (III) 0.0650 *M*, using a 1-mm sample cell.

concentrations are too small to be observed under the experimental conditions. As the concentration is increased, two additional bands appear, in the region of 3500 and 3350 cm^{-1}. A significant point is the rate at which the low-frequency 3350-cm^{-1} band increases with concentration compared to the 3500-cm^{-1} band in the various solvents. In cyclohexane solution the low-frequency band increases rapidly; in carbon tetrachloride solution it increases more slowly; in benzene solution this band is absent at the concentrations shown but does appear at higher concentrations. In addition, the peak near 3500 cm^{-1} grows more slowly in benzene solution than in the other two solvents.

The three peaks are usually attributed to monomer, dimer, and higher polymeric hydrogen-bonded species, respectively.[11,12] van Ness, *et al.*,[11] consider the dimer to be double bonded (cyclic) and the polymers to be linear (noncyclic). Bellamy and Pace,[12] however, from an analysis of data similar to that of van Ness, *et al.*, conclude that the dimer has an open (noncyclic) configuration, *i.e.*, one hydrogen-bonded hydroxyl proton and one free hydroxyl proton; the nonbonded hydroxyl proton of the open dimer also absorbs in the region of the monomer alcohol species. Tucker and Becker,[4] from an analysis of infrared data for *tert*-butyl alcohol in hexadecane, favor an open trimer as the first associated species. Fletcher and Heller,[13] from an infrared study of the self-association of 1-octanol in *n*-decane, conclude that the results are explained by monomer and tetramer species only, although, from Table III of ref 13, monomer–dimer–tetramer and monomer–trimer–tetramer models also fit the data well.

In carbon tetrachloride solution, the appearance of the "dimer" band in the infrared spectrum (Figure 5) is associated with an increase in μ_{app}^2 (Figures 1 and 2); with further increase in concentration μ_{app}^2 decreases, and this is accompanied by the first appearance of the "polymer" band in the infrared spectrum. The initial increase in μ_{app}^2 indicates a *parallel* alignment of dipoles, as a result of hydrogen bonding, with an enhancement of apparent dipole moment. The infrared peak at about 3511 cm^{-1} consequently arises from an open dimer or perhaps an open trimer, but certainly not from a closed, cyclic species. The subsequent decrease in μ_{app}^2 with concentration then represents a situation where the associated species are still small (because concentrations are still small), but now have a low apparent dipole moment, perhaps cyclic trimers or tetramers. This behavior is accompanied by the appearance of a peak near 3340 cm^{-1} in the infrared spectrum. If the concentration of the alcohol is increased still further, μ_{app}^2 again increases, due to an associated species of high apparent dipole moment, perhaps chains of four or more alcohol molecules. No additional peaks appear in the –OH stretching region of the infrared spectra to accompany this behavior but the lowest frequency peak grows in intensity compared with the other two peaks. Apparently, the force constants of the O–H bonds in the various types of hydrogen-bonded polymers, the shortest (dimer) excepted, are not much different and give rise to a broad peak centered at about 3340 cm^{-1}. The dimer and polymer peaks grow less rapidly with concentration in carbon tetrachloride solutions than in cyclohexane solutions. Evidently the monomer is stabilized by an association with the carbon tetrachloride; Fletcher[14] has postulated a 1:1 complex between the 1-octanol monomers and carbon tetrachloride.

The dielectric behavior of 1-octanol in benzene solution is similar to that in carbon tetrachloride. However, the formation of the first high dipole moment species is delayed, as shown both by the dipole moment behavior depicted in Figures 1 and 3 and by the infrared spectra in Figure 5. The infrared spectra show that the appearance of the low dipole moment species is also delayed. This suggests that the alcohol monomer is stabilized by association with the solvent, benzene. Woolley and Hepler,[15] using thermochemical data, have found similarly that phenol is more self-associated in cyclohexane than in carbon tetrachloride, and that the self-association is even smaller in benzene solutions.

Solutions of 1-octanol in cyclohexane present an interesting situation. Apparently, the monomer is little stabilized by interaction with this nonpolarizable solvent, nor is the open, high dipole moment species. This results in the early appearance of the higher polymeric absorption band in the infrared spectrum which represents a low dipole moment, presumably cyclic, species. The combined effect of the nearly simultaneous appearance of a high and a low dipole moment species results in a balance which keeps μ_{app}^2 approximately constant until the low dipole moment species dominates the equilibrium, as shown in Figures 1 and 4. Ibbitson and Moore[2] have suggested that μ_{app}^2 remains constant at low concentrations because alcohol association is delayed until the concentration is sufficiently great for cyclic higher polymers to form. This suggestion was based on the argument that the free end of an open alcohol dimer would not be stabilized by an interaction with cyclohexane as might be the case in the more polarizable carbon tetrachloride or, more particularly, with benzene molecules. It is, however, clear from the infrared results that the balance suggested above pertains, and that the closed higher polymers appear more-or-less simultaneously with the open dimer (or trimer) in cyclohexane. Although we do not present the results here, we have found that the behavior of the alcohol in *n*-hexane solution is almost identical with that in cyclohexane. These two saturated alkanes would be expected to exhibit similar solvent behavior. Fletcher and Heller[13] conclude, from a near-infrared analysis, that the self-association of 1-octanol in *n*-decane over the *whole* concentration range can be explained in terms of monomer and only two associated species, *viz.*, open tetramer and closed tetramer. However, from our present dielectric and infrared data for 1-octanol in cyclohexane, it is evident that *at least* two associated species exist from about 0.03 *M* and *at least* one additional species must be present to account for the increasing dipole moment for concentrations greater than about 0.5 *M*. It is not expected that the behavior in *n*-decane would be markedly different from that observed in cyclohexane.

The dielectric behavior in all three solvents at the lower concentrations can be accounted for using at least two associated alcohol species. The first polymer species may be an open dimer for which μ_{app}^2 is greater than μ_{app}^2 for the monomer; an alternative is an open trimer, as suggested by Tucker and Becker[4] for *tert*-butyl alcohol in hexadecane. The next species, with low dipole moment, might be a cyclic trimer or tetramer. The infrared results probably exclude a cyclic dimer at these concentrations. Each hydrogen bond in a cyclic dimer, because of its nonlinearity, would be weaker than the bond in an open dimer. We would then expect to see a peak at frequencies between the monomer and open dimer (trimer) bands, but this is absent. Finally, at high concentrations, there appears a long, open-chain polymer, or perhaps a special configuration of a cyclic polymer having a large dipole moment, as suggested by Bordewijk, Gransch, and Böttcher.[16]

We may explain the increasing extent of polymerization of the alcohol molecules as a function of concentration using thermodynamic arguments; thus, the Gibbs function is reduced by the enthalpy release on hydrogen bonding but increased by the configurational entropy decrease which occurs with the greater degree of intermolecular bonding. The presence of solute–solvent interactions partially offsets the effects of solute–solute interactions; this is most apparent at the lowest concentrations, where the monomer is the most stable species. At higher concentrations

an open dimer (or trimer) forms, but there does not appear to be a tendency to form a closed dimer, implying that the enthalpy gain from the two weak hydrogen bonds which would form cannot compensate for the entropy decrease involved. It is only when a larger polymer (trimer or tetramer, perhaps) is formed that cyclization is favored. Furthermore, such cyclization will be hindered in polarizable solvents, such as carbon tetrachloride and benzene as compared with more inert solvents such as cyclohexane (as shown by the delay in the decrease of μ_{app}^2 in benzene and in carbon tetrachloride solutions). Finally, for longer chain polymers, the enthalpy gain *per monomer molecule* on cyclization reduces so that open chains, with high dipole moments, can be expected to be stabilized in a favorable environment, as has been argued for HF.[17]

We now utilize the above ideas in a model to obtain a quantitative measure of the dipole moments of the associated species and equilibrium constants for their formation. For example, if we consider a monomer–dimer–trimer equilibrium, we may write

$$2(\text{monomer}) \longrightarrow \text{dimer}$$

$$3(\text{monomer}) \longrightarrow \text{trimer}$$

with corresponding equilibrium constants, K_2 and K_3. From this may be developed[3]

$$\mu_{app}^2 = \frac{1}{c}\left[c_1\mu_1^2 + c_2\mu_2^2 + c_3\mu_3^2\right] \quad (4)$$

or

$$\mu_{app}^2 = \frac{1}{c}\left[c_1\mu_1^2 + 2K_2c_1^2g_2\mu_1^2 + 3K_3c_1^3g_3\mu_1^2\right] \quad (5)$$

where subscripts 1, 2, and 3 refer to monomer, dimer, and trimer, respectively, c_i represents the concentration of these species, and c the total alcohol concentration. From the mass balance

$$c = c_1 + 2c_2 + 3c_3 = c_1 + 2K_2c_1^2 + 3K_3c_1^3 \quad (6)$$

For any general model these equations have the form[18]

$$\mu_{app}^2 = \frac{1}{c}\sum_i iK_i(c_1)^i g_i\mu_1^2 \quad (7)$$

and

$$c = \sum_i iK_i(c_1)^i \quad (8)$$

We may use eq 7 and 8 to obtain values for the K's and μ's by a least-squares method. We have used a simplex least-squares procedure described by Deming and Morgan,[19] where we optimized the variables only over the lower concentration range; the species which cause the final increase in apparent dipole moment have not been included, for their influence would swamp the interesting low concentration behavior. The model considered has the form: monomer–open dimer–cyclic trimer. To simplify the problem, since we have five unknown parameters, we have assumed that the dipole moment of the cyclic trimer is zero. The results are summarized in Table I and the solid lines in Figures 2–4 show the calculated μ_{app}^2 for the model in benzene, carbon tetrachloride, and cyclohexane solutions, respectively. The maximum solution concentrations used in each fit are noted in Table I.

During the least-squares optimization it became apparent that the minimum was extremely shallow, especially for cyclohexane solution. Consequently, different sets of parameters could possibly be found with about the same error. In Table I two sets of parameters are given for the cyclohexane solutions, labeled A and B, with nearly the same errors of fit. A visual inspection of the two fits in Figure 4 indicates that both are equally acceptable. Our curve-fitting experience on these systems shows that a *unique* set of parameters can be obtained if there is no error in the data, i.e., fitting synthesized data. A nearly unique set of parameters is also apparently possible if the intercept at zero concentration, μ_1^2, is well defined, when there is not much scatter in the data. In the cyclohexane data this is clearly *not* true and different combinations of the parameters can be found which give approximately the same error of fit. The intercept for the carbon tetrachloride data is better defined and the intercept for the benzene data is well defined, consequently in these two cases the minimum found during the curve fitting was less shallow. Bordewijk, *et al.*,[3] have described similar problems of nonunique sets of parameters in fitting their data for solutions of 1-heptanol in carbon tetrachloride; to obtain consistent values for their results at different temperatures they have arbitrarily fixed μ_1^2 and g_2. Our data extend to lower concentrations, so that μ_1^2 is better defined. However, there is still uncertainty in this value because of the scatter of the data at low concentrations.

TABLE I: Parameters from Least-Squares Fit for Monomer–Open Dimer–Closed Trimer ($g_3 = 0$) Models for 1-Octanol in Solution at 25°

Solvent	c_{max},[a] M		μ_1^2, D^2	K_2[b]	K_3[b]	g_2	σ[c]
			Monomer–dimer–trimer				
Cyclohexane	0.118	(A)	2.596	1.113	24.28	1.593	0.028
		(B)	2.589	0.424	19.48	2.400	0.027
Carbon tetrachloride	0.297		2.693	1.268	12.02	2.164	0.031
Benzene	0.850		2.624	0.202	0.258	2.414	0.013

[a] Maximum concentration of data used in least-squares fit of model. [b] Equilbrium constants based on concentration units of M. [c] Standard deviation of fit calculated from μ_{calcd}^2 and μ_{obsd}^2.

The values determined for benzene solution are subject to the influence of an additional high dipole moment species which is clearly present in the latter part of the concentration range, but has not been allowed for in the analysis. It is, however, not physically meaningful to fit the data in the region where only monomer and dimer are expected to be present because the parameters μ_2^2 and K_2 are then not independent and only the product $\mu_2^2K_2$ can be determined.

The results in Table I confirm our expectations about the behavior of 1-octanol in the three solvents; K_2 and K_3 in benzene are small, indicating a relatively strong interaction between the alcohol and solvent and, consequently, a smaller opportunity for self-association. The *combined* effects of K_2 and K_3 in cyclohexane indicate a greater degree of self-association of the alcohol than in carbon tetrachloride solutions. The smaller K_2 found in cyclohexane solutions compared to carbon tetrachloride solution may be due to the inherent uncertainty in the least-squares fit. The infrared results in Figure 5, however, seem to indicate that the rate of dimer formation in cyclohexane *is* about the same as in carbon tetrachloride; the extent of trimer formation is clearly greater in cyclohexane than in carbon tetrachloride. We do not attempt to rationalize the values of g_2 in Table IV; they depend on the details of the O–H $\cdots$ O interaction between two alcohol molecules *and* on

the O–H · · · solvent interaction of the "open" end of the dimer.

The monomer–dimer–trimer model considered here is highly idealized and the parameters obtained from the mathematical fit must be treated with caution since they are only mathematical parameters. Bordewijk,[3] *et al.*, have shown that a monomer–dimer–trimer model results in the same error of fit as a monomer–dimer–tetramer model. The value of this type of mathematical procedure is that it does give some quantitative feeling for the relative magnitudes of the parameters involved. We have also tried fitting 1–3–4 and 1–2–4 models but the fits are slightly worse than those given in Table I, except for cyclohexane solutions where the error of fit is about the same.

Tucker and Becker,[4] using vapor pressure measurements, have postulated a monomer–open trimer–large cyclic polymer for *tert*-butyl alcohol in hexadecane. Aveyard, *et al.*,[20] using overtone O–H stretching frequency measurements and vapor pressure osmometer measurements of 1-octanol in *n*-octane, note that at least two associated species exist up to 0.13 *M* and they favor the monomer–dimer–tetramer model.

Because of the large number of unknown parameters and the scatter in the data, it is difficult or perhaps impossible to obtain unique and physically acceptable values for both the equilibrium constants and the Kirkwood *g* factor. There are many experiments which have the potential to yield equilibrium constants, but the dielectric method is the only one which can yield the liquid structure-related *g* value. Thus, if equilibrium constants are available from other sources, they may be used in the curve fitting to obtain the important *g* values. The paper by Fletcher and Heller[13] gives equilibrium constants for various associated models for 1-octanol in *n*-decane. If we assume, as before, that the solvent properties of *n*-decane are similar to those of cyclohexane, then we can apply the equilibrium constants obtained by Heller and Fletcher to our data. We have interpolated the equilibrium constant in Table III of ref 13 to 25° for the 1–2–4 and 1–3–4 models. The dimer value for the 1–2–4 model is unfortunately uncertain and we have therefore used only the equilibrium constants for the 1–3–4 model. Applying these to our cyclohexane data we obtain a value of 2.8 for g_3 (the trimer being the high dipole moment species, in this case), with an error of fit of the same magnitude as for our fits of our 1–2–3 model. We cannot judge the significance of the isolated result, except that the value seems reasonable for an open trimer; however, this illustration does demonstrate the potential of this approach.

Conclusions

We have shown that important structural information on solute association can be obtained by measuring dielectric properties as a function of concentration. The interpretation of these results is greatly assisted by the happy combination of infrared and dielectric data. The results establish, for 1-octanol in the solvents studied, that solute association follows a general pattern: monomer–small, high dipole moment polymer–low dipole moment cyclic polymer–high dipole moment polymers.

There are interesting differences in the behavior of 1-octanol in the three solvents studied. There is a fairly large solute–solvent interaction in benzene solution which delays association; this contrasts with the behavior in cyclohexane (and in hexane) solution. In a further communication we shall compare the behavior of a number of other isomers in the same three solvents.

Acknowledgments. We wish to acknowledge the assistance of the South African Council for Scientific and Industrial Research in the purchase of equipment used in this work and of the South African Coal, Oil and Gas Corp. (S.A.S.O.L.) Ltd., for support of the research upon which this paper is based.

Supplementary Material Available. Tables containing dielectric data for 1-octanol in carbon tetrachloride, cyclohexane, and benzene over the entire concentration range at 25° will appear following these pages in the microfilm edition of this volume of the journal. Photocopies of the supplementary material from this paper only or microfiche (105 × 148 mm, 24× reduction, negatives) containing all of the supplementary material for the papers in this issue may be obtained from the Journals Department, American Chemical Society, 1155 16th St., N.W., Washington, D. C. 20036. Remit check or money order for $3.00 for photocopy or $2.00 for microfiche, referring to code number JPC-75-660.

References and Notes

(1) A referee has pointed out that the form of the Kirkwood–Frohlich equation which we use is a special case of an Onsager-based equation (eq 6.208 of C. J. F. Böttcher, "Theory of Electric Polarization," Vol. 1, 2nd ed, Elsevier, Amsterdam, 1973), when the permittivity of solute and solvent are the same. We have found, however, that the relative shapes of the curves representing the change of dipole moment with concentration, when calculated using either equation, cannot be distinguished while there is only a minor difference in the magnitude of the dipole moments so calculated. In view of the scatter in the data these minor differences appear not to be significant, and either equation may be used.
(2) D. A. Ibbitson and L. F. Moore, *J. Chem. Soc. B*, 76, 80 (1967).
(3) P. Bordewijk, M. Kunst, and A. Rip, *J. Phys. Chem.*, **77**, 548 (1973).
(4) E. E. Tucker and E. D. Becker, *J. Phys. Chem.*, **77**, 1783 (1973).
(5) A. I. Brodskii, V. D. Pokhodenko, and V. S. Kuts, *Russ. Chem. Rev.*, 347 (1970).
(6) J. C. Davis and K. K. Deb, *Advan. Magn. Resonance*, **4**, 201 (1970).
(7) M. A. Goldman and M. T. Emerson, *J. Phys. Chem.*, **77**, 2295 (1973).
(8) "Handbook for Dipolemeter," Type DM 01, Table 1, p 9; Wissenschaftlich-Technische Werkstätten, G.m.b.H., Weilheim, Bavaria, 1959. The permittivity values quoted in this handbook have been taken from other references: *viz.*, cyclohexane (2.0148 at 25°), K. Rosswog, Dissertation, Freidburg, 1953; carbon tetrachloride (2.2263 at 25°) and benzene (2.2727 at 25°), R. Mecke and K. Rosswog, *Z. Electrochem.*, **60**, 47 (1956); dibutyl ether (3.0475 at 25°), R. Mecke and H. Specht, *Z. Electrochem.*, **62**, 500 (1958).
(9) See paragraph at end of text regarding supplementary material.
(10) C. J. F. Böttcher, "Theory of Electric Polarisation," Elsevier, Amsterdam, 1952, pp 267–268.
(11) H. C. van Ness, J. van Winkle, H. H. Richtol, and H. B. Hollinger, *J. Phys. Chem.*, **71**, 1483 (1967).
(12) L. J. Bellamy and R. J. Pace, *Spectrochim. Acta*, **22**, 525 (1965).
(13) A. N. Fletcher and C. A. Heller, *J. Phys. Chem.*, **71**, 3742 (1967).
(14) A. N. Fletcher, *J. Phys. Chem.*, **73**, 2217 (1969).
(15) E. M. Woolley and L. G. Hepler, *J. Phys. Chem.*, **76**, 3008 (1972).
(16) P. Bordewijk, F. Gransch, and C. J. F. Böttcher, *J. Phys. Chem.*, **73**, 3255 (1969).
(17) R. H. Cole, *J. Chem. Phys.*, **59**, 1945 (1973).
(18) We note a typographical error in eq 8 of ref 3, where the term *i* has been omitted.
(19) S. N. Deming and S. L. Morgan, *Anal. Chem.*, **45**, 278A (1973); see also S. L. Morgan and S. N. Deming, *ibid.*, **46**, 1170 (1974).
(20) R. Aveyard, B. J. Briscoe, and J. Chapman, *J. Chem. Soc., Faraday Trans. 1*, **69**, 1772 (1973).

The Nature of Bonding in Amine–Iodine Complexes

Manjit S. Sambhi* and S. K. Khoo

Department of Chemistry, University of Malaya, Kuala Lumpur, Malaysia

(Received June 21, 1974; Revised Manuscript Received December 3, 1974)

Publication costs assisted by the Department of Chemistry, University of Malaya

The enthalpy of formation of molecular complexes arises from charge transfer and other forces, including coulombic, induction, dispersion, and exchange repulsion forces. The use of a theoretical expression which equates enthalpy of formation with energy terms arising from charge transfer and other forces can provide information about the magnitudes of these energy terms, and thus provide an insight to the nature of bonding in amine–iodine molecular complexes.

Introduction

The extent to which charge transfer and other forces contributes to the observed ground-state properties of molecular complexes is a topic of considerable interest.[1-4] A relationship[5] derived from $\Delta H°$ and the enhancement of dipole moment for amine–iodine complexes shows that the large observed $-\Delta H°$ values for these complexes is a consequence of strong charge-transfer interactions since the energy contribution made by other forces to $\Delta H°$ has essentially a constant positive value of 10.4 kcal mol^{-1}. We have confirmed[6] this result by the use of a theoretical equation of Person[7] and we now proceed to determine the magnitude of the contribution made by non-charge-transfer forces to $\Delta H°$ of amine–iodine complexes.

Theory and Results

The ground and excited states of a complex (D,A) derived from the interaction of an electron donor (D) and an electron acceptor (A) can be described[8] by the wave functions

$$\psi_N = a\psi_0(D, A) + b\psi_1(D^+\text{-}A^-)$$

and

$$\psi_E = a^*\psi_1(D^+\text{-}A^-) - b^*\psi_0(D, A)$$

The terms ψ_0 and ψ_1 refer to the no-bond and dative-bond wave functions, respectively. The ground-state energy (E_N) of a complex can be written as

$$E_N = R_N + E_0 = \Delta H°$$

where R_N is the resonance energy due to the charge-transfer force in the complex, while E_0 is the energy change due to other interactions when the donor and the acceptor come together. The coulombic, induction, and dispersion forces are attractive, while the exchange repulsion works against them, thus making E_0 either negative, zero, or positive. For molecular complexes which can be satisfactorily described by one charge-transfer state and two resonance structures ψ_0 and ψ_1, R_N is given by the theoretical expression[7]

$$R_N = \{E_1 - E_0 - 2\beta_0 S - [(E_1 - E_0)^2 - 4\beta_0 S(E_1 - E_0) + 4\beta_0^2]^{1/2}\}/2(1 - S^2) \quad (1)$$

where E_1 is the energy of the dative structure, β_0 is a resonance integral, and S is the overlap integral between ψ_0 and ψ_1. The term $(E_1 - E_0) = I_D - E_A + E_C - E_0$ where E_A is the electron affinity of the acceptor and E_C is mainly the coulombic attractive energy associated with the dative structure of the complex. If $(E_A - E_C + E_0)$ is designated by C_1, then $\Delta H°$ is given by the expression

$$\Delta H° = \{I_D - C_1 - 2\beta_0 S - [(I_D - C_1)^2 - 4\beta_0 S(I_D - C_1) + 4\beta_0^2]^{1/2}\}/2(1 - S^2) + E_0 \quad (2)$$

Equation 2 can be conveniently expressed as

$$\Delta H° = Z + E_0 \quad (3)$$

where Z represents the first term on the right-hand side of eq 2.

For a series of complexes derived from structurally related donors with a common acceptor, it has been shown[9] that the parameters β_0, C_1, and S can be assumed to be fairly constant, but the empirical procedure used[9] to obtain these parameters can only provide a range of reasonable rather than precise values. Hence, direct substitution of the values of these parameters obtained empirically can lead to erroneous estimations of R_N and E_0 if the values used turn out to be significantly different from the true values of the complexes.

For amine–iodine complexes it was found[10] that a Hammett plot of $\Delta H°$ against σ^* is linear for complexes which are relatively free of steric factors and we will assume β_0, C_1, and S as constant for these complexes. Table I shows the I_D and $\Delta H°$ values for these complexes. It was empirically found by the use of a least-squares fit program that a linear relationship with a correlation coefficient of 0.99 exists between $\Delta H°$ and Z values calculated for values of β_0, C_1, and S of -1 to -4 eV, 6 to 9 eV, and 0.15 to 0.55, respectively, at parameter intervals of 0.05. This result can be formalized by the expression

$$\Delta H° = mZ + k \quad (4)$$

where

$$m = f(\beta_0, C_1, S)$$

and

$$k = f(\beta_0, C_1, S)$$

Thus, when $m = 1$, eq 4 becomes identical with eq 3 and $k = E_0$. Table II shows the solutions obtained for E_0 together with the appropriate values of β_0, C_1, and S.

The recommended range of values[9] for β_0, C_1, and S are

TABLE I: $\Delta H°$ and I_D Data for Amine–Iodine Complexes[a]

Donor	$-\Delta H°$, eV	I_D, eV
Methylamine	0.308	8.97
Ethylamine	0.321	8.86
n-Butylamine	0.364	8.71
Dimethylamine	0.425	8.24
Trimethylamine	0.525	7.82

[a] Reference 10.

TABLE II: Solutions of E_0 with Appropriate Values of β_0, C_1, and S

Solution	$-\beta_0$, eV	C_1, eV	S	m	$k = E_0$, eV
1	1.500	6.500	0.200	0.990	0.298
2	1.500	7.000	0.450	1.018	0.293
3	2.000	6.000	0.250	1.006	0.536
4	2.000	6.500	0.400	0.990	0.520
5	2.500	6.000	0.400	0.999	0.756
6	2.500	6.500	0.550	0.996	0.737
7	3.000	6.000	0.500	0.983	0.966

−1.7 to −3 eV, 6.5 to 7.5 eV, and 0.4 to 0.5, respectively, thus solution 4 provides the best values of E_0 of 0.520 eV mol^{-1} (11.99 kcal mol^{-1}) as values of β_0, C_1, and S_1 associated with this solution have values which fall within the recommended range of values. Solutions 1 and 3 can be rejected on the grounds that S values associated with these solutions are markedly different from the recommend values of S, while solutions 2, 5, 6, and 7 may be reasonable since two out of three parameters β_0, C_1, and S associated with these solutions have values which are within the recommended range of values.

Conclusion

A linear relationship can be found between $\Delta H°$ and R_N for these amine–iodine complexes which suggests that E_0 is essentially a constant. It has a large positive value of 11.99 kcal mol^{-1} which is in good agreement with the value of 10.4 kcal mol^{-1} obtained from the use of a relationship between $\Delta H°$ and the enhancement of dipole moment.[5] The large positive value indicates that repulsive forces dominate the term E_0 and that charge-transfer forces account for the large observed $-\Delta H°$ values for these complexes. The R_N contribution to $\Delta H°$ of these complexes varies from −19.1 to −24.1 kcal mol^{-1}.

References and Notes

(1) M. W. Hanna, *J. Amer. Chem. Soc.*, **90**, 285 (1968).
(2) J. L. Lippert, M. W. Hanna, and P. J. Trotter, *J. Amer. Chem. Soc.*, **91**, 4035 (1969).
(3) R. J. W. Le Fèvre, D. V. Radford, and P. J. Stiles, *J. Chem. Soc. B*, 1297 (1968).
(4) R. S. Mulliken and W. B. Person, *J. Amer. Chem. Soc.*, **91**, 3409 (1969).
(5) H. Ratajczak and W. J. Orville-Thomas, *J. Mol. Structure*, **14**, 149 (1972).
(6) M. S. Sambhi, *J. Mol. Structure*, submitted for publication.
(7) W. B. Person, *J. Chem. Phys.*, **38**, 109 (1963).
(8) R. S. Mulliken, *J. Amer. Chem. Soc.*, **74**, 811 (1952).
(9) R. S. Mulliken and W. B. Person, "Molecular Complexes: A Lecture and Reprint Volume," Wiley, New York, N.Y., 1969.
(10) H. Yada, J. Tanaka, and S. Nagakura, *Bull. Chem. Soc. Jap.*, **33**, 1660 (1960).

COMMUNICATIONS TO THE EDITOR

Some Unmeasured Chlorine Atom Reaction Rates Important for Stratospheric Modeling of Chlorine Atom Catalyzed Removal of Ozone

Publication costs assisted by the Division of Research, U.S. Atomic Energy Commission

Sir: Chlorine atoms when injected into the stratosphere at 25 km or above can initiate a chain reaction with odd oxygen involving principally reactions 1–3.[1-9] The primary

$$Cl + O_3 \longrightarrow ClO + O_2 \quad (1)$$

$$ClO + O \longrightarrow Cl + O_2 \quad (2)$$

$$ClO + NO \longrightarrow Cl + NO_2 \quad (3)$$

manner in which this ClO_x chain is interrupted in the stratosphere is through the reaction of Cl with various hydrogen-containing species with the formation of HCl. The Cl atoms can then be released again through the attack of OH and HCl as in (4). From the measured concentrations

$$OH + HCl \longrightarrow H_2O + Cl \quad (4)$$

of CH_4[10] and the reaction rate coefficients,[11] it is clear that reaction 5 with CH_4 is quite important in the stratosphere,

$$Cl + CH_4 \longrightarrow HCl + CH_3 \quad (5)$$

and it has been regularly assumed to be the chief HCl forming reaction between about 30–50 km. Our purpose here, however, is to estimate the possible contributions from other hydrogen-containing species in the stratosphere, with the primary intention of discovering whether CH_4 is an overwhelmingly dominant H-abstraction source. Several recent calculations indicate that ClO_x-catalyzed removal of odd oxygen is becoming an increasingly serious global environmental problem through the release of Cl atoms in the stratospheric photodissociation of CF_2Cl_2 and $CFCl_3$.[1-3,7-9]

TABLE I: Calculated Rates of Removal of Cl Atoms at Various Stratospheric Altitudes[a]

Altitude, km	25	30	35	40	45	50	55
Temp, °K	227	235	252	268	275	274	274
Density, molecules cm^{-3}	7.7(17)	3.6(17)	1.7(17)	8.1(16)	4.3(16)	2.3(16)	1.3(16)
Estimated concn, cm^{-3}							
O_3	4(12)	4(12)	2(12)	6(11)	2(11)	7(10)	3(10)
CH_4	5(11)	2(11)	8(10)	3(10)	1(10)	6(9)	3(9)
H_2	6(11)	3(11)	1(11)	5(10)	2(10)	9(9)	4(9)
HO_2	2(7)	3(7)	2(7)	9(6)	6(6)	4(6)	3(6)
H_2O_2	2(9)[b]	2(9)[b]	3(8)	4(7)	1(7)	4(6)	2(6)
HNO_3	4(9)	5(8)	2(8)	3(7)	2(6)	1(6)	
Estimated rates[c] of removal of Cl atoms, cm^{-3} sec^{-1} Reaction with							
O_3	74	70	33	11	3.7	1.3	0.5
CH_4	10(−3)	5(−3)	3(−3)	2(−3)	1(−3)	4(−4)	2(−4)
H_2	2(−3)	1(−3)	8(−4)	6(−4)	3(−4)	1(−4)	5(−5)
HO_2	1(−3)	1(−3)	8(−4)	4(−4)	3(−4)	2(−4)	2(−4)
H_2O_2	6(−3)	6(−3)	1(−3)	2(−4)	7(−5)	3(−5)	2(−5)
HNO_3	4(−3)	6(−4)	2(−4)	3(−5)	3(−6)		

[a] All exponential figures have been written with the exponential in parentheses, i.e., 7.7×10^{17} is written as 7.7(17). The data have all been read to two places from smoothed curves, and then rounded off to one place in the table in view of the large uncertainties in modeling calculations for the stratosphere. [b] Other models show lower values for H_2O_2 at these altitudes. Crutzen, for example, has given values of 3(8) and 4(8) at 25 and 30 km, respectively. [c] Summary of rate equations, in cm^3 molecules^{-1} sec^{-1}, for reaction of Cl with O_3,[14] $(1.85 \pm 0.36) \times 10^{-11}$; CH_4,[11] $5.1 \times 10^{-11} \exp(-1790/T)$; H_2,[11] $5.7 \times 10^{-11} \exp(-2260/T)$; HO_2,[17] 5×10^{-11}; H_2O_2,[16] $1.7 \times 10^{-10} \exp(-910/T)$; HNO_3,[17] $6 \times 10^{-12} \exp(-400/T)$.

The most abundant hydrogen-containing species in the stratosphere are, roughly in order of decreasing abundance, H_2O, CH_4, H_2, H_2O_2, HNO_3, HO_2, and OH. Hydrogen abstraction by Cl atoms is endothermic by 10 kcal/mol with H_2O, and is therefore of negligible importance at stratospheric temperatures. Except for H_2, further calculations can only be estimates since the rate coefficients for reaction with Cl atoms has not been measured for the last four species in the list above. The reaction of Cl with OH must have an activation energy of at least 3 kcal/mol since the forward reaction is 0.8 kcal/mol exothermic and the reverse reaction of O atoms with HCl has an activation energy of at least 4 kcal/mol.[12] Abstraction of H from OH can therefore be neglected relative to abstraction from CH_4.

From the measured or estimated concentrations of these species in the stratosphere,[13] and with appropriate approximations for the rate coefficients as described below, we have calculated in Table I the approximate rates for formation of HCl by reaction with each of the five possible species between 25 and 55 km. Table I also includes the rate of reaction of Cl atoms with O_3,[14] showing it to be $>10^3$ times faster than the sum of all of the HCl-forming reactions at all of these altitudes. The reaction of Cl with H_2 is consistently about 20–30% as probable as with CH_4.

Our estimated rate coefficients for reactions 6–8 in Table

$$Cl + HO_2 \longrightarrow HCl + O_2 \quad (6)$$

$$Cl + H_2O_2 \longrightarrow HCl + HO_2 \quad (7)$$

$$Cl + HNO_3 \longrightarrow HCl + NO_3 \quad (8)$$

I have been based on comparison with the known rates for OH reaction with the same species, since OH is isoelectronic in the valence shell with Cl, and the thermochemistry of Cl and OH reactions is similar. However, since the measured rates for Cl reaction with CH_4 and H_2 are respectively 16 and 5 times faster than the corresponding OH reaction rates in the 225–275°K temperature range,[15] we have also used more rapid rate estimates for Cl reaction with the three hydrogen species of (6) to (8). Our assumptions for reactions 7 and 8 are each ten times faster than the measured rates for OH with H_2O_2[16] and HNO_3. The radical termination reaction 6 is almost certainly fast, but probably does not occur on every collision for geometric reasons. Our estimate in Table I (~1 collision in 6) falls in the middle of recent estimates for the reaction of OH + HO_2.[17] Even the assumption of reaction on every collision of Cl with HO_2 still leaves reaction 6 less important than reaction 5 throughout the 35–50 km range.

Present calculations of the rates of odd oxygen removal by ClO_x indicate that the region between 35–45 km is heavily dominant[1-3,7-9] (for example, see Figure 10 in ref 2), and in this region the data of Table I indicate that (a) reaction with CH_4 is more important in HCl formation than the other four reactions combined; and (b) omission of reactions 7 and 8 in earlier studies has not introduced major errors into the estimates of ozone depletion by ClO_x.

The estimates in Table I do suggest that H_2O_2 may be equally important with CH_4 in HCl formation near 25–30 km, and that HO_2 probably becomes more important than CH_4 somewhere above 50 km. Moreover, the uncertainty in these estimates must be considerable since neither HO_2 nor H_2O_2 has actually even been observed in the stratosphere, let alone accurately measured, and the concentrations of Table I have been inferred from model calculations. (Since our chief concern here has been to avoid ignoring a potentially important but poorly understood hydrogen-containing species, we believe that the removal rates for reactions 6 and 7 in Table I are more likely to be over- than underestimated.) [NOTE ADDED IN PROOF: R. T. Watson and D. D. Davis gave a preliminary value of less than 10^{-12} for the rate constant of reaction 7 (4th C.I.A.P. Meeting, Cambridge, Mass., Feb 1975). With this rate constant, reaction

7 has only minor importance throughout the stratosphere.]

The stratospheric concentrations of HNO_3 have been measured,[18] and it is therefore unlikely that reaction 8 is of much importance relative to reaction 5 in HCl formation. Nevertheless, completeness in the stratospheric modeling should include reaction 8 as well as reactions 6 and 7. Consequently, experimental measurements of both the high altitude concentrations of HO_2, H_2O_2, and HNO_3, plus the laboratory rate coefficients for their reactions with Cl atoms are important for a more detailed understanding of stratospheric chlorine chemistry.

Measurement of the reaction rates for the stable molecules in (7) and (8) should be relatively easy, but the radical–radical reaction of (6) seems much more difficult. Finally, all of the model calculations used in these estimates have been one-dimensional (vertical) global average models, and detailed calculations in two or three dimensions may well show portions of the stratosphere in which one or more of reactions 6–8 has more importance than in the average calculations.

References and Notes

(1) M. J. Molina and F. S. Rowland, *Nature (London)*, **249**, 810 (1974).
(2) M. J. Molina and F. S. Rowland, *Geophys. Res. Lett.*, **1**, 309 (1974).
(3) F. S. Rowland and M. J. Molina, AEC Report No. UCI-1974-1, Sept 1974; to be published in *Rev. Geophys. Space Phys.*
(4) R. S. Stolarski and R. J. Cicerone, *Can. J. Chem.*, **52**, 1610 (1974).
(5) P. Crutzen, *Can. J. Chem.*, **52**, 1569 (1974).
(6) S. C. Wofsy and M. B. McElroy, *Can. J. Chem.*, **52**, 1582 (1974).
(7) R. J. Cicerone, R. S. Stolarski, and S. Walters, *Science*, **185**, 1165 (1974).
(8) P. Crutzen, *Geophys. Res. Lett.*, **1**, 205 (1974).
(9) S. C. Wofsy, M. B. McElroy, and N. D. Sze, *Science*, **187**, 545 (1975).
(10) D. H. Ehhalt, *Can. J. Chem.*, **52**, 1510 (1974).
(11) M. A. A. Clyne and R. F. Walker, *J. Chem. Soc. Faraday Trans. 1*, **69**, 1547 (1973).
(12) The activation energy for the reverse reaction was measured as 4 kcal/mol by V. P. Balaknin, V. I. Egorov, and E. I. Intezarova, *Kinet. Catal.*, **12**, 258 (1971), and as 7 kcal/mol by E. L. Wong and F. E. Belles, NASA Technical Note, NASA TN-D-6495, 1971: *Chem. Abstr.*, **76**, 18326*q* (1972). The agreement is not good, but both groups found an activation energy of at least 4 kcal/mol.
(13) These concentrations are generally those given in ref 6, but are semiquantitatively similar to those found in ref 1–5 and other stratospheric modeling papers, except as noted.
(14) M. A. A. Clyne and R. T. Watson, *J. Chem. Soc. Faraday Trans. 1*, in press.
(15) "Chemical Kinetics Rate Survey," NBS-74-430, Jan 1974, contains a summary of the various measurements made for the OH reactions used in these estimates.
(16) These rate coefficients are ten times faster than the rate for OH + H_2O_2 given in ref 15. At 275°K, this estimated rate is only three times slower than the measured rate for Cl + O_3.
(17) The rate equation for OH + HO_2 is still subject to considerable disagreement, and values between 2×10^{-11} and 2×10^{-10} cm^3 molecule^{-1} sec^{-1} have been recommended for modelers.
(18) H. I. Schiff, *Can. J. Chem.*, **52**, 1536 (1974).
(19) This research was supported by AEC Contract No. AT(04-3)034, P.A. 126.

Department of Chemistry[19]
University of California
Irvine, California 92664

Mario J. Molina
F. S. Rowland*

Received October 21, 1974

Quantum Yield for the Photolysis of CF_2Cl_2 in O_2

Publication costs assisted by the Division of Research, U.S. Atomic Energy Commission

Sir: Large quantities (~0.5 Mtons/year) of CF_2Cl_2 are manufactured each year for use as an aerosol propellant and as a refrigerator coolant.[1,2] Essentially all of the aerosol propellant is released to the atmosphere within 1 year of manufacture, while most of that used as a refrigerant is probably also eventually released as well. The accumulation of CF_2Cl_2 in the earth's atmosphere presents a hazard to stratospheric ozone through its photolysis by reaction (1), and the subsequent chain reaction of Cl with O_3 and ClO with O.[1-5] All of our calculations concerning the atmospheric residence time of CF_2Cl_2 and the rate of formation of Cl atoms have been based on the assumption that the quantum yield for (1) is 1.0, and that the subsequent reaction of CF_2Cl with O_2 leads to the release of a second chlorine-containing free radical (either Cl or ClO). While this sequence seemed highly probable to us on the basis of analogy with CCl_4 photolysis,[6] as well as relative quantum yields for $CFCl_3$ photolysis, we have measured the actual quantum yield for photooxidation of CF_2Cl_2 in the laboratory for confirmation of the postulated photochemical steps in the atmospheric mechanisms.

$$CF_2Cl_2 + h\nu \longrightarrow CF_2Cl + Cl \qquad (1)$$

The absorption of CF_2Cl_2 has its long wavelength edge near 2150 Å, increasing rapidly to shorter wavelengths with a maximum near 1800 Å.[2,7] In the earth's atmosphere, the cross product of flux penetrating to 25–35-km altitudes and absorption cross section, assuming unit (or constant) quantum yield, causes photodissociation to occur with roughly constant probability between 1900 and 2100 Å. In this laboratory, we have used a low-pressure Hg lamp flushed with N_2 as the light source and have photolyzed CF_2Cl_2 with 1849-Å light. Our photolysis cell had one 1-in. quartz window and a path length of 11 cm. The CF_2Cl_2 (Matheson Co.) had a stated purity of 99.6% and was thoroughly degassed at −196°. Molecular oxygen from Liquid Carbonic was used. The light intensity of the lamp was determined by N_2O actinometry to be $5.7 \pm 0.5 \times 10^{14}$ photons sec^{-1} (cm)$^{-2}$. Approximately 11–15% of CF_2Cl_2 was decomposed in each photolysis experiment, as measured by differences in chromatographic peak heights.

The first step in photolysis was assumed to be reaction 1 followed by the rapid secondary reaction of CF_2Cl with O_2. While the expected product of this reaction is CF_2O, our chromatographic analysis utilized a 50-ft silicone oil column known to convert CF_2O to CO_2. Consequently, our measurement provides only the quantum yields for the removal of CF_2Cl_2 and for the complementary appearance of a corresponding photooxidized molecule capable of further reaction to form CO_2. The quantum yields for six runs with O_2 concentration $\leq [CF_2Cl_2]$ are given in Table I. Within the accuracy of our actinometry, the quantum yields for the removal of CF_2Cl_2 and for the appearance of CO_2 are both unity. Since the cross sections for absorption of 1849-Å light are 1.0×10^{-18} cm^2 for CF_2Cl_2[2] and 3×10^{-20} cm^2 for O_2,[8] >95% of the initial light absorption occurs with CF_2Cl_2.

The initial absorption step occurs in the lone pair of one of the chlorine atoms,[7] and the energy relationships overwhelmingly favor the release of Cl rather than F.[2] By analogy with the reactions of CF_3 and CCl_3, the reaction of CF_2Cl with O_2 should give CF_2O as the product, indicating the release of either Cl or ClO in the second step. Independent CF_2Cl_2–O_2 photolysis experiments utilizing infrared analysis have shown that CF_2O absorption bands are observed afterward with no indication of CFClO formation.[9] For stratospheric computations, the mechanistic difference

TABLE I: Quantum Yields for Removal of CF_2Cl_2 and Formation of Oxidized Product in the 1849-Å Photolysis of CF_2Cl_2–O_2 Mixtures

Pressure, Torr			
O_2	CF_2Cl_2	$\Phi(-CF_2Cl_2)^b$	$\Phi(CO_2)^{a,b}$
49.4	49.8	1.1_6	1.0_4
49.5	49.7	1.0_6	1.1_0
12.1	49.6	1.2_6	1.1_1
12.3	49.8	1.0_7	1.0_8
49.8	49.7	1.0_2	1.2_0
49.6	49.7	1.1_7	1.1_3
		Av 1.12 ± 0.09	1.11 ± 0.05

[a] Measured as CO_2 after reaction on the chromatographic column. [b] Quantum yields are given on the basis of absorption by CF_2Cl_2 alone.

between Cl and ClO formation in the second step is not important because the two are rapidly interconverted in chain processes involving O_3, O, and NO. The photooxidation of CF_2Cl_2 with a quantum yield of unity is thus accompanied by the appearance of ClO_x species with a quantum yield of $\Phi(Cl + ClO) = 2$. Both measurements are actually made at 1849 Å, and we infer that the same values are applicable for the 1950–2150-Å band because of the absence of any structure in the absorption band in this region, and because all of the energies are far above the minimum needed for rupture of the C–Cl bond in CF_2Cl_2. We have not sought higher precision in these experiments since our purpose was only to confirm the postulate that photooxidation was the usual fate for these molecules following absorption of a quantum of light in the 1800–2150-Å region.

The earlier measurements with $CFCl_3$,[10] the other major aerosol propellant gas in current usage, demonstrated that a constant relative quantum yield was obtained for its decomposition in O_2 or NO on widely varying ratios to the $CFCl_3$ molecule. This constancy strongly suggested that the quantum yield for decomposition is unity, unaffected by changes in photolysis conditions.[10] In view of the CF_2Cl_2 results given above, we have concluded without further experiment that $\Phi(Cl + ClO)$ is also 2 for $CFCl_3$ photolyzed in O_2 or air. In the atmosphere, the number of Cl atoms eventually released from $CFCl_3$ depends upon the ultimate fate of the CFClO residue, since its further photolysis or hydrolysis would release a third Cl atom.

Acknowledgment. This research was supported by A.E.C. Contract No. AT(04-3)-34, P.A. 126.

References and Notes

(1) M. J. Molina and F. S. Rowland, *Nature (London)*, **249** 810 (1974).
(2) F. S. Rowland and M. J. Molina, A.E.C. Report No. UCI-1974-1, Sept 1974; to be published in *Rev. Geophys. Space Phys.*
(3) R. J. Cicerone, R. S. Stolarski, and S. Walters, *Science*, **185**, 1165 (1974).
(4) P. Crutzen, *Geophys. Res. Lett.*, **1**, 205 (1974).
(5) S. C. Wofsy, M. B. McElroy, and N. D. Sze, *Science*, **187**, 545 (1975).
(6) J. Heicklen, *Adv. Photochem.*, **7**, 59 (1969).
(7) J. Doucet, P. Sauvageau, and C. Sandorfy, *J. Chem. Phys.*, **58**, 3708 (1973).
(8) M. Ackerman, F. Baume, and G. Kockarts, *Planet. Space Sci.*, **18**, 1639 (1970). The absorption is on the wing of a sharp absorption peak ($\sigma_{max} \sim 1 \times 10^{-19}$ cm^2) in the Schumann–Runge system.
(9) G. Breuer, private communication.
(10) D. Marsh and J. Heicklen, *J. Phys. Chem.*, **69**, 4410 (1965).

Department of Chemistry
University of California
Irvine, California 92664

Richard Milstein
F. S. Rowland*

Received October 17, 1974

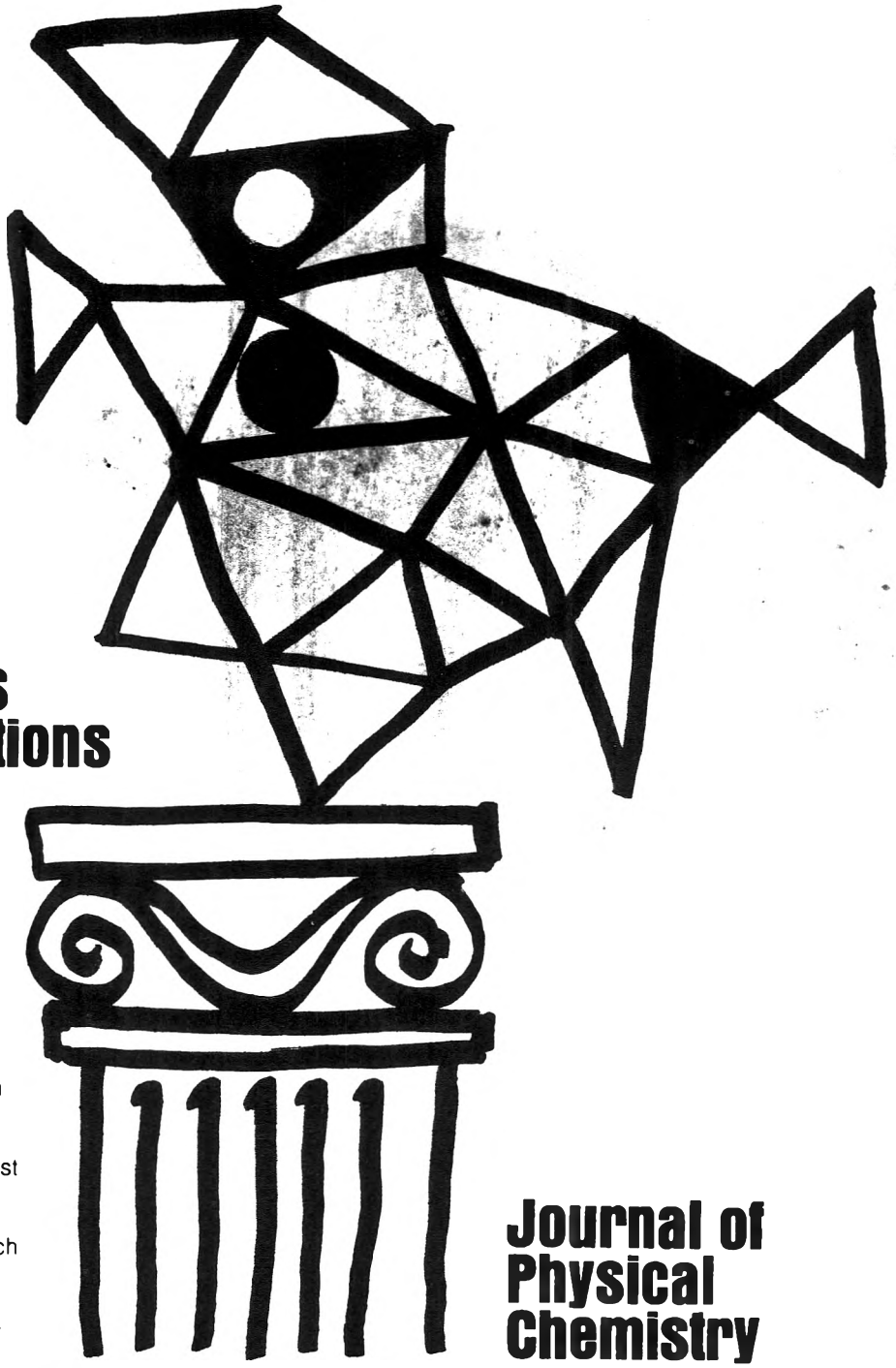

New concepts new techniques new interpretations

. . . together with valuable reports on classical areas

They are all waiting for you between the covers of our well-balanced JOURNAL OF PHYSICAL CHEMISTRY. Whatever your particular interest in physical chemistry, you'll find the JOURNAL's broad range of experimental and theoretical research reports are relevant and beneficial to your work. Each biweekly issue brings you an average of 30 authoritative, comprehensive reports on fundamental aspects of atomic and molecular phenomena, as well as timely notes, communications and reports plus the proceedings of selected symposia.

Join your fellow physical chemists who rely on JPC as an excellent biweekly source of data in both new and classical areas. Just complete and return the form to start your own subscription.

. . . *another ACS service*

Journal of Physical Chemistry

The Journal of Physical Chemistry
American Chemical Society
1155 Sixteenth Street, N.W.
Washington, D.C. 20036

1975

Yes, I would like to receive the JOURNAL OF PHYSICAL CHEMISTRY at the one-year rate checked below:

	U.S.	*Canada***	*Latin America***	*Other Nations***
ACS Member One-Year Rate*	☐ $20.00	☐ $24.50	☐ $24.50	☐ $25.00
Nonmember	☐ $80.00	☐ $84.50	☐ $84.50	☐ $85.00

Bill me ☐ Bill company ☐ Payment enclosed ☐

Air freight rates available on request

Name _____

Street _____ Home ☐ Business ☐

City _____ State _____ Zip _____

Journal subscriptions start on January '75

*NOTE: Subscriptions at ACS member rates are for personal use only. **Payment must be made in U.S. currency, by international money order, UNESCO coupons, U.S. bank draft, or order through your book dealer.

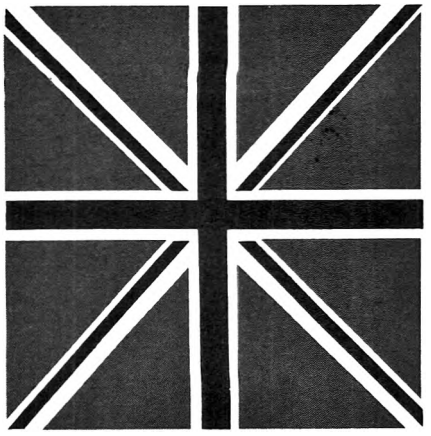

ANNOUNCING
The American Chemical Society is now distributing **SPECIALIST PERIODICAL REPORTS** published by The Chemical Society

The highly-praised **SPECIALIST PERIODICAL REPORTS** are now available for the first time through the American Chemical Society.

This outstanding series provides critical and comprehensive coverage of the latest progress in major areas of chemical research. Each field is examined in depth by foremost authorities on the subject, making each volume an essential resource for the specialist chemist as well as for the newcomer seeking an introduction to the state of the art.

Titles are published annually, and in some cases, biennially. All books postpaid in U.S. and Canada, plus 40 cents elsewhere.

Titles from the series currently available:

Aliphatic Chemistry, Senior Reporter: Prof. W. Parker, Vol. 2, 534 pp., 1974 (1972 literature), Cloth bound, $30.25.

The Alkaloids, Senior Reporter: Dr. J. E. Saxton, Vol. 3, 337 pp., 1973, (July 1971-June 1972 literature), Cloth bound $23.50.

Amino-acids, Peptides, and Proteins, Senior Reporter: Dr. R. C. Sheppard, Vol. 5, 515 pp., 1974, (1972 literature), Cloth bound $22.00.

Aromatic and Heteroaromatic Chemistry, Senior Reporters: Dr. C. W. Bird & Dr. G. W. H. Cheeseman, Vol. 1, 445 pp., 1973, (Jan. 1971-May 1972 literature), Cloth bound $30.00.

Biosynthesis, Senior Reporter: Prof. T. A. Geissman, Vol. 2, 308 pp., 1973, (1972 literature), Cloth bound $22.00.

Carbohydrate Chemistry, Senior Reporter: Prof. J. S. Brimacombe, Vol. 6, 620 pp., 1973, (1972 literature), Cloth bound $22.00.

Chemical Thermodynamics, Senior Reporter: Prof. M. L. McGlashan, Vol. 1, 362 pp., 1973, (recent literature to Dec. 1971), Cloth bound $22.00.

Colloid Science, Senior Reporter: Prof. D. H. Everett, Vol. 1, 264 pp., 1973, (1970-1971 literature), Cloth bound $18.00.

Dielectric and Related Molecular Processes, Senior Reporter: Prof. Mansel Davies, Vol. 1, 394 pp., 1972, (five years up to Sept. 1971), Cloth bound $22.00.

Electrochemistry, Senior Reporter: Prof. H. R. Thirsk, Vol. 4, 349 pp., 1974, (April 1972-March 1973 literature coverage), Cloth bound $24.75.

Electron Spin Resonance, Senior Reporter: Prof. R. O. C. Norman, Vol. 1, 273 pp., 1973, (Jan. 1971-May 1972 literature), Cloth bound $19.25.

Electronic Structure and Magnetism of Inorganic Compounds, Senior Reporter: Dr. P. Day, Vol. 2, 372 pp., 1973, (Jan. 1971-March 1972 literature), Cloth bound $22.00.

Fluorocarbon and Related Chemistry, Senior Reporters: Dr. R. E. Banks & Dr. M. G. Barlow, Vol. 2, 307 pp., 1974 (1971-1972 literature), Cloth bound, $44.00.

Foreign Compound Metabolism in Mammals, Senior Reporter: Dr. D. E. Hathway, Vol. 2, 513 pp., 1972, (1970-1971 literature), Cloth bound $30.00.

Inorganic Chemistry of the Main Group Elements, Senior Reporter: Prof. C. C. Addison FRS, Vol. 1, 444 pp., 1973, (July 1971-Sept. 1972 literature), Cloth bound $24.75.

Inorganic Chemistry of the Transition Elements, Senior Reporter: Dr. B. F. G. Johnson, Vol. 2, 501 pp., 1973, (Oct. 1971-Sept. 1972 literature), Cloth bound $26.25.

Inorganic Reaction Mechanisms, Senior Reporter: Dr. J. Burgess, Vol. 2, 393 pp., 1972, (Aug. 1970-Dec. 1971 literature), Cloth bound $22.00.

Mass Spectrometry, Senior Reporter: Dr. D. H. Williams, Vol. 2, 356 pp., 1973, (July 1970-June 1972 literature), Cloth bound $22.00.

Molecular Spectroscopy, Senior Reporters: Prof. D. A. Long, Prof. D. J. Millen & Dr. R. F. Barrow, Vol. 1, 622 pp., 1973, (recent literature to Jan. 1972), Cloth bound $33.00.

Molecular Structure by Diffraction Methods, Senior Reporters: Prof. G. A. Sim & Dr. L. E. Sutton, Vol. 1, 824 pp., 1973, (Jan. 1971-Mar. 1972 literature), Cloth bound $41.50.

Nuclear Magnetic Resonance, Senior Reporter: Dr. R. K. Harris, Vol. 2, 406 pp., 1973, (July 1971-May 1972 literature), Cloth bound $24.75.

Organic Compounds of Sulphur, Selenium, and Tellurium, Senior Reporter: Dr. D. H. Reid, Vol. 2, 827 pp., 1973, (April 1970-March 1972 literature), Cloth bound $41.50.

Organometallic Chemistry, Senior Reporters: Prof. E. W. Abel & Prof. F. G. A. Stone, Vol. 2, 612 pp., 1973, (1972 literature), Cloth bound $35.75.

Organophosphorus Chemistry, Senior Reporter: Prof. S. Trippett, Vol. 5, 313 pp., 1974 (July 1972-June 1973 literature), Cloth bound, $27.50.

Photochemistry, Senior Reporter: Prof. D. Bryce-Smith, Vol. 5, 1974 (July 1972-June 1973 literature), Cloth bound, $55.00.

Radiochemistry, Senior Reporter: Dr. G. W. A. Newton, Vol. 1, 131 pp., 1972, (July 1969-Aug. 1971 literature), Cloth bound $12.50.

Spectroscopic Properties of Inorganic and Organometallic Compounds, Senior Reporter: Prof. N. N. Greenwood, Vol. 6, 663 pp., 1973, (1972 literature), Cloth bound $30.00.

Statistical Mechanics, Senior Reporter: Dr. K. Singer, Vol. 1, 256 pp., 1973, (literature up to July 1972), Cloth bound $18.00.

Surface and Defect Properties of Solids, Senior Reporters: Prof. M. W. Roberts & Prof. J. M. Thomas, Vol. 2, 277 pp., 1973, (May 1971-April 1972 literature), Cloth bound $20.75.

Terpenoids and Steroids, Senior Reporter: Dr. K. H. Overton, Vol. 3, 527 pp., 1973, (Sept. 1971-Aug. 1972 literature), Cloth bound $33.00.

Earlier volumes in some titles available on request.

Order from:
Special Issues Sales
American Chemical Society
115 Sixteenth St., N.W.
Washington, D.C. 20036